Modelling the interactions of advanced micro- and nanoparticles with novel entities

Zhang, F.

Modelling the Interactions of Advanced Micro- and Nanoparticles with Novel Entities

Fan Zhang

张帆

Modelling the Interactions of Advanced Micro- and Nanoparticles with Novel Entities

PhD thesis, Leiden University, The Netherlands

The research as described in this thesis was conducted at the Institute of Environmental Sciences (CML), Leiden University, The Netherlands.

ISBN: 978-90-5191-232-6
Cover: Fan Zhang
Layout: Fan Zhang
Printed by: Print & Bind

Modelling the Interactions of Advanced Micro- and Nanoparticles with Novel Entities

Proefschrift

ter verkrijging van

de graad van doctor aan de Universiteit Leiden,

op gezag van rector magnificus prof.dr.ir. H. Bijl,

volgens besluit van het college voor promoties

te verdedigen op dinsdag 7 november 2023

klokke 10:00 uur

door

Fan Zhang

geboren te Shanxi, China

in 1995

Promotores:

Prof. dr. ing. M.G. Vijver

Prof. dr. ir. W.J.G.M. Peijnenburg

Promotiecommissie:

Prof. dr. G.R. de Snoo

Prof. dr. A. Tukker

Prof. dr. M. Barz

Prof. dr. A.M. de Roda Husman (Utrecht University)

Dr. P.N.H. Wassenaar (National Institute for Public Health and the Environment)

Dr. B.W. Brinkmann

Table of contents

Chapter 1

General Introduction

1.1 Novel entities

In September 2021 Claire Asher wrote an essay entitled: Novel chemical entities: Are we sleepwalking through a planetary boundary? This title gives the exact expression for humans' low state of consciousness while performing activities with increasing pollution which result in affecting the Earth system in a variety of ways. These "new substances with potential geophysical and/or biological effects" are referred to as "novel entities" (Persson et al., 2022). Scientists generally recognize that novel entities become the focus of global environmental attention when they exhibit the potential for lasting impact, large-scale distribution, and influence on important Earth system processes (De Souza Machado et al., 2019). The majority of man-made chemical "novel entities" have been reported to enter the environment (L. Chen et al., 2023; Kuznetsova et al., 2023; Nunes et al., 2023; Zhang et al., 2023), including engineered nanoparticles (ENPs), microplastics (MPs), pesticides, per- and polyfluoroalkyl substances, flame retardants, antibiotics even novel living organisms.

The Planetary Boundaries framework created by the international scientific team of the Stockholm Resilience Centre is trying to get a handle on the myriad of environmental impacts of this chemical onslaught (Steffen et al., 2015). Because novel entities are so pluriform, just recently quantification of the extent and magnitude of the pollution was estimated (Diamond et al., 2015; MacLeod et al., 2014; Persson et al., 2022, 2013; Steffen et al., 2015) with a lot of focus and help of visible plastic pollution (Arp et al., 2021).

The "planetary boundary" is the boundary value used to define the global "safe operating space" (Rockström et al., 2009), which relates

to e.g., biosphere integrity, climate change, and novel entities (Steffen et al., 2015). "Planetary boundaries" are proposed to maintain the normal functioning of the Earth system and human society by defining variables that humans need to control, setting thresholds, and reducing the risk of human activities exceeding Earth system thresholds (MacLeod et al., 2014). However, these "novel entities" are being created at such a rapid pace that they are far outpacing the risk assessments conducted by governments and organizations. This makes that the majority of the novel entities are still existing in the natural environment, and production and associated contamination are likely to rise further (Persson et al., 2022).

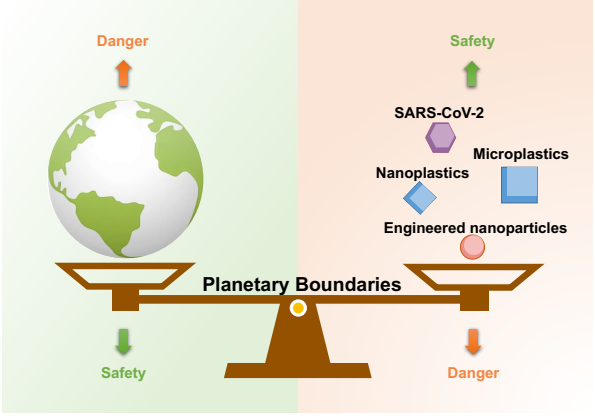

Figure 1.1. *Potential control of the quality of the Earth's ecosystem by novel entities.*

At present, it is still difficult to control the impacts on the Earth's ecosystem from these "novel entities". To maintain the balance of planetary health in relation to the continued increase of novel entities (Figure 1.1), there is an urgent need to investigate the environmental behavior and toxicological effects of novel entities. Toxicological testing has confirmed the ecotoxicity of typical novel entities such as

ENPs and MPs (Minetto et al., 2016; Rai et al., 2021). Most notably, novel entities often enter the environment as mixtures (Kar and Leszczynski, 2019; Martinez et al., 2022; Trinh and Kim, 2021). Simultaneous exposure to multiple novel entities requires consideration of the possible interactions between these novel entities and their effects on organisms.

1.1.1 Engineered nanoparticles

Nanotechnology has emerged as the most promising technology of the 21st century (Sharma et al., 2023). Nanomaterials are widely used in many fields (Singh et al., 2023), and most of them are engineered and gradually integrated into people's lives and used in thousands of products (Pérez-Hernández et al., 2021), such as cosmetics, sunscreens, fabrics, pharmaceuticals, and sports equipment. Along with the large-scale industrial production, transportation, and disposal processes of nanomaterials, especially during the wash-off process of personal care products doped with nanomaterials (e.g., cosmetics, sunscreens, textiles, etc.) and during the use and decomposition of industrial products, ENPs are released or flow into and seep into the atmosphere, water bodies, and soil environment, becoming "environmental nano-pollutants" (Abbas et al., 2020; Ahmed et al., 2018).

ENPs have been detected in surface water (Azimzada et al., 2021; Sanchís et al., 2020; Wu et al., 2020) and sediments (Tou et al., 2021), and nanoparticles containing titanium, copper, zinc, and silver have been detected in aquatic organisms for instance marine mollusks (e.g., oysters, mussels, scallops, and clams) (Xu et al., 2020). When a particle is small and approaches the nanoscale, its physicochemical

properties are greatly altered and it has the potential to freely cross cell membranes and enter the cells of organisms (Verma et al., 2008). Numerous studies have confirmed that ENPs have a significant impact on ecology and human health (Das et al., 2016; Jogaiah et al., 2021; Tiede et al., 2016). In fact, environmental nano-pollutants have become one of the most dominant and important objects of environmental science research and environmental protection technologies.

1.1.2 Microplastics and nanoplastics

In terms of time span change, humankind has taken a big step into the "plastic era" (Lee et al., 2022). However, with the growing awareness of environmental protection, it has been recognized that "microplastics" (MPs, < 5 mm) pollution has taken over the world (Jung et al., 2022). MP pollution not only affects the development of human society, but also negatively affects the function of marine organisms, biomes, and the entire global ecosystem, and is a potential global boundary threat (Allen et al., 2021; González-Pleiter et al., 2021; Romera-Castillo et al., 2023). MP pollution has posed an unprecedented challenge to geoscience research and has become a global challenge to address. MPs include micron- to millimeter-scale plastics (> 1000 nm to 5 mm) as differentiated from nanoplastics (NPs, 1 to 1000 nm) (Junaid et al., 2023). NPs are characterized by large fugitive quantities, high adsorption efficiency, and high trans-biofilm capacity, and may exhibit more intense ecological and toxic effects compared to MPs (Z. Chen et al., 2023; Qi et al., 2023).

MPs and NPs can cause damage to biological organisms through oxidative stress (Rodrigues et al., 2023), cytotoxicity (Shi et al., 2022),

inflammatory responses (Wang et al., 2023), metabolic alterations (Zhao et al., 2023), and neurotoxicity (J.-L. Xu et al., 2022). MPs and NPs are frequently found in the environment and are easily ingested by organisms and can enter the food chain by virtue of their small size (Kim et al., 2022; Zhu et al., 2021), ultimately affecting human health (Dong et al., 2023; W. Wang et al., 2022). *In vitro* studies have also confirmed that MPs and NPs have toxic effects on the human digestive, respiratory, immune, and reproductive systems (Bastyans et al., 2022; J.-L. Xu et al., 2022). Due to the strong specific surface area, MPs and NPs may have more serious negative effects on organisms when they act as "Trojan horses" carrying other contaminants through biofilms or across tissues (Katsumiti et al., 2021; Roje et al., 2019; Sun et al., 2023). Therefore, the phenomenon of complex contamination caused by the interaction of MPs and NPs with harmful "novel entities" coexisting in the environment cannot be ignored.

1.1.3 Viral particles

Different from engineered chemical "novel entities", biological "novel entities" include amongst others viruses (like, among others the coronavirus). Viruses can exist in sizes ranging in between 1–100 nm, with novel coronaviruses typically having a diameter of 60–140 nm (Gunathilake et al., 2022).

These biological entities distribute globally. Severe acute respiratory syndrome coronavirus 2 (SARS-CoV-2) spreads mostly through direct contact and respiratory droplets (Jennings and Perez, 2020; Ragab et al., 2020), although pathways via water, air, and soil may also be important vectors of coronavirus transmission (Sanchez-Galan et al.,

2021). Coronavirus-containing waste or wastewater can enter the aquatic environment, especially in urban water environments, by several routes (Saingam et al., 2023). Wastewater contains a large number of viruses, bacteria, fungi and chemical reagents, which are mixed together and are highly infectious. This allows them to easily cause various human diseases and complications, posing a serious public health risk. At the same time, the aquatic environment contains a large number of viruses and other pathogens that are extremely destructive to other ecological species. A more comprehensive understanding of the environmental behavior of viruses or viral ribonucleic acid (RNA) in environmental media is not only beneficial to the development of more scientific-based control and prevention strategies, but also allows for a deeper understanding and scientific cognition of the relevance of ecological changes to viruses.

1.2 Interactions of micro- and nanoparticles with other novel entities

Small particles have a relative large surface area (e.g., ENPs, MPs, NPs, and virus) and inherently have good adsorption capacity owing to their special physicochemical properties, including small particle size, huge specific surface area, and high hydrophobicity at nanostructured surfaces. Once these micro- and nanoparticles (MNPs) enter the environment, they are likely to sorb, enrich and carry other pollutants in the environment. This will not only alter the transport and transformation behavior of other pollutants in the environment, but these pollutants will also change the dissolution, agglomeration, precipitation, bioconcentration and migration, microbial degradation

and other behavioral properties of MNPs themselves in the environment (Figure 1.2). In addition, when MNPs act simultaneously with other novel entities on organisms, they may induce toxic responses that are different from the effects of a single toxicant (Figure 1.2). Thus, it can be seen that the carrier effect is the key by which MNPs influence the environmental behavior and toxic effects of other novel entities.

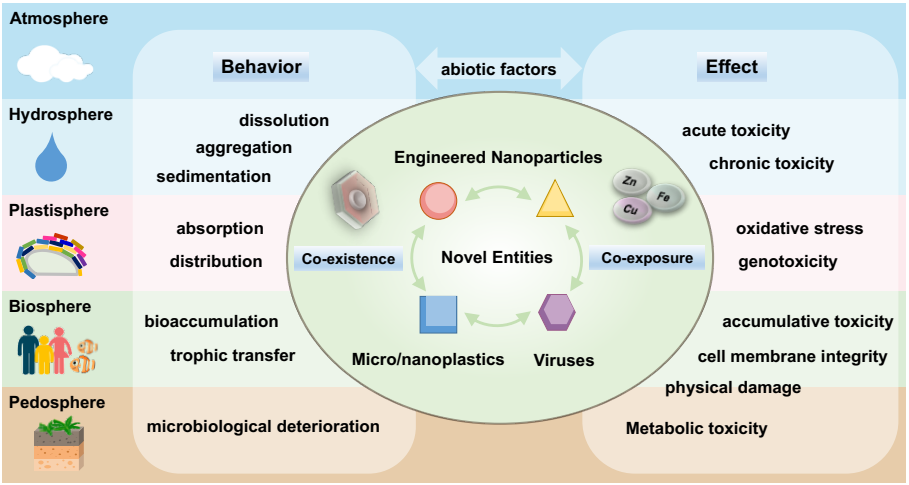

Figure 1.2. *Interactions between novel entities and their potential environmental behavior and toxicological effects.*

1.2.1 Interaction of ENPs with metals

ENPs readily adsorb metals/metal ions and their oxides from the environment (Deshwal et al., 2023; Rosenfeldt et al., 2016). This adsorption behavior can affect not only the physicochemical properties of ENPs such as particle size and surface charge, but also the environmental transport and transformation of the adsorbed substances. When the composite system belongs to the category of colloids (particle size between 1 nm and 10 μm), the particles have

well-defined physicochemical properties such as surface charge and kinetic diameter. Meanwhile, the classical colloid dispersion theory — the Derjaguine-Landaue-Verwaye-Overbeek (DLVO) theory — can provide a solid theoretical basis for the analysis of nanoparticle composite systems (Nur et al., 2015).

1.2.2 Interaction of ENPs with organic pollutants

ENPs have large chemical activity and surface energy, which make them have strong interaction with organic pollutants and allows them to adsorb a large amount of organic pollutants (Pan and Xing, 2008; Qi et al., 2014; Xin et al., 2023; Yang and Xing, 2010). In recent years, scientists have conducted various studies on the ENPs' capacity to bind organic contaminants and demonstrated that the interaction of ENPs with organic pollutants is mainly related to the hydrophilicity and polarity of organic pollutants (Chen et al., 2007). The mechanisms of interaction between ENPs and hydrophobic organic pollutants are mainly based on hydrophobic and π-π interactions, while the adsorption of hydrophilic organic pollutants is mainly through partitioning, electrostatic force, and hydrogen bonding (Pan and Xing, 2008).

1.2.3 Interaction of ENPs with microorganisms

The interactions between ENPs and microorganisms are complex and diverse. For instance, once ENPs are released into the environment, a large fraction of the nanoparticles flow into wastewater treatment plants and come into contact with microorganisms present in the wastewater treatment (Saravanan et al., 2022; Zhou et al., 2023). These microorganisms can be present in biological wastewater

treatment systems in many forms. ENPs discharged from wastewater plants or directly into the environment can also come into contact with environmental microorganisms such as bacteria and algae (Gong et al., 2023). Therefore, understanding the interaction between ENPs and microorganisms is important to recognize the migration, toxicity, and elimination of ENPs in the microbial environment.

Recently, scientists have identified novel coronaviruses in wastewater in several countries (Conde-Cid et al., 2021). Previous studies have shown that both hepatitis viruses (Brisebois et al., 2018) and enteroviruses (Upfold et al., 2021) are transmitted to humans through wastewater. Therefore, wastewater containing novel coronaviruses can pose a serious threat to the population. After going through the entire standard wastewater treatment process, it may be sufficient to remove or destroy the virus. However, if there is still virus remaining in the effluent of wastewater treatment plants or in the effluent of treatment plants with poor wastewater treatment, the virus may still enter surface waters (Kolarević et al., 2022) with the effluent discharge (e.g., lakes, rivers, and various recreational sites) and may also become a source of infection. In addition, virus-laden effluent that seeps into natural waterways can cause infection through airborne aerosols (Q. Wang et al., 2022). Furthermore, the consumption of fruits and vegetables irrigated with wastewater that has not been properly disinfected may also be an indirect route of infection (Fernandes et al., 2023). Studies have reported that novel coronavirus RNA fragments have been detected in wastewater samples (Langeveld et al., 2023). The residence of novel coronaviruses and their RNA fragments in different water bodies and aerosols provides an opportunity for their coexistence with ENPs in

the environment.

The interaction between ENPs and microorganisms involves three main processes: physical, chemical, and biological. Both the agglomeration of nanoparticles and their deposition on microbial surfaces involve common physical interaction forces, as described by the traditional DLVO theory, hydrophobic interactions, spatial site resistance, and multimer bridging. ENPs also undergo a number of chemical transformation processes in the microbial environment, including redox transformations, photochemical degradation processes, surface adsorption, precipitation, complexation and cation bridging. In addition to physicochemical processes, some biologically relevant processes also occur between ENPs and microorganisms, including endocytosis, mitochondrial effects and biodegradation.

1.2.4 Interaction of MPs and NPs with microorganisms

MPs and NPs provide substrates and ecological niches for microorganisms to attach and selectively enrich environmental microorganisms to form biofilms, a new artificial ecosystem called the "plastisphere" (Zettler et al., 2013). Harmful microorganisms in the environment are adsorbed by MPs or NPs and transported over long distances in the environmental media. In these media they propagate and spread, facilitating the spread of antibiotic resistance genes and thus causing potential harm to the ecosystem. Numerous studies have focused on the enrichment and succession of microbial communities (algae, bacteria, archaea, fungi, viruses, protozoa, etc.) in the plastisphere, exploring the interactions within microbial communities, metabolic capabilities, and how microbial communities affect the surrounding environment (Barros and Seena, 2021; Junaid et al.,

2022; Wang et al., 2022). Thus, the impact of MPs and NPs is not only associated with themselves, but the microbial impact on their surface may be even more profound.

Possibly harmful effects on biota being amplified by interactions between SARS-CoV-2 and plastic pollutants in the aquatic environment is another growing subject. For example, recent studies have shown that particles of the SARS-CoV-2 virus can adhere to MPs' surfaces (Belišová et al., 2022), raising concerns about potential increased infectivity and virus transmission in humans, as well as the possibility of ecotoxicological risk that such interactions could present to organisms that are not the targets. For example, MPs can bind SARS-CoV-2 pseudoviruses on their surface and enhance infection of human cells *in vitro*, suggesting that plastic particles present in the environment or in the respiratory or gastrointestinal tracts of humans (target organism) have the potential to interact with SARS-CoV-2 and increase the risk of viral infection (Zhang et al., 2022). In addition, airborne MPs from waste could also serve as a transmission vector for SARS-CoV-2 (Liu and Schauer, 2021), and knowledge on this interaction can help to understand the transmission process.

1.2.5 Main factors affecting the interaction between MNPs and other novel entities

The adsorption of novel entities to MNPs can be described by considering that:

1) The ability of MNPs to adsorb other novel entities is closely related to the inherent properties of MNPs. It is both size and surface

related. Additionally, the physicochemical properties of MNPs are essentially determined by their composition, morphology, and internal structure.

2) The ability of MNPs to adsorb other novel entities is also related to the physicochemical properties of the other novel entities with which it has the interaction, such as the molecular size, structure and polarity of novel entities.

3) The ability of MNPs to adsorb other novel entities is also influenced by external field conditions such as pH, ionic strength and temperature.

1.3 Combined toxic effects of MNPs and other novel entities

MNPs can affect the biotoxicity and bioefficacy of other novel entities through adsorption, enrichment, and carrier effects, while altering their environmental behavior and fate. However, the current ecological risk assessment of MNPs typically relies on toxicity data regarding the toxicity of single constituents, and the potential risks caused by combined adverse effects are not fully taken into account. Therefore, the study of the mixture toxicity of MNPs has important theoretical value and practical significance, which is conducive to improving the scientific and rational nature of ecological risk evaluation.

To address the ecological risks caused by MNPs and their mixtures, studies on the combined toxicity of MNPs with other novel entities are gradually emerging. Current studies have focused on the mixture toxicity of MNPs with metals and organic pollutants, while studies on

the mixture toxicity of MNPs with other novel entities in the particulate state (other ENPs, M/NPs) have lagged behind. Up-to-date 1st generation metal oxide ENPs were tested most frequently on these test systems (Das et al., 2022; Mansouri et al., 2016; Yu et al., 2016a).

The mechanisms of interaction of MNPs and other novel entities in the particulate state and the combined toxicity of the mixture of these two entitites to ecological species are relatively complex, and the mechanisms of toxicity due to particle-particle interactions may also differ from those of particle-organic substance and particle-metal ion interactions. In addition, a non-homogeneous mixture composed of multiple particulate components has very different properties as compared to the properties of a single particulate component. This makes the combined toxicity of MNPs and other novel entities in the particulate state being affected by a combination of factors, including the composition, structure, and properties of each particulate component, the agglomeration and stability of particles, and the composition of exposure medium.

There are currently two approaches to determine the mixture toxicity of novel entities, namely a bottom-up approach (i.e., component-based or reductionist approach) and a top-down approach (i.e., whole mixture-based or holistic approach). Mixture toxicity studies depend on the methodology chosen. In the bottom-up approach, the challenge may be to relate experimental results of carefully controlled and well-defined mixtures to real-world situations. To respond to this challenge, mixtures consisting of chemicals with actual scenario exposure information or with common toxicity indicators can be prioritized for evaluation in studies of

mixture toxicity (Rider and Simmons, 2018). In the top-down approach, on the other hand, whole mixtures are often treated like single chemicals. However, such method is needed to determine the similarity between different mixtures. It is also essential to determine the interacting effects between components in a mixture.

1.4 Computational simulation methods for interactions between MNPs and other novel entities

Computational simulation models can be used to assist in solving complex problems and in data-rich situations. Along with the innovation of computer technology and the explosive development of big data, machine learning (ML) and artificial intelligence, as well as computational simulation (or *in silico*) methods have been rapidly applied to investigate the environmental behavior of novel entities (Gastaldi et al., 2023). Currently, the use of computational simulation methods in the field of nanotoxicology has increased significantly. Computational simulation methods can not only reduce the time and money spent on identifying the impacts of novel entities for *in vivo* and *in vitro* experiments, but also improve the understanding of the toxicity of novel entities.

Four major categories of computational simulation methods are commonly used: molecular simulations, physiologically based pharmacokinetics (PBPKs), quantitative structure-activity relationship (QSAR) models, and ML. Among them, molecular simulation methods are frequently used to study the structure-effect relationship of nanoparticle-novel entity interactions (Brinkmann et al., 2022; Dowlatabadi et al., 2019; Geitner et al., 2017). Molecular simulation uses computers to simulate the structure and behavior of

molecular models at the microscopic (atomic), nanoscopic, and mesoscopic scales, and then obtain various physical and chemical properties of molecular systems (Figure 1.3).

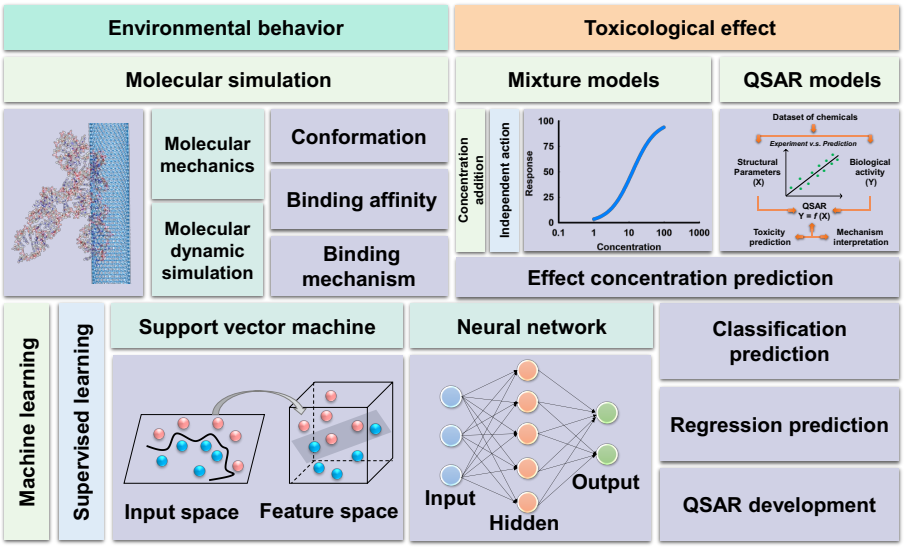

Figure 1.3. *Computational simulation methods for environmental behavior and toxicological effects of mixtures of novel entity.*

It constructs a set of models and algorithms based on physical laws with basic principles to calculate reasonable molecular structures and molecular behaviors. Molecular simulation can simulate not only the static structure of molecules, but also the dynamics of molecular systems. The typical methods of molecular simulation are: quantum mechanics (QM), molecular mechanics (MM), molecular dynamics (MD) simulation, molecular docking, Monte Carlo simulation.

MD simulation can simulate the flexible binding processes of multi-molecular systems and the dynamic conformations of complexes, providing more comprehensive information on the interaction mechanisms. Unlike other molecular simulation methods

(e.g., molecular docking, Monte Carlo simulation) that can deal with the static binding properties of multi-molecular systems, a MD method is capable of simulating both static and dynamic processes in multi-molecular systems. In addition, the MD method is more time efficient in dealing with multi-molecular systems than a QM method that takes the electron motion into account. Moreover, the MD method can also increase the accuracy. Therefore, the method has an irreplaceable advantage in simulating multi-molecular systems at the microscopic scale.

A QSAR is a statistical model that relates a set of structural parameters that describe a chemical compound to its biological activity (Buglak et al., 2019; Chen et al., 2017), as depicted in Figure 1.3. These parameters, which are called descriptors, are typically related to the steric and electronic properties of the compound, and they can be computed or measured in experiments. Biological activity, however, is determined through biological assays involving organisms of different trophic levels like algae, daphnids, and fish. Currently, the development of QSAR can offer a new way to rapidly screen chemicals alone or in mixtures and prioritize testing (Chatterjee and Roy, 2023; Reddy et al., 2023).

Recently, ML algorithms and deep learning (DL) algorithms have been developed for the study of multi-component interactions. ML modeling mainly uses publicly available structural information and *in chemico*, *in vivo*, and *in vitro* bioactivity data to construct QSAR models built on ML algorithms to further deepen the analysis of contaminant-biomolecule interactions in complex biological contexts (Figure 1.3). Therefore, ML modeling becomes a new computational technique that is completely different from molecular simulation.

Commonly used ML algorithms include support vector machines, neural networks, and random forests. These algorithms are capable of uncovering the intrinsic connections between numerous molecular features and predicted endpoints. Each algorithm has its own strengths, and the ability to make good use of such strengths is related to a variety of factors (e.g., the structure of the data). However, there is a key problem with ML modeling — poor interpretability. Previous statistical methods with excellent predictive power for linear data, such as linear-based multiple linear regression and partial least squares regression, are no longer able to cope with the explosive growth of biological "big data". The huge volume of data and the complexity of biological processes have led to a more advanced nonlinear class of data analysis methods. ML algorithms as applied to QSAR models with decision boundaries and hyperparametric dependence prediction problems that allow ML modeling with both high prediction accuracy and low interpretability. Combining multiple computational toxicology techniques to develop an integrated workflow for analysis of the underlying mechanisms can compensate for their respective shortcomings and allows to obtain optimal results. However, how to add computational flux screening while maintaining mechanistic analysis is still a critical issue to be addressed in the future.

1.5 Mixtures modeling

In ecotoxicological studies, screening of contaminant compound risks is mainly achieved by qualitatively assessing the mode of action of combined toxicity and quantitatively predicting the magnitude of combined toxicity. Two pharmacological concepts can be used for

data description and data interpretation for mixture toxicity, namely: "concentration addition" (CA) is used to predict the toxicity of mixed systems composed of compounds with similar modes of toxic action (Loewe and Muischneck, 1926); whilst "independent action" (IA) is used to predict the toxicity of mixed systems composed of compounds with different modes of toxic action (Bliss, 1939).

The CA and IA models have been applied to the assessment and prediction of nanoparticle mixture toxicity (Baek et al., 2020; Lai et al., 2022; Liu et al., 2016; Martín-de-Lucía et al., 2019). For example, the CA and IA models were used to effectively predict the combined toxicity of Cu and ZnO nanoparticles to *Lactuca sativa* L., and it was found that the fit of the IA model to experimental data on the combined toxicity of the two ENPs was better than the fit in case of the CA model (Liu et al., 2016). However, it is worth pointing out that the CA and IA models also require toxicity tests to determine the concentration-response relationships for single components. This increases the resources, money and time invested in the experiments on the one hand. On the other hand, it reduces the efficiency of the risk assessment of mixtures.

1.6 Extrapolation methods for assessing and predicting the combined toxicity of MNPs with other novel entities

Testing the toxicity of all chemicals and their mixtures is impractical, so there is an increasing need to rely on expert systems and computational methods (e.g., PBPKs, QSAR models) in future risk assessments. QSAR models can compensate for the low predictive efficiency of CA and IA models for mixture toxicity. As mentioned

above, QSAR models are mathematical relationships between toxicity indicators (e.g., lethality) and descriptors (e.g., physicochemical properties of chemicals) (Chen et al., 2017). In particular, QSAR model inputs do not require information on the concentration-response relationships of all single components in a mixture.

In previous studies, many breakthroughs have been achieved in the application of QSAR approaches to predict single toxicity studies of ENPs (Ehret et al., 2014; Epa et al., 2012; Huang et al., 2020; Puzyn et al., 2011), and hence QSAR model has become one of the most effective approaches for predicting the toxicity of single ENPs. However, QSAR studies on quantitative prediction of the toxicity of nanoparticles in combination with other novel entities are still in their infancy. The primary problem could be a lack of sufficient experimental data and standardized toxicity endpoints for developing predictive models. In addition to toxicity indicators, descriptors are also important for the development of QSAR models. Descriptors for nanoparticles can be obtained based on their properties at different multiple scales (Wang et al., 2018), which include quantum chemical properties of nanoclusters (e.g., total energy, orbital energy, and thermodynamic parameters), intrinsic structural properties of nanoparticles (e.g., chemical components, primary size, surface charge, specific surface area, and solubility), and colloidal properties of nanoparticles at mesoscopic scales (e.g., zeta potential and hydrodynamic diameter). Since nanoparticle mixtures contain both nanoparticle and mixture components, it is necessary to screen or calculate the features that can describe the hybrid system. Currently, some pioneering studies have developed QSAR models for predicting the biotoxicity of nTiO_2-based nanoblends (Mikolajczyk et al., 2019;

Trinh et al., 2022). The aforementioned $nTiO_2$-based nano-mixtures are mainly concerned with mixtures composed of metals and organics (Mikolajczyk et al., 2019; Trinh et al., 2022). However, there are still limited studies on the application of QSAR models for toxicity prediction of mixtures between nanoparticles and other novel entities in granular form.

1.7 Aims, research questions and objectives

The Earth will be under constant threat when the pressure from new types of entities persists over time. The coexistence of multiple novel entities in the environment is bound to exacerbate this threat. Exploring the interactions between different novel entities and clarifying the effects of these interactions on the environmental behavior, exposure pathways, toxic effects, and toxicity mechanisms of novel entities is a key part to understand and to enable mitigation actions. Thus, in this thesis, three novel entities of interest, namely ENPs, MPs, and SARS-CoV-2, were selected for study.

This thesis aimed to (scheme as shown in Figure 1.4):

1) Assess and quantify the interactions of carbon nanoparticles (CNPs) of different types and dimensions with the key fragment of the SARS-CoV-2 RNA.

2) Characterize the interactions of MPs with the non-enveloped structural materials of SARS-CoV-2 including a nucleocapsid protein and a SARS-CoV-2 RNA fragment in the water phase and in vacuum.

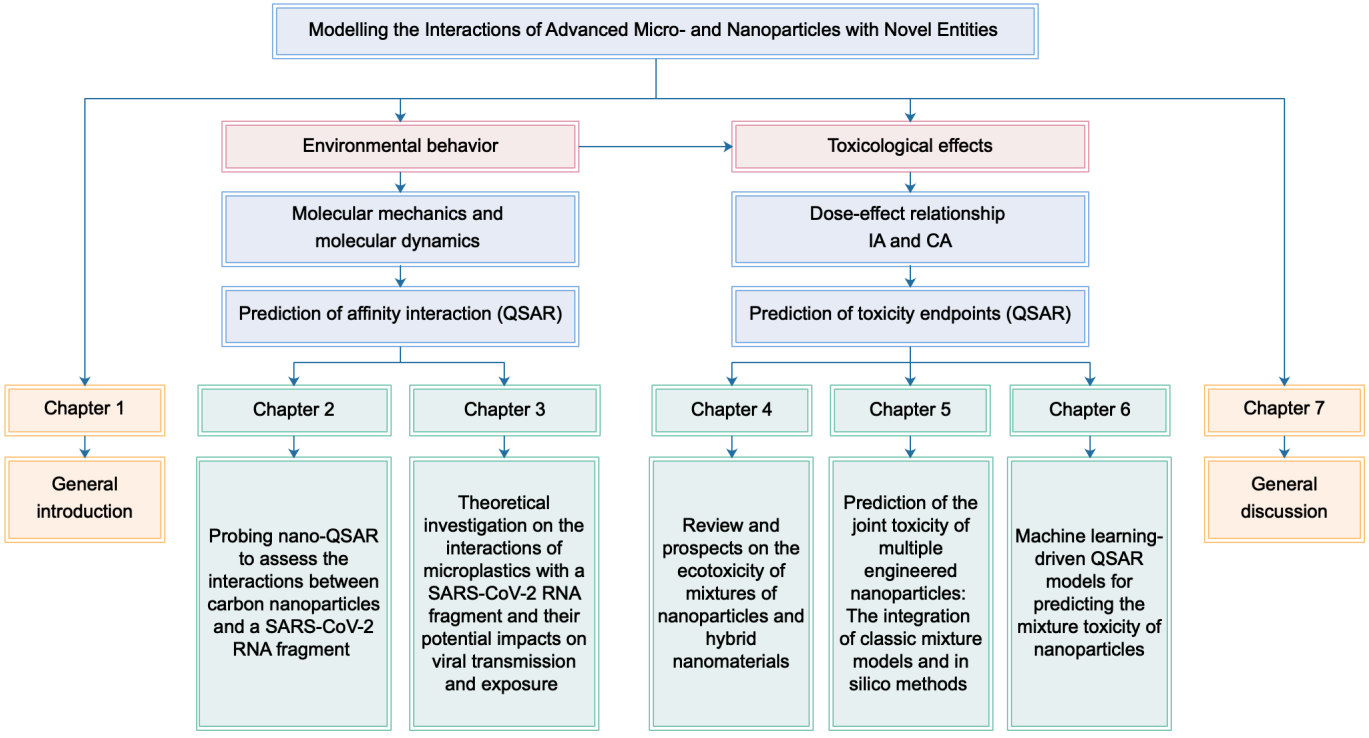

Figure 1.4. *Scheme of main research contents in this thesis.*

3) Collate information on the mixture toxicity of ENPs spanning trophic levels as well as aquatic and terrestrial environments available in the literature.

4) Propose a smart strategy for forecasting the toxicity of a mixture of ENPs.

5) Rebuild existing nano-QSAR models by incorporating ML methods to describe the toxicity of a mixture of ENPs.

According to the aims, the following research questions were addressed:

1) What is the mechanism of interaction between CNPs and the SARS-CoV-2 RNA fragment? How can the interactions be predicted? How do these interactions affect the human exposure and transmission of novel coronavirus? (**Chapter 2**)

2) What is the mechanism of interaction between MPs and the SARS-CoV-2 RNA fragment? What are the factors affecting this interaction? How does the interaction affect exposure and transmission of novel coronavirus? (**Chapter 3**)

3) What joint interactions have been reported after exposure of a range of aquatic and terrestrial test species to multiple ENPs? Which factors determine the toxicity of a mixture of multiple ENPs? Is there a difference between the environmental behavior and fate of multiple ENPs compared to single ENPs and do such differences subsequently affect the induced ecotoxicological effects? Which important knowledge gaps and further research needs have been identified in assessing mixture-nanoecotoxicology by experimentalists, computational modelers, risk assessors, and regulators? (**Chapter 4**)

4) How to quantitatively predict the joint toxicity of emerging or untested/unknown mixtures of multiple ENPs? How to establish reliable prediction models for mixed toxicity of multicomponent ENPs based on ML methods? Which ML models have better predictive performance and efficacy based on study samples? How do ML methods differ from traditional hybrid models in terms of predictive ability? (**Chapters 5 and 6**)

Focusing on the above scientific issues, theoretical models and computational simulations were used to assess and predict the interaction of MNPs with other novel entities and their combined toxicity. To accomplish this overall purpose the following objectives were achieved:

1) Probe the molecular interactions between CNPs and a SARS-CoV-2 RNA fragment using molecular mechanics simulations; Develop QSAR models to describe the interactions of 17 different types of CNPs from three dimensions with the SARS-CoV-2 RNA fragment. (**Chapter 2**)

2) Explore the molecular interactions between five MPs and a SARS-CoV-2 RNA fragment at temperatures ranging from 223 to 310 K in vacuum and in water using MD simulations. (**Chapter 3**)

3) Assess the toxicity of mixtures of ENPs to a variety of different species, covering algae, bacteria, daphnia, fish, fungi, insects, and plants using data mining methods. (**Chapter 4**)

4) Develop nano-QSAR models by ML techniques to predict the joint toxicity of seven metallic ENPs for *Escherichia coli* at different mixing ratios; Compare the differences in the ability to predict the

joint toxicity by means of ML-based nano-QSAR models and component-based mixture models. (**Chapters 5 and 6**)

1.8 Thesis outline

Chapter 1 A general introduction is given to the definition of novel entities and to the types of micron or nano scaled novel entities. Moreover, the interactions between MNPs and other novel entities and the impacts of these interactions on the behavior and toxicity of novel entities are illustrated. Meanwhile, the theoretical models and *in silico* methods for the studies of the interactions between MNPs and other novel entities and their joint toxicity are provided. Furthermore, the objectives and research questions of this thesis are proposed in this chapter.

Chapter 2 The molecular interactions between CNPs and a SARS-CoV-2 RNA fragment were investigated using molecular mechanics simulations. The mechanism of molecular interactions between the CNPs and the SARS-CoV-2 RNA fragment was elucidated. A predictive model was developed that quantifies the relationship between the structural properties of CNPs and these interactions.

Chapter 3 The molecular interactions between five model MPs and a SARS-CoV-2 RNA fragment at temperatures ranging from 223 to 310 K in vacuum and in water were investigated using MD simulations. The mechanism of the molecular interactions between the MPs and the SARS-CoV-2 RNA fragment was elucidated. A correlation was established between the interaction affinity and molecular parameters of MP monomers.

Chapter 4 The toxicity of mixtures of individual ENPs and of hybrid nanomaterials to a variety of different species, covering algae, bacteria, daphnia, fish, fungi, insects, and plants was reviewed. The strength of the joint interactions of multiple nanoparticles and the main factors influencing the joint response of the mixtures were identified. The knowledge of building a computational approach that is able to reduce the experimental costs of ecotoxicity testing of mixtures of nanoparticles of varying composition and to include both nanohybrids and mixtures of different ENPs was concluded.

Chapter 5 The classical mixture toxicology models and advanced computational toxicology models for toxicity prediction of chemical mixtures are summarized and demonstrated. The key strategy to quantitatively predict the joint toxicity of an emerging or untested/unknown mixtures of multiple ENPs is proposed.

Chapter 6 Nano-QSAR models by incorporating ML methods to predict the cytotoxicity of a mixture of ENPs were developed. The differences in the ability to predict the combined toxicity by means of the ML-based methods and two component-based mixture models (IA and CA) are compared.

Chapter 7 The research questions and main findings of the thesis are discussed. This includes discussion of the interactions between ENPs and SARS-CoV-2 genetic materials, mechanisms and influencing factors, and the impacts of these interactions on exposure and transmission of novel coronavirus; modes of action, influencing factors and assessment methods for the toxicity of ENP mixtures to ecological species; computational simulation methods for interaction and joint toxicity prediction between nanoparticles and other novel

entities; research perspectives on experimental and computational simulations for the study of environmental behavior, toxic effects and mechanisms of mixtures of novel entities; and future risk and hazard assessment of novel entities and their mixtures.

Chapter 2

Probing Nano-QSAR to Assess the Interactions between Carbon Nanoparticles and a SARS-CoV-2 RNA Fragment

Fan Zhang, Zhuang Wang, Martina G. Vijver and
Willie J.G.M. Peijnenburg

Published in Ecotoxicology and Environmental Safety 219 (2021), 112357.

Abstract

The coronavirus disease-19 (COVID-19) pandemic caused by the severe acute respiratory syndrome coronavirus 2 (SARS-CoV-2) is rampant in the world and is a serious threat to global health. The SARS-CoV-2 RNA has been detected in various environmental media, which speeds up the pace of the virus becoming a global biological pollutant. Because many engineered nanomaterials (ENMs) are capable of inducing anti-microbial activity, ENMs provide excellent solutions to overcome the virus pandemic, for instance by application as protective coatings, biosensors, or nano-agents. To tackle some mechanistic issues related to the impact of ENMs on SARS-CoV-2, we investigated the molecular interactions between carbon nanoparticles (CNPs) and a SARS-CoV-2 RNA fragment (i.e., a model molecule of frameshift stimulation element from the SARS-CoV-2 RNA genome) using molecular mechanics simulations. The interaction affinity between the CNPs and the SARS-CoV-2 RNA fragment increased in the order of fullerenes < graphenes < carbon nanotubes. Furthermore, we developed quantitative structure-activity relationship (QSAR) models to describe the interactions of 17 different types of CNPs from three dimensions with the SARS-CoV-2 RNA fragment. The QSAR models on the interaction energies of CNPs with the SARS-CoV-2 RNA fragment show high goodness-of-fit and robustness. Molecular weight, surface area, and the sum of degrees of every carbon atom were found to be the primary structural descriptors of CNPs determining the interactions. Our research not only offers a theoretical insight into the adsorption/separation and inactivation of SARS-CoV-2, but also allows to design novel ENMs which act efficiently on the genetic material RNA of SARS-CoV-2. This

contributes to minimizing the challenge of time-consuming and labor-intensive virus experiments under high risk of infection, whilst meeting our precautionary demand for options to handle any new versions of the coronavirus that might emerge in the future.

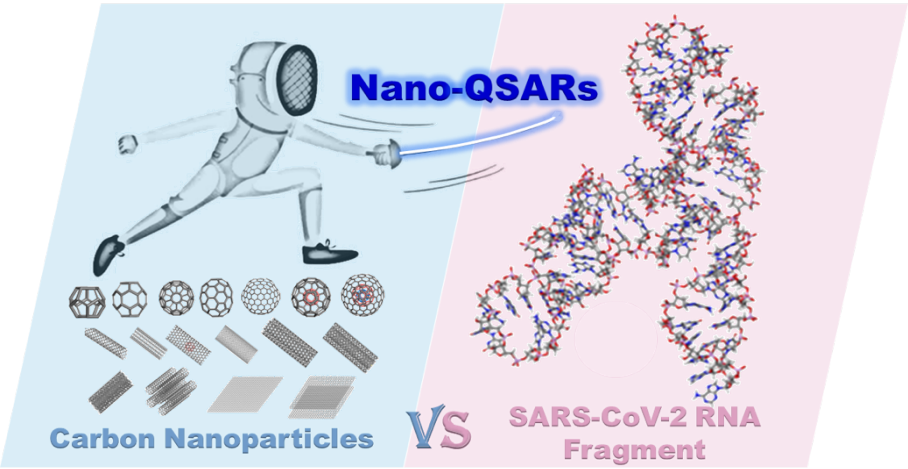

Graphical abstract

Keywords: COVID-19; Coronavirus; Genetic material; Nanomaterials; Interaction.

2.1 Introduction

The outbreak of a new coronavirus which by now has lasted for more than a year, has brought great disaster to human beings (Diffenbaugh et al., 2020; Slot et al., 2020; Snape and Viner, 2020). To deal with the most serious global public health emergency in recent decades, the governments of various countries have employed a number of measures to control the epidemic situation (Cheng et al., 2020). Scientists from various fields are stimulated to either improve existing or to develop new "weapons" against the coronavirus (Allawadhi et al., 2020; Florindo et al., 2020; Talebian et al., 2020). In response to the virus pandemic, nanoscience and nanotechnology are offering opportunities and challenges (Figure 2.1).

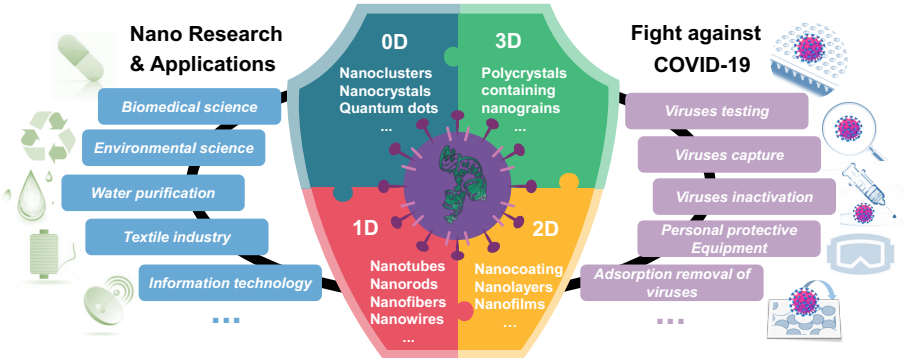

Figure 2.1. *Use of compositional and combinatorial ENM libraries, including metals, metal oxides, carbon nanotubes, and silica-based nanomaterials, to perform mechanism-based toxicological screening that links material composition and systematic variation of specific properties to biological outcomes.*

Viruses such as the avian influenza virus (H5N1), the severe acute respiratory syndrome coronavirus (SARS), the swine influenza virus (H1N1), and the Middle East respiratory syndrome coronavirus (MERS-CoV) are nature's nanostructures (Kostarelos, 2020) which

easily enter biological entities because of their special nanostructure-related advantages. Similarly, engineered nanomaterials (ENMs) also have such special properties due to the small size and hence relative large surface to volume ratio, which is in part why ENMs have been widely used for a variety of biomedical applications. In this respect there is a growing need for design of ENMs that are highly specific and efficiently taken up into target cells. The controllable physicochemical properties (e.g., size, shape, and surface) of ENMs facilitate their direct interactions with viral particles (e.g., interacting with viral envelope proteins and nucleic acids) or with host cell surface receptors to inhibit virus-cell interactions (Y. Chen et al., 2020). Hence, there is an urgent need to realize whether ENMs as anti-viral nano-agents can offer effective therapeutic strategies to combat the emergence of the coronavirus disease-19 (COVID-19). Although there has been criticism about the negative impact of nano-technology, the time for the severe acute respiratory syndrome coronavirus 2 (SARS-CoV-2) pandemic has now come to highlight the knowledge and previous experience of nanotechnologists in vaccine and drug development, delivery, and distribution (Anonymous, 2020). At the same time, the presence of the SARS-CoV-2 RNA in the environment such as in air (Mohan et al., 2021; Morawska and Cao, 2020) and water (Kitajima et al., 2020; Mohan et al., 2021) requires us to confirm whether ENMs because of their strong tendency to adsorb to any biotic or abiotic moiety, can efficiently remove the novel coronavirus. Understanding the interaction mechanisms between ENMs and macromolecules that are part of SARS-CoV-2 is an important foundation for the application of ENMs versus COVID-19.

Molecular simulation methods could be effective tools in exploring the interactions between ENMs and biomacromolecules with key biological functions (Ge et al., 2011), which would facilitate the design of novel nano-agents and improve the development and application of new therapeutic techniques. Quantitative structure-activity relationships for nanomaterials (nano-QSARs) are guided by the classical QSAR model and combine impacts of (non-tested) ENMs with their specific physicochemical properties (Chen et al., 2017; Puzyn et al., 2011). This provides a new way for rapid screening and priority testing of those ENMs that are predicted to be the most effective anti-viral agents. Combined with molecular simulation, nano-QSAR will play an increasingly important role in the fight against COVID-19 and future virus pandemics.

Many ENMs are known to exhibit high anti-microbial activity; either via induction of oxidative stress by for instance metal-based ENMs from which ions dissolve having the ability to generate oxidative stress (Sánchez-López et al., 2020), or via photothermal/ photocatalytic effects, lipid extraction, inhibition of bacterial metabolism, isolation by wrapping the microbes (Maleki Dizaj et al., 2015) with a nano-layer due to the high adsorption and high mechanical strength of ENMs. Also carbon nanoparticles (CNPs) are recognized as a promising nanomaterial for the detection, filtering, and inactivation of viruses. According to recent studies the physical interaction of carbon-based nanomaterials with bacteria, rather than oxidative stress, is the primary antimicrobial activity of these nanostructures (Maleki Dizaj et al., 2015). An additional benefit of carbon-based nanoparticles is that their high bio-safety and high biological compatibility, which are the characteristics used to comply

with various medical drugs (Aasi et al., 2020; Łoczechin et al., 2019; Palmieri and Papi, 2020; Vermisoglou et al., 2020). Therefore, this work is devoted to assessing and quantifying the interactions of the key fragment of the SARS-CoV-2 RNA (K. Zhang et al., 2021) with CNPs of different type and dimension. The fragment is a model molecule of frameshift stimulation element (FSE) from the SARS-CoV-2 RNA genome (K. Zhang et al., 2021). What is more, the FSE plays an important role in the virus replication cycle and has emerged as a major drug target (Lan et al., 2022). Subsequently, a predictive model is developed which quantifies the relationship between the structural properties of CNPs and these interactions.

2.2 Computational methods

2.2.1 Annealing simulations

The three-dimensional structure of the SARS-CoV-2 fragment determined by K. Zhang et al. (2021) was used for the simulations. Seventeen CNPs from three families of fullerenes, carbon nanotubes (CNTs), and graphene were selected as model molecules (Figure 2.2). The constructed fullerene molecular models include C_{20}, C_{36}, C_{70}, C_{240}, carbon nanoballs C_{60} and $C_{20}@C_{60}$, as well as the carbon nano-onion $C_{20}@C_{60}@C_{240}$. The constructed carbon nanotube molecular models include single-walled carbon nanotube (SCNT) (10,0), SCNT (6,6), SCNT (28,0), double-walled carbon nanotube (DCNT) (10,0), DCNT (6,6), triple-walled carbon nanotube (TCNT) (10,0), nanorope (NR) (6,6), and the complexes SCNT (16,0) with C_{60} named SCNT (16,0)@C_{60}. The constructed graphene molecular models include mono-layer graphene (MG) and bilayer graphene (BG).

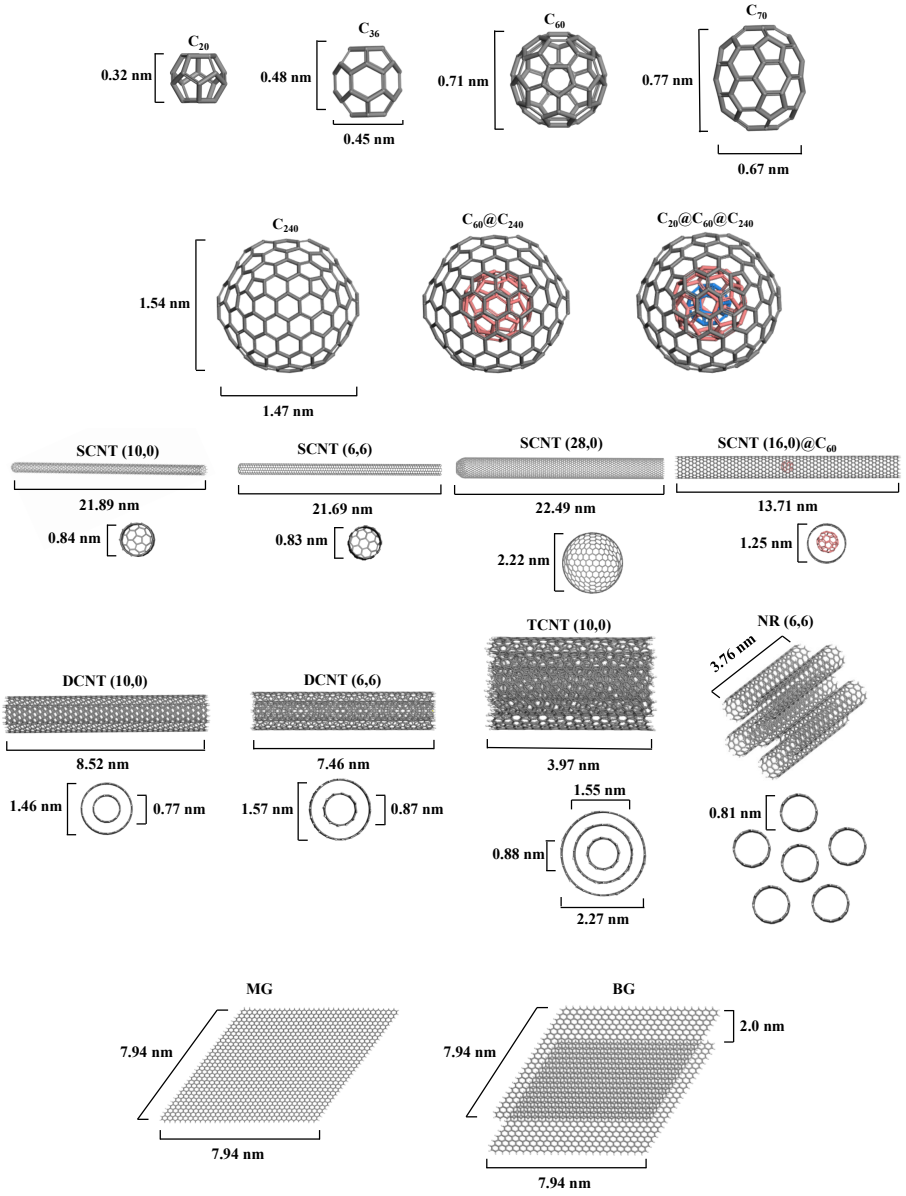

Figure 2.2. *Structure, morphology, and character of the studied models of carbon nanoparticles.*

To search for the best geometry with various forms of energy for each complex of the CNPs with the SARS-CoV-2 RNA fragment, a classical

annealing simulation was performing with the Materials Studio software package (ver. 8.0). The universal force field was adopted to perform this simulation. The cutoff radius was chosen to be 18.5 Å. The annealing simulation was performed as follows: a total of 200 annealing cycles which represented an optimal balance of total energy (Appendix Figure S2.1) were simulated with an initial temperature of 200 K, a midcycle temperature of 300 K, and 50 heating ramps per cycle, with 100 dynamic steps per ramp. The canonical ensemble (NVT ensemble, in which the number of molecules [N], volume [V], and temperature [T] of the system are kept constant) was used and the molecular dynamic simulations were performed with a time step of 1.0 fs and a Nosé thermostat. After each cycle, the lowest energy configuration was optimized. The van der Waals energies, electrostatic and total potential energies of the studied systems were calculated using the annealing simulation.

For the interaction systems, interaction energy (E_{int}) is used to evaluate the stability of the complexes of the CNPs with the SARS-CoV-2 RNA fragment. The magnitude of E_{int} is an indication of the magnitude of the driving force towards complexation. A negative value reflects a stable adsorption on the CNPs. E_{int} was calculated by

$$E_{\text{int}} = E_{\text{CNP-covRNA}} - E_{\text{CNP}} - E_{\text{covRNA}} \qquad (2.1)$$

where $E_{\text{CNP-covRNA}}$, E_{CNP}, and E_{covRNA} represent the energies (van der Waals, electrostatic, or total potential energies) of the complex, the isolated CNPs, and the individual SARS-CoV-2 RNA fragment, respectively.

2.2.2 Development of a predictive nano-QSAR model for E_{int}

Based on the interactions between the CNPs and the SARS-CoV-2 RNA fragment implied by the annealing simulations, several constitutional geometric and topological descriptors (Table 2.1) such as molecular weight (M_W), overall surface area (*OSA*), volume (*Vol*), specific surface area (*SSA*), and sum of degrees (*SDeg*), were selected to correlate with E_{int} so as to construct predictive models. *OSA* and *Vol* were calculated using Multiwfn 3.8 software (Lu and Chen, 2012a, 2012b). The *SSA* values were obtained directly from the derivation of *OSA* and *Vol*. *SDeg* was calculated using Chem3D Ultra (ver. 19.0). Orthogonal partial least squares (OPLS) regression was performed with Simca (ver. 14.1 Umetri AB & Erisoft AB) to select variables and to develop models. Randomization tests proposed for testing the rationality of the models were performed using the RAND () function to generate the pseudo-random numbers of the E_{int} derived from the total potential energy.

2.3 Results and discussion

2.3.1 Modeling the interaction of CNPs with the SARS-CoV-2 RNA fragment

In order to reveal the mechanisms of the interactions of CNPs with the SARS-CoV-2 RNA fragment, the E_{int} derived from the total potential energies, the van der Waals energies, and electrostatic energies are summarized in Figure 2.3 and Appendix Table S2.1. The optimized conformations obtained after the annealing simulations are shown in Figure 2.3A. The computed values are negative, indicating that the CNPs can form stable complexes with the SARS-CoV-2 RNA fragment.

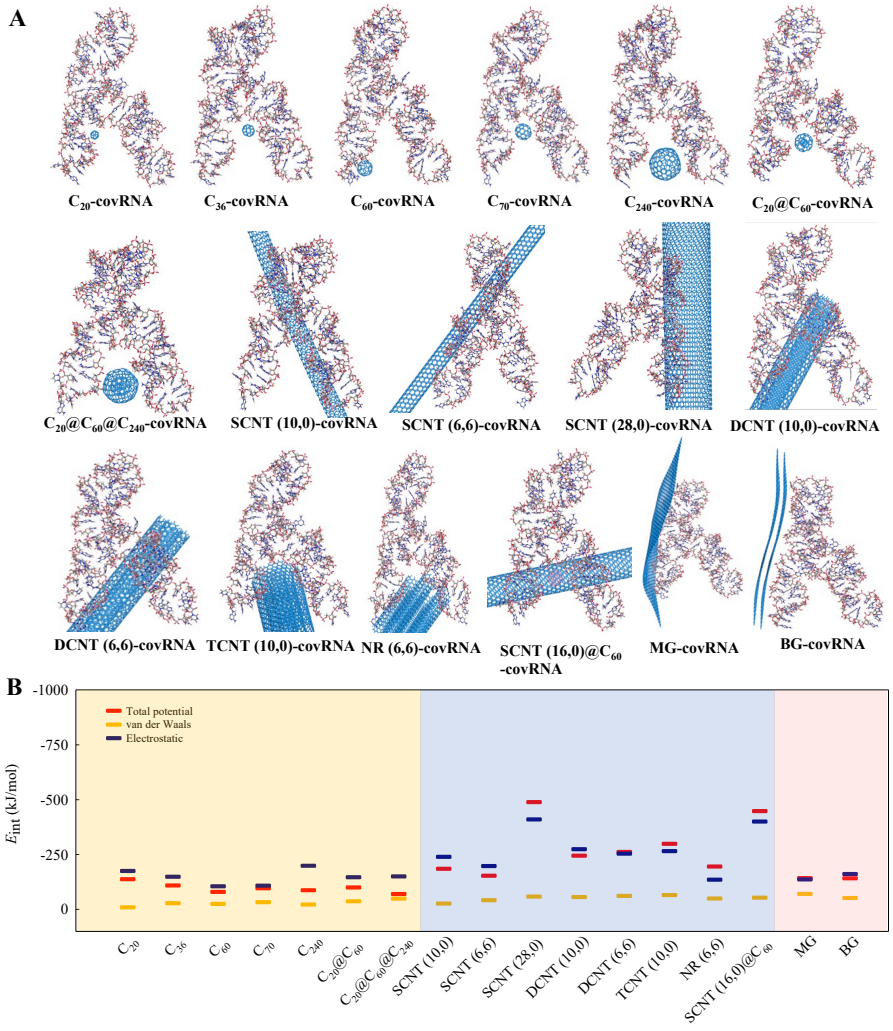

Figure 2.3. *Optimized structures of the complexes of the CNPs with the SARS-CoV-2 RNA fragment (abbreviated as covRNA) obtained after the annealing/geometry optimization procedure (A) and the calculated total potential energy interaction energies (E_{int}), van der Waals interaction energies, and electrostatic interaction energies between the CNPs and the SARS-CoV-2 RNA fragment using the simulated annealing method. The first 7 pictures (A) and the orange block (B) represent the fullerenes, the middle 8 pictures (A) and blue block (B) represent the nanotubes, the last 2 pictures (A) and the pink block (B) represent the graphenes.*

Figure 2.3B shows that CNTs have the highest absolute energy of interaction with the SARS-CoV-2 RNA fragment among the studied CNPs, as derived from the total potential energies. This suggests a strong interaction between the CNTs and the SARS-CoV-2 RNA fragment.

Generally, the interaction affinity between the CNPs and the SARS-CoV-2 RNA fragment increased in the order of fullerenes < graphenes < CNTs. In addition, the computed electrostatic interaction energies between the CNPs and the SARS-CoV-2 RNA fragment are similar to the E_{int} values derived from the total potential energies (Figure 2.3B). This implies that the electrostatic interaction contributes mainly to the mechanism of interaction. Wang et al. (2017) also concluded that electrostatic interactions contribute to the gaseous adsorption energies of organic molecules onto carbon-based nanomaterials by means of polyparameter linear free energy relationships. As the SARS-CoV-2 has a positive charge (K. Zhang et al., 2021), whereas the studied CNPs are neutral, the electrostatic interactions are mainly ion-induced dipole interactions.

2.3.2 Nano-QSAR prediction of the interaction of CNPs with the SARS-CoV-2 RNA fragment

The OPLS regression technique was used to find the most suited descriptors (Table 2.1) for developing models to quantify the E_{int} derived from the total potential energies Equations 2.2–2.4. *SSA* is the parameter that most significantly correlates with the E_{int} values of fullerenes, and there is a positive correlation between *SSA* and the absolute value of E_{int}. For CNTs and graphenes, *OSA* and *SDeg* are the parameters that correlate most significantly with the E_{int} values. At

the same time, *OSA* showed a positive correlation with the absolute E_{int}, whereas *SDeg* displayed a negative correlation with the absolute E_{int}. For the whole set of fullerenes, CNTs, and graphenes, M_W and *SDeg* are the parameters correlating most significantly with the E_{int} values. Moreover, M_W presented a positive correlation with the absolute value of E_{int}, while *SDeg* had a negative correlation with the absolute value of E_{int}.

Table 2.1. *Molecular parameters of the carbon nanoparticles.*

CNPs *	Chemical formula	Mol Weight (g/mol)	Overall surface area (nm^2)	Volume (nm^3)	Specific surface area (m^2/g)	Sum of Degrees
C_{20}	C20	240.220	1.859	0.234	4659.147	60
C_{36}	C36	432.396	2.678	0.404	3729.094	108
C_{60}	C60	720.660	3.812	0.645	3185.747	180
C_{70}	C70	840.770	4.325	0.750	3098.086	210
C_{240}	C240	2882.640	13.127	2.538	2742.369	720
$C_{20}@C_{60}$	C80	960.880	4.340	0.824	2720.323	240
$C_{20}@C_{60}@C_{240}$	C320	3843.520	10.283	3.047	1611.094	960
SCNT (10,0)	C2010H22	24164.286	108.576	21.858	2705.906	6010
SCNT (6,6)	C2100	25223.100	113.148	22.822	2701.464	6288
SCNT (28,0)	C5846	70291.912	314.016	62.889	2690.280	1098
DCNT (10,0)	C2282H58	29767.822	65.384	22.949	1322.735	1495
DCNT (6,6)	C2080H68	27148.064	61.193	21.367	1357.418	1454
TCNT (10,0)	C2146H130	28069.814	50.583	21.944	1085.212	2173
NR (6,6)	C2160H144	28266.192	92.495	23.584	1970.605	3204
SCNT (16,0)@C_{60}	C2108H32	27415.828	109.455	22.416	2404.270	1091
MG	C2046H126	26763.882	124.221	23.031	2795.087	6012
BG	C2112H180	27677.568	77.180	22.648	1679.300	6156

**= more details in Figure 2.2.*

Among the selected descriptors, M_W usually describes the size of a molecule. *SDeg* as a molecular descriptor of topology is the sum of degrees of every atom, and an atom's degree is the number of nonhydrogen atoms to which it is bonded. Moreover, *SSA* and *OSA* are known to be associated with the steric structures of NPs. Note that surface properties such as surface area generally dominate the behavior (Yang and Xing, 2010) and effects (Mottier et al., 2016) of CNPs. Taken together, the selected nano-specific descriptors not only are easy to obtain, but also can explain the interaction mechanism.

Fullerenes:

$$E_{\text{int}} = -32.241 - 0.021 \cdot SSA \qquad (2.2)$$

n = 7, R^2 = 0.804, RMSE = 0.485, Q^2_{CUM} = 0.737.

CNTs and graphenes:

$$E_{\text{int}} = -309.469 - 0.742 \cdot OSA + 0.039 \cdot SDeg \qquad (2.3)$$

n = 10, R^2 = 0.849, RMSE = 0.440, Q^2_{CUM} = 0.681.

Fullerenes, CNTs, and graphenes:

$$E_{\text{int}} = -110.679 - 0.007 \cdot Mw + 0.020 \cdot SDeg \qquad (2.4)$$

n = 17, R^2 = 0.804, RMSE = 0.473, Q^2_{CUM} = 0.710.

where n stands for the number of CNPs, R^2 is squared regression coefficient, *RMSE* is root mean squared error, and Q^2_{CUM} is the cumulative percentage of variance explained for extracted components. The values of Q^2_{CUM} of the models are higher than 0.5, suggesting the good robustness and internal predictability of the models and the models thus have high goodness-of-fit.

To further ensure the reliability of the obtained models, randomization tests were carried out by generating a fake pool of data for the E_{int} values derived from the total potential energies (Appendix Table S2.2). The E_{int} values were scrambled in two ways, namely a single sample one and a full one, to generate the pseudo-random numbers. As shown in Appendix Table S2.2, all the OPLS models obtained with the scrambled data exhibited non-competitive R^2 and Q^2_{CUM} values, as comparison to the three models provided in Equations 2.2–2.4. Thus, it is clear that the developed models are reliable and grasp the most significant information used to interpret the interactions of CNPs with the SARS-CoV-2 RNA fragment. The outcome of the randomization testing also shows that the nano-specific descriptors are relevant.

2.3.3 Implications of nano-QSAR based approaches in battling coronaviruses

A virus can be regarded as a nanoscale particle consisting of outer-capsid proteins and inner-core nucleic acids (RNA or DNA). ENMs can not only directly interact with viral particles including the envelope protein and the nucleic acids, but they can also competitively bind with the cell receptors. As aforementioned, CNPs can interact with the SARS-CoV-2 RNA fragment and stabilize it. Knowing the interaction affinity between ENMs and virus particles is important for accurately inferring the efficacy of antiviral nano-agents, which can be applied to disrupt the viral replication cycle (Y. Chen et al., 2020) and even directly to destroy its structure.

The SARS-CoV-2 RNA has been detected in environmental media (Al Huraimel et al., 2020; Kitajima et al., 2020; Mohan et al., 2021;

Morawska and Cao, 2020), which causes the novel coronavirus to become an environmental pollutant especially in air, in sewage (e.g., via the stool of contaminated patients) and in watersheds. It is known that ENMs, especially carbon-based nanomaterials, are widely utilized in the adsorption and separation of environmental pollutants because of their strong adsorption capacity and high adsorption efficiency (Ji et al., 2013; Pan and Xing, 2008; Wang et al., 2017; Yang and Xing, 2010). It is reported that the SARS-CoV-2 RNA is likely to persist for a long time in untreated wastewater (Ahmed et al., 2020). Hence, it is important to elucidate the interactions of the CNPs with the SARS-CoV-2 RNA fragment. Besides, the knowledge of these interactions can deepen and expand related research in other nanotechnology-based applications, e.g., disinfectants for personal protective equipment and sensors for SARS-CoV-2 detection.

All human beta-coronaviruses share a certain degree of genetic and structural homology (Shin et al., 2020). As reported, the SARS-CoV-2 genome sequence homology with SARS-CoV and MERS-CoV is 77 % and 50 %, respectively (Kim et al., 2020). Hence, the nano-QSAR models developed for SARS-CoV-2 in the present study are likely to be suitable for forecasting the interactions between the CNPs and other beta-coronaviruses. Furthermore, we advocate to keep the modeling as simple as it can be, and to filter those molecular descriptors which are easy to obtain and are related to antimicrobial (physical) properties. In the face of the urgency of the COVID-19 pandemic, nano-QSAR is a useful tool to investigate the impacts of nanotechnology on the novel coronavirus, and it has the advantages of preliminary screening of effective ENMs that will save valuable research time — the step towards validating the models by means of

experimental research can be started and done faster in a justified way. Eventually this may lead to saving efforts and preventing infection during experimental testing.

Nanomaterials entered the consumer market around 2000, meaning that by now nanoparticles are used in many products. For instance, within toothpaste titanium dioxide nanoparticles can be found as well as in creams to whiten products (Braakhuis et al., 2021; Rompelberg et al., 2016), and silver nanoparticles are used within many cosmetics like anti-aging creams (Kaul et al., 2018). The use of carbon-based nanomaterials for antiviral purposes is not so far off (Patel et al., 2019), and the virus killing activity of differently shaped carbon-based nanomaterials is intensively discussed (Innocenzi and Stagi, 2020; Serrano-Aroca et al., 2021). Serrano-Aroca et al. (2021) concluded that carbon-based nanomaterials had antiviral activity against 13 enveloped positive-sense single stranded RNA viruses, including SARS-CoV-2. It has been shown that the toxicity of nanomaterials is difficult to unravel, the antimicrobial activity of the nanoparticles depends on their composition, surface modification, intrinsic properties (Innocenzi and Stagi, 2020). Especially for unwanted toxicity, rigid high aspect ratio carbon fibers might be an issue in this respect that need to be dived furth into. Nonetheless, the use of carbon-based biocompatible nanomaterials as antivirals is still an almost unexplored field, while the published results show promising prospects.

2.4 Conclusions

To sum up, through molecular mechanics simulations, we have mainly addressed the molecular interactions between CNPs and the

SARS-CoV-2 RNA fragment. The estimated E_{int} suggests that the electrostatic interaction could be the predominant driving force for the interactions. The models on E_{int} developed by OPLS show high goodness-of-fit and robustness. Four nanostructural descriptors (M_W, *SSA*, *OSA*, and *SDeg*) were found to be the decisive factors controlling E_{int}.

Acknowledgements

This article pays tribute to those who are fighting against COVID-19. This work was supported by the National Natural Science Foundation of China (31971522) to Zhuang Wang and the European Union's Horizon 2020 research and innovation program "NanoinformaTIX" (814426) that supported Willie J.G.M. Peijnenburg and Martina G. Vijver. Fan Zhang greatly acknowledges the support from the China Scholarship Council (202008320308). We also thank the reviewers for their valuable comments on the manuscript.

Chapter 3

Theoretical Investigation on the Interactions of Microplastics with a SARS-CoV-2 RNA Fragment and Their Potential Impacts on Viral Transport and Exposure

Fan Zhang, Zhuang Wang, Martina G. Vijver and
Willie J.G.M. Peijnenburg

Published in Science of the Total Environment 842 (2022), 156812.

Abstract

The severe acute respiratory syndrome coronavirus 2 (SARS-CoV-2) causes the coronavirus disease-19 (COVID-19) pandemic spread across the world and remains difficult to control. Environmental pollution and habitat conditions do facilitate SARS-CoV-2 transmission as well as increase the risk of exposure to SARS-CoV-2. The coexistence of microplastics (MPs) with SARS-CoV-2 affects the viral behavior in the indoor and outdoor environment, and it is essential to study the interactions between MPs and SARS-CoV-2 because they both are ubiquitously present in our environment. To determine the mechanisms underlying the impact of MPs on SARS-CoV-2, we used molecular dynamic simulations to investigate the molecular interactions between five MPs and a SARS-CoV-2 RNA fragment at temperatures ranging from 223 to 310 K in vacuum and in water. We furthermore compared the interactions of MPs and SARS-CoV-2 RNA fragment to the performance of SARS-CoV-1 and Hepatitis B virus (HBV) RNA fragments in interacting with the MPs. The interaction affinity between the MPs and the SARS-CoV-2 RNA fragment was found to be greater than the affinity between the MPs and the SARS-CoV-1 or HBV RNA fragments, independent of the environmental media, temperature, and type of MPs. The mechanisms of the interaction between the MPs and the SARS-CoV-2 RNA fragment involved electrostatic and hydrophobic processes, and the interaction affinity was associated with the inherent structural parameters (i.e., molecular volume, polar surface area, and molecular topological index) of the MPs monomers. Although the evidence on the infectious potential of SARS-CoV-2 RNA is not fully understood, humans are exposed to MPs via their lungs, and the strong

interaction with the gene materials of SARS-CoV-2 likely affects the exposure of humans to SARS-CoV-2.

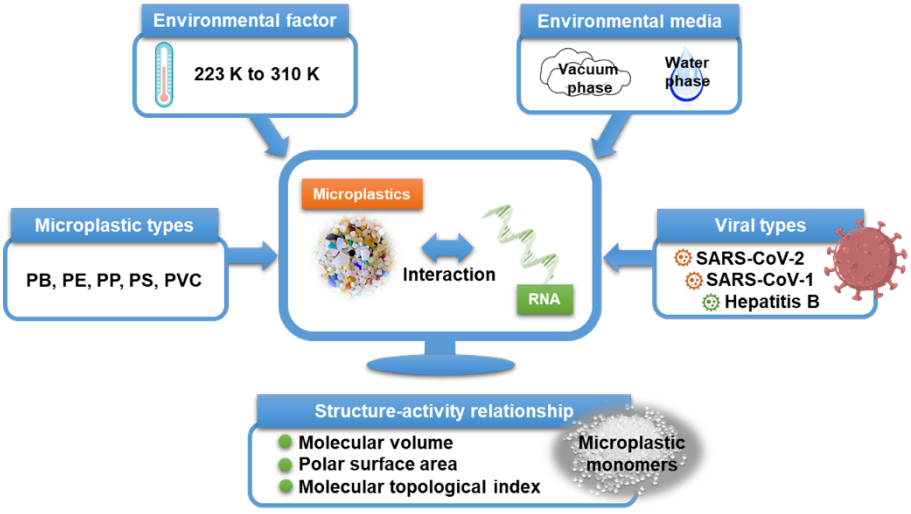

Graphical abstract

Keywords: Microplastic pollution; SARS-CoV-2; Nucleic acid material; Behavior and fate; Environmental conditions.

3.1 Introduction

The global pandemic of the coronavirus disease-19 (COVID-19) has suddenly made us realize that viruses have become important biological pollutants. The outbreak of the severe acute respiratory syndrome coronavirus 2 (SARS-CoV-2) not only seriously threatens human health (Topol, 2020; Turner et al., 2021), but also greatly increases environmental stress (Adelodun et al., 2021a, 2021b; Bedrosian et al., 2021). It is thus essential to understand the environmental fate and the behavioral dynamics of the coronavirus. The SARS-CoV-2 can travel in all environmental compartments like water (Navarro et al., 2021; Sala-Comorera et al., 2021), air (Dubey et al., 2021; Razzini et al., 2020), and soil (Anand et al., 2021; Steffan et al., 2020). A nucleic acid material (DNA or RNA) enclosed in a nucleocapsid protein is referred to as the non-enveloped structure of a virus particle (Müller et al., 2019). This is in contrast to the enveloped structure of a virus particle which contains a biological membrane. An envelope increases viral sensitivity to external physical stressors (pH, heat, dryness, etc.) as biological membranes are relatively fragile structures. Consequently, the SARS-CoV-2 as an enveloped virus is more sensitive to environmental factors than non-enveloped viruses (Achak et al., 2021). Thus, it is reasonable to believe that the non-enveloped structural materials of the SARS-CoV-2 could be more resistant to these inactivation factors and are likely to maintain their stability for a long time. Furthermore, studies on the nucleic acid material of SARS-CoV-2 are used for its detection and control in the environment and even for the implementation of personal health prevention measures.

Microplastics (MPs, i.e. particle sizes < 5 mm) are one of the most common and persistent emerging human-made pollutants. MPs are widespread in a ubiquitous fashion (Sheng et al., 2021), like they are detected in coastal waters (Roscher et al., 2021), freshwater and sediment (Q. Zhang et al., 2021), influents and effluents of sewage treatments (Nakao et al., 2021), agricultural soils (Boughattas et al., 2021), the atmosphere (Amato-Lourenço et al., 2020), and biosphere (Patil et al., 2022; Rezania et al., 2018).

The plethora of sources that can contribute to the release of MPs into air have been summarized in (Catarino et al., 2018; UNEP, 2016). In addition, the main sources of indoor and outdoor plastic debris released into the air and subject to human inhalation are illustrated by Amato-Lourenço et al. (2020). The indoor concentrations ranged between 1.0 and 60.0 fibers/m^3 whereas outdoor concentrations were significantly lower as they range between 0.3 and 1.5 fibers/m^3 (Dris et al., 2017). This is important to quantify and realize, because MPs have been reported as carriers or vectors for concurrent pollutants, e.g., metals (R. Li et al., 2021), organic pollutants (Yu et al., 2021), and they exhibit diverse interactive effects (Bhagat et al., 2021; Kim et al., 2017; Sun et al., 2021). In addition, MPs are becoming a novel ecological habitat termed the plastisphere (Zettler et al., 2013), and could facilitate the survival and dissemination of bacterial and fungal pathogens (Moresco et al., 2021), and antibiotic resistance genes (R. Li et al., 2021). Importantly, plastic pollution could be a secondary pathway for the transmission of human pathogenic viruses (Moresco et al., 2021) via the respiratory exposure route. We focus here on the MPs–SARS-CoV-2 interactions because both the virus as well as the sources of MPs (like fibers from clothes, building materials,

household objects, polymer fragments in urban dust) are closely correlated to the presence of human. It was also reported that SARS-CoV-2 remains more stable on plastic surfaces than on stainless steel, glass, and ceramics (Gidari et al., 2021) which has its consequences for the oral and hand contact exposure routes for humans. Amato-Lourenço et al. (2022) found that SARS-CoV-2 aerosols may bind to total suspended particles, such as MPs, and facilitate virus entry into the human body. Moreover, SARS-CoV-2 virus particles have the ability to sorb to the surface of MPs released during washing processes (Belišová et al., 2022). Hence, there is an urgent need to further explore the interactions and mechanisms of MPs and SARS-CoV-2.

Virus stability in the environment is strongly influenced by the size and structure of the virus particle (including the presence or absence of an envelope), the type of genome (DNA or RNA), a transmission route such as faecal-oral and air droplets, the presence of vectors or carriers like the MPs, and the viral concentration of the contamination source. As known, the intrinsic properties such as polymer type of MPs dictate their interaction affinity with other co-contaminants (Fred-Ahmadu et al., 2020; Menéndez-Pedriza and Jaumot, 2020). Besides, many environmental factors can affect the stability of viruses in the environment (Aboubakr et al., 2021; Achak et al., 2021; Paul et al., 2021), in humans (Matson et al., 2020), and on common touch surfaces (Aboubakr et al., 2021). Notably, temperature (Paul et al., 2021) and relative humidity (Zhao et al., 2020) are the two critical factors that determine the fate and transport of coronaviruses given certain environmental conditions.

Therefore, searching for some key characteristics that may affect the interaction of the MPs and SARS-CoV-2 is a noteworthy issue.

In silico methods are a promising approach and play a significant role in elucidating the mechanisms of the interactions of pollutants and biomacromolecules (Chen et al., 2019; Ge et al., 2011). In particular, the molecular simulation method such as molecular dynamics (MD) simulation is a practical *in silico* method in environmental applications (Chen et al., 2021; Feng et al., 2022; Sun et al., 2013). In addition, the molecular simulation method has shown to be an effective tool in exploring the interactions between MPs and SARS-CoV-2, and offered theoretical insights into the adsorption/separation and inactivation of carbon nanoparticles with a SARS-CoV-2 RNA fragments (F. Zhang et al., 2021a). This way *in silico* methods can not only contribute to minimizing the challenge of time-consuming and labor-intensive virus experiments under high risks of infection, but also to meeting our precautionary demand for options to handle any new versions of the coronavirus that might emerge in the future.

In light of the demands from the exploration of the interaction and mechanism between MPs and SARS-CoV-2, this knowledge gap needs to be addressed. Hence, in this work for the first time MPs were studied theoretically by MD simulation to characterize their interactions with the non-enveloped structural materials of SARS-CoV-2 including a nucleocapsid protein and a SARS-CoV-2 RNA fragment in the water phase and in the vacuum phase (as a reference for the water phase and as an approximation to the gas phase). Two reference viruses, namely SARS-CoV-1 (homologous coronavirus similar to SARS-CoV-2) and Hepatitis B virus (HBV,

non-coronavirus dissimilar to SARS-CoV-2) were selected to compare the performance in interacting with MPs. The influence of five different MP types and the temperature as an environmental factor is considered. The objectives of this study were divided in several parts: 1) Comparison of the interactions of the MPs with the nucleocapsid protein and with the viral RNA fragments; 2) Interaction mechanisms between the MPs and viral RNA fragments; and 3) Correlation of the interaction affinity and molecular parameters of MP monomers.

3.2 Computational methods

3.2.1 MD simulation

The selected three-dimensional structure models of the SARS-CoV-2 RNA fragment determined by K. Zhang et al. (2021), the SARS-CoV-1 RNA fragment determined by Robertson et al. (2004), and the HBV RNA fragment determined by LeBlanc et al. (2022) were used as model compounds for the simulation of the interactions between MPs and the viral RNA fragments. It should be noted that the SARS-CoV-2 RNA fragment is a model molecule of a frameshift stimulation element (FSE) from the SARS-CoV-2 RNA genome (K. Zhang et al., 2021). The FSE plays an important role in the virus replication cycle and has emerged as a major drug target (Lan et al., 2022). The selected three-dimensional structure models of the SARS-CoV-2 nucleocapsid protein determined by Kang et al. (2020), the SARS-CoV-1 nucleocapsid protein determined by Huang et al. (2004), and the HBV nucleocapsid protein determined by Böttcher and Nassal (2018) were used as model compounds for the simulation of the interactions between MPs and the viral nucleocapsid protein. The structures of the RNA fragments [PDB ID: 6XRZ (SARS-CoV-2),

1XJR (SARS-CoV-1), 6VAR (HBV)] and nucleocapsid proteins [(PDB ID: 6M3M (SARS-CoV-2), 1SSK (SARS-CoV-1), 6HU7 (HBV)] were obtained from the RCSB Protein Data Bank (Burley et al., 2019).

The polymer chains derived from five plastic monomers were built as model compounds for MPs including polybutene (PB), polyethylene (PE), polypropylene (PP), polystyrene (PS), and polyvinyl chloride (PVC) within the simulation. All the simulations were carried out in a box with three-dimensional boundary conditions. The dimensions of the simulation boxes were a = b = c = 85 Å, a = b = c = 90°. The length of the simulation box in each direction was large enough to enable the interactions between the MP polymer chain and the materials of the viruses. The process of building the MP models refers to the simulation methods developed by Guo et al. (2019) with slight modifications. The MP polymer chains were built and energy minimized using the smart geometry optimization algorithm, which is the combination of steepest descent, conjugate gradient, and quasi-Newton geometry optimization algorithms. Then the optimized polymer chain was randomly packed in rectangular boxes with three-dimensional periodic boundary conditions by Amorphous Cell Construction. For each box, only one polymer chain was added. The amount of PB, PE, PP, PS, and PVC monomer molecules were 200, 600, 500, 200, and 600. The MP-virus systems included one polymer chain, one RNA fragment or one nucleocapsid protein, and either a vacuum layer (83 Å) or a water layer (83 Å). For the water system, 1000 water molecules were incorporated in each unit cell. The smart geometry optimization algorithm was used to minimize the energy of the simulation systems. Then the MD calculations were performed in the canonical ensemble NVT system in which the number of

molecules [N], volume [V], and temperature [T] of the system are kept constant at 223, 263, 273, 298, and 310 K. These temperatures represent the range from a low-temperature environment to the temperature of the human body. The universal force field was adopted in the simulation framework. The van der Waals interaction cut-off was 12.5 Å, and the Ewald method (accuracy 0.001 kcal/mol) was used. The simulation was performed for 100 ps which allowed the studied system to reach equilibrium, and each step was 1.0 fs. A Nose thermostat was adopted. All the simulations were performed with the Materials Studio software package (ver. 8.0).

3.2.2 Interaction energy

For the interaction systems, the magnitude of the interaction energy (E_{int}) is an indication of the magnitude of the driving force towards complexation. A negative value reflects stable adsorption on the plastisphere. E_{int} was calculated by

$$E_{\text{int}} = E_{\text{MP-virus}} - E_{\text{MP}} - E_{\text{virus}} \qquad (3.1)$$

where $E_{\text{MP-virus}}$, E_{MP}, and E_{virus} represent the energies of the complex, the isolated MPs, and the viral RNA fragment or nucleocapsid protein, respectively.

3.2.3 Molecular parameters and linear correlation models

The MP monomers' molecular parameters (Appendix Table S3.1) such as volume of molecule (V_M), polar surface area (PSA), and molecular topological index (MTI) were selected to correlate with E_{int} so as to develop a quantitative relationship between the inherent properties of MPs and E_{int}. The molecular parameters were calculated using Multiwfn 3.8 software (Lu and Chen, 2012a, 2012b).

Correlation of interaction affinity and molecular parameters of the MP monomers was described using a polynomial relationship by performing linear regression models in Sigma Plot, ver. 14.0 (Systat Software Inc., San Jose, CA).

3.2.4 Statistical analysis

Statistically significant differences between test groups were determined by independent *t*-test and one-way analysis of variance with the Waller-Duncan test post hoc, at a significance level of $p < 0.05$ (IBM SPSS Statistics for Windows, ver. 23.0, IBM Corp., Armonk, NY). Linear regression analysis at the significant level of $p < 0.05$ was carried out using the SPSS.

3.3 Results

3.3.1 Comparison of interactions of MPs with viral nucleocapsid protein and RNA fragments

To fully understand the interactions between the MPs and the non-enveloped structures of the virus, the interactions of the MPs with the nucleocapsid protein and with the viral RNA fragments were compared after geometry optimization (Figure 3.1). As shown in Figure 3.1A, for the SARS-CoV-2, the absolute E_{int} values between the MPs and the nucleocapsid protein were significantly lower ($p < 0.05$) than those between the MPs and the RNA fragment. In contrast, for the HBV (Figure 3.1C), the absolute E_{int} values between the MPs and the nucleocapsid proteins were significantly higher ($p < 0.05$) than those between the MPs and the RNA fragments. For the SARS-CoV-1 (Figure 3.1B), the absolute E_{int} values between the MPs and the nucleocapsid proteins were higher than the corresponding values

between the MPs and the RNA fragments, but the two groups showed no significant difference ($p > 0.05$). Moreover, there was no significant difference in the absolute E_{int} values between the interactions of the MPs with the nucleocapsid proteins of the SARS-CoV-2 and the SARS-CoV-1. However, the absolute E_{int} values between the MPs and the nucleocapsid proteins of the HBV were significantly higher than those between the MPs and the nucleocapsid proteins of the SARS-CoV-2 or the SARS-CoV-1 ($p < 0.05$). In addition, the absolute E_{int} values between the MPs and the RNA fragments of the SARS-CoV-2 were significantly higher than those between the MPs and the nucleocapsid proteins of the SARS-CoV-1 or the HBV ($p < 0.05$). Moreover, no significant difference in the absolute E_{int} values between the interactions of the MPs with the RNA fragments of the SARS-CoV-1 and the HBV was found.

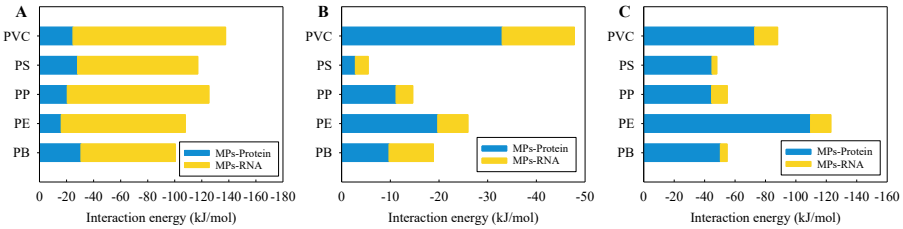

Figure 3.1. *Interaction energies of five types of MPs with the SARS-CoV-2 RNA fragment and the nucleocapsid protein (A), the SARS-CoV-1 RNA fragment and the nucleocapsid protein (B), as well as the HBV RNA fragment and the nucleocapsid protein (C), as obtained by geometry optimization.*

Generalizing, when comparing the nucleocapsid protein and the RNA fragment, then the MPs exhibited a stronger interaction with the RNA fragment for the SARS-CoV-2, while the MPs exhibited a stronger interaction with the nucleocapsid protein for the HBV. Furthermore, this difference in the interactions was not affected by the type of MP.

The plastic types were a bit more discriminative for SARS-CoV-1 and HBV compared to the SARS-CoV-2 that had interactions energies all similar for each type of MPs.

3.3.2 Interaction mechanisms between MPs and viral RNA fragments

To reveal the mechanisms of the interactions of the MPs with the viral RNA fragments, the values of E_{int} as derived from the total energy (E_t), the potential energy (E_p), the van der Waals energy (E_v), and the electrostatic energy (E_e) are summarized in Figure 3.2, Appendix Figures S3.1 and S3.2. As shown in Figure 3.2A and B, the computed E_{int} values were negative across most of the temperature range in vacuum and the full temperature range in water. This indicates that the MPs can form stable complexes with the SARS-CoV-2 RNA fragment. Furthermore, the computed E_{int} derived from the E_e between the MPs and the SARS-CoV-2 RNA fragment were generally closer to the E_{int} values derived from the E_t/E_p than the E_{int} values derived from the E_v in both vacuum and water. Moreover, there were no significant differences between the E_{int} values derived from the E_e and E_t/E_p ($p > 0.05$) in vacuum, but significant differences between the E_{int} values derived from the E_v and E_t/E_p ($p < 0.05$). This implies that the electrostatic interaction contributed mainly to the mechanism of interaction between the MPs and SARS-CoV-2 RNA fragment. The genetic material of the SARS-CoV-2 is positive single-stranded RNA (K. Zhang et al., 2021), whereas the studied MPs are neutral and the electrostatic interactions are mainly ion-induced dipole interactions.

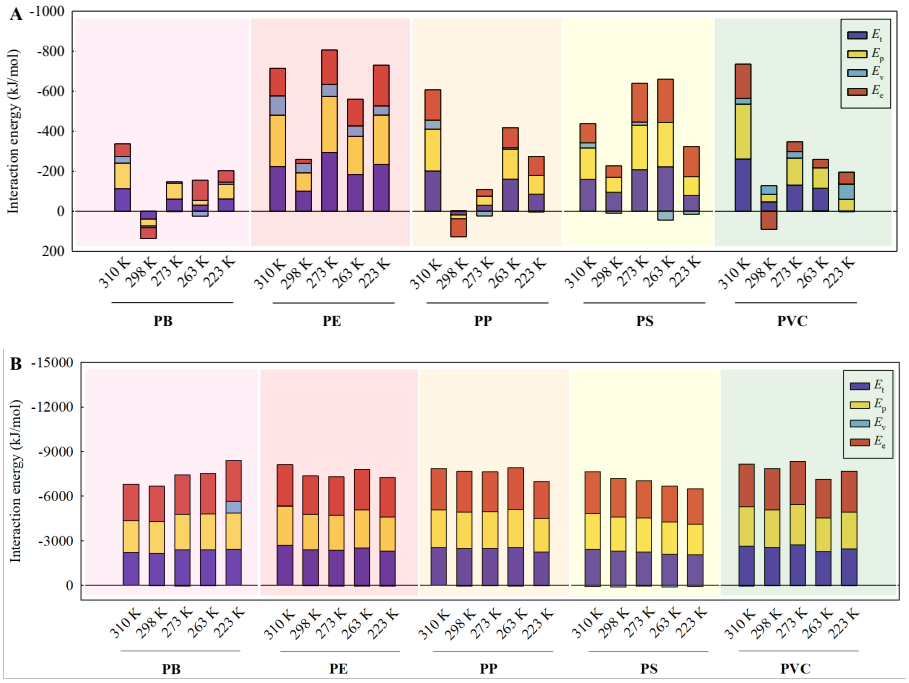

Figure 3.2. *Interaction energies of the five types of MPs with the SARS-CoV-2 RNA fragment in vacuum (A) and in water (B) at different temperatures.* E_t*: interaction energy derived from total energy,* E_p*: interaction energy derived from potential energy,* E_v*: interaction energy derived from van der Waals energy, and* E_e*: interaction energy derived from electrostatic energy.*

Moreover, the absolute E_{int} values derived from the E_t, E_p, or E_e for the interactions between the MPs and the SARS-CoV-2 RNA fragment (Figure 3.2B) in water were significantly greater than those in vacuum ($p < 0.05$) (Figure 3.2A), implying that the interaction affinity of the MPs with the SARS-CoV-2 RNA fragment in water was stronger compared with the affinity in vacuum. This may be caused by the hydrophobicity of MPs (Ding et al., 2020; J. Zhang et al., 2020), which can provide stronger interactions with the viral RNA fragment in water.

As depicted in the Appendix Figures S3.1 and S3.2, the E_{int} values derived from the E_t and E_p for the interaction between the MPs and the SARS-CoV-1 RNA or HBV RNA fragments in vacuum and water phases were significantly lower than those for the interaction between the MPs and SARS-CoV-2 RNA fragment ($p < 0.05$). This means that the MPs exhibited stronger interaction with the SARS-CoV-2 RNA fragment than with the SARS-CoV-1 RNA and the HBV RNA fragments. Moreover, most of the E_{int} values for the interaction between the MPs and the SARS-CoV-1 RNA fragment or the HBV RNA fragment tended to be positive. This implies that the complexes of the MPs with SARS-CoV-1 RNA fragment or HBV RNA fragment were instable. As a result, it is difficult to analysis the interaction mechanisms of the MPs and the SARS-CoV-1 RNA fragment or the HBV RNA fragment.

3.3.3 Correlation of interaction affinity and temperatures

To test the impact of the studied temperature on the interactions of the MPs with the viral RNA fragments, the variation of the interaction affinity with the temperatures was plotted (Figure 3.3, Appendix Figures S3.3 and S3.4). In general, for each of the MPs, the E_{int} values derived from the total energies fluctuated with the temperature. In particular, the E_{int} values between the MPs and SARS-CoV-2 RNA fragment tended to reach the highest value at 298 K in vacuum (Figure 3.3A), implying that the interaction affinity between the MPs and SARS-CoV-2 RNA fragment was lowest at 298 K. In water, the E_{int} values between the PS MPs and SARS-CoV-2 RNA fragment decreased with an increase of the temperature (Figure 3.3B). A similar phenomenon occurs in the interaction between the PS MPs and SARS-CoV-1 RNA fragment in water (Appendix Figure S3.3B). In

terms of considering the various types of MPs as a whole, the E_{int} values were not significantly different between the temperatures (Figure 3.3, Appendix Figures S3.3 and S3.4). This also means that temperature was not a determinative factor affecting the interaction affinity between the MPs and viral RNA fragments in the present simulation study.

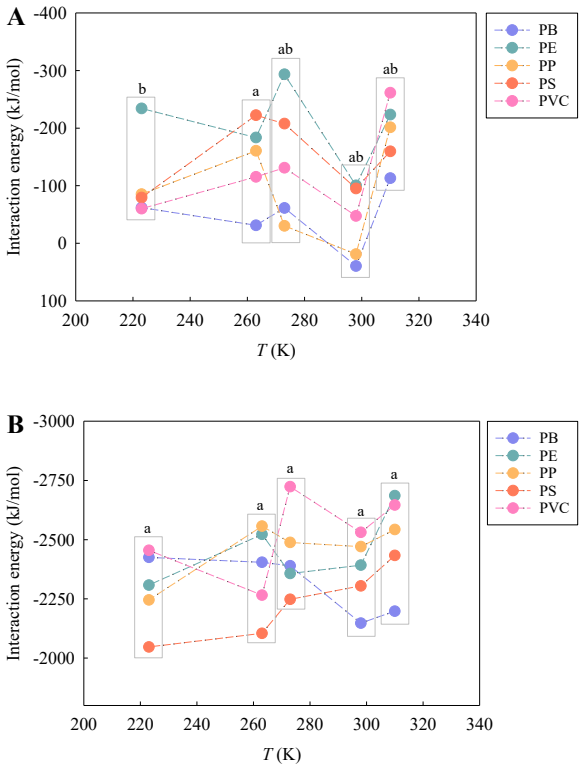

Figure 3.3. *Variation of the interaction energies derived from the total energies of the five types of MPs with the SARS-CoV-2 RNA fragment in vacuum (A) and in water (B) with the studied temperatures (223, 263, 273, 298, and 310 K). Different letters represent statistically significant differences between the treatments ($p < 0.05$).*

3.3.4 Correlation of interaction affinity and molecular parameters of MP monomers

To explore the impact of the inherent properties of MPs on their interactions with the viral RNA fragments, a correlation was conducted between the interaction affinity and molecular parameters of MP monomers (Table 3.1, Appendix Tables S3.2 and S3.3, and Figure 3.4).

Table 3.1. *Correlation coefficients between the E_{int} values derived from the total energies between the MPs and SARS-CoV-2 RNA fragment and the molecular parameters of the MP monomers*[a].

Correlation model	Temperature (K)	Volume (nm^3)		Polar surface area (nm^2)		Molecular topological index	
		$n = 5$	$n = 4$	$n = 5$	$n = 4$	$n = 5$	$n = 4$
E_{int} in vacuum	310	0.652	**0.839**	0.648	**0.821**	0.427	**0.892**
	298	0.068	**0.929**	0.063	**0.927**	0.399	**0.866**
	273	0.065	0.791	0.073	0.797	0.235	0.683
	263	0.203	**0.888**	0.194	**0.896**	0.502	**0.917**
	223	0.510	0.739	0.523	0.760	0.274	0.645
E_{int} in water	310	0.615	***0.959***	0.616	***0.959***	0.326	***0.989***
	298	0.535	0.704	0.530	0.704	0.346	**0.803**
	273	0.577	0.123	0.563	0.123	0.621	0.223
	263	0.749	0.171	0.756	0.171	**0.800**	0.168
	223	0.669	0.334	0.659	0.334	**0.817**	0.376

[a] *The correlation was tested for five types (n = 5) of MPs (PB, PE, PP, PS, and PVC)/four types (n = 4) of MPs (PB, PE, PP, and PVC) and the SARS-CoV-2 RNA fragment; The magnitude of correlation coefficient (R) reflects the degree of correlation between the E_{int} and molecular parameter values; The bold numbers indicate high values of the correlation coefficients (R > 0.800); The numbers marked in both bold and italic indicate a significant correlation at the 0.05 level (p < 0.05).*

As shown in Table 3.1, the E_{int} values derived from the total energies for the interaction of each of the MPs with the SARS-CoV-2 RNA fragment in vacuum and water phases correlated with the molecular parameters V_M, PSA, and MTI of the MP monomers to varying degree. The degree of correlation tended to be higher in vacuum and at 310

and 298 K in water except for the PS MPs with aromatic hydrocarbons. In particular, the E_{int} values correlated highly (Figure 3.4A–C) and significantly (Figure 3.4D–F) with the molecular parameters except for the PS MPs. On the whole, the greater the V_M, PSA, and MTI values, the stronger the interactions between the MPs and the SARS-CoV-2 RNA fragment (Figure 3.4).

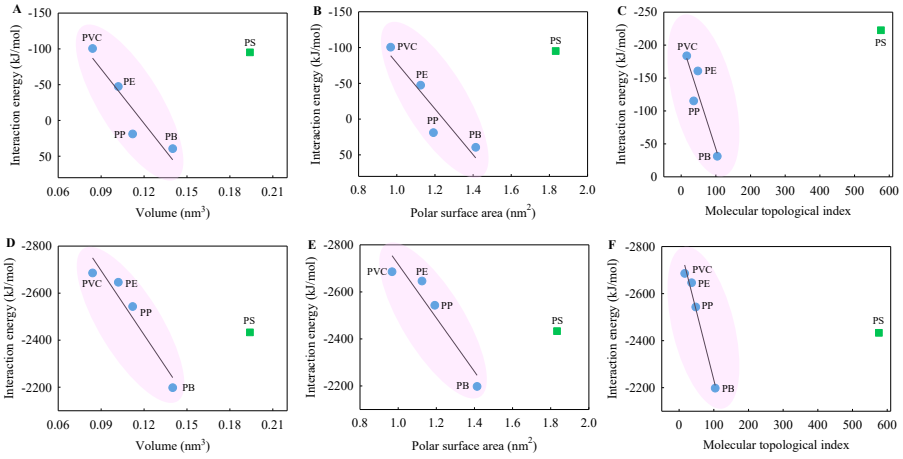

Figure 3.4. *Variation of the interaction energies derived from the total energies of the five types of MPs with the SARS-CoV-2 RNA fragment at 298 K (A and B) and 263 K (C) in vacuum and at 310 K (D, E, and F) in water with the molecular parameters of the MP monomers.*

Generally, the E_{int} values derived from the total energies for the interaction of the SARS-CoV-1 (Appendix Table S3.2) or the HBV (Appendix Table S3.3) RNA fragment with the MPs in vacuum and water phases correlated moderately or weakly with the molecular parameters V_M, PSA, and MTI of the MP monomers. It can be also found that there was a higher correlation between the E_{int} values for the interaction of the SARS-CoV-1 RNA fragment with the MPs and the molecular parameters of the MP monomers at 310 K in vacuum

except for the PS MPs. In addition, for the interaction of the MPs with the SARS-CoV-1 and the HBV RNA fragment, no significant correlation was found between the E_{int} values and the molecular parameters of the MP monomers.

3.4 Discussion

Owing to the high prevalence of both enteric and respiratory viruses in the population and the environment, there is significant potential for human viruses to become associated with the plastisphere (Moresco et al., 2021). There are many sources of MPs in the environment and potential pathways for the interaction, colonisation, and dissemination of viruses. We have studied the interaction between three different viruses and five different MPs in water and vacuum air. For these exposure routes we have taken different conditions; being different temperatures, and different coating of the virus. These coatings have been modelled theoretically how the genetic material such as the RNA of a virus is released into cells after the virus undergoes fusion. There, the RNA segments are covered with the nucleocapsid protein enabling to travel to specific organelles such as the ribosome.

The first pathway described is via the respiratory path: MPs can enter the human body through breathing, mainly due to the presence of MP pollution in the air (Amato-Lourenço et al., 2020); indoor dust as well as air in cities were shown to be large contributors. So not only the virus and MPs dose will be higher indoors, also interaction effectivity is large. It makes it a large potential exposure route for humans. It has been proven that face masks can release large numbers of MPs, which were detected in nasal mucus of mask

wearers and can be inhaled by human beings (Ma et al., 2021). In a way face masks are preventing inhalation of virus for human not infected, but those infected may even breathe the virus out. It is speculated that the virus can bind to MPs from the mask and human beings inhale them again as an agglomerate.

Second, the SARS-CoV-2 is transmitted primarily through respiratory droplets (Stadnytskyi et al., 2020) and/or aerosols (Yuan Liu et al., 2020). Airborne dust is another transmission route linked to infectious diseases (Maestre et al., 2021; Moreno et al., 2021). More severe weather phenomena such as sandstorms may exacerbate the migration of the virus (Meo et al., 2021). The adsorption of the SARS-CoV-2 on these airborne media can contribute to the long-range transport of the virus. Note that the airborne transmission route refers to the presence of particles with diameter < 5 μm, who can remain in the air for long periods (Morawska and Cao, 2020). The particle sizes of the MPs are also in this scale range. Thus, MPs dispersed in air can be inhaled by humans (Amato-Lourenço et al., 2020). The MPs can be released into the atmospheric air via several sources, e.g., synthetic textiles (G. Chen et al., 2020), tire wear particles (Lee et al., 2020), domestic laundry dryers (O'Brien et al., 2020), etc. Hence, there is a high probability that the MPs and the SARS-CoV-2 will meet in the atmospheric environment. It has been reported that SARS-CoV-2 aerosols may bind to MPs and facilitate virus entry into the human body (Amato-Lourenço et al., 2022). Our results show that the MPs stabilized the SARS-CoV-2 RNA fragment in both vacuum and water. This also means that the MPs could act as a carrier capable of carrying the gene materials of the SARS-CoV-2 and become a new airborne media for the transport of the virus.

Third, a non-droplet transmission is also possible, as the infectious SARS-CoV-2 particles are also present in human excretions (Wiktorczyk-Kapischke et al., 2021). The fragment of the SARS-CoV-2 RNA has been frequently detected in various countries in wastewater (M. Kumar et al., 2020; La Rosa et al., 2020; Randazzo et al., 2020), particularly hospital effluent (Gonçalves et al., 2021). The transmission of SARS-CoV-2 via the fecal-oral route highlights the presence and persistence of SARS-CoV-2 in the aquatic environment (Arslan et al., 2020). Moreover, the SARS-CoV-2 RNA is relatively stable in sewage and non-chlorinated drinking water (Ahmed et al., 2020). The viral RNA was also found to be relatively stable in contrast to the rapid inactivation of infectious SARS-CoV-2 in river and in sea water (Sala-Comorera et al., 2021). The COVID-19 pandemic has a huge impact on the plastic waste management in many countries, in large due to the sudden surge of medical waste which has led to a potential significant release of MPs (Khoo et al., 2021). Recent studies indicated that MPs have a significant abundance in sewage. Therefore, the sewage treatment system may be an important site for the interaction between the MPs and the gene materials of SARS-CoV-2. Belišová et al. (2022) also confirmed the ability of SARS-CoV-2 virus particles to sorb to the surface of MPs, specifically microfibers in wastewater. The present results implied that the MPs stabilized the SARS-CoV-2 RNA fragment in the water phase, regardless of temperature and MP types. Additionally, the persistence of the SARS-CoV-2 RNA fragment when present on the MPs was different from the persistence of the SARS-CoV-1 and HBV RNA fragments. In comparison, the SARS-CoV-2 RNA fragment preferred to maintain on the MPs, which may cause the gene materials of the SARS-CoV-2 to be long lasting on the MPs.

The fourth path is via the oral route such as food and water. The results in Figure 3.2 also indicated that the interaction affinity of the MPs with the SARS-CoV-2 RNA fragment in water was stronger compared with the affinity in vacuum by a factor of 10 at least. This means the MPs and viral genetic material may co-present in dairy products we eat. If the MPs are entered through the food chain (Bouwmeester et al., 2015; Mercogliano et al., 2020), the MPs enter cells via endocytosis and then are released into the cytoplasm. Particularly, the intestinal tract is the main place where MPs exist and is the channel into the circulatory system (Fournier et al., 2021; Visalli et al., 2021). In the meanwhile, it is confirmed that the SARS-CoV-2 can effectively infect intestinal epithelial cells and their precursors (Lamers et al., 2020), which reveals the fact that the intestinal tract is the potential infection site of the SARS-CoV-2 in humans. Taken together, an intercellular environment provides an opportunity for interaction between the MPs and the viral RNA segments/nucleocapsid protein. In our study, we revealed that the MPs showed stronger interaction with the SARS-CoV-2 RNA fragment than with its nucleocapsid protein. Comparison and analysis on the E_{int} also supported the finding that the MPs interacted with the SARS-CoV-2 RNA fragment more strongly than with the SARS-CoV-1 or HBV RNA fragments. This also means that the MPs are more apt to stabilize the genetic materials of the SARS-CoV-2 in the intercellular environment, whereas this interaction may limit the transcription and replication of the viral RNA genomes.

The fifth potential route is via inanimate surfaces such as plastic, stainless steel, and glass has been established (Corpet, 2021; Gidari et al., 2021) on which the persistence of the SARS-CoV-2 is detected.

For instance, Gidari et al. (2021) showed the ability of SARS-CoV-2 to persist on most common materials such as glass, stainless steel, and plastic with half-lives of 4.2, 4.4, and 5.3 h respectively. The SARS-CoV-2 is thus more stable on plastics than on steel or on glass. With the global outbreak and spread of COVID-19, disposable surgical masks as effective and cheap protective medical equipment have been widely used by the public. The random disposal of masks may result in new and greater MP pollution, because masks made of polymer materials would release MPs after entering the environment. More importantly, potential co-release of the MPs and the SARS-CoV-2 into the environment will be ineluctable. This might be expected as the result of the unreasonable disposal of the masks, especially the masks contaminated with the virus. MPs have been detected in the air. Thus, MPs can deposit upon the surface of various materials. Thus, there may be an opportunity for the interaction of MPs and the virus RNA. There is evidence that the SARS-CoV-2 RNA fragment has been detected on frozen food packaging (Han et al., 2021; Peipei Liu et al., 2020), and aquatic products can be a route of transmission of COVID-19. Positive detection of COVID-19 nucleic acid in the samples of frozen food packaging is still occurring. Our theoretical investigation also indicated that the MPs stabilized the SARS-CoV-2 RNA fragment at very low temperatures ranging from 273 to 223 K. The presence of the genetic material of SARS-CoV-2 on the surfaces is not the same as the presence of the infectious virus, but indicates the transit and contact of infected individuals (Casabianca et al., 2022). Therefore, theoretical evidence of interactions between the MPs and the SARS-CoV-2 RNA fragment could support practices (e.g., strict sanitization of medical equipment, supplies, fabrics, environmental surfaces, and air contaminated with

pathogens) that reduce the risk of SARS-CoV-2 infection and cut off its transmission route.

The plastisphere is a diverse microbial community of heterotrophs, autotrophs, predators, and symbionts (Zettler et al., 2013). Several studies demonstrated that the gene materials of microorganisms can be extracted from MPs and subsequently identified (Debeljak et al., 2017; Zettler et al., 2013). Regardless of environmental media and temperature, a stable binding between the MPs and the SARS-CoV-2 fragment was proven theoretically. After such a binding, the SARS-CoV-2 fragment is more difficult to degrade in the natural environment. This also means that entering the plastisphere appears to be an important process that significantly affects the global environmental fate of SARS-CoV-2.

SARS-CoV-2 belongs to the family of enveloped, single-strand RNA viruses (Mei and Tan, 2021). The viral membrane of SARS-CoV-2 surrounds a helical nucleocapsid in which the viral genome is encapsulated by the nucleocapsid protein (Savastano et al., 2020). The biological membrane, known as an envelope, contains lipids and proteins. An envelope may increase the viral sensitivity to physical influencing factors (pH, heat, dryness, etc.) as biological membranes are relatively fragile structures. The nucleocapsid protein of SARS-CoV-2 is produced at high levels within infected cells, enhances the efficiency of viral RNA transcription, and is essential for viral replication (Savastano et al., 2020). It is reported that the SARS-CoV-2 RNA is likely to persist for a long time in untreated wastewater (Ahmed et al., 2020). Consequently, it is essential to elucidate the interactions of the MPs with the nucleocapsid protein and SARS-CoV-2 RNA fragment. Further studies are warranted to

evaluate the interaction of the MPs with other structural proteins of SARS-CoV-2, e.g., spike, membrane, and envelope. Furthermore, the interactions as addressed in this study are the first stepping stone to meet our precautionary demand for options to handle any new versions of the coronavirus that might emerge in the future.

It was also found that there are differences in the interaction affinity between the MPs with different compositions and SARS-CoV-2 RNA fragment (Figures 3.1 and 3.2). Notably, the molecular parameters of the PS monomer performed very different in affecting the interaction affinity as compared to the other MP monomers (Figure 3.4). The benzene ring contained in PS allowed it to form π-π interactions with the SARS-CoV-2 RNA fragment that might modulate the interaction affinity. The differences in the composition of MPs are most directly reflected in the functional groups contained in their polymeric structural units. The properties of the MP monomer compounds can determine the mechanism of interaction of MPs with organic pollutants, which in turn exhibit a different interaction affinity for organic pollutants (Lee et al., 2014). In addition, changes in environmental conditions such as temperature can modulate the interaction between the MPs and SARS-CoV-2 RNA fragment (Figure 3.3). Other factors such as pH, salinity, and dissolved organic matter which may result in differences in the interaction can also not be neglected. Accordingly, the single and combined effects of different environmental factors on the interaction of the MPs and SARS-CoV-2 will need to be considered in subsequent studies.

It is undeniable that *in silico* methods still have limitations in both space and time scales, which weakens their correlation with experimental observations and available experimental data. Moreover,

quality assurance is required to minimize uncertainty in the calculation of toxicological data. In spite of this, in the face of the urgency of the COVID-19 pandemic, *in silico* methods are a useful tool to investigate the interaction of environmental pollutants such as MPs with the novel coronavirus, particularly the proposed methodologies that rely upon alternatives to biological testing with high risk of infection. Furthermore, *in silico* methods have the advantages of preliminary screening of high-risk combinations of multiple co-existing pollutants (e.g., SARS-CoV-2 and MPs) in the environment, and it will save valuable research time and efforts (e.g., model validation) as well as prevent infection during experimental testing.

3.5 Conclusions

In this work, we carried out MD simulations to investigate the interactions between five MPs and RNA fragments of three viruses including, SARS-CoV-2, SARS-CoV-1, and HBV at temperatures ranging from 223 to 310 K, in vacuum and in water phases. The estimated E_{int} implied that the interactions of the MPs with the SARS-CoV-2 RNA fragment were stronger than those with the SARS-CoV-1 and HBV RNA fragments, regardless of the environmental media, temperature, and MP types. Furthermore, the electrostatic and hydrophobic processes were the predominant mechanisms for the interactions between the MPs and the SARS-CoV-2 RNA fragment, and the interaction affinity was associated with the inherent structural parameters (i.e., V_M, PSA, and MTI) of the MP monomers. Our theoretical results suggest that MPs are capable of regulating the behavior and fate of the SARS-CoV-2 RNA fragment in the environment. While MPs are within air, food

and water, this plastic pollution could be a secondary pathway for the transmission of human pathogenic virus and hence have consequences for the exposure of humans to SARS-CoV-2, both by the respiratory pathway (enhancing potential exposure) and the touch pathway where the plastic surface binds the SARS-CoV-2 RNA fragment and thus lowers potential exposure and infectious risks for human. It should be noted that the SARS-CoV-2 RNA fragment can be immobilized by MPs which are ubiquitous in the human environments and thus their persistence and circulation would prolong the presence of virus RNA in the environment. This *in silico* work serves to minimize the challenges of conducting time-consuming and labor-intensive virus experiments with a high risk of infection, while meeting our precautionary need for options to deal with any new versions of coronaviruses that may emerge in the future.

Acknowledgements

This article pays tribute to those who are fighting COVID-19. This work was supported by the European Union's Horizon 2020 research and innovation program "NanoinformaTIX" (814426) that supported W.J.G.M.P. and M.G.V. and the National Natural Science Foundation of China (31971522) to Z.W. F.Z. greatly acknowledges the support from the China Scholarship Council (202008320308). We also thank the reviewers for their valuable comments on the manuscript.

Chapter 4

Review and Prospects on the Ecotoxicity of Mixtures of Nanoparticles and Hybrid Nanomaterials

Fan Zhang, Zhuang Wang, Willie J.G.M. Peijnenburg and Martina G. Vijver

Published in Environmental Science & Technology 56 (2022), 15238–15250.

Abstract

The rapid development of nanomaterials (NMs) and the emergence of new multicomponent NMs will inevitably lead to simultaneous exposure of organisms to multiple engineered nanoparticles (ENPs) at varying exposure levels. Understanding the joint impacts of multiple ENPs and predicting the toxicity of mixtures of ENPs are therefore evidently of importance. We reviewed the toxicity of mixtures of ENPs to a variety of different species, covering algae, bacteria, daphnia, fish, fungi, insects, and plants. Most studies used the independent-action (IA)-based model to assess the type of joint effects. Using co-occurrence networks, it was revealed that 53 % of the cases with specific joint response showed antagonistic, 25 % synergistic, and 22 % additive effects. The combination of nCuO and nZnO exhibited the strongest interactions in each type of joint interaction. Compared with other species, plants exposed to multiple ENPs were more likely to experience antagonistic effects. The main factors influencing the joint response type of the mixtures were 1) the chemical composition of individual components in mixtures, 2) the stability of suspensions of mixed ENPs, 3) the type and trophic level of the individual organisms tested, 4) the biological level of organization (population, communities, ecosystems), 5) the exposure concentrations and time, 6) the endpoint of toxicity, and 7) the abiotic field conditions (e.g., pH, ionic strength, natural organic matter). This knowledge is critical in developing efficient strategies for the assessment of the hazards induced by combined exposure to multiple ENPs in complex environments. In addition, this knowledge of the joint effects of multiple ENPs assists in the effective prediction of hybrid NMs.

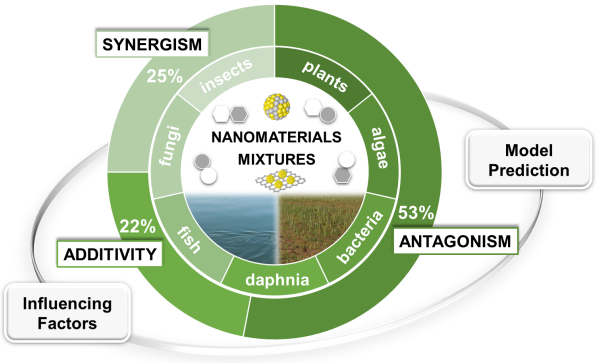

Graphical abstract

Keywords: Nanosafety; Mixture toxicity; Nanotechnology; Multicomponent nanomaterials; Independent joint action.

4.1 Introduction

Nanotechnology has undergone enormous developments recently (P. Kumar et al., 2020; Leonel et al., 2021; Lowry et al., 2019; Oksel Karakus et al., 2021). With the uninterrupted development of new emerging nanomaterials (NMs), engineered nanoparticles (ENPs) are becoming potential environmental pollutants (Stuart and Compton, 2015). Mixtures of ENPs can occur due to multiple single-component NMs entering an ecosystem (Wu et al., 2021). Mixtures of individual ENPs have been detected within municipal wastewater treatment systems (Georgantzopoulou et al., 2020; Musee et al., 2014; Simelane and Dlamini, 2019; Singh and Kumar, 2020; Sundaram and Kumar, 2017) and subsequently in the receiving waters and soils. Mixtures of individual ENPs may harm aquatic and terrestrial species (including humans) by coaccumulating in the food chain. Considering that multiple distinct ENPs may coexist in the same environmental compartments, it is critical to determine how mixtures of individual ENPs may affect environmental receptors. Additionally, multicomponent NMs, so-called hybrid or advanced NMs, are by definition a mixture but need to be distinguished from mixtures of individual ENPs. There currently is a clear trend of technological innovations moving toward the development of more complex advanced materials. However, limited information is available on the occurrence, fate, and toxicity of mixtures of NMs as well as for multicomponent NMs in the environment. It thus is imperative to perform studies that characterize the hazards of hybrid NMs at an early stage of their development, starting at the research phase. The knowledge built from mixtures of NMs can be used to get an estimate of the (magnitude of) quantification of the joint impacts of multiple

elements and particles. There is also an urgent need for extrapolating knowledge gained on individual ENPs toward hybrid NMs. This will minimize undesirable impacts on human and environmental health at later stages of development and production and will allow a conscious move toward sustainable nanotechnology and responsible innovation (Hutchison, 2016).

Assessing the joint impacts of chemicals is already notoriously difficult, and for ENPs this could be even more challenging. After all, the chemical composition and the particle characteristics need to be accounted for. Subsequently, the toxicity of NMs is inherently composed of the toxicity of the particle constituents as well as the particle-specific fate and toxicity. Analyzing the scattered experimental data on mixtures of ENPs will lead to a better understanding and will allow verification of whether conventional mixture models can be used to describe joint impacts of NMs (Li et al., 2020).

In this paper, we therefore addressed the following subresearch questions. 1) What joint interactions have been reported after exposure of a range of aquatic and terrestrial test species to multiple ENPs? 2) Which factors determine the toxicity of a mixture of multiple ENPs? 3) Is there a difference between the environmental behavior and fate of multiple ENPs compared to single ENPs and do such differences subsequently affect the induced ecotoxicological effects? 4) Which important knowledge gaps and further research needs have been identified in assessing mixture-nanoecotoxicology for experimentalists, computational modelers, risk assessors, and regulators? To address these scientific questions, we have collated information on the mixture toxicity of ENPs spanning trophic levels

as well as aquatic and terrestrial environments available in the literature. Herein, we focus on two types of multiple ENPs, namely mixtures of individual ENPs and hybrid NMs. Meanwhile, the nanohybrids of concern are mainly synthetic materials with organic or inorganic ENP components that are linked together by noncovalent bonds or covalent bonds at the nanometer scale. The strength of the joint interactions of multiple ENPs and the main factors influencing the joint response of the mixtures were identified for the first time in this work. Ultimately this knowledge constitutes the first building blocks that allow building a computational approach able to reduce the experimental costs of ecotoxicity testing of mixtures of ENPs of varying composition and to include both nanohybrids and mixtures of different ENPs.

4.2 Methods

Data were mined from peer-reviewed articles as published between 2003 and 2022, making use of the search machines Web of Science and PubMed (last access date March 10th, 2022). The inclusion criteria were as follows: (Toxicity OR Ecotoxicity) AND (Nanomaterial* OR Nanoparticle* OR Nanoplastic*) AND (Mixture* OR hybrid) AND (Alga* OR Bacteria* OR Daphnia OR Fish OR Insect* OR Plant*).

On the basis of these search terms, we obtained 1263 publications and removed duplicate papers as well as those in which the title, abstract, or text was not related to the toxicity of mixtures of NMs to ecological species (e.g., papers on microsized plastic particles). A final total of 86 papers were filtered and extracted for future reviewing, as shown in the Appendix Figure S4.1.

Data were collected for representative ecological species (algae, bacteria, daphnia, fish, fungi, insects, and plants). Binary and ternary ENP toxicity data reported from laboratory-derived studies were collected, as well as effect data on nanohybrids. The types of joint interactions (additive, synergistic, and antagonistic) of the mixtures of ENPs given in the original literature were extracted from the eligible papers. The mixtures induced additive effects or deviated from additivity, either by synergistic (toxicity of the mixture higher than the summed toxicity of the individual ENPs) or antagonistic (toxicity of the mixture lower than the summed toxicity of the individual ENPs) mixture toxicity.

In the selected papers, three common concepts enabling to assess mixture toxicity — concentration addition (CA), independent action (IA), and toxic unit (TU) — were used. In addition to assessing the impacts of the mixtures, the abiotic conditions expected to influence toxicity and information on the existing predictive methods for evaluating the mixture toxicity were collected as well.

Following the evaluation of the first 86 papers, an association rule analysis (which is a technique to uncover how items are associated with each other) was performed to mine the literature data. Calculated networks based on co-occurrence explain which combination of NMs has been most studied, which combination of NMs is more likely to have an additive, synergistic, or antagonistic effect, which species are more sensitive to additive, synergistic, or antagonistic effects, and which method is commonly used in assessing the joint toxicity of multi-ENP mixtures. The association rule analysis was performed using the Apriori algorithm in the

classification of association rule in IBM SPSS Modeler (ver. 18.0) and was further visualized using Cytoscape (ver. 3.9.0).

4.3 Results and discussion

4.3.1 Types of joint interactions of multiple ENPs

The data in the Appendix Tables S4.1 and S4.2 illustrate the different combination types of individual ENPs, ecological species, test concentrations and mixture ratios, endpoints, and intentions in joint action analyses of mixtures. Figure 4.1A depicts a network that connects ENPs in different combinations on the basis of the data gathered from the literature (Appendix Tables S4.1 and S4.2).

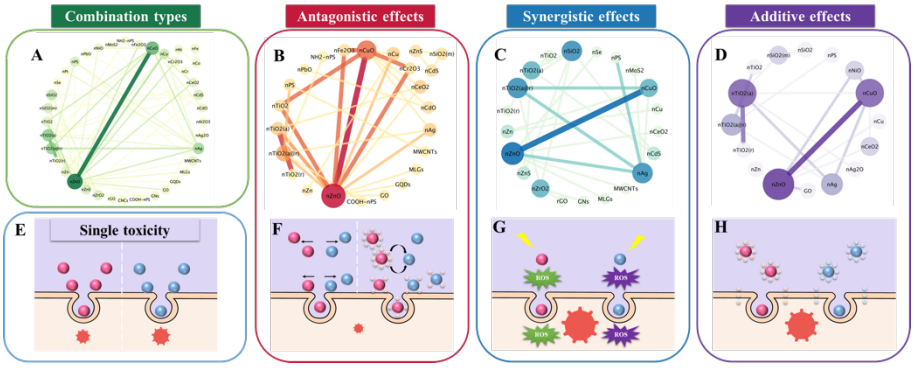

Figure 4.1. *Co-occurrence network showing the correlations between different ENPs (**A**, **B**, **C**, and **D**) and illustration of the main mechanisms of single toxicity (**E**) and joint interactions (**F**: antagonism; **G**: synergism; **H**: additivity) of mixtures of individual ENPs.*

The binary mixture of nCuO and nZnO is the most studied combination in the available reports, as indicated in Figure 4.1A. As is known, nCuO and nZnO are among the most produced and commonly used ENPs (Muhammad et al., 2022). In addition, frequently studied combinations are $nTiO_2$ (anatase) + $nTiO_2$ (rutile)

and nCu + nZnO in order of preference. Generally, at the current stage, studies have mainly focused on examining the toxicity of mixtures of metal-based ENPs (75 % of all combinations).

Figure 4.1B–D depicts a network that connects ENPs in different types of joint interactions, on the basis of the data gathered from the literature (Appendix Tables S4.1 and S4.2). In all combinations with a known joint response, 53 % of the interactions induced antagonistic effects, 25 % of the interactions induced synergistic effects, and 22 % of the interactions were additive. In addition, note that the same combinations such as nCuO and nZnO might induce antagonistic and synergistic as well as additive effects. It is important to note that the reported data involved both aquatic and terrestrial environments and different trophic levels. Following that, the prevalent concentration levels, bioavailability, and physical-chemical behavior of ENPs in mixtures and present as hybrids vary in different compartments. The effects of the mixtures could potentially be affected by this inherent difference with regard to the fate of ENPs in the environmental compartments. The interaction strengths that were found by using a co-occurrence network analysis (Figure 4.1B–D) are described in detail below.

Antagonistic effects

Antagonism is the most common mode of joint interactions of multiple ENPs observed in the current studies on mixture toxicity of ENPs. As shown in Figure 4.1B, nCuO showed the strongest antagonistic interactions with nZnO. The $nTiO_2$ (anatase) and $nTiO_2$ (rutile) combination was also found to be more inclined to show antagonistic effects, followed by nCr_2O_3 + nZnO, nCuO + nCr_2O_3,

$nCuO + nFe_2O_3$, $nCuO + nTiO_2$, $nFe_2O_3 + nZnO$, and $nTiO_2 + nZnO$. In most instances, the occurrence of antagonistic responses implies that the presence of one ENP component in a mixture reduces the uptake of other ENP components by an organism or allows for adsorption of toxic metal ions released by the dissolution of other ENP components (Figure 4.1E, F). This leads in turn to an overall reduction of the toxicity of the mixture. For example, the combined toxicity of nCu and nCuO to the luminescent bacterium *Vibrio fischeri* is antagonistic, and this joint response is associated with the saturation of Cu uptake by the bioreceptor (H. Zhang et al., 2020). This differs from the general assumption that an additive effect is expected as both nCu and nCuO release Cu ions. This assumption tends to take into account only the intrinsic properties of the ENPs and does not take into account the interactions between the mixed components and the interactions between organisms and ENPs. The binary mixtures of nCu and nZnO exhibit antagonistic effects on *V. fischeri*, which is associated with the adsorption of nCu ions released by dissolution of nCu onto nZnO (H. Zhang et al., 2020). Yu et al. (2016b) found that the mode of joint toxic action of $nCeO_2$ and $nTiO_2$ against *Nitrosomonas europaea* was antagonistic, and the impacts of $nCeO_2$ were mitigated as a function of the exposure dose of $nTiO_2$. As both negatively charged $nCeO_2$ and $nTiO_2$ particles can interact with bacterial cells, and as the electrostatic repulsion between the particles may prevent their coagglomeration/aggregation, the two nanoparticles may compete for adsorption sites on the cell wall, thus mitigating the toxic effect of $nCeO_2$ exposed solely (Yu et al., 2016b).

Synergistic effects

As shown in Figure 4.1C, the coexistence of nCuO and nZnO also showed the strongest synergistic interactions among all of the combinations with known synergistic effects. The interactions between nAg and polystyrene nanoplastics (nPS), nAg and $nTiO_2$ (anatase@rutile), nAg and nZnO, and nCuO and $nTiO_2$ (anatase@rutile) are slightly weaker than the interaction between nCuO and nZnO. The synergistic effects of ENPs can be largely due to the fact that they synergistically induce elevated levels of reactive oxygen species (ROS) (Figures 4.1E, G). For example, the synergistic effect of exposure of *Escherichia coli* to a mixture of nAg and $nTiO_2$ was associated with enhanced photocatalytic activity and elevated intracellular ROS levels (Wilke et al., 2018). H. Zhang et al. (2020) also found that the effects of the binary mixtures of nCu and nZn, nCuO and nZn, and nCuO and nZnO were synergistic to *V. fischeri*. This is related to the enhancement of intracellular ROS levels induced by these mixtures. Additionally, Z. Wang et al. (2021) addressed that the synergistic cytotoxicity induced by graphene nanoplatelets (GNs) or reduced graphene oxide (rGO) and metal-based $nZrO_2$ to *Chlorella pyrenoidosa* and the mechanism underlying this synergistic action were associated with the induction of intracellular oxidative stress and cellular membrane functional changes by the carbon-metal-based mixtures. In addition, the effects of mixtures of nAg and nZnO on *Daphnia magna* were synergistic, while their respective salts ($AgNO_3$ and $ZnCl_2$) behaved antagonistically (Lopes et al., 2016). This finding indicates that the dissolved ions are not always responsible for ENP toxicity but that ions + nanoparticles together can cause different effects to aquatic organisms (Lopes et al., 2016). The synergistic

effects of ENPs can be more harmful to ecologically relevant species and to human health, and there is an urgent need to examine the toxicity of mixtures of various combinations of ENPs and thus assess their potential synergistic risks.

Additive effects

Relatively fewer studies have reported on the combined toxicity of ENPs in an additive manner. As shown in Figure 4.1D, the combination of nCuO and nZnO displays stronger additive interactions than other ENP combinations. An additive effect is also frequently found in the mixtures of $nTiO_2$ (anatase) and $nTiO_2$ (rutile). H. Zhang et al. (2020) reported that a binary mixture of nZn and nZnO exhibited additive toxicity to *V. fischeri*. An analysis of the type of joint response suggested that nZn did not interact with nZnO and that the bioreceptor might not be saturated with Zn (H. Zhang et al., 2020). Singh and Kumar (2020) found that a combination of nanosilver oxide (nAg_2O) and $nTiO_2$ caused additive toxicity to *Spinacia oleracea* and improved the plant biomass. In addition, graphene oxide (GO) and nZnO also exerted combined toxic effects on *D. magna* in an additive manner (Ye et al., 2018). The toxicity of multiple ENPs works in an additive manner in the sense that the toxicity of a mixture of individual ENPs is equal to the sum of the toxicity of each ENP component acting alone (Figure 4.1E, H). The additive effect is characterized by the fact that each ENP component in the mixture can proportionally substitute for another ENP component without altering the overall toxicity of the mixture. Furthermore, the additive type of joint interaction is further divided into concentration-additive and effect-additive modes. Future studies are needed to identify the types of additive modes of action in order

to elucidate the main pathways by which multiple ENPs achieve additive joint interaction.

4.3.2 Potentiation or attenuation of effects

Some of the studies shown in the Appendix Tables S4.1 and S4.2 do not directly indicate the type of joint interactions for mixtures of ENPs but imply a difference between combined and single exposures. The mixture effects caused by this scenario are expressed in detail in the Appendix Table S4.3. Multiple ENPs cause enhanced toxic effects in a manner where one ENP in a mixture is less toxic or nontoxic to the organism, but its toxic effects are enhanced by concurrent exposure with another ENP. An example of potentiation effects was that coexposure to the binary mixtures of nCu and nZnO caused mortality of *Oncorhynchus mykiss* at no-effect concentration levels for each of the individual ENPs (Hernández-Moreno et al., 2019). The authors explained this by the higher Zn-ion accumulation in the fish when nCu was present. Collectively, the current studies indicated that the potentiation of the effects of multiple ENPs was mainly correlated with increased bioaccumulation of toxic components (Haghighat et al., 2021; Yin et al., 2022) and oxidative stress (Das et al., 2022; Yin et al., 2022). Conversely, an attenuated toxic effect was found by Zhao et al. (2018), who reported that nAl_2O_3 was shown to mitigate the growth inhibition toxicity of GO to *C. pyrenoidosa*. Zhao et al. (2018) explained the reduced exposure of alga to GO in the presence of nAl_2O_3 due to GO-nAl_2O_3 heteroaggregation. Evidently, the proposed reason for the attenuation effect is related to coaggregation and surface complexation (Jahan et al., 2018), a reduction in the bioavailability of toxic components (Haghighat et al., 2021; Sayadi et al., 2021), and oxidative stress symptoms (Haghighat et al., 2021;

Skiba et al., 2021). In addition, such potentiation or attenuation of effects is relative if the mixture effect lies between the effects of the individual ENPs (Kaur et al., 2019).

4.3.3 Exposure of biota to hybrid NMs

To date, concerns about the toxicity and safety of nanohybrids on release into the environment have also increased considerably. In particular, the strong interactions between nanoparticles in hybrid NMs (the primary concern here is that enhanced toxicity is induced when ENPs are mixed within a (crystalline) matrix of different NMs) could allow the nanocomposite to act in a mode of toxic action that may be different from the mode(s) of toxic action of a mixture that is composed of the separate nanosized components. The collected publications addressing the ecotoxicity of advanced NMs are summarized in the Appendix Table S4.4. Generally, there is controversy about the ecotoxicity of nanohybrids. Some studies addressed that hybrid NMs show no signs of toxicity to ecological species. For instance, Da Silva et al. (2018) found that $nTiO_2$ and multiwalled carbon nanotubes (MWCNTs) hybrids presented no acute toxicity to zebrafish embryos. However, most of the studies indicated that hybrid NMs exhibited diverse levels of toxic effects on ecological species (Azevedo et al., 2017; de Medeiros et al., 2021; Sellami et al., 2017). In particular, the minimum inhibitory concentration (MIC) of selected hybrid NMs (i.e., α-nFe_2O_3@nCo_3O_4, Chit-nAg@GO, nAg@GO, nAg@MWCNT, nAu@nAg, and rGO@nCu_2O) to bacteria ranges from 1 to 1000 μg/mL (Appendix Table S4.4 and Figure S4.2), implying that nanohybrids could be harmful to ecological species. Moreover, hybrid NMs containing nAg and any other material with a lower MIC may provoke more toxic

effects, as shown in the Appendix Figure S4.2. Furthermore, hybrid NMs can be either more or less toxic than that where each separate component of the nanohybrid was to act on its own. This implies that the ecotoxicity of multicomponent NMs is either between (de Medeiros et al., 2021) or higher than the toxicities (Azevedo et al., 2017) of the individual ENP components. In particular, some studies have highlighted that the enhanced bactericidal activity of binary ENP nanocomposites was the result of the synergistic effect of their individual ENP components (Bhaisare et al., 2016; Bhushan et al., 2018; Yang et al., 2017). The combination of multiple NMs allows new properties to emerge and/or adds to the targeted properties (Da Silva et al., 2018). Because of this, the properties that determine the toxicity of a single NM may not be the same for multicomponent NMs. Therefore, an understanding of the risks of nanohybrids remains uncertain and needs to be clarified.

With the emergence of new hybrid NMs, such as early-transition-metal carbides and nitrides (MXene) (Shao et al., 2020) and graphitic carbon nitride based nanohybrids (Liang et al., 2021), the areas of application are widening and the value of their applications is increasing (Wu et al., 2022). However, due to the diversity and complexity of hybrid NMs, toxicological studies and assessment methods on these hybrid materials are challenging. In particular, nanohybrids which have abundant interfaces and active sites (e.g., defects, dangling bonds, and functional groups) tend to be very sensitive and unstable in the exposure medium (being the mimicked environment). Therefore, there is an urgent need to carry out studies on the physical, chemical, and biological transformations that occur

in hybrid NMs in environmental media and to determine how these transformation behaviors ultimately affect their ecotoxicity.

4.3.4 Main factors influencing mixture toxicity of multiple ENPs

From the above results, it appears that multiple ENPs in different studies exhibit different or even opposite mixture effects. For example, the joint toxicity of nCuO and nZnO was determined to be antagonistic in most studies, while some studies determined it to be synergistic or additive. This is because the type and intensity of the joint response of multiple ENPs are influenced by a number of factors, such as chemical composition, physicochemical behavior, organismal factors, and the environmental conditions in which multiple ENPs and organisms would be located. Scientifically, the determination of the various factors influencing toxic effects is an important part of the study of mechanisms of toxic action and an important building block for exploring methods and mechanisms to reduce the biological toxicity of multiple ENPs before they are widely used or released into the environment. From an engineering perspective, it is particularly important to guide environmental remediation, which is the use of physical, chemical, and biological techniques to reduce the concentration or toxicity of pollutants present in the environment or to render them completely harmless (Ge et al., 2022; He et al., 2021). In environmental remediation, depending on the toxic factors, control can be sought to make environmental remediation efforts relevant. Therefore, there is a need to explore ways and mechanisms to reduce the toxicity of a mixture of multiple ENPs by analyzing how each factor affects the mixture toxicity.

Chemical composition of mixed components

The toxicological effects of ENPs are closely related to especially their chemical composition. Mixtures composed of ENPs of different chemical compositions also exhibit markedly different toxic effects on the same species. For example, the joint toxicity of nCuO and nCu against *V. fischeri* showed antagonistic effects, while the joint toxicity of nCuO and nZn against *V. fischeri* showed synergistic effects (H. Zhang et al., 2020). Similarly, $nCeO_2$ had an antagonistic toxic effect on *N. europaea* in a combination with $nTiO_2$, while $nCeO_2$ had a synergistic toxic action with nZnO (Yu et al., 2016b). It can also be deduced that the presence of $nTiO_2$ alleviated the toxicity of nAg to *E. coli* (Wilke et al., 2016), whereas the presence of nPt strengthened the toxicity of nAg to *E. coli* (Breisch et al., 2020). Moreover, the hybrid NM nAg@GO (MIC: 3.2 µg/mL (Zhu et al., 2013)) is more toxic to *E. coli* than the hybrid NM nAu@nAg (MIC: 10 µg/mL (Yang et al., 2017)). The type of joint interaction between $nSiO_2$ and other ENPs (nCdS, $nTiO_2$, and nZnS) to *Heterosigma akashiwo* was also significantly influenced by the absence and presence of metal inclusions in $nSiO_2$ (Pikula et al., 2022). In addition, the mode of joint toxic action of three metal oxide ENPs (nCuO, $nCeO_2$, and nZnO) against *Carassius auratus* changes from synergistic or antagonistic to additive effects when the chemical composition of a mixture changes from a binary to a ternary mixture (Xia et al., 2013).

Stability of suspensions of mixed ENPs

The stability of suspensions of ENPs is affected by processes such as aggregation/agglomeration, dispersion, sedimentation, dissolution, and other transformations of ENPs. These processes affect the size,

morphology, or form (nano or ionic) of ENPs in environmental media, and they are therefore important factors affecting the toxicity of ENPs. By means of the Derjaguine-Landaue-Verwaye-Overbeek (DLVO) theory, it was shown that the aggregation of a mixture of ENPs such as nCuO and nZnO in aquatic systems might be happening due to the combined effects of ionic layer compression, charge neutralization, and van der Waals attraction (Parsai and Kumar, 2019). These interaction forces drive the occurrence of coaggregation or agglomeration of multiple ENPs and also contribute to the distinct differences in their modes of joint toxic action (Yu et al., 2016b). It has also been found that the copresence of naturally derived cellulose nanocrystals (CNCs) significantly reduced the aggregation of nZnO, resulting in enhanced bioavailability and toxicity to *Eremosphaera viridis* (Yin et al., 2022). Furthermore, interactions between individual ENPs in a mixture play a mediating role in ENP toxicity, particularly for a mixed system consisting of a soluble ENP such as nZnO and other stable ENPs such as $nTiO_2$ (Tong et al., 2014). The concentration of free Zn ions released from nZnO can be scavenged due to the formation of Zn(II)-TiO_2 surface complexes, which may consequently alter the exposure and bioavailability of nZnO to organisms (Tong et al., 2014). This interaction would often cause antagonistic effects of multiple ENPs (Tong et al., 2015; Yu et al., 2016a). Besides, the ability of an ENP in a mixed system to act as "Trojan horses" carrying a dissolved ion released from another soluble ENP to targeted organs and sites cannot be underestimated. This may elevate the mixture effects of individual ENPs, though the effects of such interactions on the toxicity of multiple ENPs still need further investigation.

Types and trophic level of individual organisms tested

Figure 4.2A depicts a network that connects tested organisms with types of joint interactions of multiple ENPs. An association analysis indicated that antagonistic effects occur particularly in plants, followed by algae. Synergistic effects frequently take place in algae. An additive effect is also mostly observed in algae and plants. For the frequency of occurrence of types of joint responses, all three types of joint interactions are observed in algae, bacteria, daphnids, fish, and plants. Furthermore, it is evaluated that 68 % of the interactions are more likely to have an effect on lower trophic level organisms, including algae and plants. This means that organisms which are at lower trophic levels present more sensitivity to joint responses to the mixtures of multiple ENPs than those which are at higher trophic levels. Consequently, the trophic level may have an important impact on the mixture toxicity of multiple ENPs.

This sensitivity is particularly observed when mixtures of ENPs with the same composition exhibit different toxic effects on different species. For example, enhanced toxicity of the binary mixtures of nCu and nZnO to *Oncorhynchus mykiss* was observed (Hernández-Moreno et al., 2019), while the binary mixture showed an antagonistic effect on *V. fischeri* (H. Zhang et al., 2020) and lettuce (*Lactuca sativa* L.) (Liu et al., 2016). The binary mixtures of GO and nZnO had an additive toxicity against *D. magna*, while the binary mixtures had an antagonistic toxicity against zebrafish (*Danio rerio*) (Ye et al., 2018). In addition, the joint toxicity of spherical $nTiO_2$ and tubular $nTiO_2$ to *C. pyrenoidosa* was observed to be significantly higher than their joint toxicity to *Scenedesmus obliquus*, and the mode of interaction of the binary mixtures of spherical $nTiO_2$ and

tubular $nTiO_2$ to *C. pyrenoidosa* was found to be effect addition, whereas the joint toxicity to *S. obliquus* was based on concentration addition (Wang et al., 2020).

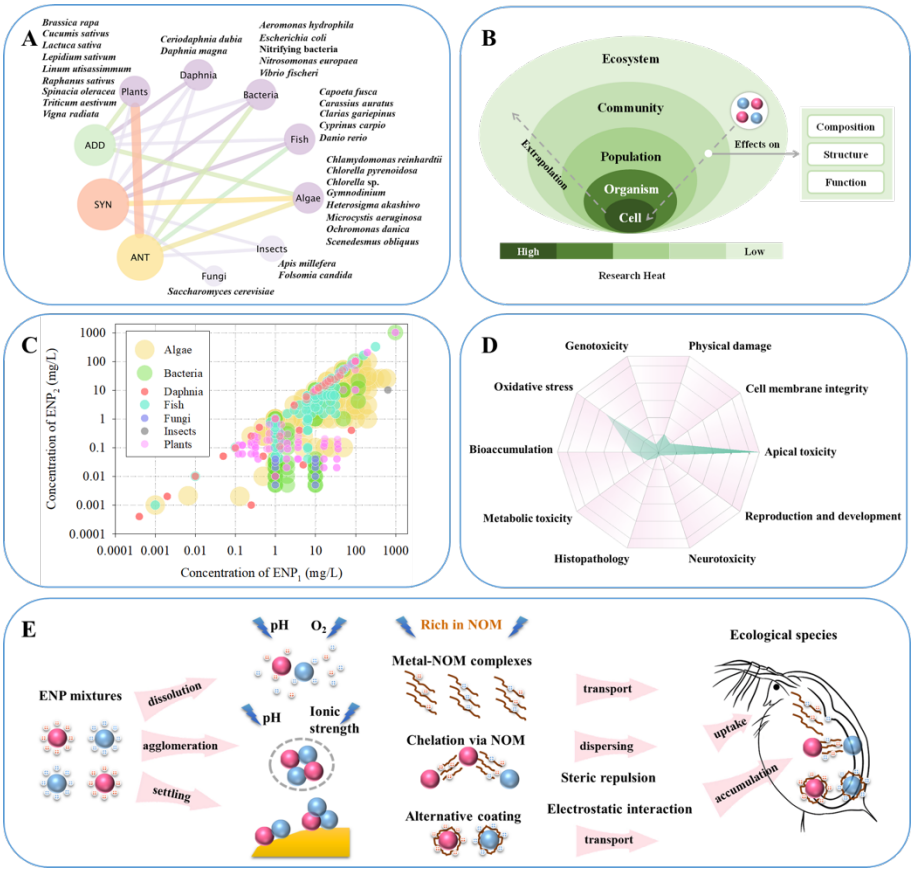

Figure 4.2. *Main factors influencing mixture toxicity of multiple ENPs.* ***A:*** *Network diagram of association rules of ecotoxicological test species combined with types of joint interactions of multiple ENPs. ANT: antagonism, SYN: synergism, and ADD: additivity.* ***B:*** *Biological levels of organization in ecosystems relevant ecological toxicology of multiple ENPs.* ***C:*** *Comparison of the ENP concentrations used in exposure studies with binary ENP mixtures.* ***D:*** *Endpoints of toxicity selected in current studies on mixture toxicity of multiple ENPs.* ***E:*** *Schematic description of the effects of natural organic matter (NOM) on the toxicity of the mixture of individual ENPs.*

Biological level of organization

Ecotoxicological effects resulting from exposure to ENPs can be attributed to changes in the state or dynamics of biological organization, because fitness differences at individual organism levels can have a range of ecological consequences (Figure 4.2B). Overall, most existing nanoecotoxicological studies have focused on the cellular and individual levels, for which mortality, ROS, and reproduction rates are the most often reported endpoints for the standard laboratory species. If for at least three trophic levels (e.g., algae, daphnids, fish) data are collected, a species sensitivity distribution (SSD) curve can be generated to assess the impact of the NMs on the potential affected species at the community level. For a variety of nAg these SSDs have been calculated and reported by Chen et al. (2018). For mixtures these types of SSD curves can be calculated as well, making use of the multisubstance formulas. However, these types of SSDs have not yet been reported in the literature for mixtures of ENPs or for hybrid NMs. The main reason for this is the lack of toxicity data for sublethal effects of mixtures of NMs: i.e., the median effect concentration (EC_{50}), the lowest observed effect concentration (LOEC), or data on the no observed effect concentration (NOEC) of mixtures.

Experimentally, some data have been reported on mixtures of individual ENPs, mostly how they affect microbial communities (Kumar et al., 2012; Londono et al., 2019; Sundaram and Kumar, 2017; Wu et al., 2021) for a range of exposure scenarios. A river bacterial community structure was shifted significantly as a consequence of addition of $nTiO_2$, nZnO, and nAg in different combinations, and with the dominant population being suppressed,

the community exposed to ENPs became more diverse (Londono et al., 2019). Another study reported that, even at the relatively modest concentrations used, a combination of nAg, nCu, and $nSiO_2$ has the potential to disrupt an arctic soil community (Kumar et al., 2012). Additionally, a mixture of nAg_2O and $nTiO_2$ had a greater impact on activated sludge than the individual ENPs when they were present at the same concentrations (Sundaram and Kumar, 2017). It is evident that the effect of ENP mixtures is not diminished by the increased biological level of organization. By modulating ENP properties such as ion release and shape, ENPs such as nAg can play a significant role in the functional composition of microbial communities (Zhai et al., 2016). This warrants the consideration of the combined effects of individual ENPs with different properties on a biological community and associated ecosystem processes in environmental science and management.

Exposure concentrations and time

The concentration distribution of the mixture components in the toxicity studies of the selected binary mixtures for different species is given in Figure 4.2C. A wide range of concentrations used for mixture toxicity testing was studied. The concentrations studied have been more focused on the range between 0.1 to 100 mg/L, which corresponds mainly to joint toxic effects on algae, bacteria, daphnia, fish, and plants. A combination of available examples found the type of joint interactions can be dependent on the doses of ENPs. For example, when the doses are close to the concentration that causes 50 % of immobilization, the synergism between nAg and nZnO in *D. magna* changes to antagonism (Azevedo et al., 2017). In addition, lower mixture concentrations of $nTiO_2$ (0.025 or 0.25 mg/L) and 1

mg/L nPS showed an antagonistic type of interactions in *S. obliquus* (Das et al., 2022). In contrast, an additive interaction was observed between the highest concentration of $nTiO_2$ (2.5 mg/L) and 1 mg/L nPS (Das et al., 2022). It is evident that the ratio of exposure concentration of individual ENPs in a mixture also plays a role in determining the type of joint response.

The type of joint response for mixtures of individual ENPs is also time-dependent. For instance, the antagonistic and synergistic effects of Zn- and Cu-based ENPs on the reproduction reduction of *Folsomia candida* were observed in soil samples after 1 and 90 days, respectively (Jośko et al., 2022). Combined treatment of ENPs triggered different physiological, chemical, and transcriptional effects on soil-grown barley *Hordeum vulgare* than those caused by individual exposure to nCuO or nZnO in a time-dependent manner (Jośko et al., 2021). The distinct joint effects of multiple ENPs may be caused by the differences in the transformation of ENPs (e.g., aggregation/agglomeration, dissolution) over time in environmental media.

Endpoints of toxicity

Figure 4.2D depicts the endpoints of toxicity used for mixture toxicity testing. Current tests examining the toxicity of mixtures of multiple ENPs include various endpoints of toxicity, which characterize their toxic effects from the apical to the mechanistic level. In existing studies apical toxicity endpoints (e.g., growth inhibition, mortality) are used as the primary toxic endpoints for characterizing the impacts of mixtures of multiple ENPs on ecological species, as shown in Figure 4.2D. It can also be observed that oxidative stress has become

the primary endpoint of toxicity assessment in elucidating the mechanisms of joint responses of biota to exposure to mixtures of multiple ENPs. Furthermore, the selection of toxicological endpoints has an obvious impact on the manner in which the joint responses of multiple ENPs are interpreted. For instance, multilayer graphenes (MLGs) and nZnO showed synergistic effects on *Capoeta fusca* using mortality rate as an endpoint, whereas MLGs and nZnO showed antagonistic effects on the same species when behavioral responses and histopathological changes were used as endpoints (Sayadi et al., 2022). Likewise, chitosan-functionalized molybdenum disulfide nanosheets ($nMoS_2$) attenuated the oxidative stress induced by nAg on yeast cells, while $nMoS_2$ had a synergistic effect with nAg in destroying the yeast cell membrane integrity (Yang et al., 2018). Generally, apical toxicity endpoints provide the most robust findings to describe multiple ENP toxicity.

Field conditions

Under different abiotic field conditions (i.e., pH, ionic strength, dissolved organic carbon, etc.), ENPs can undergo various physicochemical transformations (Lowry et al., 2012) such as dissolution, adsorption, aggregation/agglomeration, and dispersion. Each of these processes can affect the biological availability of ENPs (Figure 4.2E). The multi-ENP mixtures can also undergo these physicochemical transformation processes, thus affecting the fate and toxicity of individual ENPs in the mixtures (Liu et al., 2016; Tong et al., 2015). Understanding the extent of physicochemical transformation of multi-ENP mixtures in environmental media is therefore essential for estimating ecological risks (Geitner et al., 2020). The extent of these transformations such as dissolution and

aggregation/agglomeration will be controlled by abiotic field conditions. The aggregation and settling behavior of a mixture of ENPs such as nCuO and nZnO within aquatic systems was found to be dependent on pH, ionic strength, and concentration, and dissolution of the ENPs was observed to be significantly affected by a change in the pH of a suspension (Parsai and Kumar, 2019). Furthermore, the stability of suspensions containing a mixture of nCuO and nZnO was found to decrease with increasing pH, ionic strength, and ENP concentration (Parsai and Kumar, 2019). Another study showed that aggregation in a suspension containing a mixture of nCuO and nZnO in natural water was significantly affected by the ENP concentration, clay concentration, and humic acid (Parsai and Kumar, 2020).

It is known that abiotic field conditions, such as UV exposure (Gomes et al., 2021), pH (Xiao et al., 2016), ionic strength (Chao et al., 2021), and natural organic matter (NOM) (Deng et al., 2017; Xiao et al., 2016), can influence how ENPs affect different organisms. Consequently, ecotoxicological testing for mixtures of ENPs should include assessment of the exposure of organisms under a variety of exposure conditions to fully represent the field conditions found in the natural environment. One critical parameter influencing chemical interactions is exposure to light. In the dark, $nTiO_2$ attenuated bacterial stress caused by low concentrations of nAg due to Ag^+ adsorption (Wilke et al., 2016). Yet, since both $nTiO_2$ and nAg are photoactive, their photochemistry may play a key role in their interactions. In a further study by Wilke et al. (2018), the chemical interactions of nAg and $nTiO_2$ mixtures in a natural aqueous medium under simulated solar irradiation were studied to investigate

photoinduced stress. Wilke et al. (2018) observed that $nTiO_2$ and nAg together exert synergistic toxic stress in *E. coli* by using adenosine triphosphate levels and cell membrane integrity as probes. In addition, NOM is demonstrated to be an important parameter affecting the behavior and effect of ENP mixtures. Zhao et al. (2018) found that humic acid decreased GO-Al_2O_3 toxicity to *C. pyrenoidosa* due to enhanced steric hindrance through a surface coating of GO-Al_2O_3 heteroaggregates. In contrast, Yu et al. (2022) demonstrated that Suwannee River NOM increased the relative contribution of dissolved ions released from nCu and nZnO to the toxicity of the binary mixtures at high-effect concentrations of individual ENPs to *D. magna*. Moreover, the presence of Suwannee River NOM significantly enhanced the accumulation of either nCu or nZnO in *D. magna* exposed to the ENP mixtures (Yu et al., 2022). As depicted in Figure 4.2E, the increase in the accumulation of a mixture of ENPs in the presence of NOM may be related to the direct ingestion of metal-NOM complexes and ENP-NOM complexes by water-exposed free-swimming species.

Once released into the environment, nanoparticles can also adsorb naturally occurring biomacromolecules such as secreted proteins and polysaccharides onto their surface: namely, an eco-corona formation (Martinez et al., 2022). The presence of an eco-corona can alter the surface properties and aggregation state of nanoparticles in the aquatic environment (Yanjun Liu et al., 2020; Saavedra et al., 2019), as well as alter their ecotoxicity (Chakraborty et al., 2021; Nasser and Lynch, 2016). However, there is a paucity of literature reporting on the properties, patterns, and mechanisms of competitive formation of an eco-corona on multiple ENPs or formation of mixtures of

individual ENP-eco-corona complexes. Consequently, the impact of eco-corona formation on the combined adverse effects of mixtures of ENPs has also become one of the scientific challenges to be solved.

Additionally, biochar as a sustainable and renewable source has been used successfully for the *in situ* remediation of various pollutants during different environmental governance processes (Shao et al., 2022; Zhao et al., 2021). The concurrence of biochar also induces a positive effect in reducing the biotoxicity and bioavailability of ENPs (Abbas et al., 2019; Nyoka et al., 2018). However, the current understanding of the interactive effects of biochar and multiple ENPs on ecological species is rather limited. The impacts of biochar on the combined toxicity of individual ENPs need to be highlighted and potential opportunities identified to maximize the understanding of the environmental risk of biochar and ENPs.

It is also worth emphasizing that multiple ENPs in different studies exhibit different mixture effects, since the mixture effects are commonly caused by the interaction of multiple factors. Thus, the toxicity of ENP mixtures can be reduced by modulating several controllable factors, such as changes in the chemical composition of the components present in the mixture, reduction of the effective exposure dose, and adjustment of the external environmental conditions. Note that abiotic field conditions can drive the transformation of ENPs in the natural environment, causing a reduction in the mixture effects of multiple ENPs. With respect to the mechanism of toxicity, it should be noted that the interaction of multiple ENPs with biological systems can cause different levels of damage, such as at the tissue level, organ level, cellular level, subcellular level, and biomolecular (glycans, lipids, proteins, and

genes) level. In particular, the production of ROS can cause biomolecular damage and therefore excessive ROS production induced by multiple ENPs needs to be controlled by the organism. By optimizing the inherent structures and physicochemical properties of ENPs (e.g., size, purity, and surface properties), the direct interaction of ENPs with organisms and the uptake, accumulation, distribution, action, and clearance of ENPs in organisms can be improved. This also requires more purposely designed experiments investigating the impacts of the structure and properties of individual ENPs on the mixture effects induced by multiple ENPs.

4.3.5 Assessment and prediction methods for the mixture toxicity of multiple ENPs

Screening the risks of contaminants is mainly achieved by qualitatively assessing the types of joint interactions and quantitatively predicting the magnitude of mixture toxicity. Assessed and predictive methods (Figure 4.3A) may help to reduce the intensive laboratory experiments needed to determine the toxicity of mixtures of ENPs. An association analysis indicated that the most common way of assessing the joint interactions of multiple ENPs reported in existing studies is the IA-based model (Figure 4.3B). Moreover, the most frequently evaluated combination applying the IA-based method is the combination of nCuO and nZnO. Furthermore, it is estimated that the type of joint interaction of an ENP mixture is predicted correctly or overpredicted by default in approximately 42 % of all combinations.

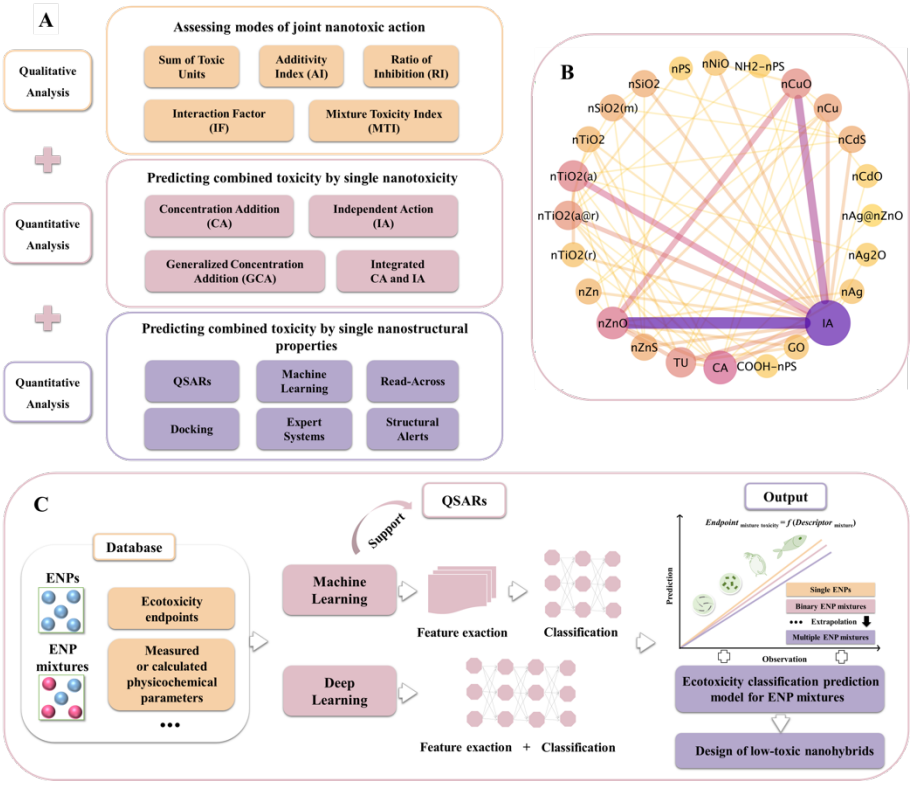

Figure 4.3. *Assessment and prediction methodology of multi-ENP mixtures.* ***A:*** *Schematic framework for the methodology.* ***B:*** *Network diagram of association rules of ENPs in binary mixtures combined with the assessment methods for their joint toxicity. CA: Concentration Addition, IA: Independent Action, and TU: Toxic Unit.* ***C:*** *Scheme of machine learning- or deep learning-based QSAR approach used for the ecotoxicity prediction of the mixtures of individual ENPs.*

CA and IA models have been preliminarily applied to the assessment and prediction of the mixture toxicity of multiple ENPs. For example, Liu et al. (2016) applied CA and IA models to effectively predict the combined toxicity of nCu and nZnO to *Lactuca sativa* L., and the fit of the IA model to the experimental data on the combined toxicity of the two ENPs was higher than that of the CA model. Wang et al. (2020) used the IA model to effectively predict the combined toxicity

of spherical $nTiO_2$ and tubular $nTiO_2$ to *C. pyrenoidosa*, while the CA model effectively predicted the combined toxicity of this binary mixture to *S. obliquus*. Although the CA and IA models offer some promise toward predicting the mixture toxicity of multiple ENPs, a great deal of validation will be necessary. In addition, one important realization is that the CA and IA models also require experiments to determine the toxicity characters (i.e., effect concentrations and concentration-response relationships) of all single components of a mixture. Taken together, the CA and IA models have become the two most commonly used methods in assessing and predicting the combined toxic effects of multiple ENPs, as shown in Figure 4.3B. Furthermore, the two methods are frequently used for the mixtures consisting of nCuO, nZnO, or $nTiO_2$. In particular, toxicity assessment and prediction of mixtures containing nCuO and nZnO prefer IA models.

Quantitative structure-activity relationship (QSAR) models are mathematical relationships between indicators of toxicity (e.g., lethality) and descriptors (e.g., physicochemical properties of chemicals) (Chen et al., 2017, 2015). QSAR models have been successfully applied to predict the single toxicity of ENPs. However, the data that have been used for QSAR models were mostly generated from toxicity studies with single ENPs rather than making use of multiple ENPs. Currently, a limited number of studies have been developed to establish QSAR models for the photocatalytic activity and toxicity of $nTiO_2$-based nanomixtures (Mikolajczyk et al., 2019, 2018, 2016). These studies aimed to develop models for predicting the photocatalytic activity and cytotoxicity of nanoblends consisting

of $nTiO_2$ and (poly) metal clusters (Au, Ag, Pd, and Pt) (Mikolajczyk et al., 2019, 2018, 2016).

QSAR models can fill in the limitations of CA and IA models (Trinh and Kim, 2021). QSAR model inputs do not require the toxicity of all single components in a mixture or the dose-response curves of single components in the mixture. However, QSAR studies on the quantitative prediction of the mixture toxicity of multiple ENPs still constitute a knowledge gap. The main reason for this may be the lack of sufficient experimental data and the absence of uniform toxicity endpoints to develop predictive models. In addition to quantitative data on toxicity endpoints, descriptors are also important for the development of QSAR models. Descriptors for ENPs can be obtained based on the properties of nanoparticles at different scales (Wang et al., 2018), including physicochemical properties (e.g., chemical composition, shape, particle size, surface charge, specific surface area, and solubility), quantum chemical properties of nanocluster structures, and mesoscale nanoparticle properties. However, because ENP mixtures contain both nanoparticle and mixture components, there is a need to develop mixture descriptors for multiple ENPs and hence QSAR models can quantitatively predict the toxicity of multi-ENP mixtures. The weighted descriptor approach in Equation 4.1 represents a preferred approach to developing descriptors for chemical mixtures (D_{mix}) (Altenburger et al., 2003; Giner et al., 2020). Then, a generic QSAR model for the prediction of activities of chemical mixtures can be expressed by Equation 4.2 (Altenburger et al., 2003)

$$D_{\mathrm{mix}} = \sum(x_i D_i) \qquad (4.1)$$

$$\log A_{\text{mix}} = a \log \sum(x_i D_{1i}) + b \log \sum(x_i D_{2i}) + \cdots + z \qquad (4.2)$$

where A_{mix} represents the activity of the chemical mixtures to be modeled, x_i represents the molar fraction of a component (i) in the mixtures, D_1 and D_2 are the structural descriptors used for each component, and a, b, and z are the coefficients of the regression function. A QSAR approach with mixture descriptors was implemented in a user-friendly application for assessing the aquatic toxicity of nanomixtures containing $nTiO_2$ and one of the selected inorganic/organic compounds (Trinh et al., 2022).

Assessing and predicting the toxicity of mixtures of multiple ENPs is facing unprecedented opportunities and challenges. Computational nontesting methods (i.e., *in silico* models) representing a fast and reliable alternative approach to *in vivo* and *in vitro* methods, for example, machine learning, read-across, docking, expert systems, and structural alerts, are expected to play key roles in the toxicity prediction of mixtures of ENPs. In particular, the integration of QSAR and machine-learning methods (e.g., support vector machine, random forest, K-nearest neighbor, naïve Bayes, decision tree, neural network, and logistic regression) can serve as a very powerful tool for solving the problem of toxicity prediction of mixtures of NMs (Figure 4.3C). The reality, however, is that the lack of databases on the mixture toxicity of ENPs hinders the development and application of artificial-intelligence-based methods for toxicity prediction. As the size of the data increases, deep-learning methods perform better than machine-learning methods. It is worth noting that deep learning attempts to obtain high-level features directly from the data, which is the main difference between deep-learning and traditional machine-learning algorithms. In addition to the prediction of

ecotoxicity endpoints/classification, machine-learning methods combined with QSAR notions can provide valuable hints for the design of low-toxicity nanohybrids. On balance, comprehensive and predictive knowledge about NM risks to environmental and ecological health must include explicit consideration of interactions in multiple ENP mixtures.

4.4 Outlook and prospects

The mixture toxicity of multiple ENPs is an emerging topic, and this topic faces numerous opportunities and challenges. Based on the current state of the science, the following key research needs have emerged.

(1) Currently, single-component ENPs as the first generation have reached full market penetration. New-generation multi-component NMs, made up of e.g. binary or ternary or quaternary constituents or ENP components with sometimes advanced properties, are just starting to enter the market. The association rule analysis performed shows that applying the notion of simple additivity is often justified, and the predictability of mixtures of ENPs can be done with approximately 42 % accuracy by taking single ENP hazard information and using a simple additive approach. An understanding of joint interactions for those novel materials is in its infancy. Continued studies will be required to investigate the combined toxicity of hybrid NMs, particularly at environmentally relevant concentrations.

(2) Based on the single ENP data, the physicochemical behavior (e.g., stability, aggregation/agglomeration, dissolution) is the most important of all characteristics of ENPs. It is known that the

presence of ligands to bind to and pH drive the single toxicity of ENPs. Thus, the effects of the physicochemical behavior such as stability (versus binding ligands) and pH versus dissolution on the toxicity of mixtures of ENPs need to be recognized. At the higher biological levels most experimental data collected for microbial communities and all other communities need to be estimated by making use of SSDs or other modeling techniques that are built from the standard laboratory test species data.

(3) When facing the continuous emergence of various new ENPs, the workload of the assessment and prediction of the mixture toxicity of multiple ENPs will multiply. In particular, the interaction behavior between different particles in the mixtures of ENPs has been screened but a mechanistic understanding has not been explored. In this study, we used the classical addition models and assumed antagonistic or synergistic joint interactions when a deviation on additivity was found. A 75 % chance of a correct prediction would be given approximately when drawing lessons from making use of the CA and IA models for metal mixtures (Liu et al., 2017; Vijver et al., 2011, 2010). The importance of modeling is recognized for screening purposes not only in prospective but also in retrospective effect assessments. Comprehensive computational approaches of predicting the mixture toxicity of multiple ENPs need to be developed further. This study gives the first building blocks on what data are currently present and accessible, and what types of joint interactions exist for mixtures of multiple ENPs and provides insights into what we can expect as response types for hybrid NMs.

Acknowledgements

The research described in this work was supported by the European Union's Horizon 2020 research and innovation program via the projects "NanoinformaTIX" (grant number 814426) and SUNSHINE (grant number 952924), and by the National Natural Science Foundation of China (grant number 31971522). M.G.V. acknowledges the support of the ERC-C grant entitled EcoWizard no. 101002123. F.Z. greatly acknowledges support from the China Scholarship Council (grant number 202008320308). We also thank the reviewers for their valuable comments on the manuscript.

Chapter 5

Prediction of the Joint Toxicity of Multiple Engineered Nanoparticles: The Integration of Classic Mixture Models and *In Silico* Methods

Fan Zhang, Zhuang Wang, Martina G. Vijver and
Willie J.G.M. Peijnenburg

Published in Chemical Research in Toxicology 34 (2021), 176–178.

Abstract

An approach to solve the emerging need of prediction of the toxicity of mixtures of engineered nanoparticles (ENPs) is presented. The integration of classic approaches to mixture toxicity assessment and computational toxicology approaches is proposed to be a smart strategy for forecasting the toxicity of a mixture of ENPs.

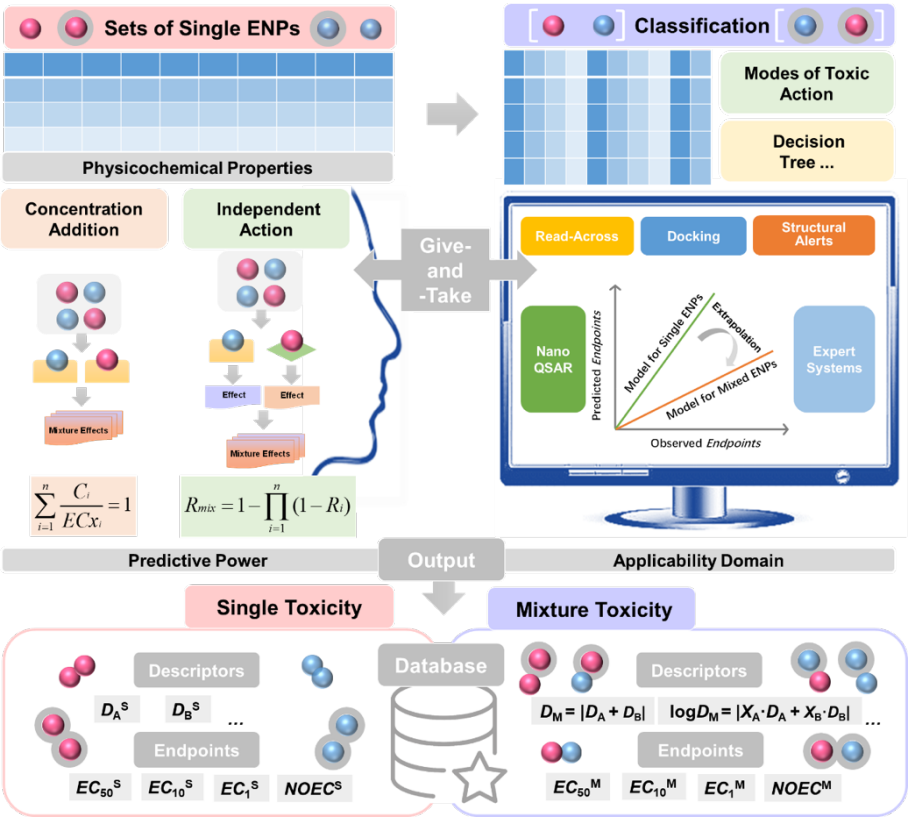

Graphical abstract

Various nanostructured materials have been found to be attractive for applications due to their distinctive physicochemical properties from atoms, molecules, and traditional bulk materials. With the increasing market entry of existing nanomaterials and the uninterrupted development of new nanomaterials, a wide diversity of engineered nanoparticles (ENPs) will inevitably be released into the atmosphere, water, and soil, which also raises concerns about the risks of these ENPs to human and ecological health (Peijnenburg et al., 2015). Assessing the environmental risks of ENPs is not only a challenge for the scientific community but also a major international demand for the sustainable development of nanotechnology.

The presence of chemical contaminants in the form of mixtures in the environment is a common rule rather than an exception. Due to the extensive use of ENPs in industrial and consumer products, ENPs will inevitably be released into the environment. Natural ecosystems will thus be exposed to a mixture of ENPs. At present, with the ongoing development and application of nanocomposites, different types of ENPs will be jointly discharged into the environment. In addition, sewage systems and municipal wastewater treatment plants have become important in-between ways to transfer ENPs to the environment. Thereupon, industrial and municipal sewage is viewed as the main source of mixtures of ENPs of varying composition. The formulation of current environmental quality standards and risk assessments is usually based on toxicity data of individual ENPs (Guinée et al., 2017), and the potential hazards of their combined toxic effects are not fully considered. This may be because the intrinsic toxicity of a mixture of ENPs (addition, synergism, or antagonism) is strikingly different from the toxicity of the individual

ENPs. Meanwhile, a standardized and trustworthy method for estimation of ENP-mixture toxicity is lacking.

We propose that the key strategy to quantitatively predict the joint toxicity of an emerging or untested/unknown mixtures of multiple ENPs is to integrate the classical mixture toxicology methods with computational toxicology approaches. This integration not only allows to properly incorporate the characteristics of the underlying mechanisms of toxicity (from the intrinsic structure information) as based on the classical mixture toxicology approaches but also strengthens the theorization (from the basic principles of mixture toxicology) of computational toxicology approaches.

On the basis of the classical mixture toxicology, the toxicity induced by exposure to mixtures of ENPs can be assessed using a component-based (CB) method. The CB method relies upon the response of the individual components of a mixture to predict the joint toxicity of the mixture (Bopp et al., 2018). The CB method for the toxicity prediction of chemical mixtures can be further classified as following joint actions in toxicodynamic processes: similar joint action (concentration addition, CA), dissimilar joint action (independent action, IA), and synergistic/antagonistic actions. The CA and IA models are usually applied to quantify the joint toxicity (including toxicity indicators and full dose/concentration-response/ effect relationships) of chemical mixtures. CA is accustomed to predicting the toxicity of mixtures consisting of chemicals with a similar mode of toxic action (MOA), and IA is conditioned to predicting the toxicity of mixtures comprising chemicals with a dissimilar MOA. Joint action as induced by chemical mixtures is a fundamental hypothesis (Kar and Leszczynski, 2019). Note that the

assessment of distinctive types of MOA of individual ENP-induced toxicity is prerequisite for the assessment of joint action of ENP mixtures. Furthermore, CA and IA have become two prevailing approaches for the quantitative prediction of mixture toxicity based upon the hypothesis of joint action. It is reasonable to believe that the widely accepted approaches to modeling mixture toxicity are applicable to mixtures of ENPs.

The development of nanotechnology has advanced by leaps and bounds, but our knowledge of the toxicological effects and risks of ENPs lags far behind the speed of their production and utilization. Most importantly, emerging nanomaterials are continuously being developed, introduced, and released. Nonetheless, different organism toxicity data are insufficient for single ENPs and yet are considerably scarcer for mixtures of ENPs. In addition, the experimental evaluation of the toxicity of single and mixtures of ENPs by means of biological models has a high cost and is time-consuming. In response to these issues, environmental scientists and toxicologists around the world have generally recognized the need to develop and validate theoretical prediction methods for ENPs, namely *in silico* (i.e., computational) toxicology models or predictive-toxicology models (mainly used for the prediction of toxicological indicators) (Chen et al., 2017). Computational toxicology can offer powerful technique support to fill a vacancy in mixture toxicity data, as the majority of mixtures even lack toxicity data for the individual ENPs. Additionally, computational toxicology methods have the potential of being capable of in advance prediction of the joint toxicity of ENP mixtures of any composition. There have been notable examples of the prediction of toxicity of chemical mixtures through computational toxicology

methods (Kar and Leszczynski, 2019), for example, the quantitative structure-activity relationship (QSAR) model, the structural alerts model, the rule-based model, the uncertainty factors model and read-across, docking, and expert systems. Such methods could be applicable to the toxicity prediction of mixtures of ENPs.

The physicochemical and steric structures of ENPs determine the intrinsic mechanisms and linkages of their environmental behavior and toxicological effects, which are the core issues and challenges in constructing a predictive toxicology model, such as nano-QSAR. Through theoretical chemistry calculations such as molecular simulation, many nanodescriptors/parameters (such as energy levels, frontier orbital energy levels, charge, etc.) describing the characteristics of a single ENP structure can be obtained. Mechanism-based nanodescriptors for discriminating the toxicity of ENPs can be further screened via classification/regression methods, for example, decision tree, logistic regression, and support vector machine. The mechanism of toxicity of ENPs can also be revealed at the molecular level. The computation of descriptors for mixtures of ENPs is the real challenge. The weighted descriptor approach represents a preferred practice to work out descriptors for chemical mixtures (Giner et al., 2020).

To achieve the integration of the classical mixture toxicity and computational toxicology methods, we suggest that research priorities for the prediction of the toxicity of mixtures of ENPs are identified to systematically sort out the toxicity and ecotoxicity information (macroscopic and microscopic toxicity end points) of ENPs gathered into "databases". Moreover, expected and/or actual environmental concentrations of ENPs need to be obtained to be implemented for

actual risk profiling of various combinations of ENPs in the environment. These environmental concentrations can be further used for the estimation of mixture ratios of multiple ENPs, and then the weighted descriptors of ENP mixtures can be evaluated by the mixture ratios. Furthermore, it is essential that information on the MOA of single ENPs to species is systematically documented, and this issue deserves priority in the selection of methods to assess mixture toxicity and the selection of mechanism-based nanodescriptors.

Acknowledgements

The research described in this work was supported by the European Union's Horizon 2020 research and innovation program "NanoinformaTIX" (grant number 814426) and the National Natural Science Foundation of China (31971522). F.Z. greatly acknowledges the support from the China Scholarship Council (202008320308).

Chapter 6

Machine Learning-Driven QSAR Models for Predicting the Mixture Toxicity of Nanoparticles

Fan Zhang, Zhuang Wang, Willie J.G.M. Peijnenburg and Martina G. Vijver

Published in Environment International 177 (2023), 108025.

Abstract

Research on theoretical prediction methods for the mixture toxicity of engineered nanoparticles (ENPs) faces significant challenges. The application of *in silico* methods based on machine learning is emerging as an effective strategy to address the toxicity prediction of chemical mixtures. Herein, we combined toxicity data generated in our lab with experimental data reported in the literature to predict the combined toxicity of seven metallic ENPs for *Escherichia coli* at different mixing ratios (22 binary combinations). We thereafter applied two machine learning (ML) techniques, support vector machine (SVM) and neural network (NN), and compared the differences in the ability to predict the combined toxicity by means of the ML-based methods and two component-based mixture models: independent action and concentration addition. Among 72 developed quantitative structure-activity relationship (QSAR) models by the ML methods, two SVM-QSAR models and two NN-QSAR models showed good performance. Moreover, an NN-based QSAR model combined with two molecular descriptors, namely enthalpy of formation of a gaseous cation and metal oxide standard molar enthalpy of formation, showed the best predictive power for the internal dataset (R^2_{test} = 0.911, adjusted R^2_{test} = 0.733, $RMSE_{test}$ = 0.091, and MAE_{test} = 0.067) and for the combination of internal and external datasets (R^2_{test} = 0.908, adjusted R^2_{test} = 0.871, $RMSE_{test}$ = 0.255, and MAE_{test} = 0.181). In addition, the developed QSAR models performed better than the component-based models. The estimation of the applicability domain of the selected QSAR models showed that all the binary mixtures in training and test sets were in the applicability domain. This study

approach could provide a methodological and theoretical basis for the ecological risk assessment of mixtures of ENPs.

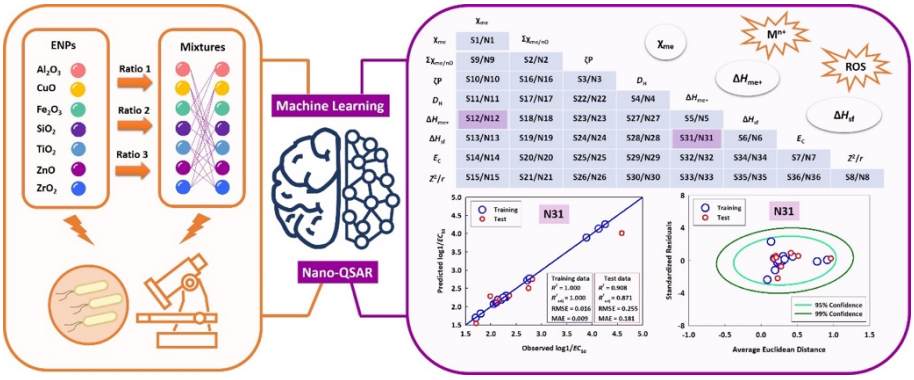

Graphical abstract

Keywords: Nanotoxicity; Advanced nanomaterials; Support vector machine; Neural network; Mixture toxicity.

6.1 Introduction

The unique physicochemical features of nanostructured materials make them particularly appealing for specific applications (Wyrzykowska et al., 2022). Developments go with a fast pace, with first-generation nanomaterials (NMs) already embedded in a variety of products and advanced NMs such as nanocomposites continuously generated (Jayaramulu et al., 2022). With the continuous development and application of NMs, different types of engineered nanoparticles (ENPs) will now be co-discharged into the environment. Municipal wastewater treatment facilities and sewage systems are becoming crucial intermediary routes for the release of the mixtures of ENPs into the environment (Georgantzopoulou et al., 2020; Simelane and Dlamini, 2019; Singh and Kumar, 2020). It is expected that industrial and municipal wastewater are a major source of mixtures of ENPs of different compositions. As a consequence, a wide range of structurally and chemically diverse ENPs will unavoidably be released into the environmental compartments (Hong et al., 2021), raising worries about potential ENPs-induced human and ecological impacts (Avellan et al., 2021). This requires to explore the scientific challenge of assessing mixture toxicity of multiple ENPs (Zhang et al., 2022a).

Fortunately experimental data on the mixture toxicity of ENPs is expanding quite recently, while progress on methods for evaluating and predicting the mixture toxicity of ENPs is lagging (Zhang et al., 2022a). Enabling ENPs' mixture predictions, classical component-based mixture models have been used (Lopes et al., 2016; Martín-de-Lucía et al., 2019). However, these mixture models such as concentration addition (CA), independent action (IA), and a

combination of the two models rely on the assessment of the concentration-response relationship of the single components and on the identification of the toxic mode of action of the single components (F. Zhang et al., 2021b). *In silico* predictive toxicology appears to be a promising alternative to the mixture modeling. Among the novel approach methodologies based on *in silico* predictions, quantitative structure-activity relationships (QSAR) modeling proves to be a useful tool for the prediction of the biological activity or property of a compound by providing a mathematical correlation with its structural features (Tropsha, 2010). Recently, QSAR methods are being applied in methodological studies for the quantitative prediction of the toxicity of mixtures of ENPs (Kar et al., 2022; Mikolajczyk et al., 2016; Na et al., 2023; Zhang et al., 2022b). Meanwhile, machine learning (ML) methods, which seek to construct an explicit or implicit model based on current data (known as training data) to make predictions or decisions on complicated issues (M. Wang et al., 2021), have already stepped into the spotlight for *in silico* prediction of toxicology. ML methods to date have shown unprecedented predictive power in predicting the toxicity of ENPs (Balraadjsing et al., 2022; Ji et al., 2022; Jia et al., 2021; Trinh et al., 2022). Thus, ML-powered QSAR modeling approaches could be a strong tool to deal with the problem of predicting the toxicity of mixtures of ENPs, and would perform better and more cost-effective than the classical mixture models. However, there is still a scarcity of QSAR models based on ML approaches for predicting the mixture toxicity of multiple ENPs.

The present study aimed at rebuilding existing QSAR for use with NMs (nano-QSAR) by incorporating ML methods to describe the toxicity of a mixture of ENPs and comparing the performance with

the mixture models. This enables the understanding of the link between the physicochemical properties describing the components in the mixture and the cytotoxicity of 22 binary mixtures of metal oxide nanoparticles (MO_X NPs) against *Escherichia coli*, a commonly used bacterium species in toxicity screening. Toxicity data for 12 binary mixtures with two different mixing ratios from our laboratory were used as an internal dataset. Toxicity data for 10 binary mixtures with another mixing ratio from the literature were used as an external dataset. The selected ML methods, namely support vector machine (SVM) (Ban et al., 2022; Liu et al., 2013) and neural network (NN) (Yang et al., 2022), are well-known and commonly utilized ML algorithms. The study involves eight indicative physicochemical parameters implicated in the mechanism of toxicity of MO_X NPs: surface charge, dispersion stability, dissolution, oxidative stress, and particle reactivity. Then, for the first time, SVM- and NN-based QSAR models for predicting the cytotoxicity of mixtures of individual MO_X NPs with diverse metal elements and different mixture ratios were developed. The goal of this study is to develop a rapid and cost-effective model for predicting the toxicity of mixtures of ENPs and provide a more suitable method for the risk assessment of multiple ENPs.

6.2 Materials and methods

6.2.1 Experimental sections

Test materials

CuO NPs with a primary size of 40 nm (advertised specific surface area > 10 m^2/g; purity 99 %), ZnO NPs with a primary size of 14 nm (advertised specific surface area of 30 ± 5 m^2/g; purity > 99 %), TiO_2

NPs with a primary size of 21 ± 5 nm (advertised specific surface area 50 ± 10 m^2/g; purity > 99.5 %), and ZrO_2 NPs with a primary size of 5–25 nm (advertised specific surface area 130 ± 20 m^2/g; purity > 97.2 %) were purchased from PlasmaChem GmbH (Berlin, Germany). The MO_X stock suspensions were freshly prepared in pure water after 30 min sonication in a water bath sonicator and then stored at 4 °C until use.

Physicochemical analysis

Zeta potential (ζP) and hydrodynamic diameters (D_H) of the MO_X NP suspensions at 10 mg/L were analyzed in water using a ZetaSizer instrument (Nano ZS90, Malvern Instruments Ltd., Worcestershire, UK).

Toxicity testing

Cytotoxicity tests were performed with *E. coli* using the microtitration plate assay (Patton et al., 2006). The initial number of bacteria was set at 1×10^8 cells/mL. Bacterial solution after exposure to the test materials was added into a 96-well white flat-bottom microplate, which subsequently was maintained at 37 °C with shaking incubation for 12 h in a constant temperature shaker. Bacteria were exposed to increasing concentrations of the suspensions of CuO NPs (from 1.26×10^{-4} to 3.02×10^{-3} mol/L), ZnO NPs (from 6.14×10^{-5} to 6.76×10^{-4} mol/L), TiO_2 NPs (from 3.76×10^{-4} to 3.76×10^{-3} mol/L), and ZrO_2 NPs (from 4.06×10^{-4} to 9.74×10^{-3} mol/L). Each test concentration was replicated four times. The optical density (OD) values corresponding to the cell number of *E. coli* were monitored using an enzyme-labeled instrument (Thermo Multiskan FC, USA), and the

inhibition rate was calculated from the measured OD values. The cytotoxicity of the tested materials was expressed in terms of effect concentrations (EC_{50} and EC_{10}: the effective concentration of a toxicant that induces 50 and 10 % bacteria inhibition), which were calculated using a concentration-response curve (CRC). For the binary mixtures in the internal dataset, *E. coli* cells were treated with various concentrations of MO_X NPs with a fixed mixture ratio, where the first and second mixtures were based on the initial EC_{50} and the EC_{10} of each MO_X NP, respectively. Thus, the two mixtures were named Int ($R1$) mixture and Int ($R2$) mixture.

6.2.2 Computational methods

Determination of concentration-response curve

The Logistic regression model, as shown in Equation 6.1, was used to fit the CRCs for single and binary MO_X NPs.

$$E = \frac{100}{\left(1+\left(\frac{C}{EC_{50}}\right)^{\theta}\right)} \qquad (6.1)$$

where E is the effect confined to the range of 0–100 %, C is the exposure concentration of the test materials, and θ represents the slope parameter.

Joint effect modeling

As the most representative approaches used are the IA and CA models (Bliss, 1939; Loewe and Muischneck, 1926), which were applied to predict the toxicity (denoted EC_{50} values) of the mixtures of MO_X NPs. Throughout the modeling EC_{50} values were transformed to inverted logarithm i.e., $\log 1/EC_{50}$.

The general expression shown in Equation 6.2 was used for the IA model,

$$E(C_{\text{mix}}) = 1 - \prod_{i=1}^{n}(1 - E(C_i)) \qquad (6.2)$$

where $E(C_{\text{mix}})$ is the effect expected at the total concentration of the mixture (scaled between 0 % and 100 %) and $E(C_i)$ is the effect that the ith mixture component would provoke if applied singly at concentration C_i.

The total concentration of a mixture causing x % effect ($EC_{x\text{mix}}$) was calculated from the CRC of the individual component using the CA model, as shown in Equation 6.3,

$$EC_{x\text{mix}} = \left(\sum_{i=1}^{n} \frac{P_i}{EC_{xi}}\right)^{-1} \qquad (6.3)$$

where P_i is the fraction of component i in the mixture and EC_{xi} is the concentration of component i that would result in x % effect if used alone.

Construction of datasets

Two datasets were constructed for the development and validation of the predictive models. The dataset was chosen not only to take into account data sample diversity (i.e., diversity of mixed components and mixed concentration ratios), but also to reduce the variability of inter-laboratory toxicity testing conditions. The first dataset (named internal dataset) consists of experimental data from our laboratory. The internal dataset consists of 12 data rows, consisting of the binary mixtures of four MO_X NPs (CuO, ZnO, TiO_2, and ZrO_2) at two different mixture ratios. The results of physicochemical analysis which included the assessment of the ζP and the D_H of MO_X NPs in

the single and binary mixture systems and the CRCs for the mixtures obtained from the *E. coli* toxicity testing and predicted by the IA and CA models are described in the Appendix.

The second dataset (named combined dataset) comprised both internal data and external data. The external data of the toxicity of 10 binary mixtures of five MO_X NPs (Al_2O_3, Fe_2O_3, SiO_2, TiO_2, and ZnO) to *E. coli* was collected from Kar et al. (2022). The binary nano-mixtures in the external dataset and the internal dataset have both different kinds of combinations and different mixture ratios of components between them. The external dataset was named Ext (*R*3) mixture. The combined dataset has a total of 22 data rows.

Calculation of mixture descriptors

A mixture descriptor (D_{mix}) is a weighted descriptor that quantifies how much each component contributes to the overall activity of a mixture (Altenburger et al., 2003). D_{mix} has been practically applied in the toxicity prediction studies of ENP mixtures (Kar et al., 2022; Trinh et al., 2022). D_{mix} is expressed by arithmetic mean (Equation 6.4):

$$D_{\text{mix}} = x_i D_i + x_j D_j \qquad (6.4)$$

where x_i and x_j are the mole fractions of constituent i and j in the mixtures, and D_i and D_j are descriptors of the individual MO_X NPs. The selected descriptors of the individual MO_X NPs and the calculated D_{mix} based on Equation 6.4 are shown in the Appendix Table S6.1 and Table S6.2, respectively. In the selection of descriptors for the individual MO_X NPs, we referred to the qualities summarized by Roy et al. (2015). Moreover, the selected descriptors are universal

descriptors, which are effectively used to construct QSAR models of individual MO_X NPs. Furthermore, these descriptors not only reflect the characteristics of nanostructures but also directly respond to toxicologically relevant properties. In details, there were eight descriptors of the individual MO_X NPs from three different types: two periodic table-based descriptors (electronegativity of metal atoms, χ_{me} and sum of metal electronegativity for an individual metal oxide divided by the number of oxygen atoms present in a particular metal oxide, $\Sigma\chi_{me/nO}$) derived from the publicly available periodic table information (Kar et al., 2014), two experimental descriptors (ζP and D_H) determined in our laboratory (CuO, ZnO, TiO_2, and ZrO_2 NPs) and obtained from a previous study (Al_2O_3, Fe_2O_3, SiO_2, TiO_2, and ZnO NPs) (Kar et al., 2022), three metal oxide energy descriptors including the enthalpy of formation of a gaseous cation having the same oxidation state as the oxidation state of the metal in the metal oxide structure (ΔH_{me+}) (Puzyn et al., 2011), the metal oxide standard molar enthalpy of formation (ΔH_{sf}) (Haynes, 2011), and the energy of the conduction band (E_C) (Zhang et al., 2012) of the nanoparticle, as well as the ionic index of the metal cation (Z^2/r) (Walker et al., 2003). Stepwise multiple linear regression in SPSS 23.0 was used to perform a preliminary screening of the descriptions obtained, and the *t* value was selected to determine the comparative importance of the descriptors on the toxic effect concentrations ($\log 1/EC_{50}$) of binary mixtures of MO_X NPs.

Machine Learning-based modeling

Two popular ML algorithms, namely SVM and NN, were used to develop the QSAR models for predicting the toxicity of binary mixtures of MO_X NPs. The datasets were divided into training (60 %

data) and test (40 % data) sets at random. For the SVM algorithm, the Gaussian radial basis function (RBF) was used. For the NN algorithm, the hyperbolic tan function for the hidden layer and the quasi-Newton method for weight optimization were applied. We used the data mining toolbox in Python for developing the ML-based predictive models (Demšar et al., 2013). To validate the models, the squared correlation coefficient (R^2) and the adjusted squared correlation coefficient (R^2_{adj}) between observed and predicted log1/EC_{50}, the root mean square error (RMSE), and the mean absolute error (MAE) of the training and test datasets were used. These statistical parameters are commonly used in current nano-QSAR studies and are widely accepted (Gajewicz et al., 2015; Kar et al., 2022; Trinh et al., 2022). Randomization tests proposed for testing the robustness of the selected models were performed using the metric $^cR^2_P$ (Kar et al., 2014). If the $^cR^2_P$ value is more than the stipulated threshold value of 0.5 then an acceptable model has been developed. The second-order bias-corrected Akaike Information Criterion (*AICc*) index as an additional statistical measure was employed on the full set to evaluate the relationship between variables. The *AICc* value was calculated using *R* software.

Applicability domain

The OECD principles of QSAR validation recommend that: *A (Q)SAR should be associated with a defined domain of applicability* (OECD, 2014). The function of the applicability domain (AD) is to define the compounds that can be reliably predicted by the QSAR model, which can also be understood as the set of compounds to which the model applies. The AD in this work was generated by using the Student's *t*-distribution on Euclidean distances (structural domain) and

standardized residuals (response domain) of a training dataset to define the space where accurate predictions can be made with a specified level of confidence (Gajewicz, 2018).

6.3 Results and Discussion

6.3.1 Toxicity of binary ENP mixtures

CRCs established for the binary mixtures of CuO, ZnO, TiO_2, and ZrO_2 NPs are shown in the Appendix Figure S6.1. Based on the curves, the log1/EC_{50} values were determined and these are summarized in Table 6.1.

Table 6.1. *Toxicity data of binary mixtures of MO_X NPs for the internal dataset* [a]

Mixture system of MO_X NPs	Observed log1/EC_{50} (mol/L)	Predicted log1/EC_{50} (mol/L)					
		QSAR models				Mixture models	
		S12	S31	N12	N31	IA	CA
Int ($R1$)							
CuO + ZnO NPs	2.72	2.68	2.70	2.72	2.72	2.85	3.05
TiO_2 + ZrO_2 NPs	2.10	2.14	2.13	2.10	2.10	2.32	2.44
ZnO + TiO_2 NPs	2.17	2.20	2.18	2.18	2.18	2.96	3.00
ZnO + ZrO_2 NPs*	2.30	2.23	2.14	2.37	2.37	2.39	2.54
CuO + TiO_2 NPs*	2.77	2.81	2.80	2.88	2.80	2.70	2.80
CuO + ZrO_2 NPs	2.29	2.25	2.27	2.29	2.29	2.30	2.46
Int ($R2$)							
CuO + ZnO NPs*	2.82	2.68	2.70	2.69	2.66	2.92	3.15
TiO_2 + ZrO_2 NPs*	2.11	2.14	2.13	2.11	2.10	2.32	2.44
ZnO + TiO_2 NPs	2.20	2.21	2.18	2.19	2.18	2.77	3.05
ZnO + ZrO_2 NPs	2.37	2.23	2.14	2.37	2.37	2.39	2.54
CuO + TiO_2 NPs	2.74	2.71	2.72	2.75	2.75	2.70	2.80
CuO + ZrO_2 NPs	2.14	2.21	2.18	2.14	2.15	2.31	2.41

[a] * *indicates the test data.*

For the binary mixtures with a certain mixture ratio, TiO_2 and ZrO_2 NPs induced the least toxicity in the combined exposure setting. Comparative analysis also revealed that the toxicity of CuO NPs combined with ZnO or TiO_2 NPs was higher than for other binary combinations.

6.3.2 Machine learning-based QSAR prediction

Based on the ML methods, 72 QSAR models integrating different D_{mix} (Figure 6.1) were developed. The performance of 36 SVM-and 36 NN-based QSAR models is shown in the Appendix Tables S6.3 and S6.4, respectively.

	χ_{me}							
χ_{me}	S1/N1	$\Sigma\chi_{me/nO}$						
$\Sigma\chi_{me/nO}$	S9/N9	S2/N2	ζP					
ζP	S10/N10	S16/N16	S3/N3	D_H				
D_H	S11/N11	S17/N17	S22/N22	S4/N4	ΔH_{me+}			
ΔH_{me+}	S12/N12	S18/N18	S23/N23	S27/N27	S5/N5	ΔH_{sf}		
ΔH_{sf}	S13/N13	S19/N19	S24/N24	S28/N28	S31/N31	S6/N6	E_C	
E_C	S14/N14	S20/N20	S25/N25	S29/N29	S32/N32	S34/N34	S7/N7	Z^2/r
Z^2/r	S15/N15	S21/N21	S26/N26	S30/N30	S33/N33	S35/N35	S36/N36	S8/N8

Figure 6.1. *SVM (S1–S36)- and NN (N1–N36)-based QSAR models prepared from the pool of different mixture descriptors. χ_{me} — metal electronegativity, $\Sigma\chi_{me/nO}$ — sum of metal electronegativity for individual metal oxide divided by the number of oxygen atoms present in particular metal oxide, ζP — zeta potential, D_H — hydrodynamic diameters, ΔH_{me+} — enthalpy of formation of a gaseous cation, ΔH_{sf} — metal oxide standard molar enthalpy of formation, E_C — nanoparticle energy of conduction band, and Z^2/r — ionic index of metal cation.*

We selected a good prediction model according to the following three criteria: (i) $R^2 \geq 0.81$ for *in vitro* data (Kubinyi, 1993); (ii) adjusted $R^2 > 0.60$ (Olasupo et al., 2020); (iii) the above two conditions need

to be satisfied not only for both the training and the test sets but also for both the internal and combined datasets, as well as for both the SVM- and NN-based models when applying the same descriptors. Among the developed QSAR models, two SVM-based models (S12 and S31) and two NN-based models (N12 and N31) performed comparably better than other models for both the internal and combined datasets. This also means that the selected QSAR models can reliably predict the toxicity of mixtures of individual MO_X NPs under multiple different experimental conditions.

Moreover, the predicted $\log 1/EC_{50}$ values by the good models (S12, S31, N12, and N31) are shown in Table 6.1 (the internal dataset) and in Table 6.2 (the combined dataset). The percental difference averaged between the experimental and predicted values by the selected models for the internal and combined datasets was 2.34, 2.50, 1.08, 1.04 and 7.16, 7.29, 2.87, 2.61 % respectively. In addition, the obtained ${}^{c}R^{2}_{P}$ values for the selected models via the Y-randomization test are higher than 0.5 (Appendix Tables S6.5 and S6.6), demonstrating that the models were not created randomly and that they are robust.

Experimentally determined $\log 1/EC_{50}$ are plotted against predicted $\log 1/EC_{50}$ for the internal and combined datasets (Figure 6.2 and Figure 6.3, respectively). The green dotted line indicates that the experimental and the predicted values correspond exactly. The bule straight line depicts a linear relationship between the experimental and predicted values based on the training sets.

Table 6.2. *Toxicity data of binary mixtures of MOx NPs for the combined dataset* [a]

Mixture system of MO_X NPs	Observed $\log 1/EC_{50}$ (mol/L)	Predicted $\log 1/EC_{50}$ (mol/L)			
		QSAR models			
		S12	S31	N12	N31
Int (*R*1)					
CuO + ZnO NPs	2.72	2.80	2.89	2.72	2.72
TiO_2 + ZrO_2 NPs	2.10	2.18	2.05	2.10	2.11
ZnO + TiO_2 NPs*	2.17	1.92	2.09	2.21	2.18
ZnO + ZrO_2 NPs	2.30	2.22	2.13	2.30	2.30
CuO + TiO_2 NPs	2.77	2.82	2.94	2.77	2.77
CuO + ZrO_2 NPs	2.29	2.27	2.47	2.27	2.26
Int (*R*2)					
CuO + ZnO NPs*	2.82	2.88	2.92	2.74	2.75
TiO_2 + ZrO_2 NPs*	2.11	2.18	2.05	2.11	2.11
ZnO + TiO_2 NPs	2.20	1.92	2.10	2.19	2.18
ZnO + ZrO_2 NPs*	2.37	2.22	2.13	2.30	2.30
CuO + TiO_2 NPs*	2.74	2.27	2.58	2.05	2.50
CuO + ZrO_2 NPs	2.14	2.22	2.31	2.17	2.19
Ext (*R*3)					
Al_2O_3 + ZnO NPs	4.26	3.93	3.88	4.26	4.26
Al_2O_3 + Fe_2O_3 NPs	2.06	2.14	2.01	2.06	2.07
Al_2O_3 + SiO_2 NPs*	1.71	1.86	1.85	1.88	1.54
Al_2O_3 + TiO_2 NPs	1.70	1.95	1.87	1.71	1.70
ZnO + Fe_2O_3 NPs	3.89	3.81	3.72	3.89	3.89
ZnO + SiO_2 NPs	4.13	3.62	3.57	4.13	4.13
Fe_2O_3 + SiO_2 NPs	2.25	2.17	2.08	2.25	2.25
Fe_2O_3 + TiO_2 NPs*	1.99	1.75	2.10	1.72	2.28
SiO_2 + TiO_2 NPs	1.80	1.88	2.01	1.81	1.80
ZnO + TiO_2 NPs*	4.59	3.76	3.69	4.46	4.01

[a] * *indicates the test data.*

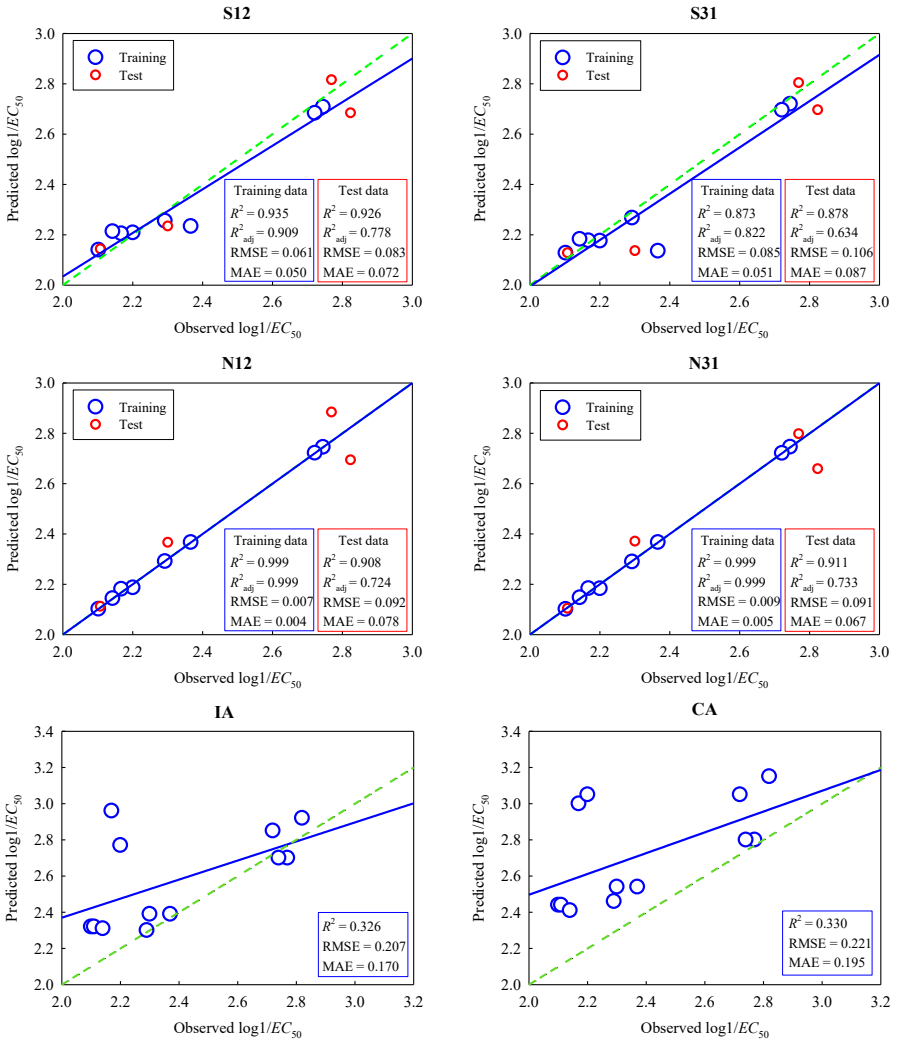

Figure 6.2. *Performance of the selected SVM- and NN-based QSAR models and the component-based mixture models developed based on the internal dataset.*

In general, the selected QSAR models exhibited good agreement ($R^2 \geq 0.81$) between the observed and predicted toxicity for the binary mixtures of MO_X NPs from the training set (blue circle) and those from the test sets (red circle). It can also be seen that the lines of the regression for the N12 and N31 models overlap with the line of

perfection, implying that the NN-based models showed better consistency between the experimental and predicted values compared to the SVM-based models. Furthermore, the percental difference averaged between the experimental and predicted values by the NN-based models was 2.17–2.40 and 2.49–2.79 times lower than the percental difference averaged between the experimental and predicted values by the SVM-based models in the internal (Appendix Table S6.7) and combined datasets (Appendix Table S6.8), respectively. Note that the N31 model had the lowest average difference between the experimental and predicted values among the selected QSARs.

In addition, the results for the statistics of the selected models are shown in the insets of Figures 6.2 and 6.3. In the internal dataset (Figure 6.2), the S12 model with higher R^2_{adj} and lower RMSE and MAE performed better than the S31 and N12 models for predicting the test data. In addition to this, the NN-based models showed better than the SVM-based models for predicting both the training and test data. Further comparisons revealed that the N31 model with higher R^2_{adj} and lower RMSE and MAE performed better than the N12 model for predicting the test data. In the combined dataset (Figure 6.3), the NN-based models with higher R^2_{adj} and lower RMSE and MAE outperformed the SVM-based models for both the training and test data. Of the four models validated, the N31 model with the highest R^2_{adj} and the lowest RMSE and MAE had the best performance capability for predicting the test data.

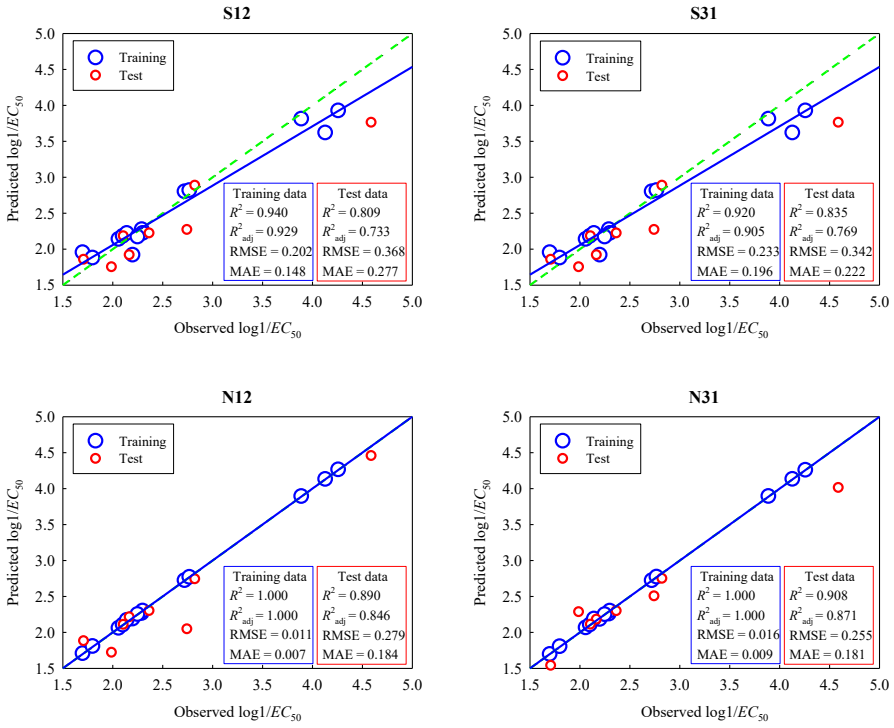

Figure 6.3. *Performance of the selected SVM- and NN-based QSAR models developed based on the combined dataset.*

Current research on biological effect prediction also indicates that NN-based models outperform SVM-based models empirically resulting from the training process and overall data prediction (Almansour et al., 2019; Bennett-Lenane et al., 2022), while other studies have shown that the SVM-based modeling approach often shows a better performance than the NN-based approach (X. Li et al., 2021; Zhao et al., 2006). In theory, both ML algorithms have advantages and disadvantages. This is reflected in that the training time for NN-based technique is higher than the training time for SVM, while the prediction time for NN models is generally lower than for SVM models. Taken together, the performance indicators of the

selected QSARs indicate that both the NN and the SVM were practical tools for the prediction of the toxicity of mixtures of ENPs.

To compare the differences between the developed QSAR models and the classical mixture models in predicting the toxicity of mixtures of MO_X NPs, we also constructed the IA and CA prediction models (Appendix Figure S6.1). As shown in Figure 6.2, the selected QSAR models gave better predictions of $\log 1/EC_{50}$ ($R^2 \geq 0.873$) compared to those models based on mixture modeling making use of IA (R^2 = 0.326) and CA (R^2 = 0.330). This implies that the QSAR models are low-cost approach to risk assessment of multiple ENP mixtures, due to the fact that the QSAR models do not need concentration-response information on each mixture component as with the commonly applied mixture models either using IA or CA. For the CuO + ZrO_2 NPs mixture at ratio 1 and the ZnO + ZrO_2 NPs mixture at ratio 2, the percental difference averaged between the experimental and predicted values by the IA model was lower than the percental difference averaged between the experimental and predicted values by the SVM-based models (Appendix Table S6.7). This means that for a particular mixture the mixture model has the ability to predict the toxicity of the mixture of MO_X NPs.

The mixture model has become a prevailing approach for the quantitative prediction of mixture toxicity with concentration addition being a conservative measure of addition of stress and independent action as assuming induced effects not at the same target and affecting a percentage at the overall response, which strengthens the theorization from the basic principles of mixture toxicology. However, the interactions between the joint chemicals are not taken into consideration in the mixture models. Especially, the

distinctive physicochemical features of ENPs, which have a high surface area for adsorption, may hinder the mixture models from accurately estimating the toxicological effects of mixtures containing ENPs (Martinez et al., 2022). A previous study indicated that the IA and CA models did not perform well in predicting the toxicity of mixtures comprising TiO_2 NPs and other pollutants to *Daphnia magna* (Trinh et al., 2022). Thus, it is reasonable to assume that the ML-integrated QSAR approach can be considered a highly promising tool for the assessment of the toxicity of a mixture of multiple ENPs.

6.3.3 Applicability domains of QSAR models

The AD of a QSAR is the physicochemical, structural, or biological space, knowledge or information on which the training set of the model has been developed, and for which it is applicable to make predictions for new compounds (Jaworska et al., 2005). The AD of the SVM-based models (S12 and S31) and NN-based models (N12 and N31) constructed from the internal and combined datasets is shown in Figures 6.4 and 6.5, respectively. The light and dark green elliptical boundaries correspond to the 95 and 99 % confidence intervals, respectively. Reliable predictions can only be generated within these confidence intervals. In the internal dataset (Figure 6.4), all the training data fall inside the 95 % confidence area, while two test data for the S12 model and only one test data for the S31 and N31 models falls between 95 % and 99 % confidence area. In the combined dataset (Figure 6.5), all the training and testing data fall inside the 95 % confidence area. Generally, all the studied binary mixtures of MO_X NPs were located within the 99 % confidence area of the selected QSAR models. Thus, the mixture toxicity predictions for each training and test mixtures of MO_X NPs are highly reliable for the selected

QSAR models. This suggests that the QSAR models can be used to predict the toxicity of any other binary combinations of MO_X NPs, especially because the predominant first-generation ENPs are within this training set as well as the mechanistically relevant descriptors.

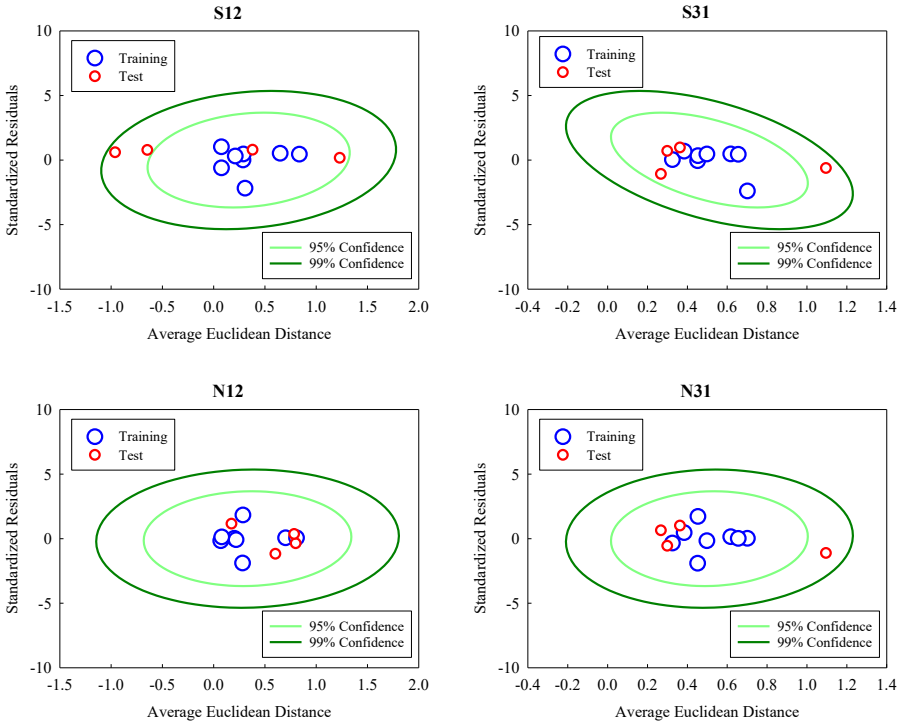

Figure 6.4. *Applicability domains of the selected SVM- and NN-based QSAR models developed based on the internal dataset.*

A QSAR model should have a well-defined AD to reflect its reliability in order to be applicable for chemical assessment and management. The dataset with 22 binary combinations has proven to be large and robust to effectively built ML-driven QSAR models for toxicity prediction. This is in line with previous conclusions confirming that ML-assisted QSAR models has good predictive power for relatively small datasets (Gajewicz et al., 2015; Puzyn et al., 2011; Zhong et al.,

2022b). These findings do give prospects of application to move the field on mixture toxicity predictions further especially when ENPs mixtures are considered in which chemicals as well as particles influence fate and responses.

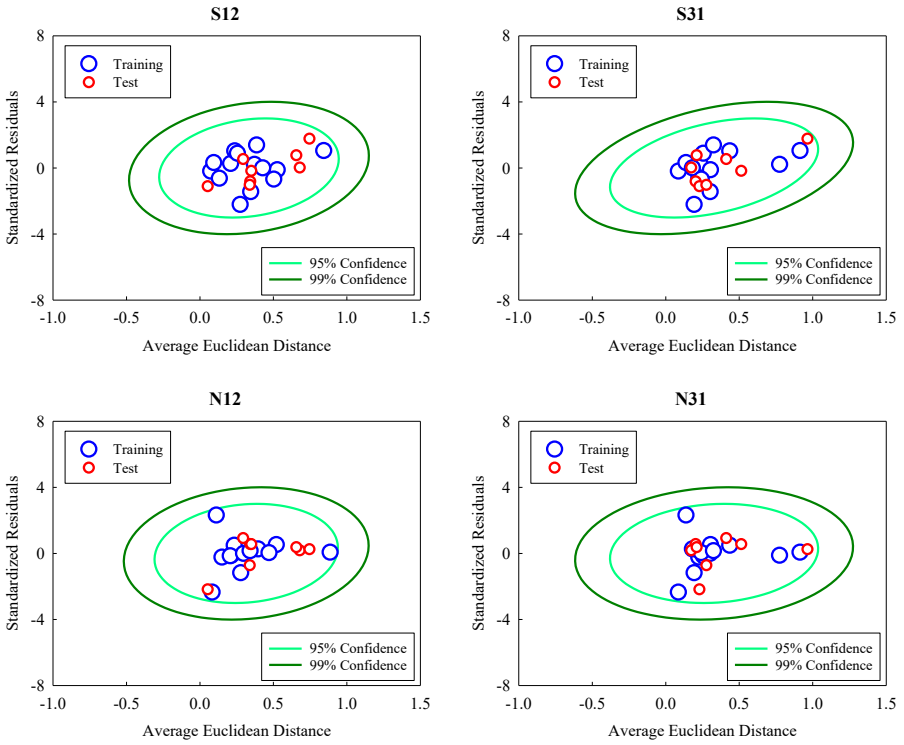

Figure 6.5. *Applicability domains of the selected SVM- and NN-based QSAR models developed based on the combined dataset.*

The characterization of the AD reflects the dependence of a QSAR model on training data (Zhong et al., 2022a). Thus, only nanostructured materials that are similar to the ENPs constituting the training set, can be reliably predicted. While artificial intelligence, ML, and big data analytics provide powerful algorithms and tools for QSAR modeling, high-quality toxicity data remain the driving force

for constructing QSAR models for the prediction of the toxicity of nano-mixtures. Therefore, further research needs to expand the amount of high-quality data available on the toxicity of mixtures of ENPs in the training set and enlarge the AD of QSAR models.

6.3.4 Importance of descriptors and mechanistic knowledge

Appendix Table S6.9 shows the comparative importance of the proposed descriptors for the toxicity prediction of binary mixtures of MO_X NPs. The magnitude of the relative importance of ΔH_{sf} (62 %) and ΔH_{me+} (47 %) is the highest in the internal and combined datasets studied respectively, suggesting that the two descriptors are very important in explaining the QSAR models. As an efficient descriptor, ΔH_{me+} was previously employed to explain the cytotoxicity of MO_X NPs to *E. coli* based on their chemical stability. The chemical stability of MO_X NPs is associated with the release of metal cation from the particles as well as the catalytic properties and redox modifications of the surface (Puzyn et al., 2011). For a given size, ΔH_{sf} might be also used as an indicator of "the ability of releasing metal cation", since it is proportional to the energy of a single metal-oxygen bond in the oxides (Gajewicz et al., 2015). The cellular damage caused by MO_X NPs may be attributed to the release of metal cations. The metal ions present in suspension can not only chelate with specific ligands of biological macromolecules to affect the toxicity of MO_X NPs to biological cells, but also can instigate the generation of free radicals such as hydroxyl radicals in both cells and mitochondria, causing DNA and mitochondrial DNA breakage (Roy et al., 2019).

In addition, χ_{me} was a significant descriptor in developing the S12 and N12 models, and indicates the energy needed to separate the metal

cation from the metal oxides as part of the mechanisms underlying the toxic effects of the metal oxides. MO_X NPs with a higher χ_{me} tend to gain electrons from the bonding pair of the electrons. This indicates an increase in the catalytic capabilities of cationic metal (Roy et al., 2019). Thus, the toxicity of MO_X NPs may be enhanced in accordance with the Haber-Weiss-Fenton cycle (Koppenol, 2001). χ_{me} is also independent of the size range of MO_X NPs (Kar et al., 2014). Following the release of metal cations, redox interactions with the molecules in biological media frequently result in the production of reactive oxygen species (ROS) (Puzyn et al., 2011). Thus, the released cations themselves, ROS-induced oxidative damage, or both may be responsible for the observed cytotoxicity. Our results indicated that these descriptors could indicate possible mechanism for the mixture toxicity of individual MO_X NPs. What is more, the descriptors used in the models are well-defined and can be derived quickly from the chemical composition information (χ_{me}) and chemical stability (ΔH_{me+} and ΔH_{sf}).

The *AICc* values were further applied to evaluate the relationship among the proposed descriptors (χ_{me}, ΔH_{me+}, and ΔH_{sf}). As shown in the Appendix Table S6.10, in both the internal dataset and the combined dataset, the *AICc* value of the model developed by applying ΔH_{me+} and ΔH_{sf} was the smallest among all the models combined with the binary descriptors. This indicates that the fitting ability of the model incorporating ΔH_{me+} and ΔH_{sf} was higher than the fitting ability of the other models using the combination of two descriptors. This is generally consistent with the results of the screening and comparative analysis regarding the performance of ML models as described previously. The models developed by applying ΔH_{sf} and

ΔH_{me+} to the internal and combined datasets, respectively, had the lowest *AICc* (Appendix Table S6.10). However, the predictive power of the ML models developed by both single descriptors cannot ensure equal predictive power for the internal dataset and the combined dataset (Appendix Tables S6.3 and S6.4).

Furthermore, we found that the *AICc* values of models developed by the combination of three descriptors (χ_{me}, ΔH_{me+}, and ΔH_{sf}) were the highest in the internal dataset, while the *AICc* values of the models developed by the combination of three descriptors in the combined dataset were higher than those of the models developed by the single descriptor (ΔH_{me+}) and the combination of ΔH_{me+} and ΔH_{sf} (Appendix Table S6.10). This implies that applying more descriptors (n = 3) to the model in this study could not significantly improve the predictive performance of the model. Furthermore, using fewer descriptors in QSAR analysis not only allows for avoiding over-fitting, but also establishes meaningful models with understandable chemical mechanisms (Wang and Chen, 2020). Thereupon, the suggested QSAR models with few utilized nano-descriptors can be regarded as robust and simple to use for predicting the mixture toxicity of ENPs.

6.4 Conclusions

Our results show that the ML methods present unprecedented opportunities and challenges for the assessment of the mixture toxicity of ENPs. The nano-QSAR models that we developed and validated, outperformed conventional mixture models. The χ_{me}, ΔH_{me+}, and ΔH_{sf} were found to be the key nano-descriptors capable of predicting the mixture toxicity. At the present stage, the synthesis of new NMs and the advanced complexity of materials has a more rapid

pace than the science to predict the fate and effects of those complexes and mixtures of ENPs. Knowledge on the mixture impacts of various shaped and chemically diverse ENPs as well as the evaluation of the environmental hazards of combinations of ENPs is a necessity to work on.

Acknowledgements

The research described in this work was supported by the National Natural Science Foundation of China (grant number 31971522) and by the European Union's Horizon 2020 research and innovation program via the projects "NanoinformaTIX" (grant number 814426). Martina G. Vijver acknowledges the support of the ERC-C grant entitled EcoWizard no. 101002123. Fan Zhang greatly acknowledges the support from the China Scholarship Council (grant number 202008320308).

Chapter 7

General Discussion

Assessing the ecological risks of novel entities is essential for the protection of human health and environmental health. When multiple novel entities act simultaneously on organisms, they often cause toxic responses that are quite different from the effects of a single novel entity. However, due to the complexities of interactions between multiple novel entities, progress in understanding their combined impacts remains slow. Most traditional assessments of chemical toxicity effects have relied on *in vivo* and *in vitro* tests of biological toxicity. Since novel entities (e.g., engineered nanoparticles, ENPs) exhibit a high degree of complexity in terms of physicochemical properties, quantum mechanical properties, and toxicological effects, their risk evaluation is gradually shifting to *in silico* approaches based on understanding of the toxicity mechanisms. In order to avoid testing each novel entity from scratch, there is an urgent need to develop a series of *in silico* models to predict the environmental fate and biotoxic effects of novel entities.

This thesis aims to reveal the mechanisms of interaction between micro- and nanoparticles (MNPs) and other novel entities, investigate the impact of such interactions on the environmental behavior and effects of novel entities, and assess and predict the combined toxicity of ENPs and other novel entities to ecological species. First, we investigated the interaction mechanisms between carbon-based nanoparticles (CNPs) and a severe acute respiratory syndrome coronavirus 2 (SARS-CoV-2) ribonucleic acid (RNA) fragment and we developed quantitative structure-activity relationship (QSAR) models to predict this interaction. Second, we revealed the interaction mechanism between microplastics (MPs) and a SARS-CoV-2 RNA fragment and its influencing factors. Third, we clarified the modes of

action and influencing factors of the combined toxicity of multiple ENPs to ecological species. Finally, we developed QSAR models based on machine learning (ML) methods to predict the ecotoxicity of mixtures of binary metal oxide nanoparticles (MO_X NPs).

7.1 Solved research questions and environmental implications

To achieve the aims described above, this thesis answered four questions to promote the understanding of the interaction between different novel entities and the impacts of the interaction on the environmental behavior and biological effects of novel entities.

7.1.1 Interaction and mechanisms of ENPs with SARS-CoV-2 macromolecules

We found that the interaction mechanism between CNPs and a SARS-CoV-2 RNA fragment is driven by electrostatic interactions through molecular mechanics simulation studies. Furthermore, we found that molecular weight, surface area, and the sum of degrees of every carbon atom as the primary structural descriptors determined the interaction between the CNPs and the SARS-CoV-2 RNA fragment. The above findings suggest that the interaction between CNPs and biomolecules mainly depends on the intrinsic properties of CNPs, especially their surface properties. CNPs have a high specific surface area, which leads to a large number of surface atoms or molecules that can interact with biomolecules.

At the same time, we found that the order of magnitude of the interaction force between the CNPs and the SARS-CoV-2 RNA fragment was: carbon nanotubes > graphene > fullerene. This also

indicates that the surface properties of CNPs are affected by various factors, such as size, shape, surface charge, hydrophobicity and chemical composition. For example, ENPs with a large surface area, high surface energy, and hydrophobicity tend to adsorb RNA and other biomolecules (e.g., proteins), leading to the formation of nanoparticle-RNA or -protein coronas on the surface of ENPs. Existing studies confirm that the formation of eco-coronas (Liu et al., 2023; Wheeler et al., 2021), represented by protein coronas, can alter the physicochemical properties of ENPs and affect their toxicity (Ekvall et al., 2021). Eco-coronas can reduce the surface charge and increase the hydrophilicity of ENPs, leading to changes in their cellular uptake, biodistribution and toxicity (Chakraborty et al., 2021; Diaz-Diestra et al., 2022). Eco-coronas may also modulate the interaction of ENPs with cell membranes and intracellular organelles (Feng et al., 2023; Liu et al., 2022), leading to alterations in their intracellular fate and toxicity.

In addition, such interactions may also have affected the structure or stability of viral RNA. In terms of viral migration and exposure, the interaction between ENPs and viral RNA may have positive effects. For example, ENPs may interfere with the ability of the virus to enter cells, replicate, or spread throughout the body (Bhatti and DeLong, 2023; Campos et al., 2020; Li et al., 2023). This may reduce the severity of infection or prevent it from occurring altogether. Furthermore, the effect of ENP-viral RNA interactions on viral migration and exposure would depend on the specific characteristics of the ENPs and the virus.

7.1.2 Interaction and mechanisms of MPs with SARS-CoV-2 macromolecules

We found that the interaction mechanism between MPs and SARS-CoV-2 RNA fragments involves electrostatic and hydrophobic processes through molecular dynamics simulation studies. Moreover, the affinity of the interaction was related to the intrinsic structural parameters of the MP monomer (i.e., molecular volume, polar surface area, and molecular topological index). It can be seen that the surface properties of MPs make biomolecules to attach to the surface of MPs. This also implies that MPs may be an important homing site for biomolecules. We also found that for the SARS-CoV-2, the interaction force between MPs and their RNA fragments was stronger than the interaction force between MPs and their nucleocapsid proteins. However, for the Hepatitis B virus (HBV), the MPs showed stronger interactions with the nucleocapsid protein than with its RNA fragment. This also suggests that the interaction between the MPs and the viral biomolecules is closely related to the type of microorganism.

The interaction between MPs and biomolecules is a complex process that can have a range of impacts on their environmental behavior and biological toxicity (Junaid and Wang, 2022; Luo et al., 2022). First, this interaction could alter the physical properties of MPs, such as surface charge, hydrophobicity, and aggregation, leading to changes in their transport and distribution in the environment. Second, the adsorption of biomolecules on MPs could affect their biological interactions with organisms. For example, the adsorption of proteins on MPs can alter the bioavailability and toxicity of MPs to organisms (Cao et al., 2022). Finally, the adsorption of biomacromolecules on

MPs could affect the fate and persistence of MPs in the environment, similar to nanomaterials (Lowry et al., 2012). MPs with adsorbed biomacromolecules may be more resistant to degradation and biofouling, making their long-term persistence in the environment more likely. Thereupon, understanding the mechanisms of interaction between MPs and biomolecules is essential for developing effective strategies to mitigate their environmental impacts and protect human and ecological health.

Currently, viral infections remain a major public health concern and the potential role of MPs in facilitating virus transmission and exposure is an area of active research. The small size of MPs may allow them to serve as carriers for transporting viral particles (Lu et al., 2022; Zhai et al., 2023). For instance, a recent study found that MPs in wastewater can carry SARS-CoV-2 (Belišová et al., 2022). This thesis also found that the high surface area of MPs and their ability to adsorb the biomolecules of SARS-CoV-2 may make them effective carriers of viral particles.

The effect of MPs on virual transmission and exposure may also depend on environmental factors. The present findings in this thesis reveal that MPs interact stronger with viral RNA fragments in an aqueous environment than in the gas phase. Previous studies have also found that the presence of MPs in water may increase the likelihood of virus particles surviving and remaining infectious (Amato-Lourenço et al., 2022; Moresco et al., 2021), but MPs may also decrease the concentration in air of virus particles by adsorbing them to the MP surface. The interaction of MPs with viral RNA may also be influenced by a range of other environmental factors, including temperature, pH, and the presence of other contaminants.

7.1.3 Joint interactions after exposure of ecological test species to multiple ENPs and factors determining the toxicity of a mixture of multiple ENPs

When multiple novel entities are present in the environment, they exert effects on ecological species (including algae, bacteria, Daphnia, fish, fungi, insects and plants) via different modes of action. Taking mixtures of multiple ENPs as an example, we found that in studies specifying the combined toxic response of mixtures of ENPs, 53 % showed antagonistic effects, 25 % synergistic effects, and 22 % additive effects. From this result, it is clear that the interactions between multiple ENPs are mainly antagonistic. This implies that if multiple ENPs coexist in the environment, their combined effects on ecological species will be smaller than the effects when each of them is present alone. However, the synergistic effects exhibited among multiple ENPs cannot be ignored. The synergistic effects occur so that the presence of multiple ENPs can have a greater effect on ecological species compared to exposure to each pollutant individually.

The combined toxic effects of multiple novel entities on ecological species depend on many factors. This thesis reveals that the main factors influencing the type of combined toxic response of biota to exposure to mixtures of ENPs are 1) the chemical composition of the individual components of the mixture, 2) the stability of the suspension of mixed ENPs, 3) the type and trophic level of the individual organisms tested, 4) the level of biological organization (population, community, and ecosystem), 5) the exposure concentration and exposure duration, 6) the toxicity endpoints, and 7) abiotic scenario conditions (e.g., pH, ionic strength, natural organic matter).

Specifically, different combinations of ENPs have different toxic effects on ecological species, and their joint effects may be influenced by their exposure concentrations in the environment. The concentration of a mixture component may be influenced by the source of the ENP mixtures and the environmental conditions which affect their distribution and transport (Buzea et al., 2007). Another factor that affects the joint toxic effects of multiple ENPs is the exposure pathway. Ecological species can be effectively exposed to mixtures of ENPs through a variety of routes, such as inhalation, ingestion, and dermal contact. Exposure routes affect the toxicity levels of mixtures of ENPs and the extent of their effects on ecological species. Duration of exposure is one factor that affects the toxic effects of multiple ENPs. Short-term exposure to mixtures of ENPs can have different effects on ecological species compared to long-term exposure (Jośko et al., 2022). Long-term exposure to low levels of ENPs can lead to chronic toxicity that may not be immediately apparent, but can have cumulative effects over time. The sensitivity of ecological species to mixtures of ENPs is also an important factor affecting their joint toxic effects. Additionally, environmental conditions, such as temperature, pH, and solution parameters, can also affect the distribution and transport of ENPs in the environment, as well as their persistence and bioavailability, and thus their joint effects on ecological species. Understanding the interactions of multiple ENPs and their joint toxic effects is critical to developing effective strategies to prevent and mitigate pollution and to protect the environment and ecological species.

7.1.4 Development of QSAR models based on ML approaches for predicting the mixture toxicity of multiple ENPs

In this thesis, a ML-based QSAR method was established to quantitatively predict the cytotoxicity of a mixture of binary ENPs against *Escherichia coli*, using MO_X NPs as a case. The QSAR model based on support vector machine and neural network methods was found to exhibit good predictive power for both the constructed internal dataset and the combined internal and external datasets. It is thus seen that the combination of ML and QSAR methods provides several advantages for predicting the toxicity of ENPs. These include:

1) Accurate predictions: ML models can identify complex relationships between nanostructure and toxicity, which can lead to more accurate toxicity predictions than traditional QSAR models.

2) Improved efficiency: ML models can analyze datasets quickly and efficiently, saving time and resources compared to traditional QSAR modeling.

3) Ability to handle large data: With the rapid growth of nano-toxicological data, ML techniques can effectively handle large and complex datasets with high dimensionality.

4) Generalizability: ML models can learn patterns from a large number of different nanostructures, making them more generalizable to new ENPs.

5) Flexible modeling: ML models can be tailored to specific toxicological endpoints and can handle complex nonlinear relationships, allowing the development of models that can predict a

wide range of toxicological endpoints.

However, there are still areas for improvement in ML-based QSAR models used to predict the toxicity of ENPs. Some of these areas include:

1) Data quality: The quality and reliability of the nanotoxicological data used to develop and validate ML models are critical to their accuracy and reliability. Further improvements in data quality are necessary to ensure the validity and reproducibility of these models.

2) Interpretability: The interpretation of ML models can be challenging and complex, which may limit their utility in regulatory decision making. Developing methods to improve the interpretability of these models is thus critical.

3) Nanostructure diversity: Many ML models are based on a relatively small subset of nanostructures. More studies are required to ensure that these models can accurately predict the toxicity of a broader range of nanostructures. Consequently, further work is needed to demonstrate the reliability and robustness of these models for use in regulatory decision making.

In short, methodologies for assessing and predicting the mixture toxicity of multiple novel entities are lagging far behind the rapid emergence of new chemicals. Big data, deep learning, and artificial intelligence present unprecedented opportunities and challenges for assessing the toxicity of mixtures of novel entities. The models developed in this thesis show that our research approach can provide a methodological and theoretical basis for ecological risk assessment

of mixtures of novel entities.

7.2 Future risk and hazard assessment of novel entities and their mixtures

7.2.1 Ecological risk assessment of multiple novel entities

Today, scientists recognize that novel entities require global environmental attention because the majority of man-made chemical "novel entities" have been reported to enter the environment and most likely in future MNPs have the potential for lasting impact, large-scale distribution, and influence on important Earth system processes. Advances in synthesizing MNPs is also occurring at a rapid pace. Therefore, risk assessment of novel entities is a critical step in ensuring the safety of chemical products, the environment and public health. It involves identifying, assessing, and quantifying the potential risks posed by chemical substances present in a variety of environments, such as water, air, and soil. The risk assessment process for novel entities could learn from the traditional chemical risk assessment process (Van Leeuwen et al., 1996), which comprises of the stages listed below:

1) Hazard identification: The potential hazards associated with chemicals are identified and described. This involves the collection and analysis of data on toxicity, exposure, and other relevant factors that might have negative health consequences.

The general paradigm of comparing exposure to hazards, also applies to novel entities albeit that it is essential to base hazard and exposure on the same metrics of exposure (number, surface area, mass concentration, etc.).

2) Exposure assessment: The extent and frequency of exposure to chemicals in the environment or related products are determined. This involves collecting data on sources, routes, and levels of exposure.

The classical chemicals are usually dealt with homogeneous solutions. However, in case of novel entities such as ENPs and MPs, we often deal with non-stable suspensions. This requires a different approach to assessment of the effective exposure and the assessment of bioavailability of the novel entities.

3) Dose-effect assessment: The relationship between the exposure dose of chemicals and their adverse health effects is assessed. This involves assessing toxicological data and establishing dose-effect relationships.

In addition to the exposure dose or concentration, the physicochemical properties (particle size, surface charge, etc.) of novel entities such as ENPs and MPs have a significant impact on their toxic effects on ecological species. Therefore, establishing the relationship between the physicochemical properties of novel entities and their effects would help to determine their biological toxicity quickly. Besides, the toxic effects of novel entities are also closely related to abiotic factors (pH, divalent cations, natural organic matter, etc.). Thereupon, the impacts of abiotic factors need to be considered when establishing the dose/concentration-effect relationships of novel entities.

4) Risk characterization: The information gathered in the previous steps to assess the overall risk posed by the chemicals is integrated. This includes assessing the likelihood and severity of

adverse effects and determining appropriate risk management measures.

A series of assessment standards and rules, index parameters, testing tools and methods for the risk management of novel entities need to be proposed. Furthermore, advanced analytical and testing technologies combined with *in silico* methods need to be used for detection, exposure assessment, hazard and risk identification of novel entities.

How to implement a scientific, systematic and comprehensive risk assessment of novel entities is an important topic for future environmental toxicology research. A powerful and extremely practical strategy for accelerating the evaluation process is the establishment of reliable assessment procedures. Moreover, essential information on risk management measures would be provided, including setting exposure limits, establishing regulations, and implementing control measures.

7.2.2 Developments in toxicity prediction for novel entities and their mixtures

The novel entities in the environment are diverse in nature and are associated with complex distribution patterns, bringing about complex ecological and environmental health effects. With the advancement of modern society and global economy, new chemicals are constantly produced and applied, and inevitably constantly released into the environment. The novel entities released into the environment are in the form of mixtures of monomers or complexes, and there are complex interactions between different novel entities such as antagonism and synergism. The study of the biological

activities of different combinations of novel entities and their joint effects is a difficult and hot research area for the international environmental science community. Therefore, the complex effects of the coexistence of multiple novel entities bring new opportunities and new challenges to environmental health research.

Development of advanced prediction methods

Chemical toxicity prediction is an important task in the fields of drug discovery, environmental protection and public health (Alves et al., 2018; Pérez Santín et al., 2021). To date, advanced methods for chemical toxicity prediction are emerging, such as QSAR models (Chen et al., 2017), ML models (Balraadjsing et al., 2022), and deep learning models (M. Xu et al., 2022), which can not only analyze the chemical structures of compounds but also predict their toxicity with high accuracy. These methods are based on the principle that the molecular structural characteristics of a chemical determine its biological activity, including its toxicity.

Advanced *in silico* methods for chemical toxicity prediction have the potential to revolutionize the field of toxicology. *In silico* predictions have the ability to handle large and complex datasets. Moreover, in contrast to traditional component-based toxicity prediction methods, *in silico* methods can provide accurate and interpretable chemical toxicity predictions that can help researchers and policy makers to make informed decisions about the safety of chemicals. More importantly, *in silico* methods can provide insight into the molecular properties that contribute to chemical toxicity. This information can be used to design safer and more effective drugs or chemicals.

For the purpose of environmental risk management of novel entities

and their mixtures, future research can develop classification and cross-comparison analogy techniques for novel entities and their mixtures by using ML algorithms such as classification-based fuzzy clustering, decision trees, and support vector machines. Meanwhile, further research can develop QSAR models for toxicity prediction of novel entities and their mixtures by utlizing nanostructure-based molecular mechanics/dynamics, Monte Carlo, quantum chemistry, and other molecular simulation methods. A complete system of intelligent detection strategies for ecotoxicological risk assessment of novel entities (including mixtures) is likely to be established in future by using *in silico* methods.

Constructing a toxicity prediction platform

Screening and assessing the toxicity effects of emerging novel entities as they are identified, is important to avoid the release of high-risk novel entities into the environment to produce more serious hazards. To quickly and accurately determine the biological toxicity effects of novel entities and their mixtures, it is necessary to develop a computer-based platform for predicting the environmental behavior and toxicity of novel entities (Figure 7.1).

The establishment of a toxicity prediction platform for novel entities (including mixtures) involves the development of a system that can accurately predict the toxicity of novel entities based on their molecular structure and properties. With the use of this platform, it is possible to evaluate any risks that could come with exposure to novel entities and to identify safer alternatives for use in various industries, including pharmaceuticals, agriculture, and consumer products. As an example of the process of building a mixture toxicity prediction

platform for multiple novel entities, the platform building process consists of the following:

1) Data collection: A process of collecting a great deal of data on the chemical structure and properties of various novel entities, as well as information on their single and combined toxic effects. These data can be obtained from various sources, including experimental studies, toxicological databases, and published literature.

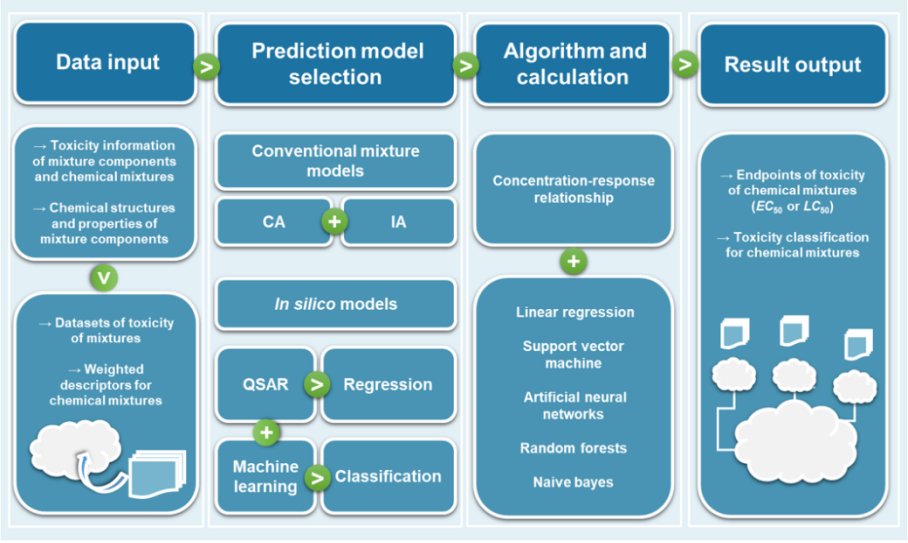

Figure 7.1. *Schematic diagram of the construction of a toxicity prediction platform for novel entities and their mixtures.*

2) Predictive model selection: Based on the completeness and richness of the collected toxicity data of mixtures of novel entities, the basic methodologies for building predictive models are selected, i.e., traditional mixture models based on mixed components and QSAR and ML models based on computational methods.

3) Predictive model development and validation: Analysis with computational methods to identify patterns and associations between

chemical structure and toxicity is carried out. This analysis typically includes the use of ML algorithms that are trained on the collected data to develop predictive models that accurately predict the toxicity of novel entities based on their molecular structures and properties. These predictive models are then validated using additional experimental data to ensure that they are accurate and reliable. This validation process typically involves comparing the predicted toxicity of the novel entities with the actual toxic effects measured in laboratory studies. To improve the accuracy and reliability of the predictive models, additional data can be included in the analysis, including information on the metabolic pathways and biological targets of the novel entities, as well as their physical and chemical properties.

4) The output of results: Once the predictive models have been validated, they can be integrated into a user-friendly platform that researchers and industry experts can use to evaluate the toxicity of the novel entities and to identify safer alternatives. This platform could include various features such as a user-friendly interface, customizable search capabilities, and interactive visualization tools.

To sum up, building a toxicity prediction platform for novel entities (including mixtures) requires a multidisciplinary approach that combines expertise in chemistry, toxicology, computational methods, and data analysis. By accurately predicting the toxicity of novel entities (including mixtures), the constructed platform can help reduce the single and joint risks associated with exposure to hazardous novel entities and promote the development of safer and more sustainable chemical products. This thesis brings the scientific community as a well as policymakers and industrial stakeholders new

information such as theoretical models and computational simulations were used to combine cytotoxicity experiments and data to understand and predict interactions between MNPs and novel entities. Within the thesis the interaction of MNPs of different dimensions with the SARS-CoV-2 RNA fragment only was investigated, but it can be used as a reference for exploring the interaction of MNPs with other RNA-based fragments. Similarly the work on the mixture and interaction models developed for metallic ENPs would also be the basis for the modeling of hybrid and other advanced metal-bearing ENPs.

References

Aasi, A., Aghaei, S.M., Moore, M.D., Panchapakesan, B., 2020. Pt-, Rh-, Ru-, and Cu-single-wall carbon nanotubes are exceptional candidates for design of anti-viral surfaces: A theoretical study. Int. J. Mol. Sci. 21, 5211. https://doi.org/10.3390/ijms21155211.

Abbas, Q., Liu, G., Yousaf, B., Ali, M.U., Ullah, H., Ahmed, R., 2019. Effects of biochar on uptake, acquisition and translocation of silver nanoparticles in rice (*Oryza sativa* L.) in relation to growth, photosynthetic traits and nutrients displacement. Environ. Pollut. 250, 728–736. https://doi.org/10.1016/j.envpol.2019.04.083.

Abbas, Q., Yousaf, B., Amina, Ali, M.U., Munir, M.A.M., El-Naggar, A., Rinklebe, J., Naushad, M., 2020. Transformation pathways and fate of engineered nanoparticles (ENPs) in distinct interactive environmental compartments: A review. Environ. Int. 138, 105646. https://doi.org/10.1016/j.envint.2020.105646.

Aboubakr, H.A., Sharafeldin, T.A., Goyal, S.M., 2021. Stability of SARS-CoV-2 and other coronaviruses in the environment and on common touch surfaces and the influence of climatic conditions: A review. Transbound. Emerg. Dis. 68, 296–312. https://doi.org/10.1111/tbed.13707.

Achak, M., Alaoui Bakri, S., Chhiti, Y., M'hamdi Alaoui, F.E., Barka, N., Boumya, W., 2021. SARS-CoV-2 in hospital wastewater during outbreak of COVID-19: A review on detection, survival and disinfection technologies. Sci. Total Environ. 761, 143192. https://doi.org/10.1016/j.scitotenv.2020.143192.

Adelodun, B., Ajibade, F.O., Tiamiyu, A.O., Nwogwu, N.A., Ibrahim, R.G., Kumar, P., Kumar, V., Odey, G., Yadav, K.K., Khan, A.H., Cabral-Pinto, M.M.S., Kareem, K.Y., Bakare, H.O., Ajibade, T.F., Naveed, Q.N., Islam, S., Fadare, O.O., Choi, K.S., 2021a.

Monitoring the presence and persistence of SARS-CoV-2 in water-food-environmental compartments: State of the knowledge and research needs. Environ. Res. 200, 111373. https://doi.org/ 10.1016/j.envres.2021.111373.

Adelodun, B., Kareem, K.Y., Kumar, P., Kumar, V., Choi, K.S., Yadav, K.K., Yadav, A., El- Denglawey, A., Cabral-Pinto, M., Son, C.T., Krishnan, S., Khan, N.A., 2021b. Understanding the impacts of the COVID-19 pandemic on sustainable Agri-food system and agroecosystem decarbonization nexus: A review. J. Clean. Prod. 318, 128451. https://doi.org/10.1016/j.jclepro.2021.128451.

Ahmed, B., Khan, M.S., Musarrat, J., 2018. Toxicity assessment of metal oxide nano-pollutants on tomato (*Solanum lycopersicon*): A study on growth dynamics and plant cell death. Environ. Pollut. 240, 802–816. https://doi.org/10.1016/j.envpol.2018.05.015.

Ahmed, W., Bertsch, P.M., Bibby, K., Haramoto, E., Hewitt, J., Huygens, F., Gyawali, P., Korajkic, A., Riddell, S., Sherchan, S.P., Simpson, S.L., Sirikanchana, K., Symonds, E. M., Verhagen, R., Vasan, S.S., Kitajima, M., Bivins, A., 2020. Decay of SARS-CoV-2 and surrogate murine hepatitis virus RNA in untreated wastewater to inform application in wastewater-based epidemiology. Environ. Res. 191, 110092. https://doi.org/10. 1016/j.envres.2020.110092.

Al Huraimel, K., Alhosani, M., Kunhabdulla, S., Stietiya, M.H., 2020. SARS-CoV-2 in the environment: Modes of transmission, early detection and potential role of pollutions. Sci. Total Environ. 744, 140946. https://doi.org/10.1016/j.scitotenv.2020.140946.

Allawadhi, P., Khurana, A., Allwadhi, S., Joshi, K., Packirisamy, G., Bharani, K.K., 2020. Nanoceria as a possible agent for the management of COVID-19. Nano Today 35, 100982. https://doi. org/10.1016/j.nantod.2020.100982.

Allen, S., Allen, D., Baladima, F., Phoenix, V.R., Thomas, J.L., Le

Roux, G., Sonke, J.E., 2021. Evidence of free tropospheric and long-range transport of microplastic at Pic du Midi Observatory. Nat. Commun. 12, 7242. https://doi.org/10.1038/s41467-021-27454-7.

Almansour, N.A., Syed, H.F., Khayat, N.R., Altheeb, R.K., Juri, R.E., Alhiyafi, J., Alrashed, S., Olatunji, S.O., 2019. Neural network and support vector machine for the prediction of chronic kidney disease: A comparative study. Comput. Biol. Med. 109, 101–111. https://doi.org/10.1016/j.compbiomed.2019.04.017.

Altenburger, R., Nendza, M., Schüürmann, G., 2003. Mixture toxicity and its modeling by quantitative structure–activity relationships. Environ. Toxicol. Chem. 22, 1900–1915. https://doi.org/10.1897/01-386.

Alves, V.M., Muratov, E.N., Zakharov, A., Muratov, N.N., Andrade, C.H., Tropsha, A., 2018. Chemical toxicity prediction for major classes of industrial chemicals: Is it possible to develop universal models covering cosmetics, drugs, and pesticides? Food Chem. Toxicol. 112, 526–534. https://doi.org/10.1016/j.fct.2017.04.008.

Amato-Lourenço, L.F., de Souza Xavier Costa, N., Dantas, K.C., dos Santos Galvão, L., Moralles, F.N., Lombardi, S.C.F.S., Júnior, A.M., Lindoso, J.A.L., Ando, R.A., Lima, F.G., Carvalho-Oliveira, R., Mauad, T., 2022. Airborne microplastics and SARS-CoV-2 in total suspended particles in the area surrounding the largest medical centre in Latin America. Environ. Pollut. 292, 118299. https://doi.org/10.1016/j.envpol.2021.118299.

Amato-Lourenço, L.F., dos Santos Galvão, L., de Weger, L.A., Hiemstra, P.S., Vijver, M.G., Mauad, T., 2020. An emerging class of air pollutants: Potential effects of microplastics to respiratory human health? Sci. Total Environ. 749, 141676. https://doi.org/10.1016/j.scitotenv.2020.141676.

Anand, U., Bianco, F., Suresh, S., Tripathi, V., Núñez-Delgado, A., Race, M., 2021. SARS-CoV-2 and other viruses in soil: An environmental outlook. Environ. Res. 198, 111297. https://doi.org/10.1016/j.envres.2021.111297.

Anonymous, 2020. Nanotechnology versus coronavirus. Nat. Nanotechnol. 15, 617. https://doi.org/10.1038/s41565-020-0757-7.

Arp, H.P.H., Kühnel, D., Rummel, C., MacLeod, M., Potthoff, A., Reichelt, S., Rojo-Nieto, E., Schmitt-Jansen, M., Sonnenberg, J., Toorman, E., Jahnke, A., 2021. Weathering plastics as a planetary boundary threat: Exposure, fate, and hazards. Environ. Sci. Technol. 55, 7246–7255. https://doi.org/10.1021/acs.est.1c01512.

Arslan, M., Xu, B., Gamal El-Din, M., 2020. Transmission of SARS-CoV-2 via fecal-oral and aerosols-borne routes: Environmental dynamics and implications for wastewater management in underprivileged societies. Sci. Total Environ. 743, 140709. https://doi.org/10.1016/j.scitotenv.2020.140709.

Asher, C., 2021. Novel chemical entities: Are we sleepwalking through a planetary boundary? (mongabay.com)

Avellan, A., Yun, J., Morais, B.P., Clement, E.T., Rodrigues, S.M., Lowry, G.V., 2021. Critical review: Role of inorganic nanoparticle properties on their foliar uptake and *in planta* translocation. Environ. Sci. Technol. 55, 13417–13431. https://doi.org/10.1021/acs.est.1c00178.

Azevedo, S.L., Holz, T., Rodrigues, J., Monteiro, T., Costa, F.M., Soares, A.M.V.M., Loureiro, S., 2017. A mixture toxicity approach to predict the toxicity of Ag decorated ZnO nanomaterials. Sci. Total Environ. 579, 337–344. https://doi.org/10.1016/j.scitotenv.2016.11.095.

Azimzada, A., Jreije, I., Hadioui, M., Shaw, P., Farner, J.M.,

Wilkinson, K.J., 2021. Quantification and characterization of Ti-, Ce-, and Ag-nanoparticles in global surface waters and precipitation. Environ. Sci. Technol. 55, 9836–9844. https://doi.org/10.1021/acs.est. 1c00488.

Baek, M.J., Son, J., Park, J., Seol, Y., Sung, B., Kim, Y.J., 2020. Quantitative prediction of mixture toxicity of $AgNO_3$ and ZnO nanoparticles on *Daphnia magna*. Sci. Technol. Adv. Mater. 21, 333–345. https://doi.org/10.1080/14686996.2020.1766343.

Balraadjsing, S., Peijnenburg, W.J.G.M., Vijver, M.G., 2022. Exploring the potential of *in silico* machine learning tools for the prediction of acute *Daphnia magna* nanotoxicity. Chemosphere 307, 135930. https://doi.org/10.1016/j.chemosphere.2022. 135930.

Ban, M.J., Lee, D.H., Shin, S.W., Kim, K., Kim, S., Oa, S.-W., Kim, G.-H., Park, Y.-J., Jin, D.R., Lee, M., Kang, J.-H., 2022. Identifying the acute toxicity of contaminated sediments using machine learning models. Environ. Pollut. 312, 120086. https://doi.org/ 10.1016/j.envpol.2022.120086.

Barros, J., Seena, S., 2021. Plastisphere in freshwaters: An emerging concern. Environ, Pollut. 290, 118123. https://doi.org/10.1016/ j.envpol.2021.118123.

Bastyans, S., Jackson, S., Fejer, G., 2022. Micro and nano-plastics, a threat to human health? Emerg. Top. Life Sci. 6, 411–422. https://doi.org/10.1042/ETLS20220024.

Bedrosian, N., Mitchell, E., Rohm, E., Rothe, M., Kelly, C., String, G., Lantagne, D., 2021. A systematic review of surface contamination, stability, and disinfection data on SARS- CoV-2 (Through july 10, 2020). Environ. Sci. Technol. 55, 4162–4173. https://doi.org/ 10.1021/acs.est.0c05651.

Belišová, N., Konečná, B., Bachratá, N., Ryba, J., Potočárová, A., Tamáš, M., Phuong, A.L., Púček, O., Kopáček, J., Mackul'ak, T.,

2022. Sorption of SARS-CoV-2 virus particles to the surface of microplastics released during washing processes. Int. J. Environ. Res. Public Health 19, 281. https://doi.org/10.3390/ijerph19010281.

Bennett-Lenane, H., Griffin, B.T., O'Shea, J.P., 2022. Machine learning methods for prediction of food effects on bioavailability: A comparison of support vector machines and artificial neural networks. Eur. J. Pharm. Sci. 168, 106018. https://doi.org/10.1016/j.ejps.2021.106018.

Bhagat, J., Nishimura, N., Shimada, Y., 2021. Toxicological interactions of microplastics/ nanoplastics and environmental contaminants: Current knowledge and future perspectives. J. Hazard. Mater. 405, 123913. https://doi.org/10.1016/j.jhazmat.2020.123913.

Bhaisare, M.L., Wu, B.-S., Wu, M.-C., Khan, M.S., Tseng, M.-H., Wu, H.-F., 2016. MALDI MS analysis, disk diffusion and optical density measurements for the antimicrobial effect of zinc oxide nanorods integrated in graphene oxide nanostructures. Biomater. Sci. 4, 183–194. https://doi.org/10.1039/c5bm00342c.

Bhatti, A., DeLong, R.K., 2023. Nanoscale interaction mechanisms of antiviral activity. ACS Pharmacol. Transl. Sci. 6, 220–228. https://doi.org/10.1021/acsptsci.2c00195.

Bhushan, M., Kumar, Y., Periyasamy, L., Viswanath, A.K., 2018. Antibacterial applications of α-Fe_2O_3/Co_3O_4 nanocomposites and study of their structural, optical, magnetic and cytotoxic characteristics. Appl. Nanosci. 8, 137–153. https://doi.org/10.1007/s13204-018-0656-5.

Bliss, C.I., 1939. The toxicity of poisons applied jointly. Ann. Appl. Biol. 26, 585–615. https://doi.org/10.1111/j.1744-7348.1939.tb06990.x.

Bopp, S.K., Barouki, R., Brack, W., Dalla Costa, S., Dorne, J.C.M., Drakvik, P.E., Faust, M., Karjalainen, T.K., Kephalopoulos, S., van Klaveren, J., Kolossa-Gehring, M., Kortenkamp, A., Lebret, E., Lettieri, T., Nørager, S., Rüegg, J., Tarazona, J.V., Trier, X., van de Water, B., van Gils, J., Bergman, Å., 2018. Current EU research activities on combined exposure to multiple chemicals. Environ. Int. 120, 544–562. https://doi.org/10.1016/j.envint.2018.07.037.

Böttcher, B., Nassal, M., 2018. Structure of mutant hepatitis B core protein capsids with premature secretion phenotype. J. Mol. Biol. 430, 4941–4954. https://doi.org/10.1016/j.jmb.2018.10.018.

Boughattas, I., Hattab, S., Zitouni, N., Mkhinini, M., Missawi, O., Bousserrhine, N., Banni, M., 2021. Assessing the presence of microplastic particles in tunisian agriculture soils and their potential toxicity effects using *Eisenia andrei* as bioindicator. Sci. Total Environ. 796, 148959. https://doi.org/10.1016/j.scitotenv.2021.148959.

Bouwmeester, H., Hollman, P.C.H., Peters, R.J.B., 2015. Potential health impact of environmentally released micro- and nanoplastics in the human food production chain: Experiences from nanotoxicology. Environ. Sci. Technol. 49, 8932–8947. https://doi.org/10.1021/acs.est.5b01090.

Braakhuis, H.M., Gosens, I., Heringa, M.B., Oomen, A.G., Vandebriel, R.J., Groenewold, M., Cassee, F.R., 2021. Mechanism of action of TiO_2: Recommendations to reduce uncertainties related to carcinogenic potential. Annu. Rev. Pharmacol. Toxicol. 61, 203–223. https://doi.org/10.1146/annurev-pharmtox-101419-100049.

Breisch, M., Loza, K., Pappert, K., Rostek, A., Rurainsky, C., Tschulik, K., Heggen, M., Epple, M., Tiller, J.C., Schildhauer, T.A., Köller, M., Sengstock, C., 2020. Enhanced dissolution of silver

nanoparticles in a physical mixture with platinum nanoparticles based on the sacrificial anode effect. Nanotechnology 31, 055703. https://doi.org/10.1088/1361-6528/ab4e48.

Brinkmann, B.W., Singhal, A., Sevink, G.J.A., Neeft, L., Vijver, M.G., Peijnenburg, W.J.G.M., 2022. Predicted adsorption affinity for enteric microbial metabolites to metal and carbon nanomaterials. J. Chem. Inf. Model. 62, 3589–3603. https://doi.org/10.1021/acs.jcim.2c00492.

Brisebois, E., Veillette, M., Dion-Dupont, V., Lavoie, J., Corbeil, J., Culley, A., Duchaine, C., 2018. Human viral pathogens are pervasive in wastewater treatment center aerosols. J. Environ. Sci. 67, 45–53. https://doi.org/10.1016/j.jes.2017.07.015.

Buglak, A.A., Zherdev, A.V., Dzantiev, B.B., 2019. Nano-(Q)SAR for cytotoxicity prediction of engineered nanomaterials. Molecules 24, 4537. https://doi.org/10.3390/molecules24244537.

Burley, S.K., Berman, H.M., Bhikadiya, C., Bi, C., Chen, L., Di Costanzo, L., Christie, C., Dalenberg, K., Duarte, J.M., Dutta, S., Feng, Z., Ghosh, S., Goodsell, D.S., Green, R.K., Guranović, V., Guzenko, D., Hudson, B.P., Kalro, T., Liang, Y., Lowe, R., Namkoong, H., Peisach, E., Periskova, I., Prlić, A., Randle, C., Rose, A., Rose, P., Sala, R., Sekharan, M., Shao, C., Tan, L., Tao, Y.-P., Valasatava, Y., Voigt, M., Westbrook, J., Woo, J., Yang, H., Young, J., Zhuravleva, M., Zardecki, C., 2019. RCSB protein data Bank: Biological macromolecular structures enabling research and education in fundamental biology, biomedicine, biotechnology and energy. Nucleic Acids Res. 47, D464–D474. https://doi.org/10.1093/nar/gky1004.

Buzea, C., Pacheco, I.I., Robbie, K., 2007. Nanomaterials and nanoparticles: Sources and toxicity. Biointerphases 2, MR17–MR172. https://doi.org/10.1116/1.2815690.

Campos, E.V.R., Pereira, A.E.S., Oliveira, J.L. de, Carvalho, L.B.,

Guilger-Casagrande, M., Lima, R. de, Fraceto, L.F., 2020. How can nanotechnology help to combat COVID-19? Opportunities and urgent need. J. Nanobiotechnol. 18, 125. https://doi.org/10.1186/s12951-020-00685-4.

Cao, J., Yang, Q., Jiang, J., Dalu, T., Kadushkin, A., Singh, J., Fakhrullin, R., Wang, F., Cai, X., Li, R., 2022. Coronas of micro/nano plastics: A key determinant in their risk assessments. Part. Fibre Toxicol. 19, 55. https://doi.org/10.1186/s12989-022-00492-9.

Casabianca, A., Orlandi, C., Amagliani, G., Magnani, M., Brandi, G., Schiavano, G.F., 2022. SARS-CoV-2 RNA detection on environmental surfaces in a university setting of Central Italy. Int. J. Environ. Res. Public Health 19, 5560. https://doi.org/10.3390/ijerph19095560.

Catarino, A.I., Macchia, V., Sanderson, W.G., Thompson, R.C., Henry, T.B., 2018. Low levels of microplastics (MP) in wild mussels indicate that MP ingestion by humans is minimal compared to exposure via household fibres fallout during a meal. Environ. Pollut. 237, 675–684. https://doi.org/10.1016/j.envpol.2018.02.069.

Chakraborty, D., Ethiraj, K.R., Chandrasekaran, N., Mukherjee, A., 2021. Mitigating the toxic effects of CdSe quantum dots towards freshwater alga *Scenedesmus obliquus*: Role of eco-corona. Environ. Pollut. 270, 116049. https://doi.org/10.1016/j.envpol.2020.116049.

Chao, S.-J., Huang, C.P., Lam, C.-C., Hua, L.-C., Chang, S.-H., Huang, C., 2021. Transformation of copper oxide nanoparticles as affected by ionic strength and its effects on the toxicity and bioaccumulation of copper in zebrafish embryo. Ecotoxicol. Environ. Saf. 225, 112759. https://doi.org/10.1016/j.ecoenv.2021.112759.

Chatterjee, M., Roy, K., 2023. "Data fusion" quantitative read-across structure-activity-activity relationships (q-RASAARs) for the prediction of toxicities of binary and ternary antibiotic mixtures toward three bacterial species. J. Hazard. Mater. 459, 132129. https://doi.org/10.1016/j.jhazmat.2023.132129.

Chen, G., Feng, Q., Wang, J., 2020. Mini-review of microplastics in the atmosphere and their risks to humans. Sci. Total Environ. 703, 135504. https://doi.org/10.1016/j.scitotenv.2019.135504.

Chen, G., Peijnenburg, W.J.G.M., Xiao, Y., Vijver, M.G., 2017. Current knowledge on the use of computational toxicology in hazard assessment of metallic engineered nanomaterials. Int. J. Mol. Sci. 18, 1504. https://doi.org/10.3390/ijms18071504.

Chen, G., Peijnenburg, W.J.G.M., Xiao, Y., Vijver, M.G., 2018. Developing species sensitivity distributions for metallic nanomaterials considering the characteristics of nanomaterials, experimental conditions, and different types of endpoints. Food Chem. Toxicol. 112, 563–570. https://doi.org/10.1016/j.fct.2017.04.003.

Chen, G., Vijver, M.G., Peijnenburg, W.J.G.M., 2015. Summary and analysis of the currently existing literature data on metal-based nanoparticles published for selected aquatic organisms: Applicability for toxicity prediction by (Q)SARs. Altern. Lab. Anim. 43, 221–240. https://doi.org/10.1177/026119291504300404.

Chen, L., Qian, Y., Jia, Q., Weng, R., Zhang, X., Li, Y., Qiu, J., 2023. A national-scale distribution of organochlorine pesticides (OCPs) in cropland soils and major types of food crops in China: Co-occurrence and associated risks. Sci. Total Environ. 861, 160637. https://doi.org/10.1016/j.scitotenv.2022.160637.

Chen, W., Duan, L., Zhu, D., 2007. Adsorption of polar and nonpolar organic chemicals to carbon nanotubes. Environ. Sci. Technol. 41,

8295–8300. https://doi.org/10.1021/es071230h.

Chen, X., Li, X., Li, Y., 2021. Toxicity inhibition strategy of microplastics to aquatic organisms through molecular docking, molecular dynamics simulation and molecular modification. Ecotoxicol. Environ. Saf. 226, 112870. https://doi.org/10.1016/j. ecoenv.2021.112870.

Chen, Y., Ma, J., Xu, M., Liu, S., 2020. Antiviral nanoagents: More attention and effort needed? Nano Today 35, 100976. https://doi.org/10.1016/j.nantod.2020.100976.

Chen, Y., Wang, M., Fu, H., Qu, X., Zhang, Z., Kang, F., Zhu, D., 2019. Spectroscopic and molecular modeling investigation on inhibition effect of nitroaromatic compounds on acetylcholinesterase activity. Chemosphere 236, 124365. https://doi.org/10.1016/j. chemosphere.2019.124365.

Chen, Z., Shi, X., Zhang, J., Wu, L., Wei, W., Ni, B.-J., 2023. Nanoplastics are significantly different from microplastics in urban waters. Water Res. X 19, 100169. https://doi.org/10.1016/j. wroa.2023.100169.

Cheng, C., Barceló, J., Hartnett, A.S., Kubinec, R., Messerschmidt, L., 2020. COVID-19 government response event dataset (CoronaNet v.1.0). Nat. Hum. Behav. 4, 756–768. https://doi.org/10.1038/ s41562-020-0909-7.

Conde-Cid, M., Arias-Estévez, M., Núñez-Delgado, A., 2021. SARS-CoV-2 and other pathogens could be determined in liquid samples from soils. Environ. Pollut. 273, 116445. https://doi.org/10.1016/ j.envpol.2021.116445.

Corpet, D.E., 2021. Why does SARS-CoV-2 survive longer on plastic than on paper? Med. Hypotheses 146, 110429. https://doi.org/ 10.1016/j.mehy.2020.110429.

Da Silva, G.H., Clemente, Z., Khan, L.U., Coa, F., Neto, L.L.R.,

Carvalho, H.W.P., Castro, V.L., Martinez, D.S.T., Monteiro, R.T.R., 2018. Toxicity assessment of TiO_2-MWCNT nanohybrid material with enhanced photocatalytic activity on *Danio rerio* (Zebrafish) embryos. Ecotoxicol. Environ. Saf. 165, 136–143. https://doi.org/10.1016/j.ecoenv.2018.08.093.

Das, J., Choi, Y.J., Song, H., Kim, J.H., 2016. Potential toxicity of engineered nanoparticles in mammalian germ cells and developing embryos: Treatment strategies and anticipated applications of nanoparticles in gene delivery. Hum. Reprod. Update 22, 588–619. https://doi.org/10.1093/humupd/dmw020.

Das, S., Thiagarajan, V., Chandrasekaran, N., Ravindran, B., Mukherjee, A., 2022. Nanoplastics enhance the toxic effects of titanium dioxide nanoparticle in freshwater algae *Scenedesmus obliquus*. Comp. Biochem. Phys. C 256, 109305. https://doi.org/10.1016/j.cbpc.2022.109305.

de Medeiros, A.M.Z., Khan, L.U., da Silva, G.H., Ospina, C.A., Alves, O.L., de Castro, V.L., Martinez, D.S.T., 2021. Graphene oxide-silver nanoparticle hybrid material: An integrated nanosafety study in zebrafish embryos. Ecotoxicol. Environ. Saf. 209, 111776. https://doi.org/10.1016/j.ecoenv.2020.111776.

de Souza Machado, A.A., Wood, C.M., Kloas, W., 2019. Novel concepts for novel entities: Updating ecotoxicology for a sustainable anthropocene. Environ. Sci. Technol. 53, 4680–4682. https://doi. org/10.1021/acs.est.9b02031.

Debeljak, P., Pinto, M., Proietti, M., Reisser, J., Ferrari, F.F., Abbas, B., van Loosdrecht, M.C.M., Slat, B., Herndl, G.J., 2017. Extracting DNA from ocean microplastics: A method comparison study. Anal. Methods 9, 1521–1526. https://doi.org/10.1039/C6AY03119F.

Demšar, J., Curk, T., Erjavec, A., Gorup, C., Hočevar, T., Milutinovič,

M., Možina, M., Polajnar, M., Toplak, M., Starič, A., Štajdohar, M., Umek, L., Žagar, L., Žbontar, J., Žitnik, M., Zupan, B., 2013. Orange: Data mining toolbox in python. J. Mach. Learn. Res. 14, 2349–2353.

Deng, R., Lin, D., Zhu, L., Majumdar, S., White, J.C., Gardea-Torresdey, J.L., Xing, B., 2017. Nanoparticle interactions with co-existing contaminants: Joint toxicity, bioaccumulation and risk. Nanotoxicology 11, 591–612. https://doi.org/10.1080/17435390.2017.1343404.

Deshwal, N., Singh, M.B., Bahadur, I., Kaushik, N., Kaushik, N.K., Singh, P., Kumari, K., 2023. A review on recent advancements on removal of harmful metal/metal ions using graphene oxide: Experimental and theoretical approaches. Sci. Total Environ. 858, 159672. https://doi.org/10.1016/j.scitotenv.2022.159672.

Diamond, M.L., de Wit, C.A., Molander, S., Scheringer, M., Backhaus, T., Lohmann, R., Arvidsson, R., Bergman, Å., Hauschild, M., Holoubek, I., Persson, L., Suzuki, N., Vighi, M., Zetzsch, C., 2015. Exploring the planetary boundary for chemical pollution. Environ. Int. 78, 8–15. https://doi.org/10.1016/j.envint.2015.02.001.

Diaz-Diestra, D.M., Palacios-Hernandez, T., Liu, Y., Smith, D.E., Nguyen, A.K., Todorov, T., Gray, P.J., Zheng, J., Skoog, S.A., Goering, P.L., 2022. Impact of surface chemistry of ultrasmall superparamagnetic iron oxide nanoparticles on protein corona formation and endothelial cell uptake, toxicity, and barrier function. Toxicol. Sci. 188, 261–275. https://doi.org/10.1093/toxsci/kfac058.

Diffenbaugh, N.S., Field, C.B., Appel, E.A., Azevedo, I.L., Baldocchi, D.D., Burke, M., Burney, J.A., Ciais, P., Davis, S.J., Fiore, A.M., Fletcher, S.M., Hertel, T.W., Horton, D.E., Hsiang, S.M., Jackson, R.B., Jin, X., Levi, M., Lobell, D.B., McKinley, G. A., Moore, F.C., Montgomery, A., Nadeau, K.C., Pataki, D.E.,

Randerson, J.T., Reichstein, M., Schnell, J.L., Seneviratne, S.I., Singh, D., Steiner, A.L., Wong-Parodi, G., 2020. The COVID-19 lockdowns: A window into the earth system. Nat. Rev. Earth Environ. 1, 470–481. https://doi.org/10.1038/s43017-020-0079-1.

Ding, L., Mao, R., Ma, S., Guo, X., Zhu, L., 2020. High temperature depended on the ageing mechanism of microplastics under different environmental conditions and its effect on the distribution of organic pollutants. Water Res. 174, 115634. https://doi.org/10.1016/j.watres.2020.115634.

Dong, X., Liu, X., Hou, Q., Wang, Z., 2023. From natural environment to animal tissues: A review of microplastics (nanoplastics) translocation and hazards studies. Sci. Total Environ. 855, 158686. https://doi.org/10.1016/j.scitotenv.2022.158686.

Dowlatabadi, M., Jahangiri, M., Farhadian, N., 2019. Prediction of chlortetracycline adsorption on the Fe_3O_4 nanoparticle using molecular dynamics simulation. J. Biomol. Struct. Dyn. 37, 3616–3626. https://doi.org/10.1080/07391102.2018.1521746.

Dris, R., Gasperi, J., Mirande, C., Mandin, C., Guerrouache, M., Langlois, V., Tassin, B., 2017. A first overview of textile fibers, including microplastics, in indoor and outdoor environments. Environ. Pollut. 221, 453–458. https://doi.org/10.1016/j.envpol.2016.12.013.

Dubey, A., Kotnala, G., Mandal, T.K., Sonkar, S.C., Singh, V.K., Guru, S.A., Bansal, A., Irungbam, M., Husain, F., Goswami, B., Kotnala, R.K., Saxena, S., Sharma, S.K., Saxena, K.N., Sharma, C., Kumar, S., Aswal, D.K., Manchanda, V., Koner, B.C., 2021. Evidence of the presence of SARS-CoV-2 virus in atmospheric air and surfaces of a dedicated COVID hospital. J. Med. Virol. 93, 5339–5349. https://doi.org/10.1002/jmv.27029.

Ehret, J., Vijver, M.G., Peijnenburg, W.J.G.M., 2014. The application of QSAR approaches to nanoparticles. Altern. Lab. Anim. 42, 43–50. https://doi.org/10.1177/026119291404200107.

Ekvall, M.T., Hedberg, J., Odnevall Wallinder, I., Malmendal, A., Hansson, L.-A., Cedervall, T., 2021. Adsorption of bio-organic eco-corona molecules reduces the toxic response to metallic nanoparticles in *Daphnia magna*. Sci. Rep. 11, 10784. https://doi.org/10.1038/s41598-021-90053-5.

Epa, V.C., Burden, F.R., Tassa, C., Weissleder, R., Shaw, S., Winkler, D.A., 2012. Modeling biological activities of nanoparticles. Nano Lett. 12, 5808–5812. https://doi.org/10.1021/nl303144k.

Feng, H., Liu, Y., Xu, Y., Li, S., Liu, X., Dai, Y., Zhao, J., Yue, T., 2022. Benzo[*a*]pyrene and heavy metal ion adsorption on nanoplastics regulated by humic acid: cooperation/competition mechanisms revealed by molecular dynamics simulations. J. Hazard. Mater. 424, 127431. https://doi.org/10.1016/j.jhazmat.2021.127431.

Feng, Y., Wu, J., Lu, H., Lao, W., Zhan, H., Lin, L., Liu, G., Deng, Y., 2023. Cytotoxicity and hemolysis of rare earth ions and nanoscale/bulk oxides (La, Gd, and Yb): Interaction with lipid membranes and protein corona formation. Sci. Total Environ. 879, 163259. https://doi.org/10.1016/j.scitotenv.2023.163259.

Fernandes, L.S., Galvão, A., Santos, R., Monteiro, S., 2023. Impact of water reuse on agricultural practices and human health. Environ. Res. 216, 114762. https://doi.org/10.1016/j.envres.2022.114762.

Florindo, H.F., Kleiner, R., Vaskovich-Koubi, D., Acúrcio, R.C., Carreira, B., Yeini, E., Tiram, G., Liubomirski, Y., Satchi-Fainaro, R., 2020. Immune-mediated approaches against COVID-19. Nat. Nanotechnol. 15, 630–645. https://doi.org/10.1038/s41565-020-0732-3.

Fournier, E., Etienne-Mesmin, L., Grootaert, C., Jelsbak, L., Syberg, K., Blanquet-Diot, S., Mercier-Bonin, M., 2021. Microplastics in

the human digestive environment: A focus on the potential and challenges facing *in vitro* gut model development. J. Hazard. Mater. 415, 125632. https://doi.org/10.1016/j.jhazmat.2021.125632.

Fred-Ahmadu, O.H., Bhagwat, G., Oluyoye, I., Benson, N.U., Ayejuyo, O.O., Palanisami, T., 2020. Interaction of chemical contaminants with microplastics: Principles and perspectives. Sci. Total Environ. 706, 135978. https://doi.org/10.1016/j.scitotenv.2019.135978.

Gajewicz, A., 2018. How to judge whether QSAR/read-across predictions can be trusted: A novel approach for establishing a model's applicability domain. Environ. Sci.: Nano 5, 408–421. https://doi.org/10.1039/C7EN00774D.

Gajewicz, A., Schaeublin, N., Rasulev, B., Hussain, S., Leszczynska, D., Puzyn, T., Leszczynski, J., 2015. Towards understanding mechanisms governing cytotoxicity of metal oxides nanoparticles: Hints from nano-QSAR studies. Nanotoxicology 9, 313–325. https://doi.org/10.3109/17435390.2014.930195.

Gastaldi, M.S., Felsztyna, I., Miguel, V., Sánchez-Borzone, M.E., García, D.A., 2023. Theoretical and experimental study of molecular interactions of fluralaner with lipid membranes. J. Agric. Food Chem. 71, 2134–2142. https://doi.org/10.1021/acs.jafc.2c06811.

Ge, C., Du, J., Zhao, L., Wang, L., Liu, Y., Li, D., Yang, Y., Zhou, R., Zhao, Y., Chai, Z., Chen, C., 2011. Binding of blood proteins to carbon nanotubes reduces cytotoxicity. Proc. Natl. Acad. Sci. 108, 16968–16973. https://doi.org/10.1073/pnas.1105270108.

Ge, L., Shao, B., Liang, Q., Huang, D., Liu, Z., He, Q., Wu, T., Luo, S., Pan, Y., Zhao, C., Huang, J., Hu, Y., 2022. Layered double hydroxide based materials applied in persulfate based advanced oxidation processes: Property, mechanism, application and

perspectives. J. Hazard. Mater. 424, 127612. https://doi.org/10.1016/j.jhazmat.2021.127612.

Geitner, N.K., Ogilvie Hendren, C., Cornelis, G., Kaegi, R., Lead, J.R., Lowry, G.V., Lynch, I., Nowack, B., Petersen, E., Bernhardt, E., Brown, S., Chen, W., de Garidel-Thoron, C., Hanson, J., Harper, S., Jones, K., von der Kammer, F., Kennedy, A., Kidd, J., Matson, C., Metcalfe, C.D., Pedersen, J., Peijnenburg, W.J.G.M., Quik, J.T.K., Rodrigues, S.M., Rose, J., Sayre, P., Simonin, M., Svendsen, C., Tanguay, R., Tefenkji, N., van Teunenbroek, T., Thies, G., Tian, Y., Rice, J., Turner, A., Liu, J., Unrine, J., Vance, M., White, J.C., Wiesner, M.R., 2020. Harmonizing across environmental nanomaterial testing media for increased comparability of nanomaterial datasets. Environ. Sci.: Nano 7, 13–36. https://doi.org/10.1039/c9en00448c.

Geitner, N.K., Zhao, W., Ding, F., Chen, W., Wiesner, M.R., 2017. Mechanistic insights from discrete molecular dynamics simulations of pesticide-nanoparticle interactions. Environ. Sci. Technol. 51, 8396–8404. https://doi.org/10.1021/acs.est.7b01674.

Georgantzopoulou, A., Farkas, J., Ndungu, K., Coutris, C., Carvalho, P.A., Booth, A.M., Macken, A., 2020. Wastewater-aged silver nanoparticles in single and combined exposures with titanium dioxide affect the early development of the marine copepod *Tisbe battagliai*. Environ. Sci. Technol. 54, 12316–12325. https://doi.org/10.1021/acs.est.0c03113.

Gidari, A., Sabbatini, S., Bastianelli, S., Pierucci, S., Busti, C., Bartolini, D., Stabile, A.M., Monari, C., Galli, F., Rende, M., Cruciani, G., Francisci, D., 2021. SARS-CoV-2 survival on surfaces and the effect of UV-C light. Viruses 13, 408. https://doi.org/10.3390/ v13030408.

Giner, B., Lafuente, C., Lapeña, D., Errazquin, D., Lomba, L., 2020. QSAR study for predicting the ecotoxicity of NADES towards

Aliivibrio fischeri. Exploring the use of mixing rules. Ecotoxicol. Environ. Saf. 191, 110004. https://doi.org/10.1016/j.ecoenv.2019.110004.

Gomes, S.I.L., Amorim, M.J.B., Pokhrel, S., Mädler, L., Fasano, M., Chiavazzo, E., Asinari, P., Jänes, J., Tämm, K., Burk, J., Scott-Fordsmand, J.J., 2021. Machine learning and materials modelling interpretation of *in Vivo* toxicological response to TiO_2 nano-particles library (UV and non-UV exposure). Nanoscale 13, 14666–14678. https://doi.org/10.1039/d1nr03231c.

Gonçalves, J., Koritnik, T., Mioč, V., Trkov, M., Bolješič, M., Berginc, N., Prosenc, K., Kotar, T., Paragi, M., 2021. Detection of SARS-CoV-2 RNA in hospital wastewater from a low COVID-19 disease prevalence area. Sci. Total Environ. 755, 143226. https://doi. org/10.1016/j.scitotenv.2020.143226.

Gong, H., Li, R., Li, F., Guo, X., Xu, L., Gan, L., Yan, M., Wang, J., 2023. Toxicity of nanoplastics to aquatic organisms: Genotoxicity, cytotoxicity, individual level and beyond individual level. J. Hazard. Mater. 443, 130266. https://doi.org/10.1016/j.jhazmat.2022.130266.

González-Pleiter, M., Edo, C., Aguilera, Á., Viúdez-Moreiras, D., Pulido-Reyes, G., González-Toril, E., Osuna, S., de Diego-Castilla, G., Leganés, F., Fernández-Piñas, F., Rosal, R., 2021. Occurrence and transport of microplastics sampled within and above the planetary boundary layer. Sci. Total Environ. 761, 143213. https://doi.org/10.1016/j.scitotenv.2020.143213.

Guineé, J.B., Heijungs, R., Vijver, M.G., Peijnenburg, W.J.G.M., 2017. Setting the stage for debating the roles of risk assessment and life-cycle assessment of engineered nanomaterials. Nat. Nanotechnol. 12, 727–733. https://doi.org/10.1038/nnano.2017.135.

Gunathilake, T.M.S.U., Ching, Y.C., Uyama, H., Hai, N.D., Chuah,

C.H., 2022. Enhanced curcumin loaded nanocellulose: A possible inhalable nanotherapeutic to treat COVID-19. Cellulose 29, 1821–1840. https://doi.org/10.1007/s10570-021-04391-8.

Guo, X., Liu, Y., Wang, J., 2019. Sorption of sulfamethazine onto different types of microplastics: A combined experimental and molecular dynamics simulation study. Mar. Pollut. Bull. 145, 547–554. https://doi.org/10.1016/j.marpolbul.2019.06.063.

Haghighat, F., Kim, Y., Sourinejad, I., Yu, I.J., Johari, S.A., 2021. Titanium dioxide nanoparticles affect the toxicity of silver nanoparticles in common carp (*Cyprinus carpio*). Chemosphere 262, 127805. https://doi.org/10.1016/j.chemosphere.2020.127805.

Han, J., Zhang, X., He, S., Jia, P., 2021. Can the coronavirus disease be transmitted from food? A review of evidence, risks, policies and knowledge gaps. Environ. Chem. Lett. 19, 5–16. https://doi.org/10.1007/s10311-020-01101-x.

Haynes, W.M., 2011. CRC Handbook of Chemistry and Physics, 92nd Edition, CRC Press.

He, M., Liang, Q., Tang, L., Liu, Z., Shao, B., He, Q., Wu, T., Luo, S., Pan, Y., Zhao, C., Niu, C., Hu, Y., 2021. Advances of covalent organic frameworks based on magnetism: Classification, synthesis, properties, applications. Coord. Chem. Rev. 449, 214219. https://doi.org/10.1016/j.ccr.2021.214219.

Hernández-Moreno, D., Valdehita, A., Conde, E., Rucandio, I., Navas, J.M., Fernández-Cruz, M.L., 2019. Acute toxic effects caused by the co-exposure of nanoparticles of ZnO and Cu in rainbow trout. Sci. Total Environ. 687, 24–33. https://doi.org/10.1016/j.scitotenv.2019.06.084.

Hong, H., Adam, V., Nowack, B., 2021. Form-specific and probabilistic environmental risk assessment of 3 engineered nanomaterials (nano-Ag, nano-TiO_2, and nano-ZnO) in European

freshwaters. Environ. Toxicol. Chem. 40, 2629–2639. https://doi.org/10. 1002/etc.5146.

Huang, Q., Yu, L., Petros, A.M., Gunasekera, A., Liu, Z., Xu, N., Hajduk, P., Mack, J., Fesik, S.W., Olejniczak, E.T., 2004. Structure of the N-terminal RNA-binding domain of the SARS CoV nucleocapsid protein. Biochemistry 43, 6059–6063. https://doi. org/10.1021/bi036155b.

Huang, Y., Li, X., Xu, S., Zheng, H., Zhang, L., Chen, J., Hong, H., Kusko, R., Li, R., 2020. Quantitative structure-activity relationship models for predicting inflammatory potential of metal oxide nanoparticles. Environ. Health Perspect. 128, 67010. https://doi.org/10.1289/EHP6508.

Hutchison, J.E., 2016. The road to sustainable nanotechnology: Challenges, progress and opportunities. ACS Sustainable Chem. Eng. 4, 5907–5914. https://doi.org/10.1021/acssuschemeng. 6b02121.

Innocenzi, P., Stagi, L., 2020. Carbon-based antiviral nanomaterials: Graphene, C-dots, and fullerenes. A perspective. Chem. Sci. 11, 6606–6622. https://doi.org/10.1039/D0SC02658A.

Jahan, S., Alias, Y.B., Bakar, A.F.B.A., Yusoff, I.B., 2018. Toxicity evaluation of ZnO and TiO_2 nanomaterials in hydroponic red bean (*Vigna angularis*) plant: Physiology, biochemistry and kinetic transport. J. Environ. Sci. 72, 140–152. https://doi.org/ 10.1016/j.jes.2017.12.022.

Jaworska, J., Nikolova-Jeliazkova, N., Aldenberg, T., 2005. QSAR applicabilty domain estimation by projection of the training set descriptor space: A review. Altern. Lab. Anim. 33, 445–459. https://doi.org/10.1177/026119290503300508.

Jayaramulu, K., Mukherjee, S., Morales, D.M., Dubal, D.P., Nanjundan, A.K., Schneemann, A., Masa, J., Kment, S., Schuhmann, W., Otyepka, M., Zbořil, R., Fischer, R.A., 2022.

Graphene-based metal–organic framework hybrids for applications in catalysis, environmental, and energy technologies. Chem. Rev. 122, 17241–17338. https://doi.org/10.1021/acs.chemrev.2c00270.

Jennings, W.G., Perez, N.M., 2020. The immediate impact of COVID-19 on law enforcement in the United States. Am. J. Crim. Justice 45, 690–701. https://doi.org/10.1007/s12103-020-09536-2.

Ji, L., Chen, W., Xu, Z., Zheng, S., Zhu, D., 2013. Graphene nanosheets and graphite oxide as promising adsorbents for removal of organic contaminants from aqueous solution. J. Environ. Qual. 42, 191–198. https://doi.org/10.2134/jeq2012.0172.

Ji, Z., Guo, W., Wood, E.L., Liu, J., Sakkiah, S., Xu, X., Patterson, T.A., Hong, H., 2022. Machine learning models for predicting cytotoxicity of nanomaterials. Chem. Res. Toxicol. 35, 125–139. https://doi.org/10.1021/acs.chemrestox.1c00310.

Jia, Y., Hou, X., Wang, Z., Hu, X., 2021. Machine learning boosts the design and discovery of nanomaterials. ACS Sustainable Chem. Eng. 9, 6130–6147. https://doi.org/10.1021/acssuschemeng.1c00483.

Jogaiah, S., Paidi, M.K., Venugopal, K., Geetha, N., Mujtaba, M., Udikeri, S.S., Govarthanan, M., 2021. Phytotoxicological effects of engineered nanoparticles: An emerging nanotoxicology. Sci. Total Environ. 801, 149809. https://doi.org/10.1016/j.scitotenv.2021.149809.

Jośko, I., Krasucka, P., Skwarek, E., Oleszczuk, P., Sheteiwy, M., 2022. The co-occurrence of Zn-and Cu-based engineered nanoparticles in soils: The metal extractability vs. toxicity to *Folsomia candida*. Chemosphere 287, 132252. https://doi.org/10.1016/j. chemosphere.2021.132252.

Jośko, I., Kusiak, M., Xing, B., Oleszczuk, P., 2021. Combined effect of nano-CuO and nano-ZnO in plant-related system: From bioavailability in soil to transcriptional regulation of metal homeostasis in barley. J. Hazard. Mater. 416, 126230. https://doi.org/10.1016/j.jhazmat.2021.126230.

Junaid, M., Liu, S., Chen, G., Liao, H., Wang, J., 2023. Transgenerational impacts of micro(nano)plastics in the aquatic and terrestrial environment. J. Hazard. Mater. 443, 130274. https://doi.org/10.1016/j.jhazmat.2022.130274.

Junaid, M., Liu., S, Liao, H., Liu, X., Wu, Y., Wang, J., 2022. Wastewater plastisphere enhances antibiotic resistant elements, bacterial pathogens, and toxicological impacts in the environment. Sci. Total Environ. 841, 156805. https://doi.org/ 10.1016/j. scitotenv.2022.156805.

Junaid, M., Wang, J., 2022. Interaction of micro(nano)plastics with extracellular and intracellular biomolecules in the freshwater environment. Crit. Rev. Env. Sci. Tec. 52, 4241–4265. https://doi.org/10.1080/10643389.2021.2002078.

Jung, Y.S., Sampath, V., Prunicki, M., Aguilera, J., Allen, H., LaBeaud, D., Veidis, E., Barry, M., Erny, B., Patel, L., Akdis, C., Akdis, M., Nadeau, K., 2022. Characterization and regulation of microplastic pollution for protecting planetary and human health. Environ. Pollut. 315, 120442. https://doi.org/10.1016/j.envpol. 2022.120442.

Kang, S., Yang, M., Hong, Z., Zhang, L., Huang, Z., Chen, X., He, S., Zhou, Z., Zhou, Z., Chen, Q., Yan, Y., Zhang, C., Shan, H., Chen, S., 2020. Crystal structure of SARS-CoV-2 nucleocapsid protein RNA binding domain reveals potential unique drug targeting sites. Acta Pharm. Sin. B 10, 1228–1238. https://doi.org/10. 1016/j.apsb. 2020.04.009.

Kar, S., Gajewicz, A., Puzyn, T., Roy, K., Leszczynski, J., 2014.

Periodic table-based descriptors to encode cytotoxicity profile of metal oxide nanoparticles: A mechanistic QSTR approach. Ecotoxicol. Environ. Saf. 107, 162–169. https://doi.org/10.1016/j.ecoenv. 2014.05.026.

Kar, S., Leszczynski, J., 2019. Exploration of computational approaches to predict the toxicity of chemical mixtures. Toxics 7, 15. https://doi.org/10.3390/toxics7010015.

Kar, S., Pathakoti, K., Leszczynska, D., Tchounwou, P.B., Leszczynski, J., 2022. *In vitro* and *in silico* study of mixtures cytotoxicity of metal oxide nanoparticles to *Escherichia coli*: A mechanistic approach. Nanotoxicology 16, 566–579. https://doi.org/10.1080/17435390.2022.2123750.

Katsumiti, A., Losada-Carrillo, M.P., Barros, M., Cajaraville, M.P., 2021. Polystyrene nanoplastics and microplastics can act as Trojan horse carriers of benzo(*a*)pyrene to mussel hemocytes in vitro. Sci. Rep. 11, 22396. https://doi.org/10.1038/s41598-021-01938-4.

Kaul, S., Gulati, N., Verma, D., Mukherjee, S., Nagaich, U., 2018. Role of nanotechnology in cosmeceuticals: A review of recent advances. J. Pharm. 2018, 3420204. https://doi.org/10.1155/2018/3420204.

Kaur, J., Khatri, M., Puri, S., 2019. Toxicological evaluation of metal oxide nanoparticles and mixed exposures at low doses using zebra fish and THP1 cell line. Environ. Toxicol. 34, 375–387. https://doi.org/10.1002/tox.22692.

Khoo, K.S., Ho, L.Y., Lim, H.R., Leong, H.Y., Chew, K.W., 2021. Plastic waste associated with the COVID-19 pandemic: Crisis or opportunity? J. Hazard. Mater. 417, 126108. https://doi.org/10.1016/j.jhazmat.2021.126108.

Kim, D., Chae, Y., An, Y.-J., 2017. Mixture toxicity of nickel and microplastics with different functional groups on *Daphnia*

magna. Environ. Sci. Technol. 51, 12852–12858. https://doi.org/10.1021/acs.est.7b03732.

Kim, J.-M., Chung, Y.-S., Jo, H.J., Lee, N.-J., Kim, M.S., Woo, S.H., Park, S., Kim, J.W., Kim, H.M., Han, M.-G., 2020. Identification of coronavirus isolated from a patient in Korea with COVID-19. Osong Public Health Res. Perspect. 11, 3–7. https://doi.org/10.24171/j.phrp.2020.11.1.02.

Kim, L., Cui, R., Il Kwak, J., An, Y.-J., 2022. Trophic transfer of nanoplastics through a microalgae-crustacean-small yellow croaker food chain: Inhibition of digestive enzyme activity in fish. J. Hazard. Mater. 440, 129715. https://doi.org/10.1016/j.jhazmat.2022.129715.

Kitajima, M., Ahmed, W., Bibby, K., Carducci, A., Gerba, C.P., Hamilton, K.A., Haramoto, E., Rose, J.B., 2020. SARS-CoV-2 in wastewater: State of the knowledge and research needs. Sci. Total Environ. 739, 139076. https://doi.org/10.1016/j.scitotenv.2020.139076.

Kolarević, S., Micsinai, A., Szántó-Egész, R., Lukács, A., Kračun-Kolarević, M., Djordjevic, A., Vojnović-Milutinović, D., Marić, J.J., Kirschner, A.K.T., Farnleitner, A.A.H., Linke, R., Đukic, A., Kostić-Vuković, J., Paunović, M., 2022. Wastewater-based epidemiology in countries with poor wastewater treatment – Epidemiological indicator function of SARS-CoV-2 RNA in surface waters. Sci. Total Environ. 843, 156964. https://doi.org/10.1016/j.scitotenv.2022.156964.

Koppenol, W.H., 2001. "The Haber-Weiss cycle-70 years later." REDOX Report: Communications in Free Radical Research 6, 229–234. https://doi.org/10.1179/135100001101536373.

Kostarelos, K., 2020. Nanoscale nights of COVID-19. Nat. Nanotechnol. 15, 343–344. https://doi.org/10.1038/s41565-020-0687-4.

Kubinyi, H., 1993. QSAR: Hansch analysis and related approaches, in: Mann-hold, R., Krogsgaard-Larsen, P., Timmerman, H. (Eds.), Methods and principles in medicinal chemistry, vol 1. VCH, Weinheim. https://doi.org/10.1002/9783527616824.

Kumar, M., Patel, A.K., Shah, A.V., Raval, J., Rajpara, N., Joshi, M., Joshi, C.G., 2020. First proof of the capability of wastewater surveillance for COVID-19 in India through detection of genetic material of SARS-CoV-2. Sci. Total Environ. 746, 141326. https://doi.org/10.1016/j.scitotenv.2020.141326.

Kumar, N., Shah, V., Walker, V.K., 2012. Influence of a nanoparticle mixture on an arctic soil community. Environ. Toxicol. Chem. 31, 131–135. https://doi.org/10.1002/etc.721.

Kumar, P., Mahajan, P., Kaur, R., Gautam, S., 2020. Nanotechnology and its challenges in the food sector: A review. Mater. Today Chem. 17, 100332. https://doi.org/10.1016/j.mtchem.2020.100332.

Kuznetsova, O.V., Keppler, B.K., Timerbaev, A.R., 2023. Analysis of engineered nanoparticles in seawater using ICP-MS-based technology: From negative to positive samples. Molecules 28, 994. https://doi.org/10.3390/molecules28030994.

La Rosa, G., Iaconelli, M., Mancini, P., Bonanno Ferraro, G., Veneri, C., Bonadonna, L., Lucentini, L., Suffredini, E., 2020. First detection of SARS-CoV-2 in untreated wastewaters in Italy. Sci. Total Environ. 736, 139652. https://doi.org/10.1016/j.scitotenv.2020.139652.

Lai, R.W.S., Zhou, G.-J., Kang, H.-M., Jeong, C.-B., Djurišić, A.B., Lee, J.-S., Leung, K.M.Y., 2022. Contrasting toxicity of polystyrene nanoplastics to the rotifer *Brachionus koreanus* in the presence of zinc oxide nanoparticles and zinc ions. Aquat. Toxicol. 253, 106332. https://doi.org/10.1016/j.aquatox.2022.106332.

Lamers, M.M., Beumer, J., van der Vaart, J., Knoops, K., Puschhof, J.,

Breugem, T.I., Ravelli, R.B.G., Paul van Schayck, J., Mykytyn, A.Z., Duimel, H.Q., van Donselaar, E., Riesebosch, S., Kuijpers, H.J.H., Schipper, D., van de Wetering, W.J., de Graaf, M., Koopmans, M., Cuppen, E., Peters, P.J., Haagmans, B.L., Clevers, H., 2020. SARS-CoV-2 productively infects human gut enterocytes. Science 369, 50–54. https://doi.org/10.1126/science.abc1669.

Lan, T.C.T., Allan, M.F., Malsick, L.E., Woo, J.Z., Zhu, C., Zhang, F., Khandwala, S., Nyeo, S.S.Y., Sun, Y., Guo, J.U., Bathe, M., Näär, A., Griffiths, A., Rouskin, S., 2022. Secondary structural ensembles of the SARS-CoV-2 RNA genome in infected cells. Nat. Commun. 13, 1128. https://doi.org/10.1038/s41467-022-28603-2.

Langeveld, J., Schilperoort, R., Heijnen, L., Elsinga, G., Schapendonk, C.E.M., Fanoy, E., de Schepper, E.I.T., Koopmans, M.P.G., de Graaf, M., Medema, G., 2023. Normalisation of SARS-CoV-2 concentrations in wastewater: The use of flow, electrical conductivity and crAssphage. Sci. Total Environ. 865, 161196. https://doi.org/10.1016/j.scitotenv.2022.161196.

LeBlanc, R.M., Kasprzak, W.K., Longhini, A.P., Olenginski, L.T., Abulwerdi, F., Ginocchio, S., Shields, B., Nyman, J., Svirydava, M., Del Vecchio, C., Ivanic, J., Schneekloth Jr., J.S., Shapiro, B.A., Dayie, T.K., Le Grice, S.F.J., 2022. Structural insights of the conserved "priming loop" of hepatitis B virus pre-genomic RNA. J. Biomol. Struct. Dyn. 40, 9761–9773. https://doi.org/10.1080/07391102.2021.1934544.

Lee, H., Ju, M., Kim, Y., 2020. Estimation of emission of tire wear particles (TWPs) in Korea. Waste Manag. 108, 154–159. https://doi.org/10.1016/j.wasman.2020.04.037.

Lee, H., Shim, W.J., Kwon, J.-H., 2014. Sorption capacity of plastic debris for hydrophobic organic chemicals. Sci. Total Environ. 470–471, 1545–1552. https://doi.org/10.1016/j.scitotenv.2013.

08.023.

Lee, M., Kim, H., Ryu, H.-S., Moon, J., Khant, N.A., Yu, C., Yu, J.-H., 2022. Review on invasion of microplastic in our ecosystem and implications. Sci. Prog. 105. https://doi.org/10.1177/00368504221140766.

Leonel, A.G., Mansur, A.A.P., Mansur, H.S., 2021. Advanced functional nanostructures based on magnetic iron oxide nanomaterials for water remediation: A review. Water Res. 190, 116693. https://doi.org/10.1016/j.watres.2020.116693.

Li, M., Liu, W., Slaveykova, V.I., 2020. Effects of mixtures of engineered nanoparticles and metallic pollutants on aquatic organisms. Environments 7, 27. https://doi.org/10.3390/environments7040027.

Li, R., Zhu, L., Yang, K., Li, H., Zhu, Y.-G., Cui, L., 2021. Impact of urbanization on anti- biotic resistome in different microplastics: Evidence from a large-scale whole river analysis. Environ. Sci. Technol. 55, 8760–8770. https://doi.org/10.1021/acs.est.1c01395.

Li, S., Liu, X., Liu, G., Liu, C., 2023. Biomimetic nanotechnology for SARS-CoV-2 treatment. Viruses 15, 596. https://doi.org/10.3390/v15030596.

Li, X., Yang, B., Yang, J., Fan, Y., Qian, X., Li, H., 2021. Magnetic properties and its application in the prediction of potentially toxic elements in aquatic products by machine learning. Sci. Total Environ. 783, 147083. https://doi.org/10.1016/j.scitotenv.2021.147083.

Liang, Q., Shao, B., Tong, S., Liu, Z., Tang, L., Liu, Y., Cheng, M., He, Q., Wu, T., Pan, Y., Huang, J., Peng, Z., 2021. Recent advances of melamine self-assembled graphitic carbon nitride-based materials: Design, synthesis and application in energy and environment. Chem. Eng. J. 405, 126951. https://doi.org/

10.1016/j.cej.2020.126951.

Liu, N., Liang, Y., Wei, T., Zou, L., Bai, C., Huang, X., Wu, T., Xue, Y., Tang, M., Zhang, T., 2022. Protein corona mitigated the cytotoxicity of CdTe QDs to macrophages by targeting mitochondria. NanoImpact 25, 100367. https://doi.org/10.1016/j.impact.2021.100367.

Liu, P., Yang, M., Zhao, X., Guo, Y., Wang, L., Zhang, J., Lei, W., Han, W., Jiang, F., Liu, W.J., Gao, G.F., Wu, G., 2020. Cold-chain transportation in the frozen food industry may have caused a recurrence of COVID-19 cases in destination: Successful isolation of SARS-CoV-2 virus from the imported frozen cod package surface. Biosaf. Health 2, 199–201. https://doi.org/10.1016/j.bsheal.2020.11.003.

Liu, Q., Schauer, J., 2021. Airborne microplastics from waste as a transmission vector for COVID-19. Aerosol Air Qual. Res. 21, 200439. https://doi.org/10.4209/aaqr.2020.07.0439.

Liu, R., Zhang, H.Y., Ji, Z.X., Rallo, R., Xia, T., Chang, C.H., Nel, A., Cohen, Y., 2013. Development of structure–activity relationship for metal oxide nanoparticles. Nanoscale 5, 5644–5653. https://doi.org/10.1039/c3nr01533e.

Liu, S., Zhang, X., Zeng, K., He, C., Huang, Y., Xin, G., Huang, X., 2023. Insights into eco-corona formation and its role in the biological effects of nanomaterials from a molecular mechanisms perspective. Sci. Total Environ. 858, 159867. https://doi.org/10.1016/j.scitotenv.2022.159867.

Liu, Y., Baas, J., Peijnenburg, W.J.G.M., Vijver, M.G., 2016. Evaluating the combined toxicity of Cu and ZnO nanoparticles: Utility of the concept of additivity and a nested experimental design. Environ. Sci. Technol. 50, 5328–5337. https://doi.org/10.1021/acs.est. 6b00614.

Liu, Yanjun, Huang, Z., Zhou, J., Tang, J., Yang, C., Chen, C., Huang,

W., Dang, Z., 2020. Influence of environmental and biological macromolecules on aggregation kinetics of nanoplastics in aquatic systems. Water Res. 186, 116316. https://doi.org/10.1016/j.watres.2020.116316.

Liu, Y., Vijver, M.G., Pan, B., Peijnenburg, W.J.G.M., 2017. Toxicity models of metal mixtures established on the basis of "additivity" and "interactions". Front. Environ. Sci. Eng. 11, 10–13. https://doi.org/10.1007/s11783-017-0916-8.

Liu, Yuan, Ning, Z., Chen, Y., Guo, M., Liu, Y., Gali, N.K., Sun, L., Duan, Y., Cai, J., Westerdahl, D., Liu, X., Xu, K., Ho, K.-F., Kan, H., Fu, Q., Lan, K., 2020. Aerodynamic analysis of SARS-CoV-2 in two Wuhan hospitals. Nature 582, 557–560. https://doi.org/10.1038/s41586-020-2271-3.

Łoczechin, A., Séron, K., Barras, A., Giovanelli, E., Belouzard, S., Chen, Y.-T., Metzler-Nolte, N., Boukherroub, R., Dubuisson, J., Szunerits, S., 2019. Functional carbon quantum dots as medical countermeasures to human coronavirus. ACS Appl. Mater. Interfaces 11, 42964–42974. https://doi.org/10.1021/acsami.9b15032.

Loewe, S., Muischneck, H., 1926. Effect of combinations: Mathematical basis of problem. Arch. Exp. Pathol. Pharmakol. 114, 313–326.

Londono, N., Donovan, A.R., Shi, H., Geisler, M., Liang, Y., 2019. Effects of environmentally relevant concentrations of mixtures of TiO_2, ZnO and Ag ENPs on a river bacterial community. Chemosphere 230, 567–577. https://doi.org/10.1016/j.chemosphere.2019.05.110.

Lopes, S., Pinheiro, C., Soares, A.M.V.M., Loureiro, S., 2016. Joint toxicity prediction of nanoparticles and ionic counterparts: Simulating toxicity under a fate scenario. J. Hazard. Mater. 320, 1–9. https://doi.org/10.1016/j.jhazmat.2016.07.068.

Lowry, G.V., Avellan, A., Gilbertson, L.M., 2019. Opportunities and challenges for nanotechnology in the agri-tech revolution. Nat. Nanotechnol. 14, 517–522. https://doi.org/10.1038/s41565-019-0461-7.

Lowry, G.V., Gregory, K.B., Apte, S.C., Lead, J.R., 2012. Transformations of nanomaterials in the environment. Environ. Sci. Technol. 46, 6893–6899. https://doi.org/10.1021/es300839e.

Lu, J., Yu, Z., Ngiam, L., Guo, J., 2022. Microplastics as potential carriers of viruses could prolong virus survival and infectivity. Water Res. 225, 119115. https://doi.org/10.1016/j.watres.2022.119115.

Lu, T., Chen, F., 2012a. Multiwfn: A multifunctional wavefunction analyzer. J. Comput. Chem. 33, 580–592. https://doi.org/10.1002/jcc.22885.

Lu, T., Chen, F., 2012b. Quantitative analysis of molecular surface based on improved Marching Tetrahedra algorithm. J. Mol. Graph. Model. 38, 314–323. https://doi.org/10.1016/j.jmgm.2012.07.004.

Luo, H., Du, Q., Zhong, Z., Xu, Y., Peng, J., 2022. Protein-coated microplastics corona complex: An underestimated risk of microplastics. Sci. Total Environ. 851, 157948. https://doi.org/10.1016/j.scitotenv.2022.157948.

Ma, J., Chen, F., Xu, H., Jiang, H., Liu, J., Li, P., Chen, C.C., Pan, K., 2021. Face masks as a source of nanoplastics and microplastics in the environment: Quantification, characterization, and potential for bioaccumulation. Environ. Pollut. 288, 117748. https://doi. org/10.1016/j.envpol.2021.117748.

MacLeod, M., Breitholtz, M., Cousins, I.T., de Wit, C.A., Persson, L.M., Rudén, C., McLachlan, M.S., 2014. Identifying chemicals that are planetary boundary threats. Environ. Sci. Technol. 48, 11057–

11063. https://doi.org/10.1021/es501893m.

Maestre, J.P., Jarma, D., Yu, J.-R.F., Siegel, J.A., Horner, S.D., Kinney, K.A., 2021. Distribution of SARS-CoV-2 RNA signal in a home with COVID-19 positive occupants. Sci. Total Environ. 778, 146201. https://doi.org/10.1016/j.scitotenv.2021.146201.

Maleki Dizaj, S., Mennati, A., Jafari, S., Khezri, K., Adibkia, K., 2015. Antimicrobial activity of carbon-based nanoparticles. Adv. Pharm. Bull. 5, 19–23. https://doi.org/10.5681/apb.2015.003.

Mansouri, B., Maleki, A., Johari, S.A., Shahmoradi, B., Mohammadi, E., Shahsavari, S., Davari, B., 2016. Copper bioaccumulation and depuration in common carp (*Cyprinus carpio*) following co-exposure to TiO_2 and CuO nanoparticles. Arch. Environ. Contam. Toxicol. 71, 541–552. https://doi.org/10.1007/s00244-016-0313-5.

Martín-de-Lucía, I., Gonçalves, S.F., Leganés, F., Fernández-Piñas, F., Rosal, R., Loureiro, S., 2019. Combined toxicity of graphite-diamond nanoparticles and thiabendazole to *Daphnia magna*. Sci. Total Environ. 688, 1145–1154. https://doi.org/10.1016/j.scitotenv.2019.06.316.

Martinez, D.S.T., Ellis, L.-J.A., Da Silva, G.H., Petry, R., Medeiros, A.M.Z., Davoudi, H.H., Papadiamantis, A.G., Fazzio, A., Afantitis, A., Melagraki, G., Lynch, I., 2022. *Daphnia magna* and mixture toxicity with nanomaterials–current status and perspectives in data-driven risk prediction. Nano Today 43, 101430. https://doi. org/10.1016/j.nantod.2022.101430.

Matson, M.J., Yinda, C.K., Seifert, S.N., Bushmaker, T., Fischer, R.J., van Doremalen, N., Lloyd-Smith, J.O., Munster, V.J., 2020. Effect of environmental conditions on SARS-CoV-2 stability in human nasal mucus and sputum. Emerg. Infect. Dis. 26, 2276–2278. https://doi.org/10.3201/eid2609.202267.

Mei, M., Tan, X., 2021. Current strategies of antiviral drug discovery

for COVID-19. Front. Mol. Biosci. 8, 671263. https://doi.org/10.3389/fmolb.2021.671263.

Menéndez-Pedriza, A., Jaumot, J., 2020. Interaction of environmental pollutants with microplastics: A critical review of sorption factors, bioaccumulation and ecotoxicological effects. Toxics 8, 40. https://doi.org/10.3390/toxics8020040.

Meo, S.A., Almutairi, F.J., Abukhalaf, A.A., Alessa, O.M., Al-Khlaiwi, T., Meo, A.S., 2021. Sandstorm and its effect on particulate matter PM 2.5, carbon monoxide, nitrogen dioxide, ozone pollutants and SARS-CoV-2 cases and deaths. Sci. Total Environ. 795, 148764. https://doi.org/10.1016/j.scitotenv.2021.148764.

Mercogliano, R., Avio, C.G., Regoli, F., Anastasio, A., Colavita, G., Santonicola, S., 2020. Occurrence of microplastics in commercial seafood under the perspective of the human food chain. A review. J. Agric. Food Chem. 68, 5296–5301. https://doi.org/10.1021/acs.jafc.0c01209.

Mikolajczyk, A., Gajewicz, A., Mulkiewicz, E., Rasulev, B., Marchelek, M., Diak, M., Hirano, S., Zaleska-Medynska, A., Puzyn, T., 2018. Nano-QSAR modeling for ecosafe design of heterogeneous TiO_2-based nano-photocatalysts. Environ. Sci.: Nano 5, 1150–1160. https://doi.org/10.1039/C8EN00085A.

Mikolajczyk, A., Malankowska, A., Nowaczyk, G., Gajewicz, A., Hirano, S., Jurga, S., Zaleska-Medynska, A., Puzyn, T., 2016. Combined experimental and computational approach to developing efficient photocatalysts based on Au/Pd–TiO_2 nanoparticles. Environ. Sci.: Nano, 3, 1425–1435. https://doi.org/10.1039/c6en00232c.

Mikolajczyk, A., Sizochenko, N., Mulkiewicz, E., Malankowska, A., Rasulev, B., Puzyn, T., 2019. A chemoinformatics approach for the characterization of hybrid nanomaterials: Safer and efficient design perspective. Nanoscale 11, 11808–11818. https://doi.org/

10.1039/c9nr01162e.

Minetto, D., Volpi, Ghirardini A., Libralato, G., 2016. Saltwater ecotoxicology of Ag, Au, CuO, TiO_2, ZnO and C_{60} engineered nanoparticles: An overview. Environ. Int. 92–93, 189–201. https://doi.org/10.1016/j.envint.2016.03.041.

Mohan, S.V., Hemalatha, M., Kopperi, H., Ranjith, I., Kumar, A.K., 2021. SARS-CoV-2 in environmental perspective: Occurrence, persistence, surveillance, inactivation and challenges. Chem. Eng. J. 405, 126893. https://doi.org/10.1016/j.cej.2020.126893.

Morawska, L., Cao, J., 2020. Airborne transmission of SARS-CoV-2: The world should face the reality. Environ. Int. 139, 105730. https://doi.org/10.1016/j.envint.2020.105730.

Moreno, T., Pintó, R.M., Bosch, A., Moreno, N., Alastuey, A., Minguillón, M.C., Anfruns-Estrada, E., Guix, S., Fuentes, C., Buonanno, G., Stabile, L., Morawska, L., Querol, X., 2021. Tracing surface and airborne SARS-CoV-2 RNA inside public buses and subway trains. Environ. Int. 147, 106326. https://doi.org/10. 1016/j.envint.2020.106326.

Moresco, V., Oliver, D.M., Weidmann, M., Matallana-Surget, S., Quilliam, R.S., 2021. Survival of human enteric and respiratory viruses on plastics in soil, freshwater, and marine environments. Environ. Res. 199, 111367. https://doi.org/10.1016/j.envres.2021.111367.

Mottier, A., Mouchet, F., Laplanche, C., Cadarsi, S., Lagier, L., Arnault, J.-C., Girard, H. A., León, V., Vázquez, E., Sarrieu, C., Pinelli, É., Gauthier, L., Flahaut, E., 2016. Surface area of carbon nanoparticles: A dose metric for a more realistic ecotoxicological assessment. Nano Lett. 16, 3514–3518. https://doi.org/10.1021/acs.nanolett.6b00348.

Muhammad, A., He, J., Yu, T., Sun, C., Shi, D., Jiang, Y., Xianyu, Y., Shao, Y., 2022. Dietary exposure of copper and zinc oxides

nanoparticles affect the fitness, enzyme activity, and microbial community of the model insect, silkworm *Bombyx mori*. Sci. Total Environ. 813, 152608. https://doi.org/10.1016/j.scitotenv.2021.152608.

Müller, T.G., Sakin, V., Müller, B., 2019. A spotlight on viruses — Application of click chemistry to visualize virus-cell interactions. Molecules 24, 481. https://doi.org/10.3390/molecules24030481.

Musee, N., Zvimba, J.N., Schaefer, L.M., Nota, N., Sikhwivhilu, L.M., Thwala, M., 2014. Fate and behavior of ZnO- and Ag-engineered nanoparticles and a bacterial viability assessment in a simulated wastewater treatment plant. J. Environ. Sci. Heal. A 49, 59–66. https://doi.org/10.1080/10934529.2013.824302.

Na, M., Nam, S.H., Moon, K., Kim, J., 2023. Development of a nano-QSAR model for predicting the toxicity of nano-metal oxide mixtures to *Aliivibrio fischeri*. Environ. Sci.: Nano, 10, 325–337. https://doi.org/10.1039/D2EN00672C.

Nakao, S., Akita, K., Ozaki, A., Masumoto, K., Okuda, T., 2021. Circulation of fibrous microplastic (microfiber) in sewage and sewage sludge treatment processes. Sci. Total Environ. 795, 148873. https://doi.org/10.1016/j.scitotenv.2021.148873.

Nasser, F., Lynch, I., 2016. Secreted protein eco-corona mediates uptake and impacts of polystyrene nanoparticles on *Daphnia magna*. J. Proteomics 137, 45–51. https://doi.org/10.1016/j.jprot.2015.09.005.

Navarro, A., Gómez, L., Sanseverino, I., Niegowska, M., Roka, E., Pedraccini, R., Vargha, M., Lettieri, T., 2021. SARS-CoV-2 detection in wastewater using multiplex quantitative PCR. Sci. Total Environ. 797, 148890. https://doi.org/10.1016/j.scitotenv.2021.148890.

Nunes, B.Z., Moreira, L.B., Xu, E.G., Castro, Í.B., 2023. A global snapshot of microplastic contamination in sediments and biota

of marine protected areas. Sci. Total Environ. 865, 161293. https://doi.org/10.1016/j.scitotenv.2022.161293.

Nur, Y., Lead, J.R., Baalousha, M., 2015. Evaluation of charge and agglomeration behavior of TiO_2 nanoparticles in ecotoxicological media. Sci. Total Environ. 535, 45–53. https://doi.org/10.1016/j.scitotenv.2014.11.057.

Nyoka, N.W.-K., Kanyile, S.N., Bredenhand, E., Prinsloo, G.J., Voua Otomo, P., 2018. Biochar alleviates the toxicity of imidacloprid and silver nanoparticles (AgNPs) to *Enchytraeus albidus* (Oligochaeta). Environ. Sci. Pollut. Res. 25, 10937–10945. https://doi.org/10.1007/s11356-018-1383-x.

O'Brien, S., Okoffo, E.D., O'Brien, J.W., Ribeiro, F., Wang, X., Wright, S.L., Samanipour, S., Rauert, C., Toapanta, T.Y.A., Albarracin, R., Thomas, K.V., 2020. Airborne emissions of microplastic fibres from domestic laundry dryers. Sci. Total Environ. 747, 141175. https://doi.org/10.1016/j.scitotenv.2020.141175.

OECD, 2014. Guidance Document on the Validation of (Quantitative) Structure-Activity Relationship [(Q)SAR] Models, OECD Series on Testing and Assessment. OECD. https://doi.org/10.1787/9789264085442-en.

Oksel Karakus, C., Bilgi, E., Winkler, D.A., 2021. Biomedical nanomaterials: Applications, toxicological concerns, and regulatory needs. Nanotoxicology 15, 331–351. https://doi.org/10.1080/17435390.2020.1860265.

Olasupo, S.B., Uzairu, A., Shallangwa, G.A., Uba, S., 2020. Chemoinformatic studies on some inhibitors of dopamine transporter and the receptor targeting schizophrenia for developing novel antipsychotic agents. Heliyon 6, e04464. https://doi.org/10.1016/j.heliyon.2020.e04464.

Palmieri, V., Papi, M., 2020. Can graphene take part in the fight against COVID-19? Nano Today 33, 100883. https://doi.org/10.

1016/j.nantod.2020.100883.

Pan, B., Xing, B., 2008. Adsorption mechanisms of organic chemicals on carbon nanotubes. Environ. Sci. Technol. 42, 9005–9013. https://doi.org/10.1021/es801777n.

Parsai, T., Kumar, A., 2019. Understanding effect of solution chemistry on heteroaggregation of zinc oxide and copper oxide nanoparticles. Chemosphere 235, 457–469. https://doi.org/10.1016/j.chemosphere.2019.06.171.

Parsai, T., Kumar, A., 2020. Stability and characterization of mixture of three particle system containing ZnO-CuO nanoparticles and clay. Sci. Total Environ. 740, 140095. https://doi.org/10.1016/j.scitotenv.2020.140095.

Patel, K.D., Singh, R.K., Kim, H.-W., 2019. Carbon-based nanomaterials as an emerging platform for theranostics. Mater. Horiz. 6, 434–469. https://doi.org/10.1039/c8mh00966j.

Patil, S.M., Rane, N.R., Bankole, P.O., Krishnaiah, P., Ahn, Y., Park, Y.-K., Yadav, K.K., Amin, M.A., Jeon, B.-H., 2022. An assessment of micro- and nanoplastics in the biosphere: A review of detection, monitoring, and remediation technology. Chem. Eng. J. 430, 132913. https://doi.org/10.1016/j.cej.2021.132913.

Patton, T., Barrett, J., Brennan, J., Moran, N., 2006. Use of a spectrophotometric bioassay for determination of microbial sensitivity to manuka honey. J. Microbiol. Methods 64, 84–95. https://doi.org/10.1016/j.mimet.2005.04.007.

Paul, D., Kolar, P., Hall, S.G., 2021. A review of the impact of environmental factors on the fate and transport of coronaviruses in aqueous environments. npj Clean Water 4, 7. https://doi.org/10.1038/s41545-020-00096-w.

Peijnenburg, W.J.G.M., Baalousha, M., Chen, J., Chaudry, Q., Von Der Kammer, F., Kuhlbusch, T.A.J., Lead, J., Nickel, C., Quik,

J.T.K., Renker, M., Wang, Z., Koelmans, A.A., 2015. A review of the properties and processes determining the fate of engineered nanomaterials in the aquatic environment. Crit. Rev. Environ. Sci. Technol. 45, 2084–2134. https://doi.org/10.1080/10643389.2015.1010430.

Pérez Santín, E., Rodríguez Solana, R., González García, M., Del García Suárez, M.M., Blanco Díaz, G.D., Cima Cabal, M.D., Moreno Rojas, J.M., López Sánchez, J.I., 2021. Toxicity prediction based on artificial intelligence: A multidisciplinary overview. WIREs Comput. Mol. Sci. 11, e1516. https://doi.org/10.1002/wcms.1516.

Pérez-Hernández, H., Pérez-Moreno, A., Sarabia-Castillo, C.R., García-Mayagoitia, S., Medina-Pérez, G., López-Valdez, F., Campos-Montiel, R.G., Jayanta-Kumar, P., Fernández-Luqueño, F., 2021. Ecological drawbacks of nanomaterials produced on an industrial scale: Collateral effect on human and environmental health. Water Air Soil Pollut. 232, 435. https://doi.org/10.1007/s11270-021-05370-2.

Persson, L., Carney Almroth, B.M., Collins, C.D., Cornell, S., de Wit, C.A., Diamond, M.L., Fantke, P., Hassellöv, M., MacLeod, M., Ryberg, M.W., Søgaard Jørgensen, P., Villarrubia-Gómez, P., Wang, Z., Hauschild, M.Z., 2022. Outside the safe operating space of the planetary boundary for novel entities. Environ. Sci. Technol. 56, 1510–1521. https://doi.org/10.1021/acs.est.1c04158.

Persson, L.M., Breitholtz, M., Cousins, I.T., de Wit, C.A., MacLeod, M., McLachlan, M.S., 2013. Confronting unknown planetary boundary threats from chemical pollution. Environ. Sci. Technol. 47, 12619–12622. https://doi.org/10.1021/es402501c.

Pikula, K., Johari, S.A., Santos-Oliveira, R., Golokhvast, K., 2022. Individual and binary mixture toxicity of five nanoparticles in marine microalga *Heterosigma akashiwo*. Int. J. Mol. Sci. 23, 990. https://doi.org/10.3390/ijms23020990.

Puzyn, T., Rasulev, B., Gajewicz, A., Hu, X., Dasari, T.P., Michalkova, A., Hwang, H.-M., Toropov, A., Leszczynska, D., Leszczynski, J., 2011. Using nano-QSAR to predict the cytotoxicity of metal oxide nanoparticles. Nat. Nanotechnol. 6, 175–178. https://doi.org/10.1038/nnano.2011.10.

Qi, P., Qiu, L., Feng, D., Gu, Z., Guo, B., Yan, X., 2023. Distinguish the toxic differentiations between acute exposure of micro- and nano-plastics on bivalves: An integrated study based on transcriptomic sequencing. Aquat. Toxicol. 254, 106367. https://doi.org/10.1016/j.aquatox.2022.106367.

Qi, Z., Hou, L., Zhu, D., Ji, R., Chen, W., 2014. Enhanced transport of phenanthrene and 1-naphthol by colloidal graphene oxide nanoparticles in saturated soil. Environ. Sci. Technol. 48, 10136–10144. https://doi.org/10.1021/es500833z.

Ragab, D., Salah Eldin, H., Taeimah, M., Khattab, R., Salem, R., 2020. The COVID-19 cytokine storm; What we know so far. Front. Immunol. 11, 1446. https://doi.org/10.3389/fimmu.2020.01446.

Rai, P.K., Lee, J., Brown, R.J.C., Kim, K.H., 2021. Environmental fate, ecotoxicity biomarkers, and potential health effects of micro- and nano-scale plastic contamination. J. Hazard. Mater. 403, 123910. https://doi.org/10.1016/j.jhazmat.2020.123910.

Randazzo, W., Truchado, P., Cuevas-Ferrando, E., Simón, P., Allende, A., Sánchez, G., 2020. SARS-CoV-2 RNA in wastewater anticipated COVID-19 occurrence in a low prevalence area. Water Res. 181, 115942. https://doi.org/10.1016/j.watres.2020.115942.

Razzini, K., Castrica, M., Menchetti, L., Maggi, L., Negroni, L., Orfeo, N.V., Pizzoccheri, A., Stocco, M., Muttini, S., Balzaretti, C.M., 2020. SARS-CoV-2 RNA detection in the air and on surfaces in the COVID-19 ward of a hospital in Milan, Italy. Sci. Total Environ. 742, 140540. https://doi.org/10.1016/j.scitotenv.2020.

140540.

Reddy, N., Lynch, B., Gujral, J., Karnik, K., 2023. Alternatives to animal testing in toxicity testing: Current status and future perspectives in food safety assessments. Food Chem. Toxicol. 179, 113944. https://doi.org/10.1016/j.fct.2023.113944.

Rezania, S., Park, J., Md Din, M.F., Mat Taib, S., Talaiekhozani, A., Kumar Yadav, K., Kamyab, H., 2018. Microplastics pollution in different aquatic environments and biota: A review of recent studies. Mar. Pollut. Bull. 133, 191–208. https://doi.org/10.1016/j.marpolbul.2018.05.022.

Rider, C.V., Simmons, J.E., 2018. Chemical mixtures and combined chemical and nonchemical stressors. Cham: Springer International Publishing.

Robertson, M.P., Igel, H., Baertsch, R., Haussler, D., Ares, M., Scott, W.G., 2004. The structure of a rigorously conserved RNA element within the SARS virus genome. PLoS Biol. 3, e5. https://doi. org/10.1371/journal.pbio.0030005.

Rockström, J., Steffen, W., Noone, K., Persson, Å., Chapin, F.S.I., Lambin, E., Lenton, T.M., Scheffer, M., Folke, C., Schellnhuber, H.J., Nykvist, B., de Wit, C.A., Hughes, T., van der Leeuw, S., Rodhe, H., Sörlin, S., Snyder, P.K., Costanza, R., Svedin, U., Falkenmark, M., Karlberg, L., Corell, R.W., Fabry, V.J., Hansen, J., Walker, B., Liverman, D., Richardson, K., Crutzen, P., Foley, J., 2009. Planetary boundaries: Exploring the safe operating space for humanity. Ecol. Soc. 14, 32. https://doi.org/10.5751/ES-03180-140232.

Rodrigues, C.C., Salla, R.F., Rocha, T.L., 2023. Bioaccumulation and ecotoxicological impact of micro(nano)plastics in aquatic and land snails: Historical review, current research and emerging trends. J. Hazard. Mater. 444, 130382. https://doi.org/10.1016/j.jhazmat.2022.130382.

Roje, Ž., Ilić, K., Galić, E., Pavičić, I., Turčić, P., Stanec, Z., Vrček, I.V., 2019. Synergistic effects of parabens and plastic nanoparticles on proliferation of human breast cancer cells. Arh. Hig. Rada. Toksikol. 70, 310–314. https://doi.org/10.2478/aiht-2019-70-3372.

Romera-Castillo, C., Lucas, A., Mallenco-Fornies, R., Briones-Rizo, M., Calvo, E., Pelejero, C., 2023. Abiotic plastic leaching contributes to ocean acidification. Sci. Total Environ. 854, 158683. https://doi. org/10.1016/j.scitotenv.2022.158683.

Rompelberg, C., Heringa, M.B., van Donkersgoed, G., Drijvers, J., Roos, A., Westenbrink, S., Peters, R., van Bemmel, G., Brand, W., Oomen, A.G., 2016. Oral intake of added titanium dioxide and its nanofraction from food products, food supplements and toothpaste by the Dutch population. Nanotoxicology 10, 1404–1414. https://doi.org/10.1080/17435390.2016.1222457.

Roscher, L., Fehres, A., Reisel, L., Halbach, M., Scholz-Böttcher, B., Gerriets, M., Badewien, T.H., Shiravani, G., Wurpts, A., Primpke, S., Gerdts, G., 2021. Microplastic pollution in the Weser estuary and the German North Sea. Environ. Pollut. 288, 117681. https://doi.org/10.1016/j.envpol.2021.117681.

Rosenfeldt, R.R., Seitz, F., Haigis, A.-C., Höger, J., Zubrod, J.P., Schulz, R., Bundschuh, M., 2016. Nanosized titanium dioxide influences copper-induced toxicity during aging as a function of environmental conditions. Environ. Toxicol. Chem. 35, 1766–1774. https://doi.org/10.1002/etc.3325.

Roy, J., Ojha, P.K., Roy, K., 2019. Risk assessment of heterogeneous TiO_2-based engineered nanoparticles (NPs): A QSTR approach using simple periodic table based descriptors. Nanotoxicology 13, 701–716. https://doi.org/10.1080/17435390.2019.1593543.

Roy, K., Kar, S., Das, R.N., 2015. A Primer on QSAR/QSPR Modeling. Cham: Springer International Publishing AG. https://doi.org/10.

1007/978-3-319-17281-1.

Saavedra, J., Stoll, S., Slaveykova, V.I., 2019. Influence of nanoplastic surface charge on eco-corona formation, aggregation and toxicity to freshwater zooplankton. Environ. Pollut. 252, 715–722. https://doi.org/10.1016/j.envpol.2019.05.135.

Saingam, P., Li, B., Nguyen Quoc, B., Jain, T., Bryan, A., Winkler, M.K.H., 2023. Wastewater surveillance of SARS-CoV-2 at intra-city level demonstrated high resolution in tracking COVID-19 and calibration using chemical indicators. Sci. Total Environ. 866, 161467. https://doi.org/10.1016/j.scitotenv.2023.161467.

Sala-Comorera, L., Reynolds, L.J., Martin, N.A., O'Sullivan, J.J., Meijer, W.G., Fletcher, N.F., 2021. Decay of infectious SARS-CoV-2 and surrogates in aquatic environments. Water Res. 201, 117090. https://doi.org/10.1016/j.watres.2021.117090.

Sanchez-Galan, J.E., Ureña, G., Escovar, L.F., Fabrega-Duque, J.R., Coles, A., Kurt, Z., 2021. Challenges to detect SARS-CoV-2 on environmental media, the need and strategies to implement the detection methodologies in wastewaters. J. Environ. Chem. Eng. 9, 105881. https://doi.org/10.1016/j.jece.2021.105881.

Sánchez-López, E., Gomes, D., Esteruelas, G., Bonilla, L., Lopez-Machado, A.L., Galindo, R., Cano, A., Espina, M., Ettcheto, M., Camins, A., Silva, A.M., Durazzo, A., Santini, A., Garcia, M.L., Souto, E.B., 2020. Metal-based nanoparticles as antimicrobial agents: An overview. Nanomaterials 10, 292. https://doi.org/10.3390/nano10020292.

Sanchís, J., Jiménez-Lamana, J., Abad, E., Szpunar, J., Farré, M., 2020. Occurrence of cerium-, titanium-, and silver-bearing nanoparticles in the Besòs and Ebro Rivers. Environ. Sci. Technol. 54, 3969–3978. https://doi.org/10.1021/acs.est.9b05996.

Saravanan, A., Kumar, P.S., Hemavathy, R.V., Jeevanantham, S., Jawahar, M.J., Neshaanthini, J.P., Saravanan, R., 2022. A review on synthesis methods and recent applications of nanomaterial in wastewater treatment: Challenges and future perspectives. Chemosphere 307, 135713. https://doi.org/10.1016/j.chemosphere.2022.135713.

Savastano, A., Ibáñez de Opakua, A., Rankovic, M., Zweckstetter, M., 2020. Nucleocapsid protein of SARS-CoV-2 phase separates into RNA-rich polymerase-containing condensates. Nat. Commun. 11, 6041. https://doi.org/10.1038/s41467-020-19843-1.

Sayadi, M.H., Pavlaki, M.D., Loureiro, S., Martins, R., Tyler, C.R., Mansouri, B., Kharkan, J., Shekari, H., 2022. Co-exposure of Zinc oxide nanoparticles and multi-layer graphenes in blackfish (*Capoeta fusca*): Evaluation of lethal, behavioural, and histopathological effects. Ecotoxicology 31, 425–439. https://doi.org/10.1007/s10646-022-02521-x.

Sayadi, M.H., Pavlaki, M.D., Martins, R., Mansouri, B., Tyler, C.R., Kharkan, J., Shekari, H., 2021. Bioaccumulation and toxicokinetics of zinc oxide nanoparticles (ZnO NPs) co-exposed with graphene nanosheets (GNs) in the blackfish (*Capoeta fusca*). Chemosphere 269, 128689. https://doi.org/10.1016/j.chemosphere.2020.128689.

Sellami, B., Mezni, A., Khazri, A., Bouzidi, I., Saidani, W., Sheehan, D., Beyrem, H., 2017. Toxicity assessment of ZnO-decorated Au nanoparticles in the mediterranean clam *Ruditapes decussatus*. Aquat. Toxicol. 188, 10–19. https://doi.org/10.1016/j.aquatox.2017.04.005.

Serrano-Aroca, Á., Takayama, K., Tuñón-Molina, A., Seyran, M., Hassan, S.S., Pal Choudhury, P., Uversky, V.N., Lundstrom, K., Adadi, P., Palù, G., Aljabali, A.A.A., Chauhan, G., Kandimalla, R., Tambuwala, M.M., Lal, A., Abd El-Aziz, T.M., Sherchan, S., Barh, D., Redwan, E.M., Bazan, N.G., Mishra, Y.K., Uhal, B.D., Brufsky,

A., 2021. Carbon-based nanomaterials: Promising antiviral agents to combat COVID-19 in the microbial-resistant era. ACS Nano 15, 8069–8086. https://doi.org/10.1021/acsnano.1c00629.

Shao, B., Liu, Z., Tang, L., Liu, Y., Liang, Q., Wu, T., Pan, Y., Zhang, X., Tan, X., Yu, J., 2022. The effects of biochar on antibiotic resistance genes (ARGs) removal during different environmental governance processes: A review. J. Hazard. Mater. 435, 129067. https://doi. org/10.1016/j.jhazmat.2022.129067.

Shao, B., Wang, J., Liu, Z., Zeng, G., Tang, L., Liang, Q., He, Q., Wu, T., Liu, Y., Yuan, X., 2020. $Ti_3C_2T_x$ MXene decorated black phosphorus nanosheets with improved visible-light photocatalytic activity: Experimental and theoretical studies. J. Mater. Chem. A 8, 5171–5185. https://doi.org/10.1039/c9ta13610j.

Sharma, B., Tiwari, S., Kumawat, K.C., Cardinale, M., 2023. Nano-biofertilizers as bio-emerging strategies for sustainable agriculture development: Potentiality and their limitations. Sci. Total Environ. 860, 160476. https://doi.org/10.1016/j.scitotenv.2022.160476.

Sheng, Y., Liu, Y., Wang, K., Cizdziel, J.V., Wu, Y., Zhou, Y., 2021. Ecotoxicological effects of micronized car tire wear particles and their heavy metals on the earthworm (*Eisenia fetida*) in soil. Sci. Total Environ. 793, 148613. https://doi.org/10.1016/j.scitotenv.2021.148613.

Shi, X., Wang, X., Huang, R., Tang, C., Hu, C., Ning, P., Wang, F., 2022. Cytotoxicity and genotoxicity of polystyrene micro- and nanoplastics with different size and surface modification in A549 cells. Int. J. Nanomedicine 17, 4509–4523. https://doi.org/10.2147/IJN.S381776.

Shin, M.D., Shukla, S., Chung, Y.H., Beiss, V., Chan, S.K., Ortega-

Rivera, O.A., Wirth, D. M., Chen, A., Sack, M., Pokorski, J.K., Steinmetz, N.F., 2020. COVID-19 vaccine development and a potential nanomaterial path forward. Nat. Nanotechnol. 15, 646–655. https://doi.org/10.1038/s41565-020-0737-y.

Simelane, S., Dlamini, L.N., 2019. An investigation of the fate and behaviour of a mixture of WO_3 and TiO_2 nanoparticles in a wastewater treatment plant. J. Environ. Sci. 76, 37–47. https://doi.org/10.1016/j.jes.2018.03.018.

Singh, D., Kumar, A., 2020. Binary mixture of nanoparticles in sewage sludge: Impact on spinach growth. Chemosphere 254, 126794. https://doi.org/10.1016/j.chemosphere.2020.126794.

Singh, N.B., Chaudhary, R.G., Desimone, M.F., Agrawal, A., Shukla, S.K., 2023. Green synthesized nanomaterials for safe technology in sustainable agriculture. Curr. Pharm. Biotechnol. 24, 61–85. https://doi.org/10.2174/1389201023666220608113924.

Skiba, E., Pietrzak, M., Glińska, S., Wolf, W.M., 2021. The combined effect of ZnO and CeO_2 nanoparticles on *Pisum sativum* L.: A photosynthesis and nutrients uptake study. Cells 10, 3105. https://doi.org/10.3390/cells10113105.

Slot, E., Hogema, B.M., Reusken, C.B.E.M., Reimerink, J.H., Molier, M., Karregat, J.H.M., IJlst, J., Novotný, V.M.J., van Lier, R.A.W., Zaaijer, H.L., 2020. Low SARS-CoV-2 seroprevalence in blood donors in the early COVID-19 epidemic in the Netherlands. Nat. Commun. 11, 5744. https://doi.org/10.1038/s41467-020-19481-7.

Snape, M.D., Viner, R.M., 2020. COVID-19 in children and young people. Science 370, 286–288. https://doi.org/10.1126/science.abd6165.

Stadnytskyi, V., Bax, C.E., Bax, A., Anfinrud, P., 2020. The airborne lifetime of small speech droplets and their potential importance in SARS-CoV-2 transmission. Proc. Natl. Acad. Sci. 117, 11875–

11877. https://doi.org/10.1073/pnas.2006874117.

Steffan, J.J., Derby, J.A., Brevik, E.C., 2020. Soil pathogens that may potentially cause pandemics, including severe acute respiratory syndrome (SARS) coronaviruses. Curr. Opin. Environ. Sci. Health 17, 35–40. https://doi.org/10.1016/j.coesh.2020.08.005.

Steffen, W., Richardson, K., Rockström, J., Cornell, S.E., Fetzer, I., Bennett, E.M., Biggs, R., Carpenter, S.R., de Vries ,W., de Wit, C.A., Folke, C., Gerten, D., Heinke, J., Mace, G.M., Persson, L.M., Ramanathan, V., Reyers, B., Sörlin, S., 2015. Sustainability. Planetary boundaries: Guiding human development on a changing planet. Science 347, 1259855. https://doi.org/10.1126/science.1259855.

Stuart, E.J.E., Compton, R.G., 2015. Nanoparticles-emerging contaminants. In environmental analysis by electrochemical sensors and biosensors; Moretto, L.M., Kalcher, K., Eds.; Springer; Nanostructure science and technology, pp 855–878. https://doi.org/10.1007/978-1-4939-1301-5_8.

Sun, N., Shi, H., Li, X., Gao, C., Liu, R., 2023. Combined toxicity of micro/nanoplastics loaded with environmental pollutants to organisms and cells: Role, effects, and mechanism. Environ. Int. 171, 107711. https://doi.org/10.1016/j.envint.2022.107711.

Sun, Q., Xie, H.-B., Chen, J., Li, X., Wang, Z., Sheng, L., 2013. Molecular dynamics simulations on the interactions of low molecular weight natural organic acids with C_{60}. Chemosphere 92, 429–434. https://doi.org/10.1016/j.chemosphere.2013.01.039.

Sun, S., Shi, W., Tang, Y., Han, Y., Du, X., Zhou, W., Zhang, W., Sun, C., Liu, G., 2021. The toxic impacts of microplastics (MPs) and polycyclic aromatic hydrocarbons (PAHs) on haematic parameters in a marine bivalve species and their potential mechanisms of action. Sci. Total Environ. 783, 147003. https://

doi.org/10.1016/j.scitotenv.2021.147003.

Sundaram, B., Kumar, A., 2017. Long-term effect of metal oxide nanoparticles on activated sludge. Water Sci. Technol. 75, 462–473. https://doi.org/10.2166/wst.2016.541.

Talebian, S., Wallace, G.G., Schroeder, A., Stellacci, F., Conde, J., 2020. Nanotechnology-based disinfectants and sensors for SARS-CoV-2. Nat. Nanotechnol. 15, 618–621. https://doi.org/10.1038/s41565-020-0751-0.

Tiede, K., Hanssen, S.F., Westerhoff, P., Fern, G.J., Hankin, S.M., Aitken, R.J., Chaudhry, Q., Boxall, A.B., 2016. How important is drinking water exposure for the risks of engineered nanoparticles to consumers? Nanotoxicology 10, 102–110. https://doi.org/10.3109/17435390.2015.1022888.

Tong, T., Fang, K., Thomas, S.A., Kelly, J.J., Gray, K.A., Gaillard, J.-F., 2014. Chemical interactions between nano-ZnO and nano-TiO_2 in a natural aqueous medium. Environ. Sci. Technol. 48, 7924–7932. https://doi.org/10.1021/es501168p.

Tong, T., Wilke, C.M., Wu, J., Binh, C.T.T., Kelly, J.J., Gaillard, J.-F., Gray, K.A., 2015. Combined toxicity of nano-ZnO and nano-TiO_2: From single- to multinanomaterial systems. Environ. Sci. Technol. 49, 8113–8123. https://doi.org/10.1021/acs.est.5b02148.

Topol, E.J., 2020. COVID-19 can affect the heart. Science 370, 408–409. https://doi.org/10.1126/science.abe2813.

Tou, F., Wu, J., Fu, J., Niu, Z., Liu, M., Yang, Y., 2021. Titanium and zinc-containing nanoparticles in estuarine sediments: Occurrence and their environmental implications. Sci. Total Environ. 754, 142388. https://doi.org/10.1016/j.scitotenv.2020.142388.

Trinh, T.X., Kim, J., 2021. Status quo in data availability and

predictive models of nano-mixture toxicity. Nanomaterials 11, 124. https://doi.org/10.3390/nano11010124.

Trinh, T.X., Seo, M., Yoon, T.H., Kim, J., 2022. Developing random forest based QSAR models for predicting the mixture toxicity of TiO_2 based nano-mixtures to *Daphnia magna*. NanoImpact 25, 100383. https://doi.org/10.1016/j.impact.2022.100383.

Tropsha, A., 2010. Best practices for QSAR model development, validation, and exploitation. Mol. Inform. 29, 476–488. https://doi.org/10.1002/minf.201000061.

Turner, J.S., Kim, W., Kalaidina, E., Goss, C.W., Rauseo, A.M., Schmitz, A.J., Hansen, L., Haile, A., Klebert, M.K., Pusic, I., O'Halloran, J.A., Presti, R.M., Ellebedy, A.H., 2021. SARS-CoV-2 infection induces long-lived bone marrow plasma cells in humans. Nature 595, 421–425. https://doi.org/10.1038/s41586-021-03647-4.

UNEP, 2016. Marine plastic debris and microplastics — Global lessons and research to inspire action and guide policy change. United Nations Environment Programme, Nairobi. https://doi.org/10. 13140/RG.2.2.30493.51687.

Upfold, N.S., Luke, G.A., Knox, C., 2021. Occurrence of human enteric viruses in water sources and shellfish: A focus on Africa. Food Environ. Virol. 13, 1–31. https://doi.org/10.1007/s12560-020-09456-8.

Van Leeuwen, C.J., Bro-Rasmussen, F., Feijtel, T.C., Arndt, R., Bussian, B.M., Calamari, D., Glynn, P., Grandy, N.J., Hansen, B., van Hemmen, J.J., Hurst, P., King, N., Koch, R., Müller, M., Solbé, J.F., Speijers, G.A., Vermeire, T., 1996. Risk assessment and management of new and existing chemicals. Environ. Toxicol. Phar. 2, 243–299. https://doi.org/10.1016/s1382-6689(96)00072-5.

Verma, A., Uzun, O., Hu, Y., Hu, Y., Han, H.-S., Watson, N., Chen, S.,

Irvine, D.J., Stellacci, F., 2008. Surface-structure-regulated cell-membrane penetration by monolayer-protected nanoparticles. Nat. Mater. 7, 588–595. https://doi.org/10.1038/nmat2202.

Vermisoglou, E., Panáček, D., Jayaramulu, K., Pykal, M., Frébort, I., Kolář, M., Hajdúch, M., Zbořil, R., Otyepka, M., 2020. Human virus detection with graphene-based materials. Biosens. Bioelectron. 166, 112436. https://doi.org/10.1016/j.bios.2020.112436.

Vijver, M.G., Elliott, E.G., Peijnenburg, W.J.G.M., de Snoo, G.R., 2011. Response predictions for organisms water-exposed to metal mixtures: A meta-analysis. Environ. Toxicol. Chem. 30, 1482–1487. https://doi.org/10.1002/etc.499.

Vijver, M.G., Peijnenburg, W.J.G.M., de Snoo, G.R., 2010. Toxicological mixture models are based on inadequate assumptions. Environ. Sci. Technol. 44, 4841–4842. https://doi.org/10.1021/es1001659.

Visalli, G., Facciolà, A., Pruiti Ciarello, M., De Marco, G., Maisano, M., Di Pietro, A., 2021. Acute and sub-chronic effects of microplastics (3 and 10 μm) on the human intestinal cells HT-29. Int. J. Environ. Res. Public Health 18, 5833. https://doi.org/10.3390/ijerph18115833.

Walker, J.D., Enache, M., Dearden, J.C., 2003. Quantitative cationic–activity relationships for predicting toxicity of metals. Environ. Toxicol. Chem. 22, 1916–1935. https://doi.org/10.1897/02-568.

Wang, J., Peng, C., Dai, Y., Li, Y., Jiao, S., Ma, X., Liu, X., Wang, L., 2022. Slower antibiotics degradation and higher resistance genes enrichment in plastisphere. Water Res. 222, 118920. https://doi.org/10.1016/j.watres.2022.118920.

Wang, M., Yu, H.L., Chen, Y., Huang, M.X., 2021. Machine learning assisted screening of non-rare-earth elements for Mg alloys with

low stacking fault energy. Comp. Mater. Sci. 196, 110544. https://doi.org/10.1016/j.commatsci.2021.110544.

Wang, Q., Li, Y., Lung, D.C., Chan, P.-T., Dung, C.-H., Jia, W., Miao, T., Huang, J., Chen, W., Wang, Z., Leung, K.-M., Lin, Z., Wong, D., Tse, H., Wong, S.C.Y., Choi, G.K.-Y., Lam, J,Y.-W., To, K.K.-W., Cheng, V.C.-C., Yuen, K.-Y., 2022. Aerosol transmission of SARS-CoV-2 due to the chimney effect in two high-rise housing drainage stacks. J. Hazard. Mater. 421, 126799. https://doi.org/10.1016/j. jhazmat.2021.126799.

Wang, W., Do, A.T.N., Kwon, J.-H., 2022. Ecotoxicological effects of micro- and nanoplastics on terrestrial food web from plants to human beings. Sci. Total Environ. 834, 155333. https://doi. org/10.1016/j.scitotenv.2022.155333.

Wang, X., Ren, X.-M., He, H., Li, F., Liu, K., Zhao, F., Hu, H., Zhang, P., Huang, B., Pan, X., 2023. Cytotoxicity and pro-inflammatory effect of polystyrene nano-plastic and micro-plastic on RAW264.7 cells. Toxicology 484, 153391. https://doi.org/10. 1016/j.tox.2022. 153391.

Wang, Y., Chen, J., Wei, X., Hernandez Maldonado, A.J., Chen, Z., 2017. Unveiling adsorption mechanisms of organic pollutants onto carbon nanomaterials by density functional theory computations and linear free energy relationship modeling. Environ. Sci. Technol. 51, 11820–11828. https://doi.org/10.1021/ acs.est.7b02707.

Wang, Y., Chen, X., 2020. A joint optimization QSAR model of fathead minnow acute toxicity based on a radial basis function neural network and its consensus modeling. RSC Adv. 10, 21292–21308. https://doi.org/10.1039/d0ra02701d.

Wang, Z., Jin, S., Zhang, F., Wang, D., 2020. Combined toxicity of TiO_2 nanospherical particles and TiO_2 nanotubes to two micro-algae with different morphology. Nanomaterials 10, 2559.

https://doi.org/10.3390/nano10122559.

Wang, Z., Vijver, M.G., Peijnenburg, W.J.G.M., 2018. Multiscale coupling strategy for nano ecotoxicology prediction. Environ. Sci. Technol. 52, 7598–7600. https://doi.org/10.1021/acs.est.8b02895.

Wang, Z., Zhang, F., Vijver, M.G., Peijnenburg, W.J.G.M., 2021. Graphene nanoplatelets and reduced graphene oxide elevate the microalgal cytotoxicity of nano-zirconium oxide. Chemosphere 276, 130015. https://doi.org/10.1016/j.chemosphere.2021.130015.

Wheeler, K.E., Chetwynd, A.J., Fahy, K.M., Hong, B.S., Tochihuitl, J.A., Foster, L.A., Lynch, I., 2021. Environmental dimensions of the protein corona. Nat. Nanotechnol. 16, 617–629. https://doi.org/10.1038/s41565-021-00924-1.

Wiktorczyk-Kapischke, N., Grudlewska-Buda, K., Wałecka-Zacharska, E., Kwiecińska-Piróg, J., Radtke, L., Gospodarek-Komkowska, E., Skowron, K., 2021. SARS-CoV-2 in the environment — Non-droplet spreading routes. Sci. Total Environ. 770, 145260. https://doi.org/10.1016/j.scitotenv.2021.145260.

Wilke, C.M., Tong, T., Gaillard, J.-F., Gray, K.A., 2016. Attenuation of microbial stress due to nano-Ag and nano-TiO_2 interactions under dark conditions. Environ. Sci. Technol. 50, 11302–11310. https://doi.org/10.1021/acs.est.6b02271.

Wilke, C.M., Wunderlich, B., Gaillard, J.-F., Gray, K.A., 2018. Synergistic bacterial stress results from exposure to nano-Ag and nano-TiO_2 mixtures under light in environmental media. Environ. Sci. Technol. 52, 3185–3194. https://doi.org/10.1021/acs.est.7b05629.

Wu, S., Gaillard, J.-F., Gray, K.A., 2021. The impacts of metal-based engineered nanomaterial mixtures on microbial systems: A

review. Sci. Total Environ. 780, 146496. https://doi.org/10.1016/j.scitotenv.2021.146496.

Wu, S., Zhang, S., Gong, Y., Shi, L., Zhou, B., 2020. Identification and quantification of titanium nanoparticles in surface water: A case study in Lake Taihu, China. J. Hazard. Mater. 382, 121045. https://doi.org/10.1016/j.jhazmat.2019.121045.

Wu, T., He, Q., Liu, Z., Shao, B., Liang, Q., Pan, Y., Huang, J., Peng, Z., Liu, Y., Zhao, C., Yuan, X., Tang, L., Gong, S., 2022. Tube wall delamination engineering induces photogenerated carrier separation to achieve photocatalytic performance improvement of tubular g-C_3N_4. J. Hazard. Mater. 424, 127177. https://doi.org/10.1016/j.jhazmat.2021.127177.

Wyrzykowska, E., Mikolajczyk, A., Lynch, I., Jeliazkova, N., Kochev, N., Sarimveis, H., Doganis, P., Karatzas, P., Afantitis, A., Melagraki, G., Serra, A., Greco, D., Subbotina, J., Lobaskin, V., Bañares, M.A., Valsami-Jones, E., Jagiello, K., Puzyn, T., 2022. Representing and describing nanomaterials in predictive nanoinformatics. Nat. Nanotechnol. 17, 924–932. https://doi.org/10.1038/s41565-022-01173-6.

Xia, J., Zhao, H.Z., Lu, G.H., 2013. Effects of selected metal oxide nanoparticles on multiple biomarkers in *Carassius auratus*. Biomed. Environ. Sci. 26, 742–749. https://doi.org/10.3967/0895-3988.2013.09.005.

Xiao, Y., Peijnenburg, W.J.G.M., Chen, G., Vijver, M.G., 2016. Toxicity of copper nanoparticles to *Daphnia magna* under different exposure conditions. Sci. Total Environ. 563–564, 81–88. https://doi.org/10.1016/j.scitotenv.2016.04.104.

Xin, X., Chen, B., Yang, M., Gao, S., Wang, H., Gu, W., Li, X., Zhang, B., 2023. A critical review on the interaction of polymer particles and co-existing contaminants: Adsorption mechanism, exposure factors, effects on plankton species. J. Hazard. Mater. 445,

130463. https://doi.org/10.1016/j.jhazmat.2022.130463.

Xu, J.-L., Lin, X., Wang, J.J., Gowen, A.A., 2022. A review of potential human health impacts of micro- and nanoplastics exposure. Sci. Total Environ. 851, 158111. https://doi.org/10.1016/j.scitotenv. 2022.158111.

Xu, L., Wang, Z., Zhao, J., Lin, M., Xing, B., 2020. Accumulation of metal-based nanoparticles in marine bivalve mollusks from offshore aquaculture as detected by single particle ICP-MS. Environ. Pollut. 260, 114043. https://doi.org/10.1016/j.envpol. 2020.114043.

Xu, M., Yang, H., Liu, G., Tang, Y., Li, W., 2022. In silico prediction of chemical aquatic toxicity by multiple machine learning and deep learning approaches. J. Appl. Toxicol. 42, 1766–1776. https://doi.org/10.1002/jat.4354.

Yang, K., Xing, B., 2010. Adsorption of organic compounds by carbon nanomaterials in aqueous phase: Polanyi theory and its application. Chem. Rev. 110, 5989–6008. https://doi.org/10.1021/cr100059s.

Yang, L., Chen, P., He, K., Wang, R., Chen, G., Shan, G., Zhu, L., 2022. Predicting bioconcentration factor and estrogen receptor bioactivity of bisphenol a and its analogues in adult zebrafish by directed message passing neural networks. Environ. Int. 169, 107536. https://doi.org/10.1016/j.envint.2022.107536.

Yang, L., Yan, W., Wang, H., Zhuang, H., Zhang, J., 2017. Shell thickness-dependent antibacterial activity and biocompatibility of gold@silver core–shell nanoparticles. RSC Adv. 7, 11355–11361. https://doi.org/10.1039/c7ra00485k.

Yang, Q., Zhang, L., Ben, A., Wu, N., Yi, Y., Jiang, L., Huang, H., Yu, Y., 2018. Effects of dispersible MoS_2 nanosheets and nano-silver coexistence on the metabolome of yeast. Chemosphere 198, 216–225. https://doi.org/10.1016/j.chemosphere.2018.01.140.

Ye, N., Wang, Z., Wang, S., Peijnenburg, W.J.G.M., 2018. Toxicity of mixtures of zinc oxide and graphene oxide nanoparticles to aquatic organisms of different trophic level: Particles outperform dissolved ions. Nanotoxicology 12, 423–438. https://doi.org/10.1080/17435390.2018.1458342.

Yin, J., Huang, G., An, C., Feng, R., 2022. Nanocellulose enhances the dispersion and toxicity of ZnO NPs to green algae *Eremosphaera viridis*. Environ. Sci.: Nano 9, 393–405. https://doi.org/10.1039/D1EN00881A.

Yu, Q., Wang, Z., Wang, G., Peijnenburg, W.J.G.M., Vijver, M.G., 2022. Effects of natural organic matter on the joint toxicity and accumulation of Cu nanoparticles and ZnO nanoparticles in *Daphnia magna*. Environ. Pollut. 292, 118413. https://doi.org/10.1016/j.envpol.2021.118413.

Yu, R., Wu, J., Liu, M., Chen, L., Zhu, G., Lu, H., 2016a. Physiological and transcriptional responses of *Nitrosomonas europaea* to TiO_2 and ZnO nanoparticles and their mixtures. Environ. Sci. Pollut. Res. 23, 13023–13034. https://doi.org/10.1007/s11356-016-6469-8.

Yu, R., Wu, J., Liu, M., Zhu, G., Chen, L., Chang, Y., Lu, H., 2016b. Toxicity of binary mixtures of metal oxide nanoparticles to *Nitrosomonas europaea*. Chemosphere 153, 187–197. https://doi.org/10.1016/j.chemosphere.2016.03.065.

Yu, Y., Mo, W.Y., Luukkonen, T., 2021. Adsorption behaviour and interaction of organic micropollutants with nano and microplastics — A review. Sci. Total Environ. 797, 149140. https://doi.org/10.1016/j.scitotenv.2021.149140.

Zettler, E.R., Mincer, T.J., Amaral-Zettler, L.A., 2013. Life in the "plastisphere": Microbial communities on plastic marine debris. Environ. Sci. Technol. 47, 7137–7146. https://doi.org/10.1021/es401288x.

Zhai, X., Zhang, X.-H., Yu, M., 2023. Microbial colonization and degradation of marine microplastics in the plastisphere: A review. Front. Microbiol. 14, 1127308. https://doi.org/10.3389/fmicb.2023.1127308.

Zhai, Y., Hunting, E.R., Wouters, M., Peijnenburg, W.J.G.M., Vijver, M.G., 2016. Silver nanoparticles, ions, and shape governing soil microbial functional diversity: Nano shapes Micro. Front. Microbiol. 7, 1123. https://doi.org/10.3389/fmicb.2016.01123.

Zhang, F., Wang, Z., Peijnenburg, W.J.G.M., Vijver, M.G., 2022a. Review and prospects on the ecotoxicity of mixtures of nanoparticles and hybrid nanomaterials. Environ. Sci. Technol. 56, 15238–15250. https://doi.org/10.1021/acs.est.2c03333.

Zhang, F., Wang, Z., Vijver, M.G., Peijnenburg, W.J.G.M., 2022b. Theoretical investigation on the interactions of microplastics with a SARS-CoV-2 RNA fragment and their potential impacts on viral transport and exposure. Sci. Total Environ. 842, 156812. https://doi.org/10.1016/j.scitotenv.2022.156812.

Zhang, F., Wang, Z., Vijver, M.G., Peijnenburg, W.J.G.M., 2021a. Probing nano-QSAR to assess the interactions between carbon nanoparticles and a SARS-CoV-2 RNA fragment. Ecotoxicol. Environ. Saf. 219, 112357. https://doi.org/10.1016/j.ecoenv.2021.112357.

Zhang, F., Wang, Z., Vijver, M.G., Peijnenburg, W.J.G.M., 2021b. Prediction of the joint toxicity of multiple engineered nanoparticles: The integration of classic mixture models and *in silico* methods. Chem. Res. Toxicol. 34, 176–178. https://doi.org/10.1021/acs.chemrestox.0c00300.

Zhang, H., Ji, Z., Xia, T., Meng, H., Low-Kam, C., Liu, R., Pokhrel, S., Lin, S., Wang, X., Liao, Y.-P., Wang, M., Li, L., Rallo, R., Damoiseaux, R., Telesca, D., Mädler, L., Cohen, Y., Zink, J.I., Nel, A.E., 2012. Use of metal oxide nanoparticle band gap to

develop a predictive paradigm for oxidative stress and acute pulmonary inflammation. ACS Nano 6, 4349–4368. https://doi.org/10.1021/nn3010087.

Zhang, H., Shi, J., Su, Y., Li, W., Wilkinson, K.J., Xie, B., 2020. Acute toxicity evaluation of nanoparticles mixtures using luminescent bacteria. Environ. Monit. Assess. 192, 484. https://doi.org/10.1007/s10661-020-08444-6.

Zhang, J., Chen, H., He, H., Cheng, X., Ma, T., Hu, J., Yang, S., Li, S., Zhang, L., 2020. Adsorption behavior and mechanism of 9-nitroanthracene on typical microplastics in aqueous solutions. Chemosphere 245, 125628. https://doi.org/10.1016/j.chemosphere.2019.125628.

Zhang, J., Zhang, X., Zhou, Y., Han, Q., Wang, X., Song, C., Wang, S., Zhao, S., 2023. Occurrence, distribution and risk assessment of antibiotics at various aquaculture stages in typical aquaculture areas surrounding the Yellow Sea. J. Environ. Sci. 126, 621–632. https://doi.org/10.1016/j.jes.2022.01.024.

Zhang, K., Zheludev, I.N., Hagey, R.J., Haslecker, R., Hou, Y.J., Kretsch, R., Pintilie, G.D., Rangan, R., Kladwang, W., Li, S., Wu, M.T.-P., Pham, E.A., Bernardin-Souibgui, C., Baric, R.S., Sheahan, T.P., Glenn, J.S., Chiu, W., Das, R., D′Souza, V., 2021. Cryo-EM and antisense targeting of the 28-kDa frameshift stimulation element from the SARS-CoV-2 RNA genome. Nat. Struct. Mol. Biol. 28, 747–754. https://doi.org/10.1038/s41594-021-00653-y.

Zhang, Q., Liu, T., Liu, L., Fan, Y., Rao, W., Zheng, J., Qian, X., 2021. Distribution and sedimentation of microplastics in Taihu Lake. Sci. Total Environ. 795, 148745. https://doi.org/10.1016/j.scitotenv.2021.148745.

Zhang, Y., Zhang, X., Li, X., He, D., 2022. Interaction of microplastics and soil animals in agricultural ecosystems. Curr. Opin. Env. Sci.

Health 26, 100327. https://doi.org/10.1016/j.coesh.2022.100327.

Zhao, C., Shao, B., Yan, M., Liu, Z., Liang, Q., He, Q., Wu, T., Liu, Y., Pan, Y., Huang, J., Wang, J., Liang, J., Tang, L., 2021. Activation of peroxymonosulfate by biochar-based catalysts and applications in the degradation of organic contaminants: A review. Chem. Eng. J. 416, 128829. https://doi.org/10.1016/j.cej.2021.128829.

Zhao, C.Y., Zhang, H.X., Zhang, X.Y., Liu, M.C., Hu, Z.D., Fan, B.T., 2006. Application of support vector machine (SVM) for prediction toxic activity of different data sets. Toxicology 217, 105–119. https://doi.org/10.1016/j.tox.2005.08.019.

Zhao, J., Dai, Y., Wang, Z., Ren, W., Wei, Y., Cao, X., Xing, B., 2018. Toxicity of GO to freshwater algae in the presence of Al_2O_3 particles with different morphologies: Importance of heteroaggregation. Environ. Sci. Technol. 52, 13448–13456. https://doi.org/10.1021/acs.est.8b00815.

Zhao, L., Qi, Y., Luzzatto-Fegiz, P., Cui, Y., Zhu, Y., 2020. COVID-19: Effects of environmental conditions on the propagation of respiratory droplets. Nano Lett. 20, 7744–7750. https://doi.org/10.1021/acs.nanolett.0c03331.

Zhao, T., Tan, L., Han, X., Ma, X., Lin, K., Wang, J., 2023. Energy metabolism response induced by microplastic for marine dinoflagellate *Karenia mikimotoi*. Sci. Total Environ. 866, 161267. https://doi.org/10.1016/j.scitotenv.2022.161267.

Zhong, S., Lambeth, D.R., Igou, T.K., Chen, Y., 2022a. Enlarging applicability domain of quantitative structure–activity relationship models through uncertainty-based active learning. ACS EST Eng. 2, 1211–1220. https://doi.org/10.1021/acsestengg.1c00434.

Zhong, S., Zhang, Y., Zhang, H., 2022b. Machine learning-assisted

QSAR models on contaminant reactivity toward four oxidants: Combining small data sets and knowledge transfer. Environ. Sci. Technol. 56, 681–692. https://doi.org/10.1021/acs.est.1c04883.

Zhou, J., Zhang, H., Liu, J., Gong, L., Yang, X., Zuo, T., Zhou, Y., Wang, J., You, X., Jia, Q., Wang, L., 2023. Effects of Fe_3O_4 nanoparticles on anaerobic digestion enzymes and microbial community of sludge. Environ. Technol. 44, 68–81. https://doi.org/10.1080/ 09593330.2021.1963324.

Zhu, H., Fu, S., Zou, H., Su, Y., Zhang, Y., 2021. Effects of nanoplastics on microalgae and their trophic transfer along the food chain: Recent advances and perspectives. Environ. Sci. Process. Impacts 23, 1873–1883. https://doi.org/10.1039/ D1EM00438G.

Zhu, Z., Su, M., Ma, L., Ma, L., Liu, D., Wang, Z., 2013. Preparation of graphene oxide–silver nanoparticle nanohybrids with highly antibacterial capability. Talanta 117, 449–455. https://doi.org/ 10.1016/j.talanta.2013.09.017.

Summary

With the rapid development and intensification of society and economy, novel entities such as engineered nanoparticles (ENPs), microplastics (MPs), nanoplastics (NPs), and viral particles are emerging. These novel entities may pose risks to humans and to the environment. Micro- and nanoparticles (MNPs) can adsorb other novel entities to form aggregated contamination, due to their small particle size and relative large surface area. In this thesis, we used advanced computational methods including molecular simulation, data mining, machine learning (ML), and quantitative structure-activity relationship (QSAR) modeling. These methods were used to investigate the mechanisms of interaction between MNPs and other novel entities (**chapters 2 and 3**), the joint toxic action of MNPs and other novel entities, the factors affecting their joint toxicity to ecological species (**chapter 4**), as well as to quantitatively predict the interaction forces between MNPs and other novel entities (**chapters 2 and 3**), and the toxicity of their mixtures (**chapters 5 and 6**).

In **chapter 2**, we have investigated the molecular interactions between carbon nanoparticles (CNPs) and the SARS-CoV-2 RNA fragment using molecular mechanics simulations to tackle some mechanistic issues related to the impact of ENPs on SARS-CoV-2. The interaction affinity between the CNPs and the SARS-CoV-2 RNA fragment increased in the order of fullerenes < graphenes < carbon nanotubes. Furthermore, we developed QSAR models to determine the interactions of 17 different types of CNPs from three dimensions with the SARS-CoV-2 RNA fragment. The QSAR models on the

interaction energies of CNPs with the SARS-CoV-2 RNA fragment show high goodness-of-fit and robustness. Molecular weight, surface area, and the sum of degrees of every carbon atom were found to be the primary structural descriptors of CNPs determining the interactions. Within this chapter a theoretical insight into the adsorption/separation and inactivation of SARS-CoV-2 was provided. The results allow to design novel ENPs which interact efficiently with the genetic materials of SARS-CoV-2. This contributes to minimizing the challenge of time-consuming and labor-intensive experiments with viruses under high risk of infection, whilst meeting our precautionary demand for options to handle any new versions of the coronavirus that might emerge in the future.

In **chapter 3**, we have used molecular dynamic simulations to investigate the molecular interactions between five MPs and the SARS-CoV-2 RNA fragment at temperatures ranging from 223 to 310 K in vacuum and in water to determine the mechanisms underlying the impact of MPs on SARS-CoV-2. Furthermore, we have compared the interactions of the SARS-CoV-2 RNA fragment with the MPs to the performance of the RNA fragments of SARS-CoV-1 and Hepatitis B virus interacting with the MPs. The interaction affinity between the MPs and the SARS-CoV-2 RNA fragment was found to be greater than the affinity between the MPs and the RNA fragments of SARS-CoV-1 or Hepatitis B virus, independent of the environmental media, temperature, and type of MPs. The mechanisms of the interaction between the MPs and the SARS-CoV-2 RNA fragment involve electrostatic and hydrophobic processes, and the interaction affinity was associated with the inherent structural parameters of the MPs monomers. The results presented in this chapter indicate that

humans are exposed to MPs via their lungs, and the strong interaction with the gene materials of SARS-CoV-2 likely affects the exposure of humans to SARS-CoV-2.

In **chapter 4**, we have applied data mining methods to understand the joint impacts of multiple ENPs and predict the toxicity of mixtures of ENPs. Accordingly, we have collected and categorized the toxicity of mixtures of ENPs to a variety of different species, covering algae, bacteria, daphnia, fish, fungi, insects, and plants. Using co-occurrence networks, it was revealed that 53 % of the cases with specific joint response showed antagonistic, 25 % synergistic, and 22 % additive effects. The combination of nCuO and nZnO exhibited the strongest interactions in each type of joint interaction. Compared with other species, plants exposed to multiple ENPs were more likely to experience antagonistic effects. The main factors influencing the joint response type of the mixtures were 1) the chemical composition of individual components in mixtures, 2) the stability of suspensions of mixed ENPs, 3) the type and trophic level of the individual organisms tested, 4) the biological level of organization (population, communities, ecosystems), 5) the exposure concentrations and time, 6) the endpoint of toxicity, and 7) the abiotic field conditions (e.g., pH, ionic strength, natural organic matter). Ultimately this knowledge constitutes the first building blocks that allow to build a computational approach able to reduce the experimental costs of ecotoxicity testing of mixtures of ENPs of varying composition, and including both nanohybrids as well as mixtures of different ENPs.

In **chapter 5**, we proposed computational toxicity approaches with classical mixture equations to quantitatively predict the joint toxicity of emerging or untested/unknown mixtures of multiple ENPs.

Research priorities for the prediction of the toxicity of mixtures of ENPs are identified and we suggest to systematically sort out the toxicity and ecotoxicity information of ENPs gathered into "databases". Moreover, expected and/or actual environmental concentrations of ENPs need to be obtained to be implemented for actual risk profiling of various combinations of ENPs in the environment. These environmental concentrations can be further used for the estimation of ratios of the individual particles present in mixtures of ENPs, and then the weighted descriptors of ENP mixtures can be evaluated by the mixture ratios. It is essential that information on the mode of toxic action of single ENPs to species is systematically documented. This issue deserves priority in the selection of methods to assess mixture toxicity and the selection of mechanism-based nano-descriptors.

In **chapter 6**, we have combined toxicity data generated in our lab with experimental data reported in the literature to predict the combined toxicity of seven metallic ENPs for *Escherichia coli* at different mixing ratios (22 binary combinations). We thereafter applied two ML techniques, support vector machine (SVM) and neural network (NN), and compared the differences in the ability to predict the combined toxicity by means of ML-based methods and two component-based mixture models: IA and CA. Among 72 developed QSAR models by the ML methods, two SVM-QSAR models and two NN-QSAR models showed good performance. Moreover, an NN-based QSAR model combined with two molecular descriptors, namely enthalpy of formation of a gaseous cation and metal oxide standard molar enthalpy of formation, showed the best predictive power for the internal dataset (R^2_{test} = 0.911, adjusted R^2_{test} = 0.733,

$RMSE_{test}$ = 0.091, and MAE_{test} = 0.067) and for the combination of internal and external datasets (R^2_{test} = 0.908, adjusted R^2_{test} = 0.871, $RMSE_{test}$ = 0.255, and MAE_{test} = 0.181). In addition, the developed QSAR models performed better than the IA and CA models. The estimation of the applicability domain of the selected QSAR models showed that all the binary mixtures in the training and test sets were within the applicability domain. Hence, this work confirms that the models developed can provide a methodological and theoretical basis for the ecological risk assessment of mixtures of ENPs.

The results of this thesis indicate that understanding the mechanisms of interactions between novel entities in the environment and their modes of joint toxic action can provide an important theoretical basis for establishing effective risk assessment procedures to mitigate the effects of novel entities on ecosystems and human health. Furthermore, this thesis provides an important technical support and practical basis for the quantitative prediction of the environmental behavior and toxicological effects of novel entities and their mixtures by applying various advanced *in silico* methods individually or in combination.

Samenvatting

Met de snelle ontwikkeling en intensivering van de samenleving en economie ontstaan er nieuwe entiteiten zoals gemanipuleerde nanodeeltjes (ENP's), microplastics (MP's), nanoplastics (NP's) en virale deeltjes. Deze nieuwe entiteiten kunnen risico's opleveren voor de mens en voor het milieu. Micro- en nanodeeltjes (MNP's) kunnen andere nieuwe entiteiten adsorberen om geaggregeerde verontreiniging te vormen, vanwege hun kleine deeltjesgrootte en relatief grote oppervlak. In dit proefschrift hebben we een verscheidenheid aan geavanceerde computationele methoden gebruikt, waaronder moleculaire simulatie, datamining, machinaal leren (ML) en kwantitatieve structuur-activiteitsrelatie (QSAR) modellering. Deze methoden zijn ingezet om de interactiemechanismen tussen MNP's en andere nieuwe entiteiten (**hoofdstuk 2** en **3**), de gezamenlijke toxische werking van MNP's en andere nieuwe entiteiten, de factoren die hun gezamenlijke toxiciteit voor ecologische soorten beïnvloeden (**hoofdstuk 4**), en ook om de interactiekrachten tussen MNP's en andere nieuwe entiteiten (**hoofdstuk 2** en **3**) en de toxiciteit van hun mengsels (**hoofdstuk 5** en **6**) kwantitatief te voorspellen.

In **hoofdstuk 2** hebben we de moleculaire interacties tussen koolstofnanodeeltjes (CNP's) en het SARS-CoV-2 RNA-fragment onderzocht met behulp van moleculaire mechanica simulaties om enkele mechanistische kwesties met betrekking tot de invloed van ENP's op SARS-CoV-2 aan te pakken. De interactieaffiniteit tussen de CNP's en het SARS-CoV-2 RNA-fragment nam toe in de volgorde fullerenen < grafeen < koolstofnanobuisjes. Verder ontwikkelden we

QSAR-modellen om de interacties van 17 verschillende typen CNP's uit drie dimensies met het SARS-CoV-2 RNA-fragment te bepalen. De QSAR-modellen voor de interactie-energieën van CNP's met het SARS-CoV-2 RNA-fragment vertonen een hoge 'goodness-of-fit' en robuustheid. Molecuulgewicht, oppervlakte en de som van de graden van elk koolstofatoom bleken de primaire structurele descriptoren van CNP's te zijn die de interacties bepalen. In dit hoofdstuk werd een theoretisch inzicht gegeven in de adsorptie/separatie en inactivatie van SARS-CoV-2. De resultaten laten toe om nieuwe ENP's te ontwerpen die efficiënt interageren met het genetisch materiaal van SARS-CoV-2. Dit draagt bij aan het minimaliseren van de uitdaging van tijdrovende en arbeidsintensieve experimenten met virussen met een hoog infectierisico (o.a. SARS-CoV-2), terwijl we tegelijkertijd voldoen aan onze voorzorgsprincipe naar opties om te gaan met eventuele nieuwe versies van het coronavirus die in de toekomst zouden kunnen opduiken.

In **hoofdstuk 3** hebben we moleculair dynamische simulaties gebruikt om de moleculaire interacties tussen 5 MPs en het SARS-CoV-2 RNA fragment te onderzoeken bij temperaturen variërend van 223 tot 310 K in vacuüm en in water om de mechanismen te bepalen die ten grondslag liggen aan de invloed van MPs op SARS-CoV-2. Verder hebben we de interacties van het SARS-CoV-2 RNA-fragment met de MP's vergeleken met de prestaties van de RNA-fragmenten van SARS-CoV-1 en Hepatitis B-virus die interacteren met de MP's. De interactieaffiniteit tussen de MP's en het SARS-CoV-2 RNA-fragment bleek groter te zijn dan de affiniteit tussen de MP's en de RNA-fragmenten van SARS-CoV-1 of Hepatitis B-virus, onafhankelijk van de omgevingsmedia, de

temperatuur en het type MP's. De mechanismen van de interactie tussen de MP's en het SARS-CoV-2 RNA-fragment omvatten elektrostatische en hydrofobe processen, en de interactieaffiniteit werd in verband gebracht met de inherente structurele parameters van de MP's-monomeren. De resultaten gepresenteerd in dit hoofdstuk geven aan dat mensen worden blootgesteld aan MPs via hun longen, en de sterke interactie met het genmateriaal van SARS-CoV-2 beïnvloedt waarschijnlijk de blootstelling van mensen aan SARS-CoV-2.

In **hoofdstuk 4** hebben we dataminingmethoden toegepast om de gezamenlijke effecten van meerdere ENP's te begrijpen en de toxiciteit van mengsels van ENP's te voorspellen. Hiervoor hebben we de toxiciteit van mengsels van ENP's voor verschillende soorten algen, bacteriën, daphnia, vissen, schimmels, insecten en planten verzameld en gecategoriseerd. Met behulp van co-occurentienetwerken werd onthuld dat 53 % van de gevallen met specifieke gezamenlijke reactie antagonistische, 25 % synergetische en 22 % additieve effecten vertoonden. De combinatie van nCuO en nZnO vertoonde de sterkste interacties in elk type van gezamenlijke interactie. Vergeleken met andere soorten hadden planten blootgesteld aan meerdere ENP's meer kans op antagonistische effecten. De belangrijkste factoren die van invloed waren op het type gezamenlijke reactie van de mengsels waren 1) de chemische samenstelling van individuele componenten in mengsels, 2) de stabiliteit van suspensies van gemengde ENP's, 3) het type en trofisch niveau van de individuele geteste organismen, 4) het biologische organisatieniveau (populatie, gemeenschappen, ecosystemen), 5) de blootstellingsconcentraties en -tijd, 6) het eindpunt van toxiciteit, en 7) de abiotische veldomstandigheden (bijv.

pH, ionensterkte, natuurlijk organisch materiaal). Uiteindelijk vormt deze kennis de eerste bouwstenen voor een computationele aanpak waarmee de experimentele kosten van ecotoxiciteitstesten van mengsels van ENP's van verschillende samenstelling, waaronder zowel nanohybriden als mengsels van verschillende ENP's, kunnen worden verlaagd.

In **hoofdstuk 5** hebben we computationele toxiciteitsbenaderingen met klassieke mengselvergelijkingen voorgesteld om de gezamenlijke toxiciteit van opkomende of ongeteste/onbekende mengsels van meerdere ENP's kwantitatief te voorspellen. Onderzoeksprioriteiten voor de voorspelling van de toxiciteit van mengsels van ENP's worden geïdentificeerd en we stellen voor om de informatie over toxiciteit en ecotoxiciteit van ENP's die in "databases" is verzameld, systematisch te sorteren. Bovendien moeten verwachte en/of actuele milieuconcentraties van ENP's worden verkregen om te kunnen worden gebruikt voor de feitelijke risicoprofilering van verschillende combinaties van ENP's in het milieu. Deze milieuconcentraties kunnen verder worden gebruikt voor de schatting van verhoudingen van de individuele deeltjes die aanwezig zijn in mengsels van ENP's, waarna de gewogen descriptoren van ENP-mengsels kunnen worden geëvalueerd aan de hand van de mengverhouding. Het is essentieel dat informatie over de toxische werking van afzonderlijke ENP's op soorten systematisch wordt gedocumenteerd. Deze kwestie verdient prioriteit bij de selectie van methoden om de toxiciteit van mengsels te beoordelen en de selectie van mechanisme-gebaseerde nano-descriptoren.

In **hoofdstuk 6** hebben we toxiciteitsgegevens uit ons laboratorium gecombineerd met experimentele gegevens uit de literatuur om de

gecombineerde toxiciteit van 7 metallische ENP's voor *Escherichia coli* bij verschillende mengverhoudingen (22 binaire combinaties) te voorspellen. Daarna pasten we twee ML-technieken toe, support vector machine (SVM) en neuraal netwerk (NN), en vergeleken we de verschillen in het vermogen om de gecombineerde toxiciteit te voorspellen door middel van ML-gebaseerde methoden en twee componentgebaseerde mengmodellen: IA en CA. Van de 72 ontwikkelde QSAR-modellen door middel van ML-methoden vertoonden twee SVM-QSAR-modellen en twee NN-QSAR-modellen goede prestaties. Bovendien vertoonde een NN-gebaseerd QSAR-model gecombineerd met twee moleculaire descriptoren, namelijk enthalpie van vorming van een gasvormig kation en standaard molaire enthalpie van vorming van metaaloxide, de beste voorspellende kracht voor de interne dataset (R^2_{test} = 0,911, aangepaste R^2_{test} = 0,733, $RMSE_{test}$ = 0,091 en MAE_{test} = 0,067) en voor de combinatie van interne en externe datasets (R^2_{test} = 0,908, aangepaste R^2_{test} = 0,871, $RMSE_{test}$ = 0,255 en MAE_{test} = 0,181). Bovendien presteerden de ontwikkelde QSAR-modellen beter dan de IA- en CA-modellen. De schatting van het toepassingsdomein van de geselecteerde QSAR modellen toonde aan dat alle binaire mengsels in de trainings- en testsets binnen het toepassingsdomein vielen. Dit werk bevestigt dus dat de ontwikkelde modellen een methodologische en theoretische basis kunnen bieden voor de ecologische risicobeoordeling van mengsels van ENP's.

De resultaten van dit proefschrift geven inzicht in de mechanismen van interacties tussen nieuwe entiteiten in het milieu en hun gezamenlijke toxische werkingsmechanismen een belangrijke theoretische basis kan vormen voor het vaststellen van effectieve

risicobeoordelingsprocedures om de effecten van nieuwe entiteiten op ecosystemen en de menselijke gezondheid te beperken. Verder biedt dit proefschrift een belangrijke technische ondersteuning en praktische basis voor de kwantitatieve voorspelling van het gedrag in het milieu en toxicologische effecten van nieuwe entiteiten en mengsels daarvan door verschillende geavanceerde *in silico* methoden afzonderlijk of in combinatie toe te passen.

Curriculum Vitae

Fan Zhang was born in 1995 in Yangquan, Shanxi Province, China. After completing senior school at Yangquan No.1 High School in 2013, she enrolled in Nanjing University of Information Science & Technology to study Environmental Science. In 2016, she was awarded the "China National Scholarship" (2 ‰) for undergraduate students. After graduating with a Bachelor's degree in 2017, She won the first prize for the "Outstanding Undergraduate Thesis" of Jiangsu Province. And then, Fan was recommended as a postgraduate candidate exempt from the admission exam, to continue her Master's study in Environmental Science and Engineering at Nanjing University of Information Science & Technology. During this period, she was mainly engaged in research on the behavior and toxicity of micro/nanoplastic particles in the freshwater environment. And in 2019 she was awarded the "China National Scholarship" (2 ‰) for postgraduate students. She graduated with a Master's degree in 2020 and was granted the "Outstanding Master's Thesis" award of the university. In the same year, Fan was awarded a scholarship by the "China Scholarship Council (CSC)" to continue her PhD research at the Institute of Environmental Sciences (CML) at Leiden University. Here, she joined the Ecotox team led by Prof. dr. Martina G. Vijver and Prof. dr. Willie J.G.M. Peijnenburg, focusing on the study of modelling the interactions of advanced micro- and nanoparticles with novel entities.

List of Publications

Fan Zhang, Zhuang Wang, Willie J.G.M. Peijnenburg & Martina G. Vijver (2023). Machine learning-driven QSAR models for predicting the mixture toxicity of nanoparticles. *Environment International*, 177, 108025. https://doi.org/10.1016/j.envint.2023.108025.

Fan Zhang, Zhuang Wang, Willie J.G.M. Peijnenburg & Martina G. Vijver (2022). Review and prospects on the ecotoxicity of mixtures of nanoparticles and hybrid nanomaterials. *Environmental Science & Technology*, 56(22), 15238-15250. https://doi.org/10.1021/acs.est.2c03333. (Supplementary Journal Cover)

Fan Zhang, Zhuang Wang, Martina G. Vijver & Willie J.G.M. Peijnenburg (2022). Theoretical investigation on the interactions of microplastics with a SARS-CoV-2 RNA fragment and their potential impacts on viral transport and exposure. *Science of the Total Environment*, 842, 156812. http://dx.doi.org/10.1016/j.scitotenv.2022.156812.

Fan Zhang, Zhuang Wang, Martina G. Vijver & Willie J.G.M. Peijnenburg (2021). Probing nano-QSAR to assess the interactions between carbon nanoparticles and a SARS-CoV-2 RNA fragment. *Ecotoxicology and Environmental Safety*, 219, 112357. https://doi.org/10.1016/j.ecoenv.2021.112357.

Fan Zhang, Zhuang Wang, Martina G. Vijver & Willie J.G.M. Peijnenburg (2021). Prediction of the joint toxicity of multiple engineered nanoparticles: the integration of classic mixture models and *in silico* methods. *Chemical Research in Toxicology*, 34(2), 176-178. https://dx.doi.org/10.1021/acs.chemrestox.0c00300.

Zhuang Wang, **Fan Zhang**, Martina G. Vijver & Willie J.G.M. Peijnenburg (2021). Graphene nanoplatelets and reduced graphene oxide elevate the microalgal cytotoxicity of nano-zirconium oxide. *Chemosphere*, 276, 130015. https://doi.org/10.1016/j.chemosphere.2021.130015.

Qi Yu, Zhuang Wang, Yujia Zhai, **Fan Zhang**, Martina G. Vijver & Willie J.G.M. Peijnenburg (2021). Effects of humic substances on the aqueous stability of cerium dioxide nanoparticles and their toxicity to aquatic organisms. *Science of the Total Environment*, 781, 146583. https://doi.org/10.1016/j.scitotenv.2021.146583.

Acknowledgements

The time I spent pursuing my PhD was not a long time in my life, but it was one of the most memorable times of my experience. I am grateful to have met and known all of you, giving my heart etched with wonderful memories!

First and foremost, I would like to express my deepest thanks to my promotors Prof. dr. Martina Vijver and Prof. dr. Willie Peijnenburg. Thank you both for creating a free, open, and inclusive research environment for me. I truly appreciate all the support, guidance, and help you have provided.

Dear Martina, when I encountered difficulties with research, you were always patient in helping me to solve the problems and provided me with useful advice and intelligent ideas to show me the way forward. Thank you for your encouragement and trust in me and for letting me explore the areas that interest me.

Dear Willie, I am really grateful for your continuous inspiration to my scientific research. Your patience, meticulousness, and rigor have always been a great example for me to follow. I appreciate what you have taught me throughout the years. Thank you for always being there for me and guiding me.

My special gratitude goes to Dr. Zhuang Wang who inspired me to pursue scientific research. Thank you for pouring in all your knowledge and guidance. I am everlastingly grateful.

I would like to thank all members of the reading committee: Prof. dr. G.R. de Snoo, Prof. dr. A. Tukker, Prof. dr. M. Barz, Prof. dr. A.M. de Roda Husman, Dr. P.N.H. Wassenaar, and Dr. B.W. Brinkmann.

Thank you very much for taking the time to read my thesis and give invaluable feedback.

I am grateful to the Ecotox group members for giving me encouragement and warmth. The time for the communications and sharing within the Ecotox meeting will be unforgettable memories for me in the future. Many thanks to our office managers for all their generous help and instructions. Thank you to all our colleagues at CML.

Finally, love and hugs to my dearest parents. Thank you for giving me a warm home and allowing me to grow up in a loving and cozy environment, and for your selfless dedication and support, which has allowed me to pursue my academic ambition without distractions. I'm so thankful to be your daughter.

Appendix

Supplementary information for Chapter 2

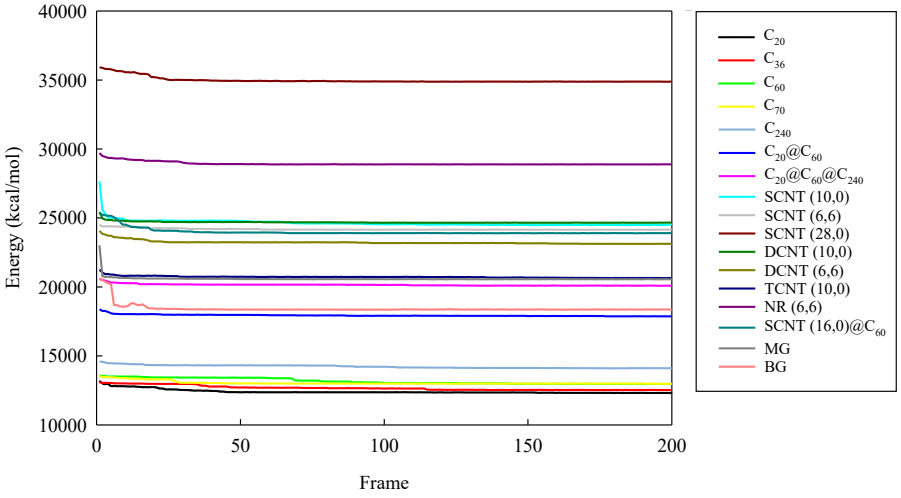

Figure S2.1. *Variation of total energy of the complexes of the carbon nanoparticles with SARS-CoV-2 RNA fragment during Forcite Anneal optimization.*

Table S2.1. *Calculated total potential energy interaction energies (E_{int}), van der Waals interaction energies, and electrostatic interaction energies between the carbon nanoparticles (CNPs) and the SARS-CoV-2 RNA fragment (covRNA)*

CNP-covRNA complex	E_{int} (kJ/mol)		
	Total potential energy	van der Waals	Electrostatic
C_{20}-covRNA	-137.608	-9.415	-175.137
C_{36}-covRNA	-108.956	-28.314	-148.972
C_{60}-covRNA	-79.874	-25.355	-105.241
C_{70}-covRNA	-96.413	-33.106	-108.117
C_{240}-covRNA	-87.358	-22.031	-198.906
C_{20}@C_{60}-covRNA	-100.055	-37.002	-146.696
C_{20}@C_{60}@C_{240}-covRNA	-70.335	-49.281	-150.333
SCNT (10,0)-covRNA	-185.127	-26.885	-239.362
SCNT (6,6)-covRNA	-153.478	-41.943	-197.572
SCNT (28,0)-covRNA	-489.113	-58.486	-410.306
DCNT (10,0)-covRNA	-244.928	-56.431	-274.291
DCNT (6,6)-covRNA	-261.953	-61.665	-253.979
TCNT (10,0)-covRNA	-298.677	-65.354	-265.589
NR (6,6)-covRNA	-195.360	-49.726	-135.640
SCNT (16,0)@C_{60}-covRNA	-448.289	-53.492	-400.611
MG-covRNA	-142.530	-70.631	-136.654
BG-covRNA	-141.717	-51.850	-161.298

Table S2.2. *OPLS regression models obtained from the fake pool data of the interaction energies derived from the total potential energy* [a]

Fullerenes		**CNTs and graphenes**		**Fullerenes, CNTs, and graphenes**	
data 1	**data 2**	**data 3**	**data 4**	**data 5**	**data 6**
-187	-116	-185.127	-334	-137.608	-71
-108.956	-119	-153.478	-124	-108.956	-156
-79.874	-135	-426	-215	-79.874	-288
-96.413	-43	-244.928	-487	-96.413	-486
-87.358	-53	-261.953	-489	-87.358	-121
-100.055	-36	-298.677	-362	-100.055	-167
-70.335	-73	-195.360	-433	-70.335	-230
		-448.289	-157	-185.127	-447
		-142.530	-412	-153.478	-473
		-141.717	-170	-489.113	-339
				-244.928	-82
				-469	-364
				-298.677	-226
				-195.360	-415
				-448.289	-168
				-142.530	-196
				-141.717	-291
Fullerenes					
Model 1	E_{int}=-22.105-0.028·*SSA* n = 7, R^2 = 0.593, RMSE = 0.698, Q^2_{CUM} = 0.247				
Model 2	E_{int}=-10.341-0.024·*SSA* n = 7, R^2 = 0.411, RMSE = 0.841, Q^2_{CUM} = 0.325				
CNTs and graphenes					
Model 3	E_{int}=-304.189-0.606·*OSA*+0.035·*SDeg* n = 10, R^2 = 0.795, RMSE = 0.480, Q^2_{CUM} = 0.614				
Model 4	E_{int}=-479.223+0.833·*OSA*+0.019·*SDeg* n = 10, R^2 = 0.255, RMSE = 0.915, Q^2_{CUM} = 0.073				
Fullerenes, CNTs, and graphenes					
Model 5	E_{int}=-92.390-0.006·M_W+0.003·*SDeg* n = 17, R^2 = 0.614, RMSE = 0.642, Q^2_{CUM} = 0.577				
Model 6	E_{int}=-197.742-0.0.01·M_W-0.018·*SDeg* n = 17, R^2 = 0.191, RMSE = 0.929, Q^2_{CUM} = 0.044				

[a] *The pseudo-random numbers of the interaction energies derived from the total potential energy are shown in red.*

Supplementary information for Chapter 3

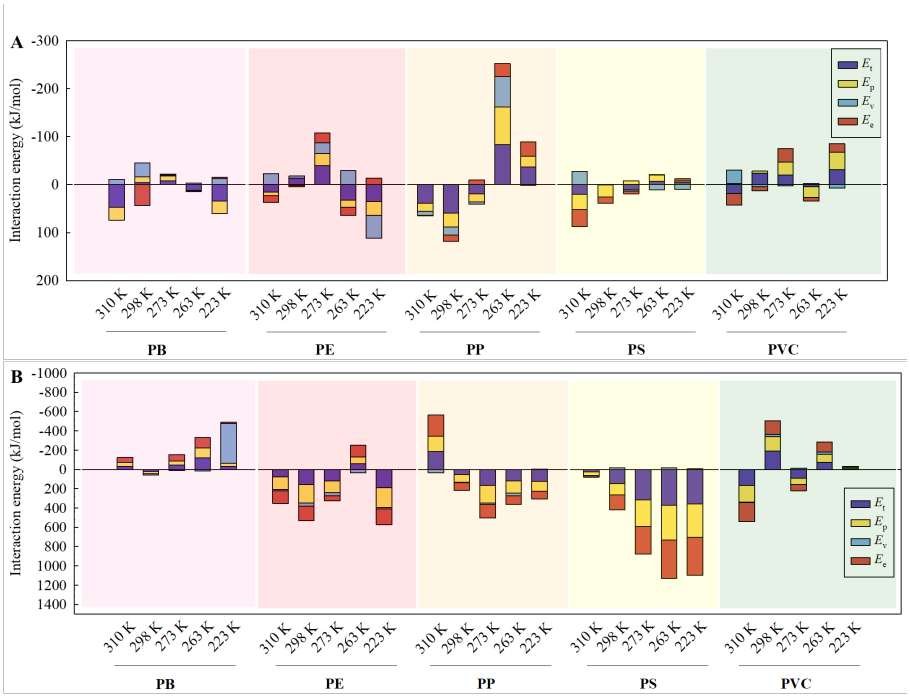

Figure S3.1. *Interaction energies of the five types of MPs with the SARS-CoV-1 RNA fragment in vacuum (A) and in water (B) at different temperatures.* E_t*: interaction energy derived from total energy,* E_p*: interaction energy derived from potential energy,* E_v*: interaction energy derived from van der Waals energy, and* E_e*: interaction energy derived from electrostatic energy.*

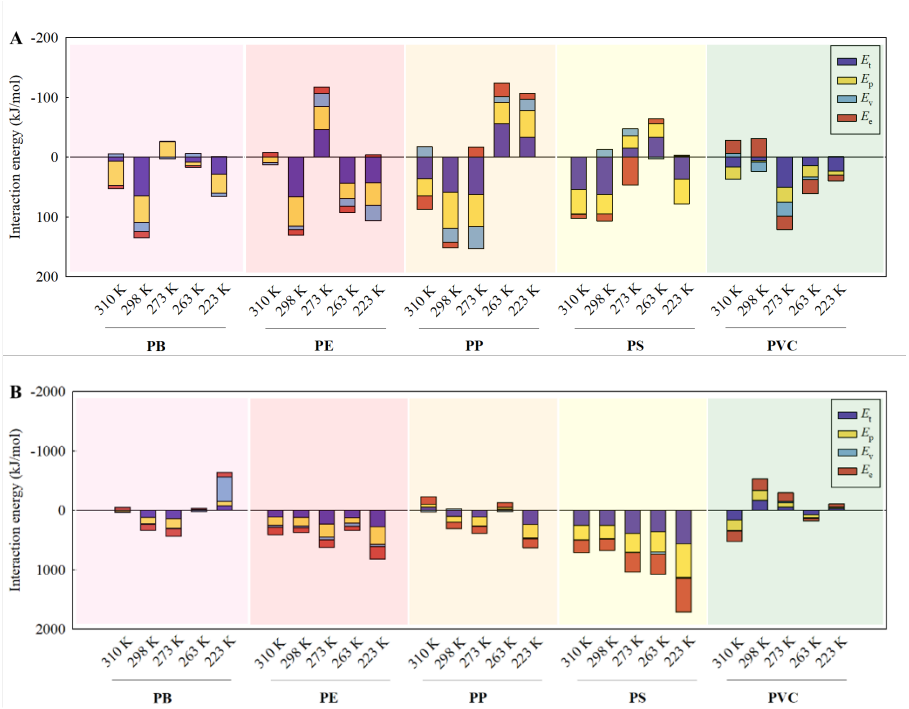

Figure S3.2. *Interaction energies of the five types of MPs with the HBV RNA fragment in vacuum (A) and in water (B) at different temperatures.* E_t*: interaction energy derived from total energy,* E_p*: interaction energy derived from potential energy,* E_v*: interaction energy derived from van der Waals energy, and* E_e*: interaction energy derived from electrostatic energy.*

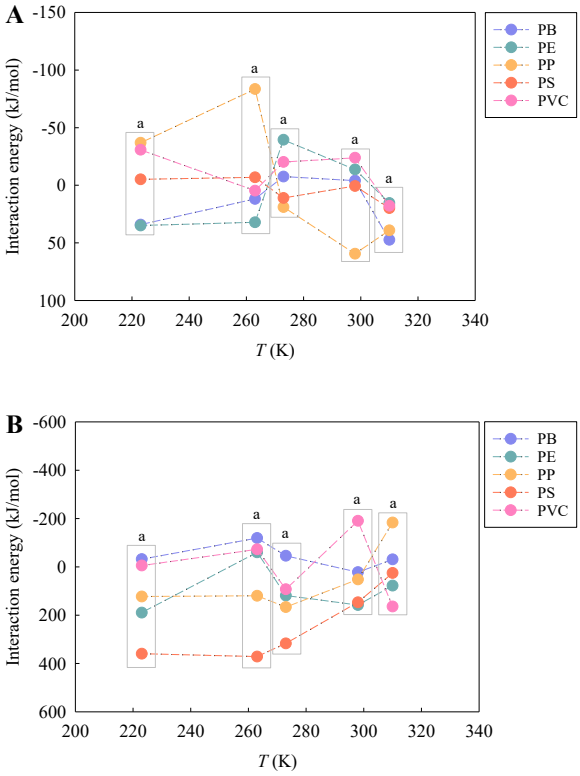

Figure S3.3. *Variation of the interaction energies derived from the total energies of the five types of MPs with the SARS-CoV-1 RNA fragment in vacuum (A) and in water (B) with the studied temperatures (223, 263, 273, 298, and 310 K). Different letters represent statistically significant differences between the treatments ($p < 0.05$).*

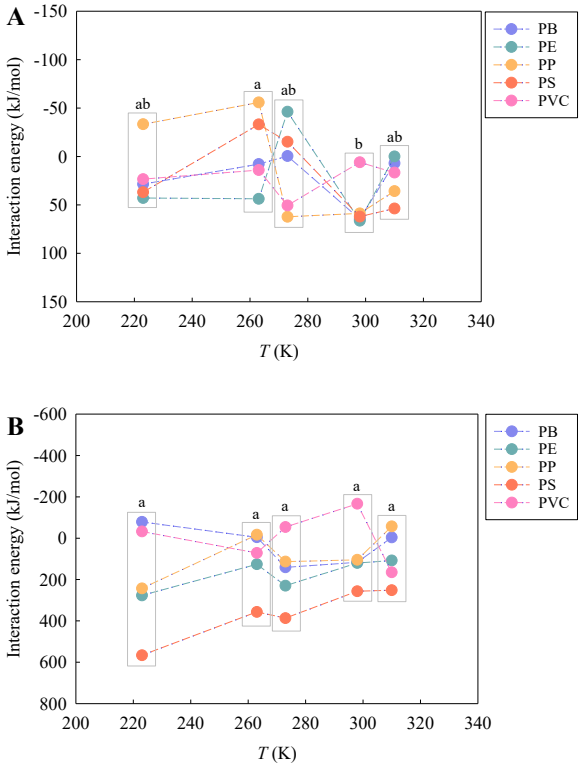

Figure S3.4. *Variation of the interaction energies derived from the total energies of the five types of MPs with the HBV RNA fragment in vacuum (A) and in water (B) with the studied temperatures (223, 263, 273, 298, and 310 K). Different letters represent statistically significant differences between the treatments ($p < 0.05$).*

Table S3.1. *Calculated molecular parameters of the MP monomers.*

Monomers	Volume (nm^3)	Polar surface area (nm^2)	Molecular topological index
PB	0.140	1.414	104
PE	0.084	0.968	16
PP	0.112	1.192	48
PS	0.194	1.833	576
PVC	0.102	1.125	36

Table S3.2. *Correlation coefficients between the E_{int} values derived from the total energies between the MPs and SARS-CoV-1 RNA fragment and the molecular parameters of the MP monomers* [a].

Correlation model	Temperature (K)	Volume (nm^3)		Polar surface area (nm^2)		Molecular topological index	
		$n = 5$	$n = 4$	$n = 5$	$n = 4$	$n = 5$	$n = 4$
E_{int} in vacuum	310	0.136	**0.918**	0.137	**0.907**	0.194	**0.890**
	298	0.055	0.212	0.049	0.197	0.036	0.107
	273	0.627	0.569	0.628	0.567	0.489	0.445
	263	0.076	0.195	0.076	0.192	0.011	0.054
	223	0.013	0.014	0.022	0.084	0.035	0.259
E_{int} in water	310	0.151	0.439	0.144	0.418	0.011	0.370
	298	0.308	0.177	0.291	0.211	0.418	0.102
	273	0.493	0.735	0.488	0.736	0.722	**0.822**
	263	0.751	0.171	0.746	0.179	**0.867**	0.294
	223	0.521	0.739	0.511	0.761	0.754	0.724

[a] *The correlation was tested for five types (n = 5) of MPs (PB, PE, PP, PS, and PVC)/four types (n = 4) of MPs (PB, PE, PP, and PVC) and the SARS-CoV-1 RNA fragment; The magnitude of correlation coefficient (R) reflects the degree of correlation between the E_{int} and molecular parameter values; The bold numbers indicate high values of the correlation coefficients (R > 0.800).*

Table S3.3. *Correlation coefficients between the E_{int} values derived from the total energies between the MPs and HBV RNA fragment and the molecular parameters of the MP monomers* [a].

Correlation model	Temperature (K)	Volume (nm^3)		Polar surface area (nm^2)		Molecular topological index	
		$n = 5$	$n = 4$	$n = 5$	$n = 4$	$n = 5$	$n = 4$
E_{int} in vacuum	310	0.744	0.162	0.744	0.169	0.784	0.546
	298	0.289	0.190	0.273	0.155	0.261	0.262
	273	0.155	0.268	0.144	0.288	0.294	0.009
	263	0.519	0.382	0.519	0.380	0.428	0.747
	223	0.186	0.204	0.185	0.202	0.303	0.679
E_{int} in water	310	0.429	0.595	0.432	0.574	0.652	0.007
	298	0.620	0.203	0.606	0.169	0.640	0.258
	273	0.649	0.106	0.636	0.140	0.765	0.114
	263	0.663	**0.834**	0.659	**0.831**	**0.876**	0.245
	223	0.507	0.668	0.496	0.689	0.729	0.062

[a] *The correlation was tested for five types (n = 5) of MPs (PB, PE, PP, PS, and PVC)/four types (n = 4) of MPs (PB, PE, PP, and PVC) and the HBV RNA fragment; The magnitude of correlation coefficient (R) reflects the degree of correlation between the E_{int} and molecular parameter values; The bold numbers indicate high values of the correlation coefficients (R > 0.800).*

Supplementary information for Chapter 4

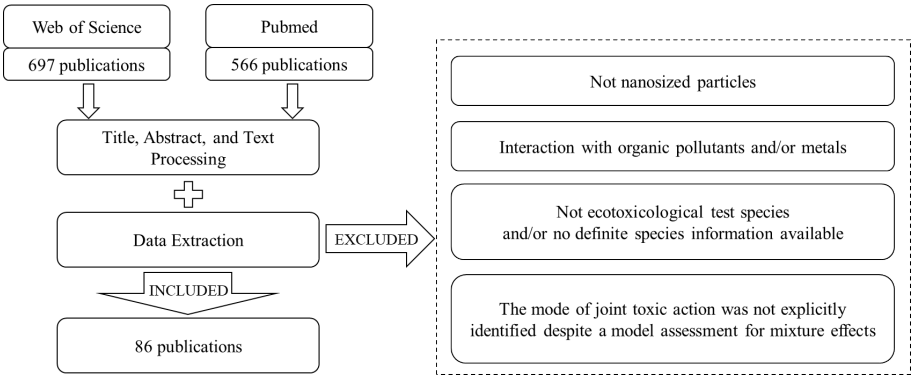

Figure S4.1. *Flowchart showing the decision process for inclusion and exclusion of literature on the ecotoxicity of mixtures of nanomaterials, identified using the ISI Web of Knowledge and PubMed search.*

Table S4.1. *List of studies on the joint toxicological effects of multiple metal-based engineered nanoparticles (ENPs) on ecological species* [a]

ENPs Types of mixtures	Ecological species	Test concentrations	Toxicity endpoints	Types of joint interactions	References
Algae					
$nTiO_2$ (anatase) + $nTiO_2$ (rutile)	*Chlorella* sp.	$nTiO_2$ (anatase) + $nTiO_2$ (rutile): 0.25+0.25, 0.25+0.5, and 0.5+0.5 mg/L	Cell viability, chlorophyll content, uptake/internalization, cell surface morphology, ultra-structural changes, DNA damage, and ROS generation	Antagonistic	Iswarya et al., 2015
		$nTiO_2$ (anatase) + $nTiO_2$ (rutile): 0.25+1, 0.5+0.25, 0.5+1, 1+0.25, 1+0.5, and 1+1 mg/L		Additive	
$nSiO_2$ + $nTiO_2$ (anatase@rutile)	*Scenedesmus obliquus*	$nSiO_2$: 1 µg/L and 1 mg/L $nTiO_2$ (anatase@rutile): 1 µg/L and 1 mg/L $nZrO_2$: 1 µg/L and 1 mg/L Mixtures (1:1 and 1:1:1 ratios)	Chlorophyll content, intracellular levels of ROS, mitochondrial membrane potential, permeability of cell membrane, antioxidant activities, and cell surface morphology	n.d.	Liu et al., 2018
$nSiO_2$ + $nZrO_2$				n.d.	
$nTiO_2$ (anatase@rutile) + $nZrO_2$				n.d.	
$nSiO_2$ + $nTiO_2$ (anatase@rutile) + $nZrO_2$				Synergistic	
nCdS + nZnS	*Heterosigma akashiwo*	nCdS: 12 mg/L $nSiO_2$ (with no inclusions): 143.5 mg/L $nSiO_2$ (with metal inclusions): 2.1 mg/L $nTiO_2$ (anatase): 79.5 mg/L nZnS: 53 mg/L	Growth inhibition, esterase activity, membrane potential, ROS generation, and cell size	Antagonistic	Pikula et al., 2022
nCdS + $nTiO_2$ (anatase)				Synergistic	
nCdS+ $nSiO_2$ (with no inclusions)				Synergistic	
nCdS + $nSiO_2$ (with metal inclusions)				Antagonistic	

$nTiO_2$ (anatase) + nZnS				Synergistic	
$nSiO_2$ (with no inclusions) + nZnS				Synergistic	
$nSiO_2$ (with metal inclusions) + nZnS				Antagonistic	
$nSiO_2$ (with no inclusions) + $nTiO_2$ (anatase)				Synergistic	
$nSiO_2$ (with metal inclusions) + $nTiO_2$ (anatase)				Additive	
$nSiO_2$ (with no inclusions) + $nSiO_2$ (with metal inclusions)				Additive	
$nTiO_2$ (Spherical, anatase@rutile) + $nTiO_2$ (Tubular)	*Scenedesmus obliquus*	$nTiO_2$ (Spherical, anatase@rutile) + $nTiO_2$ (Tubular): 2.33+13.16 and 19.75+211.26 mg/L	Growth inhibition and intracellular ROS generation	Additive	Wang et al., 2020
	Chlorella pyrenoidosa	$nTiO_2$ (Spherical, anatase@rutile) + $nTiO_2$ (Tubular): 0.13+0.002 and 5.38+4.87 mg/L		Additive	
				Synergistic	
nCuO + nZnO	*Scenedesmus obliquus*	nCuO: 2.1 μg Cu/L-4.3 mg Cu/L nZnO: 6.6 μg Zn/L-33.1 mg Zn/L Mixtures: equal toxic ratio	Growth inhibition	Additive	Ye et al., 2017
Bacteria					
nAg + nPt	*Escherichia coli*	nAg + nPt: 30+70, 50+50, and 70+30 wt%	Antimicrobial activity	n.d.	Breisch et al., 2020
	Staphylococcus aureus				
nCuO + $nTiO_2$ (anatase@rutile)	*Escherichia coli*	nCuO + $nTiO_2$ (anatase@rutile): 0.1+2, 0.2+2, 0.3+2, and 0.4+2 mg/L	Bacterial ATP levels, cell membrane integrity, and ROS production	Synergistic	Chen et al., 2020
				Slight additive	
nAg + nCuO	Nitrifying bacteria	The concentration of each	Nitrification inhibition and	Additive	Choi and Hu, 2009

nAg + $nTiO_2$ (anatase)		metallic/oxide nanoparticles was 1 mg/L	intracellular ROS concentrations	Additive	
nAg + nZnO				Antagonistic	
nAg + nCuO + $nTiO_2$ (anatase)				Additive	
$nTiO_2$ (anatase) + nZnO	*Escherichia coli*	$nTiO_2$ (anatase):1, 10, 100, and 1000 mg/L nZnO:1, 10, 100, and 1000 mg/L Mixtures (1:1 ratio)	Growth reduction and cell wall damage	Antagonistic	Srivastava and Kumar, 2017
$nTiO_2$ (anatase@rutile) + nZnO	*Escherichia coli*	$nTiO_2$ (anatase@rutile) + nZnO: 10+1 and 10+25 mg/L	ATP levels, cell membrane integrity, ROS production, and nanoparticle/bacterial surface interactions	Antagonistic	Tong et al., 2015
	Aeromonas hydrophila				
nAg + $nTiO_2$ (anatase@rutile)	*Escherichia coli*	nAg: 5, 10, 20, 30, and 40 µg/L $nTiO_2$ (anatase@rutile): 1 and 10 mg/L	ATP levels	n.d. (under dark)	Wilke et al., 2016
nAg + $nTiO_2$ (anatase@rutile)	*Escherichia coli*	nAg: 5, 10, 20, and 30 µg/L $nTiO_2$ (anatase@rutile): 1 and 2 or 10 mg/L	ATP levels, cell membrane integrity, and ROS production	Synergistic (under light)	Wilke et al., 2018
$nCeO_2$ + nZnO	*Nitrosomonas europaea*	$nCeO_2$ + nZnO: 1+10, 10+10, and 50+10 mg/L	Cell size, charge, morphology, density, membrane integrity, ammonia removal rate, amoA gene expression, and AMO activity	Synergistic	Yu et al., 2016a
$nCeO_2$ + $nTiO_2$ (anatase)		$nCeO_2$ + $nTiO_2$ (anatase): 50+1, 50+10, and 50+50 mg/L		Antagonistic	

$nTiO_2$ (anatase) + nZnO	*Nitrosomonas europaea*	$nTiO_2$ (anatase) + nZnO: 1+10, 10+10, and 50+10 mg/L	Cell size, charge, morphology, density, membrane integrity, ammonia removal rate, AMO activity, and transcriptional response	Antagonistic	Yu et al., 2016b
nAg + nCu	*Escherichia coli*	40 mL of nAg and 40 mL of nCu were separately synthesized in 3% (w/v) of chitosan and then mixed together	Bacterial growth inhibition	n.d.	Zain et al., 2014
	Bacillus subtilis				
nCuO + nZn	*Vibrio fischeri*	nCu (EC_{50}): 4.1 mg/L nZn (EC_{50}): 20.5 mg/L nCuO (EC_{50}): 118.7 mg/L nZnO (EC_{50}): 11.6 mg/L Equitoxic binary mixtures of nanoparticles were prepared based on the EC_{50} values of individual nanoparticles to determine their joint effects	Bioluminescence inhibition	Synergistic	Zhang et al., 2020
nCuO + nZnO				Synergistic	
nCu + nZn				Synergistic	
nCu + nCuO				Antagonistic	
nCu + nZnO				Antagonistic	
nZn + nZnO				Additive	
Daphnia					
nAg + nZnO	*Daphnia magna*	nAg: 0.05 to 0.25 mg·Ag/L and nZnO: 0.5 to 1.3 mg·Zn/L for immobilization tests; Combined exposures: based on a full factorial design nAg: 0.095 to 0.5 mg·Ag/L and nZnO: 0.1 to 0.4 mg·Zn/L for reproduction tests; Combined exposures: a fixed ray design based on individual toxic units	Immobilization and reproduction	Synergistic	Azevedo et al., 2017
				Antagonistic	

$nTiO_2$ (anatase) + $nTiO_2$ (rutile)	*Ceriodaphnia dubia*	$nTiO_2$ (anatase): 4.63, 9.26, 13.89, 18.52, 23.15, 27.78, and 32.41 mg/L $nTiO_2$ (rutile): 6, 12, 18, 24, 30, 36, and 42 mg/L Mixtures: equal toxic proportions	Mortality and biouptake	Antagonistic (under visible irradiation)	Iswarya et al., 2016
		$nTiO_2$ (anatase): 2.82, 5.64, 8.46, 11.28, 14.10, 16.92, and 19.74 mg/L $nTiO_2$ (rutile): 2.97, 5.94, 8.91, 11.88, 14.85, 17.82, and 20.79 mg/L Mixtures: equal toxic proportions		Additive (under UV-A irradiation)	
$nTiO_2$ (anatase) + $nTiO_2$ (rutile)	*Ceriodaphnia dubia*	Mixtures: 75, 300, and 1200 µM the mixtures treated algal diet In case of a binary mixture, the equal concentration of anatase and rutile nanoparticles forms the total concentration of binary mixture	Mortality, ultra-structural deformities, bioaccumulation, and biomagnification	Antagonistic (under visible irradiation)	Iswarya et al., 2018
				Antagonistic (under UV-A irradiation)	
$nTiO_2$ (anatase) + $nTiO_2$ (rutile)	*Ceriodaphnia dubia*	Mixtures: 75, 150, 300, 600, and 1200 µM the mixtures treated algal diet The binary mixture comprises an equal concentration of rutile and anatase nanoparticles	Mortality and oxidative stress (MDA, CAT, and GSH)	Synergistic (lower concentration, under visible irradiation)	Iswarya et al., 2019
				Additive (higher concentration, under visible irradiation)	
				Additive (lower concentration, under UV-A irradiation)	
				Antagonistic (higher concentration, under UV-A irradiation)	

nAg + nZnO	*Daphnia magna*	nAg: 1-25 µg/L and nZnO: 0.25-5 mg/L	Immobilization and feeding inhibition	Synergistic	Lopes et al., 2016
nCu + nCr	*Daphnia magna*	Joint toxicity of binary mixtures was determined at an equal concentration (1:1), and the total concentrations were 0.4, 2, 10, 50, and 100 µg/L	Reproduction and growth, rates of filtration and ingestion, as well as changes in enzyme activities: AChE, SOD, CAT, and GST	More-than-additive	Lu et al., 2017
$nTiO_2$ (anatase) + $nTiO_2$ (rutile)	*Daphnia similis*	70:30 anatase: rutile ratio (w/w) 1 to 100 mg/L TiO_2	Immobilization	n.d.	Marcone et al., 2012
nCu + nZnO	*Daphnia magna*	nCu + nZnO: 0.11 mg Cu/L+1.29 mg Zn/L nCu + nZnO: 0.40 mg Cu/L+4.01 mg Zn/L	Mortality and bioaccumulation	Additive More-than-additive	Yu et al., 2022
nCuO + nZnO	*Daphnia magna*	Binary mixtures were also tested according to an equiconcentration ratio of 1:1 and the total exposure concentrations were 0.0004, 0.002, 0.01, 0.05, and 0.25 mg/L	Immobilization, mortality, reproduction (fecundity) and growth, as well as filtration and ingestion rates	Synergistic Partial additive	Zhao et al., 2012
Fish					
nAg + $nTiO_2$ (anatase@rutile)	*Cyprinus carpio*	nAg: 0.05, 0.10, 0.20, 0.30, 0.40, 0.50, 0.60, and 0.70 mg/L for acute toxicity tests and nAg: 0.05 and 0.1 mg/L for chronic toxicity tests $nTiO_2$ (anatase@rutile): 1 mg/L	Mortality, bioaccumulation, oxidative stress (SOD, CAT, and GST), and gill histopathology	Antagonistic Synergistic Additive	Haghighat et al., 2021
nCu + nZnO	*Poeciliopsis lucida*	nCu: 0.39, 0.78, 1.56, 3.13, 6.25, 12.5, and 25 µg/mL nZnO: 6.25 µg/mL	Cell viability, cell morphology, and metal internalization	n.d.	Hernández-Moreno et al., 2016
nCu + nZnO	*Oncorhynchus mykiss*	nCu: 0.0425, 0.085, 0.17, and 0.34	Survival, metal internalization,	n.d.	Hernández-Moreno

		mg/L nZnO: 1.25 mg/L	and oxidative stress (EROD activity, GST activity, and GSH/GSSG ratio)		et al., 2019
$nTiO_2$ (spherical, anatase) + nZnO (stick-shaped)	*Danio rerio*	$nTiO_2$ (spherical, anatase): 1.5, 3, 6, 12, and 24 mg Ti/L nZnO: 2, 4, 8, 16, and 32 mg Zn/L	Mortality and hatching rate	Antagonistic	Hua et al., 2016
$nCeO_2$ + nCuO	Zebrafish embryos	$nCeO_2$: 0.01, 0.1, 1, 10, and 50 µg/mL nCuO: 0.01, 0.1, 1, 10, and 50 µg/mL Mixtures (1:1 ratio)	Mortality rate, hatching rate, malformations, oxidative stress genes, CAT enzyme activity, DNA damage, and apoptosis and necrosis	n.d.	Kaur et al., 2019
nCuO + $nTiO_2$ (anatase@rutile)	*Cyprinus carpio*	nCuO + $nTiO_2$ (anatase@rutile): 2.5+10 and 5.0+10 mg/L	Oxidative stress biomarkers in the liver, brain, and gills and acetylcholinesterase activity (a biomarker that indicates neurotoxicity) in the brain and muscle, as well as induce histopathological alterations in the gills, liver and retina	n.d.	Mansouri et al., 2016
nCuO + $nTiO_2$ (anatase@rutile)	*Cyprinus carpio*	nCuO + $nTiO_2$ (anatase@rutile): 2.5+10 and 5.0+10 mg/L	Histopathological anomalies of gill and intestine tissues in *C. carpio*	Synergistic	Mansouri et al., 2017
$nTiO_2$ + nZnO	*Prochilodus lineatus*	$nTiO_2$ + nZnO: 1+1 µg/L	Biochemical responses (AchE activity, protein carbonylation, lipid peroxidation, and non-protein thiols) and injuries in organs (histological and ultra-structural analyses)	n.d.	Miranda et al., 2016
nAg + nCuO	*Clarias gariepinus*	nCuO: 6.25, 12.5, 25, 50, and 100 mg/L nAg: 6.25, 12.5, 25, 50, and 100 mg/L Mixtures (1:1 ratio)	Frequency of micronucleus, haematology, histopathology (skin, gills and liver), and hepatic oxidative stress analysis (MDA, reduced GSH, SOD, and	Antagonistic	Ogunsuyi et al., 2019

			CAT)	Synergistic	
$nCuO + nCeO_2$	*Carassius auratus*	20, 40, 80, 160, and 320 mg/L. The binary and ternary mixtures were tested at an equi-concentration ratio of 1:1 or 1:1:1 (W/V)	AChE activity, Na^+/K^+-ATPase activity, SOD activity, and CAT activity	Antagonistic	Xia et al., 2013
$nCuO + nZnO$				Synergistic	
$nCeO_2 + nZnO$				Antagonistic	
$nCeO_2 + nCuO + nZnO$				Additive	
Fungi					
$nAg + nMoS_2$ (chitosan functionalization)	*Saccharomyces cerevisiae*	nAg: 5, 10, 20, 30, and 40 μg/L $nMoS_2$ (chitosan functionalization): 1 and 10 mg/L	Oxidative stress (intracellular ROS generation), membrane stress (intracellular lactate dehydrogenase activity), and metabolic activities	Synergistic	Yang et al., 2018
Insects					
nCdO + nPbO	*Apis millefera*	nCdO: 0.01 mg/mL nPbO: 0.65 mg/mL	Content of nCdO and nPbO in midgut tissues, survival, morphological assessment of midgut tissues, ultrastructure observations, and incidence of apoptosis and necrosis of midgut epithelia	Antagonistic	Dabour et al., 2019
nZn + nCu	*Folsomia candida*	nZn: nCu: 300+300 mg/kg	Survival and reproduction	Antagonistic	Jośko et al., 2022
nZnO + nCuO		nZnO: nCuO: 300+300 mg/kg		Synergistic	
Plants					
nCo + nFe + nNi	*Lactuca sativa*	Influent: 2,700 mg nCo + 50,000 mg nFe + 6,250 mg nNi; DI Water 123 kg	Germination and growth	n.d.	Hassanein et al., 2021
$nTiO_2$ (anatase) + nZnO	*Vigna angularis*	$nTiO_2$ (anatase): 20, 40, 60, 80, 100, and 200 μg/mL nZnO: 20, 40, 60, 80, 100, and 200 μg/mL Mixtures (1:1 ratio)	Seed germination, root/shoot length, total chlorophyll content, carotenoids and lipid peroxidation, oxidative stress and antioxidant enzyme activity,	n.d.	Jahan et al., 2018

			kinetic uptake and transport		
nCuO + nZnO	*Hordeum vulgare*	nCuO: 300 mg Cu/kg nZnO: 300 mg Zn/kg Mixtures (1:1 ratio)	Biomass, plant mineral composition as well as expression of genes regulating metal homeostasis (ZIP1,3,6,8,10,14, RAN1, PAA1,2, MTP1, COPT5) and detoxification (MT1–3)	n.d.	Jośko et al., 2021
nCuO + nZnO nCuO + $nTiO_2$ nCuO + nCr_2O_3 nCuO + nFe_2O_3 nZnO + $nTiO_2$ nZnO + nCr_2O_3 nZnO + nFe_2O_3	*Lepidium sativum*	Concentration of each nanoparticles was set to be 100 mg/L Mixtures (1:1 ratio)	Seed germination, root growth inhibition rates, and the external and internal surface area of root	Antagonistic	Jośko et al., 2017
	Linum utisassimmum				
	Cucumis sativus				
	Triticum aestivum				
nCdO + nCuO	*Vigna radiata*	0.1, 1, and 10 mg/L Mixtures (1:1 ratio)	Germination percent, relative germination rate, and metal accumulations	n.d.	Jung et al., 2020
nCuO + nZnO nCuO + nNiO nZnO + nNiO	*Lactuca sativa*	nCuO: 0.06 and 0.12 mg/L nZnO: 0.12 and 0.25 mg/L nNiO: 0.15 and 0.3 mg/L	Root and shoot growth	Additive	Kong et al., 2021
	Raphanus sativus	nCuO: 0.09 and 0.18 mg/L nZnO: 0.31 and 0.62 mg/L nNiO: 0.71 and 1.42 mg/L			
nCu + nZnO	*Lactuca sativa*	nCu: 0.10 to 0.80 mg/L nZnO: 0.50 to 50.00 mg/L	Relative root elongation rate	Antagonistic	Liu et al., 2016
$nTiO_2$ (anatase) + $nTiO_2$ (rutile)	*Pisum sativum*	800 mg of TiO_2 per kg of soil	TiO_2 particles' entry in the root	n.d.	Muccifora et al.,

		Mixture of anatase and rutile $nTiO_2$: 1:1 ratio	system, bioaccumulation, relative distribution, and localiz-ation, as well as the main crystalline form preferentially absorbed and their effect in cells ultrastructure of plant roots		2021
nCuO + nZnO	*Spinacia oleracea*	nCuO: 10, 100, and 1000 mg/L nZnO: 10, 100, and 1000 mg/L Mixtures (1:1 ratio)	Root length, shoot length, total weight, chlorophyll content, carotenoid content, and ion content of *S. oleracea* plants	n.d.	Singh and Kumar, 2016
nCuO + nZnO	*Raphanus sativus*	nCuO: 10, 100, and 1000 mg/kg nZnO: 10, 100, and 1000 mg/kg Mixtures (1:1 ratio)	Seed germination (root length, shoot length, and fresh weight) and metal uptake	Antagonistic	Singh and Kumar, 2018
nCuO + nZnO	*Raphanus sativus*	nCuO: 0.1, 1, 10, 100, and 1000 mg/L nZnO: 0.1, 1, 10, 100, and 1000 mg/L Mixtures (1:1 ratio)	Seed germination (root length, shoot length, and fresh weight) and metal uptake	Antagonistic	Singh and Kumar, 2019
nCuO + nZnO	*Spinacia oleracea*	nCuO + nZnO: $1.2\times10^{-4}+1.2\times10^{-4}$, $1.2\times10^{-3}+1.2\times10^{-3}$, $1.2\times10^{-2}+1.2\times10^{-2}$ mol/kg of soil	Maturity, plant fresh weight, root length, and metal uptake	Additive	Singh and Kumar, 2020a
nAg_2O + $nTiO_2$ (anatase)	*Spinacia oleracea*	nAg_2O: 1 and 10 mg/kg $nTiO_2$ (anatase): 1 and 10 mg/kg Mixtures (1:1 ratio)	Plant physiology and development (root length, shoot length, and fresh weight), total chlorophyll and carotenoid contents, and metal uptake	Additive	Singh and Kumar, 2020b
$nCeO_2$ + nZnO	*Pisum sativum*	Ce: 100 and 200 mg/L Zn: 100 and 200 mg/L Mixtures (1:1 ratio)	Plant growth (root and stem lengths and fresh weight), Ce and Zn concentrations in roots and shoots, photosynthesis pigments (contents of chlorophyll a, chlorophyll b, and carotenoids), and photosynthetic parameters (leaf net photosynthesis, sub-stomatal CO_2	n.d.	Skiba et al., 2021

			concentration, transpiration, stomatal conductance, photosynthetic water use efficiency, and photosynthetic CO_2 response curve		
nCdO + nCuO	*Vigna radiata*	nCdO + nCuO: 1+1, 10+10, and 100+100 mg/kg	Seed germination, plant growth, and metal accumulation	Antagonistic	Subpiramaniyam et al., 2021

[a] *N.d. = not determined. AChE – acetylcholinesterase, AMO – ammonia monooxygenase, ATP – adenosine triphosphate, ATPase – adenosine triphosphatase, CAT – catalase, COX – cyclooxygenase, EROD – ethoxyresorufin-O-deethylase, GSH – glutathione, GSSG – oxidized glutathione, GST – glutathione S-transferase, LPO – lipid peroxidation, MDA malondialdehyde, $nMoS_2$ – molybdenum disulfide nanosheets, ROS – reactive oxygen species, SOD – superoxide dismutase.*

For presentation purposes, $nSiO_2$ (with metal inclusions) is shortened to $nSiO_2$(m), $nTiO_2$ (anatase) is shortened to $nTiO_2$(a), $nTiO_2$ (anatase@rutile) is shortened to $nTiO_2$(a@r), $nTiO_2$ (rutile) is shortened to $nTiO_2$(r).

Table S4.2. *List of studies on the joint toxicological effects of multiple engineered nanoparticles (ENPs) comprising of non-metal-based components on ecological species* [a]

ENPs Types of mixtures	Ecological species	Test concentrations	Toxicity endpoints	Types of joint interactions	References
nPS + $nTiO_2$ (anatase@rutile)	*Scenedesmus obliquus*	nPS: 1 mg/L $nTiO_2$ (anatase@rutile): 0.025, 0.25, and 2.5 mg/L	Cell viability, morphological changes, oxidative stress (total ROS, superoxide radical, hydroxyl radical), antioxidant activity, photosynthetic efficiency, and esterase activity	Antagonistic	Das et al., 2022
				Additive	
nPS + nZnO	*Ctenopharyngodon idella*	nPS: 760 µg/L nZnO: 760 µg/L	Behavioral, biochemical (nitric oxide dosage, TBARS, hydrogen peroxide, total glutathione content, DPPH radicals' scavenging, SOD, and AChE activity, nutritional status), and genotoxic biomarkers	No observed antagonistic, synergistic or additive effect	Estrela et al., 2021
MWCNTs + nCuO	*Tetradesmus obliquus*	MWCNTs: 1, 10, and 100 mg/L nCuO: 2 and 200 mg/L	Growth inhibition, membrane damage, physical damage, oxidative stress (ROS level, SOD, and MDA), and internalization of Cu	n.d.	Fang et al., 2022
nSe + nZnO	Zebra fish *(D. rerio)*	nSe + nZnO (2 mg/kg each)	Survivability, growth performance parameters, intracellular ROS, gene expression, and fecundity and development	Synergetic	Fasil et al., 2021
MWCNTs + nZnO	*Brassica rapa*	MWCNTs: 10 and 100 mg/L nZnO: 10, 50, and 100 mg/L	The length of roots and stems, chlorophyll content, oxidative stress (relative ROS, soluble sugar, and MDA contents), antioxidant enzyme activity (CAT, POD, and SOD), metal element content, and root scanning electron microscopy	Synergetic	Hong et al., 2022

nPS + nAg	*Chlamydomonas reinhardtii*	nAg: 3, 10, 30, 100, and 200 µg/L nPS: 3 and 30 mg C/L	Cell-specific growth rate and subcellular distributions	Synergistic	Huang et al., 2019
	Ochromonas danica	nAg: 10, 30, 100, 200, and 300 µg/L nPS: 3 and 30 mg C/L			
nPS + $nTiO_2$ (anatase@rutile)	*Chlorella* sp.	nPS, COOH-nPS, and NH_2-nPS: 5 mg/L $nTiO_2$ (anatase@rutile): 0.25, 0.5, and 1 mg/L	Cell viability, oxidative stress (total ROS, superoxide and hydroxyl radical, CAT and SOD, and MDA), maximum quantum yield of PS II, and esterase activity	Antagonistic	Natarajan et al., 2022
COOH-nPS + $nTiO_2$ (anatase@rutile)					
NH_2-nPS + $nTiO_2$ (anatase@rutile)					
GNs + nZnO	*Capoeta fusca*	GNs + nZnO: 6.5+0.04 and 6.5+0.09 mg/L	Bioconcentration (uptake and elimination)	n.d.	Sayadi et al., 2021
MLGs + nZnO	*Capoeta fusca*	MLGs: 6.5 mg/L nZnO: 0.1, 0.4, 0.9, 1, 5, 10, 15, 20, 25, and 30 mg/L for acute toxicity test and nZnO: 0.09 mg/L for behavioural assay and histopathology	Lethality, histopathological and behavioral changes	Synergistic	Sayadi et al., 2022
				Antagonistic	
GO + nZnO	*Scenedesmus obliquus*	GO: 0.5-50 mg/L nZnO: 0.01-50 mg/L Mixture ratios: EC_{10} and EC_{50} of each component	Growth inhibition rate and total ROS level	Additive	Ye et al., 2018
	Daphnia magna	GO: 1-80 mg/L nZnO: 0.01-0.4 mg/L Mixture ratios: EC_{10} and EC_{50} of each component	Immobilization rate and total ROS level	Additive	
	Danio rerio	GO: 20-160 mg/L nZnO: 2-20 mg/L Mixture ratios: LC_{10} and LC_{50} of each component	Lethality and total ROS level	Antagonistic	

CNCs + nZnO	*Eremosphaera viridis*	CNCs: 100 mg/L nZnO: 1, 5, and 10 mg/L	Dry weight, chlorophyll a, chlorophyll b, ROS level, CAT activity, MDA content, cellular superficial- and ultra-structures, elemental distribution as well as proteins and lipids in a single algal cell	n.d.	Yin et al., 2022
GNs + $nZrO_2$	*Chlorella pyrenoidosa*	GNs: 0.1 and 1 mg/L $nZrO_2$: 1, 5, 10, 17.5, 25, and 50 mg/L GNs + $nZrO_2$: 1+EC_{10} and 1+EC_{50} mg/L	Growth inhibition, intracellular levels of ROS, mitochondrial membrane potential, permeability of cell membrane, and cellular superficial- and ultra-structures	Synergistic	Wang et al., 2021
rGO + $nZrO_2$		rGO: 0.1 and 1 mg/L $nZrO_2$: 1, 5, 10, 17.5, 25, and 50 mg/L rGO + $nZrO_2$: 1+EC_{10} and 1+EC_{50} mg/L		Synergistic	
MWCNTs + nPS	*Microcystis aeruginosa*	MWCNTs: 5, 10, 20, and 50 mg/L nPS: 5, 10, 20, and 50 mg/L	Growth (cell density), photosynthesis (chlorophyll a), total protein, antioxidant responses (SOD and MDA), membrane damage, genetic material damage, and metabolic process	Antagonistic	Zhang et al., 2022
GO + nAl_2O_3	*Chlorella pyrenoidosa*	GO: 25 mg/L nAl_2O_3: 50, 100, 150, 300, 450, and 600 mg/L	Growth inhibition, membrane damage, oxidative stress, and physical damage	n.d.	Zhao et al., 2018
GQDs + nZnO	*Gymnodinium*	GQDs + nZnO: 1+1, 20+5, and 20+20 mg/L	Cell density, specific growth rates, total intracellular ROS, enzyme activities (SOD and ATPase), and surface interaction of nanoparticles and algal cells	Antagonistic	Zhu et al., 2022

[a] *N.d. = not determined. AChE – acetylcholinesterase, ATPase – adenosine triphosphatase, CNCs – cellulose nanocrystals, COOH-nPS – carboxyl-functionalized polystyrene nanoplastics, DPPH – diphenyl-1-picrylhydrazyl, EC_{10} – 10% effect concentration, EC_{50} – 50% effect concentration, GNs – graphene nanosheets, GO – graphene oxide, GQDs – graphene quantum dots, LC_{10} – 10% lethal concentration, LC_{50} – 50% lethal concentration, MDA– malondialdehyde, MLGs –*

multi-layer graphenes, MWCNTs – multiwall carbon nanotubes, NH_2-nPS – amine-functionalized polystyrene nanoplastics, POD – peroxidase, nPS – polystyrene nanoplastics, rGO – reduced graphene oxide, nSe – nano-selenium, SOD – superoxide dismutase, SWCNTs – single walled carbon nanotubes, TBARS – thiobarbituric acid reactive species.

For presentation purposes, $nTiO_2$ (anatase@rutile) is shortened to $nTiO_2$(a@r).

Table S4.3. *List of studies on the potentiation or attenuation of effects of mixtures of individual engineered nanoparticles (ENPs) on ecological species* [a]

ENPs Types of mixtures	Ecological species	Potentiation or attenuation of effects		References
nAg + nPt	*Escherichia coli* *Staphylococcus aureus*	nPt significantly increased the toxicity of nAg	↑	Breisch et al., 2020
MWCNTs + nCuO	*Tetradesmus obliquus*	The existence of nCuO in some groups reduced cell membrane damage caused by MWCNTs	↓	Fang et al., 2022
		The highest concentration of nCuO combined with the highest concentration of MWCNTs enhanced the induced ROS level	↑	
nAg + $nTiO_2$ (anatase@rutile)	*Cyprinus carpio*	$nTiO_2$ increased acute toxicity of nAg	↑	Haghighat et al., 2021
		$nTiO_2$ increased Ag accumulation in liver and intestine	↑	
		$nTiO_2$ decreased Ag accumulation in gills	↓	
		$nTiO_2$ somewhat mitigated the effects of nAg on antioxidant enzymes activities	↓	
nCu + nZnO	*Poeciliopsis lucida*	The cytotoxicity exerted by nCu was enhanced in presence of non-toxic concentrations of nZnO	↑	Hernández-Moreno et al., 2016
nCu + nZnO	*Oncorhynchus mykiss*	The co-exposure of rainbow trout to non-toxic concentrations of nCu and a fixed non-toxic concentration of nZnO resulted in lethal effects	↑	Hernández-Moreno et al., 2019
$nTiO_2$ (anatase) + nZnO	*Vigna angularis*	The combination led to attenuated uptake and translocation behavior	↓	Jahan et al., 2018
nCuO + nZnO	*Hordeum vulgare*	After combined treatment of ENPs, the extractable concentrations of Cu and Zn were lower than upon individual exposure in bulk soil	↓	Jośko et al., 2021
		Genes related to metal uptake (ZIP) and cellular compartment (PAA2, RAN1) were mostly up-regulated by single rather than combined application of ENPs	↓	
nCdO + nCuO	*Vigna radiata*	The germination rate of the nCdO + nCuO treatment was less than that of the single metal exposure under both humidities (70% and 80%) at 48 h	↓	Jung et al., 2020
nCuO + $nCeO_2$	Zebrafish embryos	The harmful effects of the mixtures were more than $nCeO_2$ and less than that of nCuO	↑↓	Kaur et al., 2019
nCuO + $nTiO_2$ (anatase@rutile)	*Cyprinus carpio*	The joint presence of $nTiO_2$ can potentially increase the uptake of nCuO in the tissues of carp	↑	Mansouri et al., 2016
$nCeO_2$ + nZnO	*Pisum sativum*	The effects of nZnO were decreased by $nCeO_2$	↓	Skiba et al., 2021

GNs + nZnO	*Capoeta fusca*	The presence of GNs reduced the bioavailability of nZnO	↓	Sayadi et al., 2021
nAg + $nTiO_2$ (anatase@rutile)	*Escherichia coli*	$nTiO_2$ attenuated the toxicity of nAg	↓	Wilke et al., 2016
nAg + $nMoS_2$ (chitosan functionalization)	*Saccharomyces cerevisiae*	$nMoS_2$ attenuated the oxidative stress induced by nAg on the yeast cells	↓	Yang et al., 2018
		nAg inhibited the metabolic activities in yeast cells, but this inhibition phenomenon could be alleviated by $nMoS_2$	↓	
CNCs + nZnO	*Eremosphaera viridis*	The addition of CNCs enhanced the bioavailability and toxicity of nZnO to the algae	↑	Yin et al., 2022
		The nZnO-CNC association enhanced the envelopment of the algal cells and exerted strong oxidative stress as compared to bare nZnO	↑	
GO + nAl_2O_3	*Chlorella pyrenoidosa*	Algal growth inhibition by GO with coexisting nAl_2O_3 particles was much lower than the sum of inhibitions from the individual materials for nAl_2O_3, showing the toxicity mitigation by nAl_2O_3	↓	Zhao et al., 2018
		GO-induced algal membrane damage was suppressed by the nAl_2O_3	↓	

[a] *↑ indicates the potentiation of effect of mixtures of individual ENPs and ↓ indicates the attenuation of effect of mixtures of individual ENPs. CNCs – cellulose nanocrystals, GNs – graphene nanosheets, GO – graphene oxide, MWCNTs – multiwall carbon nanotubes.*

For presentation purposes, $nTiO_2$ (anatase) is shortened to $nTiO_2$(a), $nTiO_2$ (anatase@rutile) is shortened to $nTiO_2$(a@r).

Table S4.4. *List of studies on the toxicological effects of multicomponent nanomaterials (NMs) on ecological species* [a]

Types of hybrid NMs	Ecological species	Toxicity endpoints	Minimum inhibitory concentration	Toxic effects	References
nAg@nZnO	*Daphnia magna*	Immobilization and reproduction	n.d.	nAg@nZnO hybrid NMs showed higher toxicity than predicted based on the toxicity of nAg and nZnO	Azevedo et al., 2017
GO@nZnO	*Escherichia coli*	Growth of bacteria	n.d.	The antibacterial activity of GO@nZnO nanorods hybrid NMs has been demonstrated	Bhaisare et al., 2016
	Staphylococcus aureus				
α-nFe_2O_3@nCo_3O_4	*B. subtilis*	Bacterial growth inhibition	90 mg/dL	The enhanced bactericidal activity of the α-nFe_2O_3@nCo_3O_4 nanocomposite was the result of synergistic effects of iron oxide and cobalt oxide nanoparticles	Bhushan et al., 2018
	S. aureus		75 mg/dL		
	E. coli		60 mg/dL		
	S. typhi		45 mg/dL		
GO@nAg	*Fusarium graminearum*	Spore germination inhibition	n.d.	The GO@nAg nanocomposite showed almost a 3- and 7-fold increase of inhibition efficiency over pure nAg and GO suspension, respectively.	Chen et al., 2016
nTiO_2@MWCNT	*Danio rerio* embryos	Acute toxicity, hatching rate, growth, yolk sac size, and sarcomere length	n.d.	TiO_2@MWCNT hybrid NMs showed no acute toxicity to zebrafish embryos	Da Silva et al., 2018
GO@nAg	Zebrafish embryos	Mortality, malformation, edema, hatching, total length, and yolk sac size	n.d.	With chorion: LC_{50} of GO@nAg hybrid NMs: 1.4 [1.3-1.7] mg/L; Without chorion: LC_{50} of GO@nAg hybrid NMs: 1.0 [0.9-1.2] mg/L; The toxic effects of GO@nAg were lower than $AgNO_3$, but higher than GO	de Medeiros et al., 2021

nSe@nIO	*Staphylococcus aureus*	Biofilm viability	n.d.	The relative fraction of dead-to-live bacteria of the nanocomposites (400.0%) was much higher than that of nSe (51.6%) and nIO (60.0%)	Li et al., 2020
GO@polyvinylpyrrolidone-stabilized nAg	*Pseudomonas aeruginosa*	Bacterial growth inhibition	n.d.	This hybrid nanocomposite poses enhanced antibacterial activity against carbapenem-resistant *P. aeruginosa* strains through a possible synergy between toxicity mechanisms of GO nanosheets and nAg	Lozovskis et al., 2020
nTiO_2@MWCNT-CNF	*Pseudokirchneriella subcapitata*	Growth inhibition and sublethal oxidative stress	n.d.	Acute exposure of *P. subcapitata* to various concentrations of TiO_2@MWCNT-CNF nanocomposite may cause algal growth inhibition including undesirable sublethal oxidative stress effects	Malatjie et al., 2022
nZn@nCuO	*Xenopus laevis* embyos	Bioaccumulation, oxidative stress, and histopathology	n.d.	nZn@nCuO nanocomposite does induce only mild acute toxicity in *X. laevis* embryos. Nevertheless, these effects are smaller than those of nZnO. Interestingly, embryos exposed to the nanocomposite accumulate NPs more efficiently than those exposed to nCuO and nZnO, but the internalized NMs do not induce severe acute toxicity	Mantecca et al., 2015
nAg@GO Chit-nAg@GO	*Staphylococcus aureus* UCLA 8076	Bacterial growth inhibition	nAg@GO: 1.90 Ag + 1.5 GO μg/mL Chit-nAg@GO (1:8): 1.19	Chit-nAg@GO exhibit higher antibacterial activity than most of the antibacterial agents based on nAg or	Marta et al., 2015

	Staphylococcus aureus 1190R		Ag + 1.41 GO μg/mL	nAg@GO reported	
PSF-CNF@nAg	*Bacillus subtilis*	Bacterial growth inhibition	n.d.	In solid phase the gram-positive bacteria showed higher sensitivity for PSF-CNF@nAg membranes, while in liquid phase the antimicrobial activity of the hybrid membrane is more pronounced towards gram-negative species. Furthermore, in the case of *E. coli*, the growth inhibition in liquid medium is probably due to the synergetic action of the modified CNF and nAg	Mocanu et al., 2019
	Escherichia coli				
Ag-nZnO@SWCNT	*Escherichia coli*	Viable cell numbers	n.d.	All multicomponent NMs have been reported to possess strong antimicrobial activity towards *E. coli* and *S. aureus* bacteria, due to synergistic effect between metal-doped ZnO nanoparticles and carbon nanotubes	Mohammed et al., 2019
Au-nZnO@SWCNT					
Ag-nZnO@MWCNT	*Staphylococcusaureus*				
Au-nZnO@MWCNT					
nAg@GO	*Escherichia coli*	Antimicrobial effect mean inhibition zone	n.d.	An increase in the inhibition zone with the increase in amount of nAg@GO nanocomposite is obvious due to greater antimicrobial agents	Naeem et al., 2019
	Staphylococcus aureus				
rGO@nCu_2O	*Escherichia coli*	Bacterial growth inhibition	5.9 μg/mL	rGO@nCu_2O nanocomposite have a higher antimicrobial activity toward gram-negative and gram-positive bacteria when compared with reference antibiotics such as kanamycin and streptomycin	Selim et al., 2020
	Pseudo-monas aeruginosa		2.9 μg/mL		
	Bacillus subtilis		2.9 μg/mL		

nAu@nZnO	*Ruditapes decussatus*	Levels of H_2O_2, MDA, intracellular iron and calcium as well as the activities of SOD and CAT	n.d.	nAu@nZnO hybrid NMs induced biochemical and histological alterations within either the digestive gland or gill tissues at high concentration	Sellami et al., 2017
nAg@MWCNT	*Methylobacterium* spp.	Bacterial growth inhibition	30 μg/mL	30 μg/mL of synthesized Ag@MWCNTs yielded an efficient level of antibacterial activity against *Methylobacterium* spp. and *Sphingomonas* spp.	Seo et al., 2014
	Sphingomonas spp.				
nAu@nAg	*Escherichia coli*	Bacterial growth inhibition	10 μg/mL	Compared with individual nAg and the simple mixture of nAu and nAg, bimetallic nAu@nAg with remarkable stability and a long-term antibacterial efficiency while possessed synergistically enhanced antibacterial activity against both gram-negative and gram-positive bacteria, even at a lower silver concentration	Yang et al., 2017
	Staphylococcus aureus		15 μg/mL		
nAg@GO	*Escherichia coli*	Bacterial growth inhibition	3.2 μg/mL	After conjugating to GO sheets, the antibacterial activities of nAg against *E. coli* and *B. subtilis* were significantly enhanced	Zhu et al., 2013
	Bacillus subtilis		6.4 μg/mL		

[a] *N.d. = not determined, Chit – chitosan, CNCs – cellulose nanocrystals, CNF – carbon nanofiber, GO – graphene oxide, IO – iron oxide, MWCNT – multiwall carbon nanotube, PSF – polysulfone, rGO – reduced graphene oxide, SWCNT – single walled carbon nanotube.*

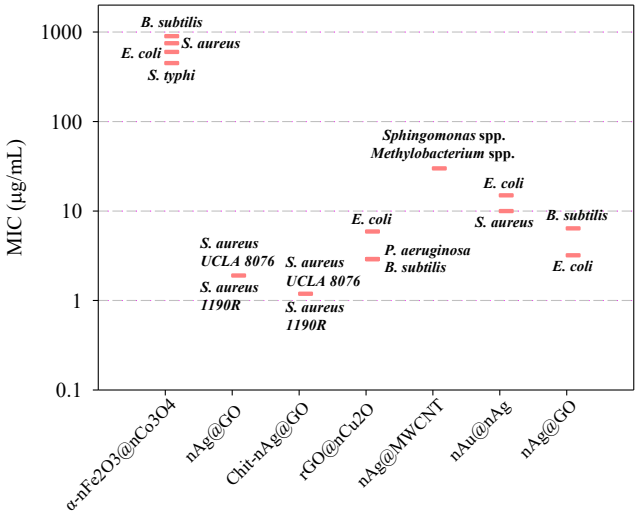

Figure S4.2. *Minimum inhibitory concentration (MIC) for bacteria exposed to multicomponent nanomaterials.*

References

Azevedo, S.L., Holz, T., Rodrigues, J., Monteiro, T., Costa, F.M., Soares, A.M.V.M., Loureiro, S., 2017. A mixture toxicity approach to predict the toxicity of Ag decorated ZnO nanomaterials. Sci. Total Environ. 579, 337–344.

Bhaisare, M.L., Wu, B.-S., Wu, M.-C., Khan, M.S., Tseng, M.-H., Wu, H.-F., 2016. MALDI MS analysis, disk diffusion and optical density measurements for the antimicrobial effect of zinc oxide nanorods integrated in graphene oxide nanostructures. Biomater. Sci. 4, 183–194.

Bhushan, M., Kumar, Y., Periyasamy, L., Viswanath, A.K., 2018. Antibacterial applications of α-Fe_2O_3/Co_3O_4 nanocomposites and study of their structural, optical, magnetic and cytotoxic characteristics. Appl. Nanosci. 8, 137–153.

Breisch, M., Loza, K., Pappert, K., Rostek, A., Rurainsky, C., Tschulik, K., Heggen, M., Epple, M., Tiller, J.C., Schildhauer, T.A., Köller, M., Sengstock, C., 2020. Enhanced dissolution of silver nanoparticles in a physical mixture with platinum nanoparticles based on the sacrificial anode effect. Nanotechnology 31, 055703.

Chen, J., Sun, L., Cheng, Y., Lu, Z., Shao, K., Li, T., Hu, C., Han, H., 2016. Graphene oxide-silver nanocomposite: Novel agricultural antifungal agent against *Fusarium graminearum* for crop disease prevention. ACS Appl. Mater. Interfaces 8, 24057–24070.

Chen, X., Wilke, C.M., Gaillard, J.-F., Gray, K.A., 2020. Combined toxicity of nano-CuO/nano-TiO_2 and $CuSO_4$/nano-TiO_2 on *Escherichia coli* in aquatic environments under dark and light conditions. NanoImpact 19, 100250.

Choi, O., Hu, Z., 2009. Role of reactive oxygen species in determining nitrification inhibition by metallic/oxide nanoparticles. J. Environ. Eng. 135, 1365–1370.

Da Silva, G.H., Clemente, Z., Khan, L.U., Coa, F., Neto, L.L.R., Carvalho, H.W.P., Castro, V.L., Martinez, D.S.T., Monteiro, R.T.R., 2018. Toxicity assessment of TiO_2-MWCNT nanohybrid material with enhanced photocatalytic activity on *Danio rerio* (Zebrafish) embryos. Ecotoxicol. Environ. Saf. 165, 136–143.

Dabour, K., Al Naggar, Y., Masry, S., Naiem, E., Giesy, J.P., 2019. Cellular alterations in midgut cells of honey bee workers (*Apis millefera* L.) exposed to sublethal concentrations of CdO or PbO nanoparticles or their binary mixture. Sci. Total Environ. 651, 1356–1367.

Das, S., Thiagarajan, V., Chandrasekaran, N., Ravindran, B., Mukherjee, A., 2022. Nanoplastics enhance the toxic effects of titanium dioxide nanoparticle in freshwater algae *Scenedesmus obliquus*. Comp. Biochem. Phys. C 256, 109305.

de Medeiros, A.M.Z., Khan, L.U., da Silva, G.H., Ospina, C.A., Alves, O.L., de Castro, V.L., Martinez, D.S.T., 2021. Graphene oxide-silver nanoparticle hybrid material: An integrated nanosafety study in zebrafish embryos. Ecotoxicol. Environ. Saf. 209, 111776.

Estrela, F.N., Batista Guimarães, A.T., Silva, F.G., Marinho da Luz, T., Silva, A.M., Pereira, P.S., Malafaia, G., 2021. Effects of polystyrene nanoplastics on *Ctenopharyngodon idella* (grass carp) after individual and combined exposure with zinc oxide nanoparticles. J. Hazard. Mater. 403, 123879.

Fang, R., Gong, J., Cao, W., Chen, Z., Huang, D., Ye, J., Cai, Z., 2022. The combined toxicity and mechanism of multi-walled carbon nanotubes and nano copper oxide toward freshwater algae: *Tetradesmus obliquus*. J. Environ. Sci. 112, 376–387.

Fasil, D.M., Hamdi, H., Al-Barty, A., Zaid, A.A., Parashar, S.K.S., Das, B., 2021. Selenium and zinc oxide multinutrient supplementation enhanced growth performance in zebra fish by modulating oxidative stress and growth-related gene expression. Front. Bioeng. Biotechnol. 9, 721717.

Haghighat, F., Kim, Y., Sourinejad, I., Yu, I.J., Johari, S.A., 2021. Titanium dioxide nanoparticles affect the toxicity of silver nanoparticles in common carp (*Cyprinus carpio*). Chemosphere 262, 127805.

Hassanein, A., Keller, E., Lansing, S., 2021. Effect of metal nanoparticles in anaerobic digestion production and plant uptake from effluent fertilizer. Bioresour. Technol. 321, 124455.

Hernández-Moreno, D., Li, L., Connolly, M., Conde, E., Fernández, M., Schuster, M., Navas, J.M., Fernández-Cruz, M.-L., 2016. Mechanisms underlying the enhancement of toxicity caused by the coincubation of zinc oxide and copper nanoparticles in a fish hepatoma cell line. Environ. Toxicol. Chem. 35, 2562–2570.

Hernández-Moreno, D., Valdehita, A., Conde, E., Rucandio, I., Navas, J.M., Fernández-Cruz, M.L., 2019. Acute toxic effects caused by the co-exposure of nanoparticles of ZnO and Cu in rainbow trout. Sci. Total Environ. 687, 24–33.

Hong, M., Gong, J.-L., Cao, W.-C., Fang, R., Cai, Z., Ye, J., Chen, Z.-P., Tang, W.-W., 2022. The combined toxicity and mechanism of multi-walled carbon nanotubes and nano zinc oxide toward the cabbage. Environ. Sci. Pollut. Res. 29, 3540–3554.

Hua, J., Peijnenburg, W.J.G.M., Vijver, M.G., 2016. TiO_2 nanoparticles reduce the effects of ZnO nanoparticles and Zn ions on zebrafish embryos (*Danio rerio*).

NanoImpact 2, 45–53.

Huang, B., Wei, Z.-B., Yang, L.-Y., Pan, K., Miao, A.-J., 2019. Combined toxicity of silver nanoparticles with hematite or plastic nanoparticles toward two freshwater algae. Environ. Sci. Technol. 53, 3871–3879.

Iswarya, V., Bhuvaneshwari, M., Alex, S.A., Iyer, S., Chaudhuri, G., Chandrasekaran, P.T., Bhalerao, G.M., Chakravarty, S., Raichur, A.M., Chandrasekaran, N., Mukherjee, A., 2015. Combined toxicity of two crystalline phases (anatase and rutile) of Titania nanoparticles towards freshwater microalgae: *Chlorella* sp. Aquat. Toxicol. 161, 154–169.

Iswarya, V., Bhuvaneshwari, M., Chandrasekaran, N., Mukherjee, A., 2016. Individual and binary toxicity of anatase and rutile nanoparticles towards *Ceriodaphnia dubia*. Aquat. Toxicol. 178, 209–221.

Iswarya, V., Bhuvaneshwari, M., Chandrasekaran, N., Mukherjee, A., 2018. Trophic transfer potential of two different crystalline phases of TiO_2 NPs from *Chlorella* sp. to *Ceriodaphnia dubia*. Aquat. Toxicol. 197, 89–97.

Iswarya, V., Palanivel, A., Chandrasekaran, N., Mukherjee, A., 2019. Toxic effect of different types of titanium dioxide nanoparticles on *Ceriodaphnia dubia* in a freshwater system. Environ. Sci. Pollut. Res. 26, 11998–12013.

Jahan, S., Alias, Y.B., Bakar, A.F.B.A., Yusoff, I.B., 2018. Toxicity evaluation of ZnO and TiO_2 nanomaterials in hydroponic red bean (*Vigna angularis*) plant: Physiology, biochemistry and kinetic transport. J. Environ. Sci. 72, 140–152.

Jośko, I., Oleszczuk, P., Skwarek, E., 2017. Toxicity of combined mixtures of nanoparticles to plants. J. Hazard. Mater. 331, 200–209.

Jośko, I., Kusiak, M., Xing, B., Oleszczuk, P., 2021. Combined effect of nano-CuO and nano-ZnO in plant-related system: From bioavailability in soil to transcriptional regulation of metal homeostasis in barley. J. Hazard. Mater. 416, 126230.

Jośko, I., Krasucka, P., Skwarek, E., Oleszczuk, P., Sheteiwy, M., 2022. The co-occurrence of Zn-and Cu-based engineered nanoparticles in soils: The metal extractability vs. toxicity to *Folsomia candida*. Chemosphere 287, 132252.

Jung, E.S., Sivakumar, S., Hong, S.-C., Yi, P.-I., Jang, S.-H., Suh, J.-M., 2020. Influence of relative humidity on germination and metal accumulation in *Vigna radiata* exposed to metal-based nanoparticles. Sustainability 12, 1347.

Kaur, J., Khatri, M., Puri, S., 2019. Toxicological evaluation of metal oxide nanoparticles and mixed exposures at low doses using zebra fish and THP1 cell line. Environ. Toxicol. 34, 375–387.

Kong, I.C., Ko, K.-S., Koh, D.-C., 2021. Comparisons of the effect of different metal oxide nanoparticles on the root and shoot growth under shaking and non-shaking incubation, different plants, and binary mixture conditions. Nanomaterials 11, 1653.

Li, S., Chang, R., Chen, J., Mi, G., Xie, Z., Webster, T.J., 2020. Novel magnetic nanocomposites combining selenium and iron oxide with excellent anti-biofilm properties. J. Mater. Sci. 55, 1012–1022.

Liu, Y., Baas, J., Peijnenburg, W.J.G.M., Vijver, M.G., 2016. Evaluating the combined toxicity of Cu and ZnO nanoparticles: Utility of the concept of additivity and a nested experimental design. Environ. Sci. Technol. 50, 5328–5337.

Liu, Y., Wang, S., Wang, Z., Ye, N., Fang, H., Wang, D., 2018. TiO_2, SiO_2 and ZrO_2 nanoparticles synergistically provoke cellular oxidative damage in freshwater microalgae. Nanomaterials 8, 95.

Lopes, S., Pinheiro, C., Soares, A.M.V.M., Loureiro, S., 2016. Joint toxicity prediction of nanoparticles and ionic counterparts: Simulating toxicity under a fate scenario. J. Hazard. Mater. 320, 1–9.

Lozovskis, P., Jankauskaitė, V., Guobienė, A., Kareivienė, V., Vitkauskienė, A., 2020. Effect of graphene oxide and silver nanoparticles hybrid composite on *P. aeruginosa* strains with acquired resistance genes. Int. J. Nanomedicine 15, 5147–5163.

Lu, G., Yang, H., Xia, J., Zong, Y., Liu, J., 2017. Toxicity of Cu and Cr Nanoparticles to *Daphnia magna*. Water Air Soil Pollut. 228, 18.

Malatjie, T.S., Botha, T.L., Kuvarega, A.T., Madima, N., de Bruyn, K., Tekere, M., Nkambule, T.T.I., Mamba, B.B., Msagati, T.A.M., 2022. Toxicity evaluation of TiO_2/MWCNT-CNF hybrid nanocomposites with enhanced photocatalytic activity toward freshwater microalgae: *Pseudokirchneriella subcapitata*. Chemosphere 291, 132891.

Mansouri, B., Maleki, A., Johari, S.A., Shahmoradi, B., Mohammadi, E., Shahsavari, S., Davari, B., 2016. Copper bioaccumulation and depuration in common carp (*Cyprinus carpio*) following co-exposure to TiO_2 and CuO Nanoparticles. Arch. Environ. Contam. Toxicol. 71, 541–552.

Mansouri, B., Maleki, A., Johari, S.A., Shahmoradi, B., Mohammadi, E., Davari, B., 2017. Histopathological effects of copper oxide nanoparticles on the gill and intestine of common carp (*Cyprinus carpio*) in the presence of titanium dioxide nanoparticles. Chem. Ecol. 33, 295–308.

Mantecca, P., Moschini, E., Bonfanti, P., Fascio, U., Perelshtein, I., Lipovsky, A.,

Chirico, G., Bacchetta, R., Del Giacco, L., Colombo, A., Gedanken, A., 2015. Toxicity evaluation of a new Zn-doped CuO nanocomposite with highly effective antibacterial properties. Toxicol. Sci. 146, 16–30.

Marcone, G.P.S., Oliveira, Á.C., Almeida, G., Umbuzeiro, G.A., Jardim, W.F., 2012. Ecotoxicity of TiO_2 to *Daphnia similis* under irradiation. J. Hazard. Mater. 211–212, 436–442.

Marta, B., Potara, M., Iliut, M., Jakab, E., Radu, T., Imre-Lucaci, F., Katona, G., Popescu, O., Astilean, S., 2015. Designing chitosan–silver nanoparticles–graphene oxide nanohybrids with enhanced antibacterial activity against *Staphylococcus aureus*. Colloid. Surface. A 487, 113–120.

Miranda, R.R., Damaso da Silveira, A.L.R., de Jesus, I.P., Grötzner, S.R., Voigt, C.L., Campos, S.X., Garcia, J.R.E., Randi, M.A.F., Ribeiro, C.A.O., Filipak Neto, F., 2016. Effects of realistic concentrations of TiO_2 and ZnO nanoparticles in *Prochilodus lineatus* juvenile fish. Environ. Sci. Pollut. Res. 23, 5179–5188.

Mocanu, A., Rusen, E., Diacon, A., Isopencu, G., Mustăţea, G., Şomoghi, R., Dinescu, A., 2019. Antimicrobial properties of polysulfone membranes modified with carbon nanofibers and silver nanoparticles. Mater. Chem. Phys. 223, 39–45.

Mohammed, M.K.A., Ahmed, D.S., Mohammad, M.R., 2019. Studying antimicrobial activity of carbon nanotubes decorated with metal-doped ZnO hybrid materials. Mater. Res. Express 6, 055404.

Muccifora, S., Castillo-Michel, H., Barbieri, F., Bellani, L., Ruffini Castiglione, M., Spanò, C., Pradas del Real, A.E., Giorgetti, L., Tassi, E.L., 2021. Synchrotron radiation spectroscopy and transmission electron microscopy techniques to evaluate TiO_2 NPs incorporation, speciation, and impact on root cells ultrastructure of *Pisum sativum* L. plants. Nanomaterials 11, 921.

Naeem, H., Ajmal, M., Qureshi, R.B., Muntha, S.T., Farooq, M., Siddiq, M., 2019. Facile synthesis of graphene oxide–silver nanocomposite for decontamination of water from multiple pollutants by adsorption, catalysis and antibacterial activity. J. Environ. Manage. 230, 199–211.

Natarajan, L., Jenifer, M.A., Chandrasekaran, N., Suraishkumar, G.K., Mukherjee, A., 2022. Polystyrene nanoplastics diminish the toxic effects of Nano-TiO_2 in marine algae *Chlorella* sp. Environ. Res. 204, 112400.

Ogunsuyi, O.I., Fadoju, O.M., Akanni, O.O., Alabi, O.A., Alimba, C.G., Cambier, S., Eswara, S., Gutleb, A.C., Adaramoye, O.A., Bakare, A.A., 2019. Genetic and systemic toxicity induced by silver and copper oxide nanoparticles, and their mixture in *Clarias gariepinus* (Burchell, 1822). Environ. Sci. Pollut. Res. 26,

27470–27481.

Pikula, K., Johari, S.A., Santos-Oliveira, R., Golokhvast, K., 2022. Individual and binary mixture toxicity of five nanoparticles in marine microalga *Heterosigma akashiwo*. Int. J. Mol. Sci. 23, 990.

Sayadi, M.H., Pavlaki, M.D., Martins, R., Mansouri, B., Tyler, C.R., Kharkan, J., Shekari, H., 2021. Bioaccumulation and toxicokinetics of zinc oxide nanoparticles (ZnO NPs) co-exposed with graphene nanosheets (GNs) in the blackfish (*Capoeta fusca*). Chemosphere 269, 128689.

Sayadi, M.H., Pavlaki, M.D., Loureiro, S., Martins, R., Tyler, C.R., Mansouri, B., Kharkan, J., Shekari, H., 2022. Co-exposure of zinc oxide nanoparticles and multi-layer graphenes in blackfish (*Capoeta fusca*): Evaluation of lethal, behavioural, and histopathological effects. Ecotoxicology 31, 425–439.

Selim, M.S., Samak, N.A., Hao, Z., Xing, J., 2020. Facile design of reduced graphene oxide decorated with Cu_2O nanocube composite as antibiofilm active material. Mater. Chem. Phys. 239, 122300.

Sellami, B., Mezni, A., Khazri, A., Bouzidi, I., Saidani, W., Sheehan, D., Beyrem, H., 2017. Toxicity assessment of ZnO-decorated Au nanoparticles in the Mediterranean clam *Ruditapes decussatus*. Aquat. Toxicol. 188, 10–19.

Seo, Y., Hwang, J., Kim, J., Jeong, Y., Hwang, M.P, Choi, J., 2014. Antibacterial activity and cytotoxicity of multi-walled carbon nanotubes decorated with silver nanoparticles. Int. J. Nanomedicine 9, 4621–4629.

Singh, D., Kumar, A., 2016. Impact of irrigation using water containing CuO and ZnO nanoparticles on *Spinach oleracea* grown in soil media. Bull. Environ. Contam. Toxicol. 97, 548–553.

Singh, D., Kumar, A., 2018. Investigating long-term effect of nanoparticles on growth of *Raphanus sativus* plants: A trans-generational study. Ecotoxicology 27, 23–31.

Singh, D., Kumar, A., 2019. Assessment of toxic interaction of nano zinc oxide and nano copper oxide on germination of *Raphanus sativus* seeds. Environ. Monit. Assess. 191, 703.

Singh, D., Kumar, A., 2020a. Quantification of metal uptake in *Spinacia oleracea* irrigated with water containing a mixture of CuO and ZnO nanoparticles. Chemosphere 243, 125239.

Singh, D., Kumar, A., 2020b. Binary mixture of nanoparticles in sewage sludge: Impact on spinach growth. Chemosphere 254, 126794.

Skiba, E., Pietrzak, M., Glińska, S., Wolf, W.M., 2021. The combined effect of ZnO and CeO_2 nanoparticles on *Pisum sativum* L.: A photosynthesis and nutrients uptake study. Cells 10, 3105.

Srivastava, S., Kumar, A., 2017. Comparative cytotoxicity of nanoparticles and ions to *Escherichia coli* in binary mixtures. J. Environ. Sci. 55, 11–19.

Subpiramaniyam, S., Hong, S.-C., Yi, P.-I., Jang, S.-H., Suh, J.-M., Jung, E.-S., Park, J.-S., Cho, L.-H., 2021. Influence of sawdust addition on the toxic effects of cadmium and copper oxide nanoparticles on *Vigna radiata* seeds. Environ. Pollut. 289, 117311.

Tong, T., Wilke, C.M., Wu, J., Binh, C.T.T., Kelly, J.J., Gaillard, J.-F., Gray, K.A., 2015. Combined toxicity of nano-ZnO and nano-TiO_2: From single- to multinanomaterial systems. Environ. Sci. Technol. 49, 8113–8123.

Wang, Z., Jin, S., Zhang, F., Wang, D., 2020. Combined toxicity of TiO_2 nanospherical particles and TiO_2 nanotubes to two microalgae with different morphology. Nanomaterials 10, 2559.

Wang, Z., Zhang, F., Vijver, M.G., Peijnenburg, W.J.G.M., 2021. Graphene nanoplatelets and reduced graphene oxide elevate the microalgal cytotoxicity of nano-zirconium oxide. Chemosphere 276, 130015.

Wilke, C.M., Tong, T., Gaillard, J.-F., Gray, K.A., 2016. Attenuation of microbial stress due to nano-Ag and nano-TiO_2 interactions under dark conditions. Environ. Sci. Technol. 50, 11302–11310.

Wilke, C.M., Wunderlich, B., Gaillard, J.-F., Gray, K.A., 2018. Synergistic bacterial stress results from exposure to nano-Ag and nano-TiO_2 mixtures under light in environmental media. Environ. Sci. Technol. 52, 3185–3194.

Xia, J., Zhao, H.Z., Lu, G.H., 2013. Effects of selected metal oxide nanoparticles on multiple biomarkers in *Carassius auratus*. Biomed. Environ. Sci. 26, 742–749.

Yang, L., Yan, W., Wang, H., Zhuang, H., Zhang, J., 2017. Shell thickness-dependent antibacterial activity and biocompatibility of gold@silver core–shell nanoparticles. RSC Adv. 7, 11355–11361.

Yang, Q., Zhang, L., Ben, A., Wu, N., Yi, Y., Jiang, L., Huang, H., Yu, Y., 2018. Effects of dispersible MoS_2 nanosheets and nano-silver coexistence on the metabolome of yeast. Chemosphere 198, 216–225.

Ye, N., Wang, Z., Fang, H., Wang, S., Zhang, F., 2017. Combined ecotoxicity of binary zinc oxide and copper oxide nanoparticles to *Scenedesmus obliquus*. J. Environ. Sci. Heal. A 52, 555–560.

Ye, N., Wang, Z., Wang, S., Peijnenburg, W.J.G.M., 2018. Toxicity of mixtures of zinc oxide and graphene oxide nanoparticles to aquatic organisms of different trophic level: Particles outperform dissolved ions. Nanotoxicology 12, 423–438.

Yin, J., Huang, G., An, C., Feng, R., 2022. Nanocellulose enhances the dispersion and toxicity of ZnO NPs to green algae *Eremosphaera viridis*. Environ. Sci.: Nano 9, 393–405.

Yu, Q., Wang, Z., Wang, G., Peijnenburg, W.J.G.M., Vijver, M.G., 2022. Effects of natural organic matter on the joint toxicity and accumulation of Cu nanoparticles and ZnO nanoparticles in *Daphnia magna*. Environ. Pollut. 292, 118413.

Yu, R., Wu, J., Liu, M., Zhu, G., Chen, L., Chang, Y., Lu, H., 2016a. Toxicity of binary mixtures of metal oxide nanoparticles to *Nitrosomonas europaea*. Chemosphere 153, 187–197.

Yu, R., Wu, J., Liu, M., Chen, L., Zhu, G., Lu, H., 2016b. Physiological and transcriptional responses of *Nitrosomonas europaea* to TiO_2 and ZnO nanoparticles and their mixtures. Environ. Sci. Pollut. Res. 23, 13023–13034.

Zain, N.M., Stapley, A.G.F., Shama, G., 2014. Green synthesis of silver and copper nanoparticles using ascorbic acid and chitosan for antimicrobial applications. Carbohyd. Polym. 112, 195–202.

Zhang, H., Shi, J., Su, Y., Li, W., Wilkinson, K.J., Xie, B., 2020. Acute toxicity evaluation of nanoparticles mixtures using luminescent bacteria. Environ. Monit. Assess. 192, 484.

Zhang, Y., Li, X., Liang, J., Luo, Y., Tang, N., Ye, S., Zhu, Z., Xing, W., Guo, J., Zhang, H., 2022. *Microcystis aeruginosa*'s exposure to an antagonism of nanoplastics and MWCNTs: The disorders in cellular and metabolic processes. Chemosphere 288, 132516.

Zhao, H-Z., Lu, G-H., Xia, J., Jin, S-G., 2012. Toxicity of nanoscale CuO and ZnO to *Daphnia magna*. Chem. Res. Chin. Univ. 28, 209–213.

Zhao, J., Dai, Y., Wang, Z., Ren, W., Wei, Y., Cao, X., Xing, B., 2018. Toxicity of GO to freshwater algae in the presence of Al_2O_3 particles with different morphologies: Importance of heteroaggregation. Environ. Sci. Technol. 52, 13448–13456.

Zhu, X., Tan, L., Zhao, T., Huang, W., Guo, X., Wang, J., Wang, J., 2022. Alone and combined toxicity of ZnO nanoparticles and graphene quantum dots on microalgae *Gymnodinium*. Environ. Sci. Pollut. Res. 29, 47310–47322.

Zhu, Z., Su, M., Ma, L., Ma, L., Liu, D., Wang, Z., 2013. Preparation of graphene

oxide–silver nanoparticle nanohybrids with highly antibacterial capability. Talanta 117, 449–455.

Supplementary information for Chapter 6

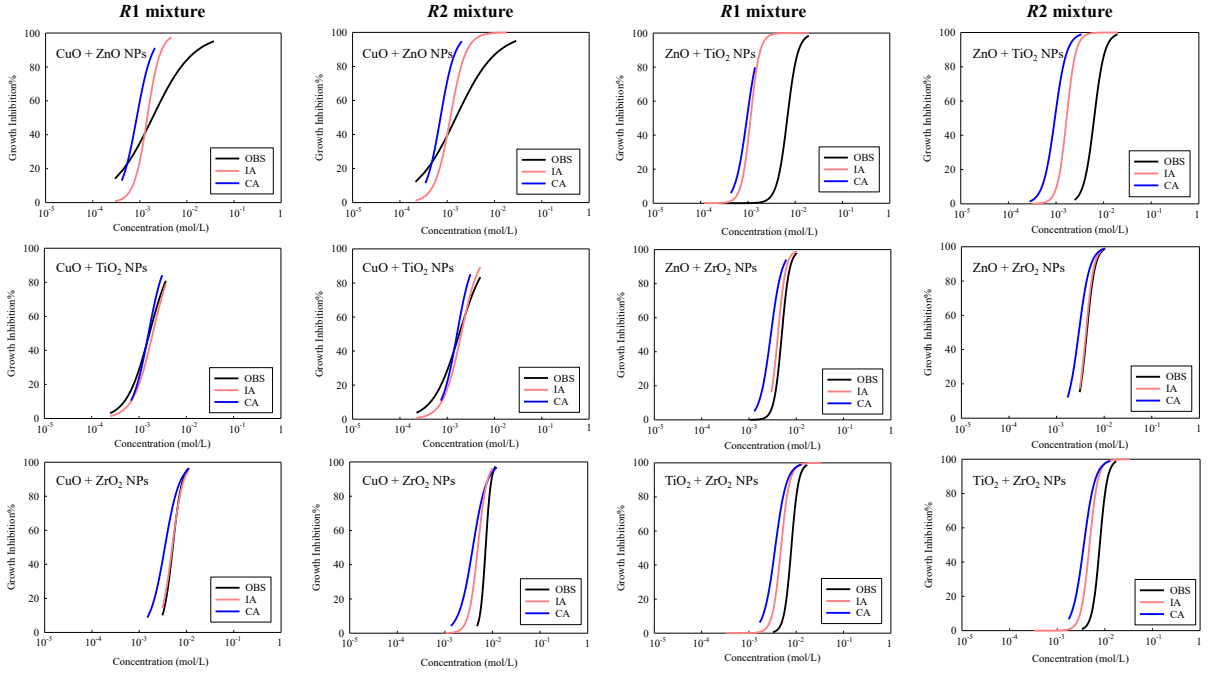

Figure S6.1. *Comparison between observed and predicted concentration-response curves for Escherichia coli exposed to the binary mixtures of CuO, ZnO, TiO_2, and ZrO_2 NPs at two different mixture ratios. OBS stands for observation. IA and CA represent independent action model and concentration addition model, respectively.*

Table S6.1. *Single descriptors of the MO_X NPs studied* [a].

MO_X NPs	Periodictable-based descriptors		Experimental descriptors		Metal oxide energy descriptors			Ionic index
	χ_{me}	$\Sigma\chi_{me/nO}$	ζP	D_H	ΔH_{me+}	ΔH_{sf}	E_C	Z^2/r
			mV	nm	kcal/mol	eV	eV	pm^{-2}
Al_2O_3 NPs	1.61	1.073	30.3	330	1,187.83	-17.345	-1.515	0.1667
CuO NPs	1.90	1.900	-15.1	201	706.25	-1.609	-5.174	0.0548
Fe_2O_3 NPs	1.83	1.220	-6.3	> 6000	1,408.29	-8.512	-4.993	0.1636
SiO_2 NPs	1.90	0.950	-29.8	1230	1,686.38	-9.410	-2.018	0.6154
TiO_2 NPs	1.54	0.770	-14.1/-10.7	383/748	1,575.73	-9.779	-4.161	0.2623
ZnO NPs	1.65	1.650	-16.6/-20.9	373/1614	662.44	-3.608	-3.891	0.0667
ZrO_2 NPs	1.33	0.665	-16.4	262	1,357.66	-11.252	-3.192	0.1905

[a] *χ_{me} — metal electronegativity, $\Sigma\chi_{me/nO}$ — sum of metal electronegativity for individual metal oxide divided by the number of oxygen atoms present in a particular metal oxide, ζP — zeta potential, D_H — hydrodynamic diameters, ΔH_{me+} — enthalpy of formation of a gaseous cation, ΔH_{sf} — metal oxide standard molar enthalpy of formation, E_C — nanoparticle energy of conduction band, and Z^2/r — ionic index of metal cation.*

Table S6.2. *Mixture descriptors of binary mixtures of MO_X NPs studied* [a].

Mixture system of MO_X NPs	Mixture descriptors							
	χ_{me}	$\Sigma\chi_{me/nO}$	ζP	D_H	ΔH_{me+}	ΔH_{sf}	E_C	Z^2/r
			mV	nm	kcal/mol			pm^{-2}
Int (*R*1)								
CuO + ZnO NPs	1.85	1.854	-15.3	232	698.225	-45.548	-113.896	0.0570
TiO_2 + ZrO_2 NPs	1.37	0.684	-16.0	285	1398.092	-253.179	-77.752	0.2038
ZnO + TiO_2 NPs	1.56	0.917	-14.5	382	1423.106	-231.185	-94.914	0.2296
ZnO + ZrO_2 NPs	1.34	0.708	-16.4	267	1327.297	-259.477	-74.313	0.1851
CuO + TiO_2 NPs	1.71	1.304	-14.6	297	1165.134	-136.538	-106.986	0.1643
CuO + ZrO_2 NPs	1.43	0.874	-16.2	252	1247.443	-221.852	-81.342	0.1675
Int (*R*2)								
CuO + ZnO NPs	1.83	1.833	-15.5	247	694.561	-49.404	-111.421	0.0580
TiO_2 + ZrO_2 NPs	1.37	0.684	-16.0	284	1396.568	-253.416	-77.596	0.2033
ZnO + TiO_2 NPs	1.56	0.920	-14.5	381	1420.099	-231.297	-94.894	0.2290
ZnO + ZrO_2 NPs	1.34	0.707	-16.4	267	1327.972	-259.477	-74.297	0.1852
CuO + TiO_2 NPs	1.67	1.178	-14.5	317	1262.020	-157.532	-104.383	0.1874
CuO + ZrO_2 NPs	1.39	0.800	-16.3	256	1286.528	-235.194	-78.600	0.1757
Ext (*R*3)								
Al_2O_3 + ZnO NPs	1.64	1.442	-2.4	1150	852.141	-8.568	-3.033	0.1028
Al_2O_3 + Fe_2O_3 NPs	1.72	1.147	11.8	3189	1299.010	-12.890	-3.269	0.1651
Al_2O_3 + SiO_2 NPs	1.74	1.016	2.4	747	1419.092	-13.664	-1.748	0.3748
Al_2O_3 + TiO_2 NPs	1.58	0.934	11.4	522	1366.300	-13.864	-2.732	0.2107
ZnO + Fe_2O_3 NPs	1.72	1.493	-15.6	3215	934.716	-5.398	-4.293	0.1021
ZnO + SiO_2 NPs	1.73	1.420	-23.8	1488	998.684	-5.513	-3.276	0.2469
Fe_2O_3 + SiO_2 NPs	1.86	1.096	-17.1	3808	1536.096	-8.925	-3.626	0.3712
Fe_2O_3 + TiO_2 NPs	1.70	1.015	-8.3	3606	1484.611	-9.090	-4.614	0.2086
SiO_2 + TiO_2 NPs	1.72	0.861	-20.3	991	1631.475	-9.593	-3.081	0.4402
ZnO + TiO_2 NPs	1.61	1.364	-17.6	1333	959.297	-5.614	-3.979	0.1303

[a] *The descriptors of the mixtures of MO_X NPs were derived from the descriptors of the individual MO_X NPs based on Equation 6.4, as shown in the main text.*

Table S6.3. *Performance of SVM-based QSAR models.*

Models	Internal dataset									Combined dataset								
	training					test				training					test			
	R^2	R^2_{adj}	RMSE	MAE		R^2	R^2_{adj}	RMSE	MAE	R^2	R^2_{adj}	RMSE	MAE		R^2	R^2_{adj}	RMSE	MAE
S1	0.838	0.757	0.096	0.093		0.875	0.813	0.108	0.086	0.097	-0.053	0.782	0.536		-0.133	-0.322	0.896	0.566
S2	0.848	0.772	0.093	0.087		0.853	0.780	0.117	0.099	0.881	0.861	0.284	0.240		0.695	0.644	0.465	0.310
S3	0.360	0.040	0.191	0.155		0.237	-0.145	0.266	0.220	0.375	0.271	0.650	0.469		-0.467	-0.712	1.020	0.746
S4	0.667	0.501	0.138	0.133		0.006	-0.491	0.304	0.263	0.343	0.234	0.666	0.555		0.389	0.287	0.658	0.537
S5	0.532	0.298	0.163	0.120		0.596	0.394	0.194	0.157	0.929	0.917	0.219	0.191		0.885	0.866	0.285	0.223
S6	0.900	0.850	0.076	0.055		0.895	0.843	0.099	0.090	0.555	0.481	0.549	0.335		0.734	0.690	0.434	0.321
S7	0.869	0.804	0.087	0.082		0.923	0.885	0.085	0.073	-0.146	-0.337	0.880	0.494		-0.119	-0.306	0.890	0.534
S8	0.376	0.064	0.189	0.131		0.338	0.007	0.248	0.187	0.408	0.309	0.633	0.436		0.399	0.299	0.653	0.427
S9	0.868	0.815	0.087	0.084		0.869	0.607	0.110	0.084	0.862	0.837	0.305	0.228		0.659	0.523	0.491	0.317
S10	0.884	0.838	0.081	0.081		0.863	0.589	0.113	0.081	0.323	0.200	0.676	0.441		-0.167	-0.634	0.909	0.608
S11	0.886	0.840	0.081	0.074		0.916	0.748	0.088	0.077	0.295	0.167	0.690	0.486		0.170	-0.162	0.767	0.516
S12	0.935	0.909	0.061	0.050		0.926	0.778	0.083	0.072	0.940	0.929	0.202	0.148		0.809	0.733	0.368	0.277
S13	0.882	0.835	0.082	0.078		0.870	0.610	0.110	0.092	0.601	0.528	0.519	0.330		0.608	0.451	0.527	0.380
S14	0.851	0.791	0.092	0.090		0.888	0.664	0.102	0.085	-0.092	-0.291	0.859	0.459		0.054	-0.324	0.819	0.479
S15	0.938	0.913	0.059	0.043		0.933	0.799	0.079	0.069	0.471	0.375	0.598	0.372		0.400	0.160	0.652	0.388
S16	0.905	0.867	0.074	0.073		0.891	0.673	0.101	0.075	0.822	0.790	0.347	0.273		0.580	0.412	0.545	0.359
S17	0.868	0.815	0.087	0.070		0.880	0.640	0.105	0.088	0.905	0.888	0.253	0.215		0.792	0.709	0.383	0.286
S18	0.881	0.833	0.082	0.046		0.859	0.577	0.114	0.100	0.955	0.947	0.175	0.156		0.855	0.797	0.320	0.239
S19	0.889	0.845	0.080	0.071		0.882	0.646	0.105	0.092	0.848	0.820	0.321	0.254		0.743	0.640	0.427	0.282
S20	0.892	0.849	0.078	0.077		0.894	0.682	0.099	0.075	0.907	0.890	0.251	0.221		0.516	0.322	0.585	0.433
S21	0.892	0.849	0.079	0.049		0.892	0.676	0.100	0.088	0.807	0.772	0.362	0.280		0.653	0.514	0.496	0.337
S22	0.888	0.843	0.080	0.073		0.746	0.238	0.153	0.111	0.420	0.315	0.626	0.489		0.094	-0.268	0.801	0.603
S23	0.888	0.843	0.080	0.080		0.881	0.643	0.105	0.078	0.874	0.851	0.292	0.236		0.785	0.699	0.390	0.268
S24	0.944	0.922	0.057	0.051		0.927	0.781	0.082	0.056	0.701	0.647	0.450	0.302		0.411	0.175	0.646	0.433

S25	0.886	0.840	0.081	0.080		0.837	0.511	0.123	0.091		0.171	0.020	0.749	0.426		-0.012	-0.417	0.847	0.514
S26	0.901	0.861	0.075	0.074		0.891	0.673	0.101	0.070		0.490	0.397	0.587	0.393		0.244	-0.058	0.732	0.453
S27	0.807	0.730	0.105	0.098		0.789	0.367	0.140	0.125		0.949	0.940	0.186	0.158		0.892	0.849	0.277	0.214
S28	0.881	0.833	0.082	0.072		0.892	0.676	0.100	0.089		0.728	0.679	0.429	0.287		0.812	0.737	0.365	0.292
S29	0.904	0.866	0.074	0.071		0.933	0.799	0.079	0.068		0.311	0.186	0.682	0.418		0.046	-0.336	0.822	0.569
S30	0.785	0.699	0.111	0.100		0.699	0.097	0.167	0.150		0.523	0.436	0.568	0.448		0.579	0.411	0.546	0.396
S31	0.873	0.822	0.085	0.051		0.878	0.634	0.106	0.087		0.920	0.905	0.233	0.196		0.835	0.769	0.342	0.222
S32	0.948	0.927	0.055	0.050		0.934	0.802	0.078	0.057		0.944	0.934	0.195	0.191		0.663	0.528	0.489	0.377
S33	0.558	0.381	0.159	0.115		0.594	-0.218	0.194	0.152		0.894	0.875	0.268	0.227		0.807	0.730	0.370	0.278
S34	0.893	0.850	0.078	0.076		0.881	0.643	0.105	0.086		0.657	0.595	0.482	0.324		0.568	0.395	0.553	0.399
S35	0.893	0.850	0.078	0.046		0.901	0.703	0.096	0.079		0.678	0.619	0.467	0.311		0.601	0.441	0.532	0.363
S36	0.953	0.934	0.052	0.043		0.944	0.832	0.072	0.056		0.206	0.062	0.733	0.408		0.323	0.052	0.693	0.443

Table S6.4. *Performance of NN-based QSAR models.*

Models	Internal dataset									Combined dataset								
	training					test				training					test			
	R^2	R^2_{adj}	RMSE	MAE		R^2	R^2_{adj}	RMSE	MAE	R^2	R^2_{adj}	RMSE	MAE		R^2	R^2_{adj}	RMSE	MAE
N1	0.999	0.999	0.009	0.006		0.904	0.856	0.095	0.076	0.472	0.384	0.598	0.429		0.089	-0.063	0.804	0.646
N2	0.893	0.840	0.078	0.058		0.906	0.859	0.094	0.092	0.972	0.967	0.136	0.087		0.730	0.685	0.438	0.339
N3	0.994	0.991	0.019	0.015		-0.316	-0.974	0.349	0.210	0.742	0.699	0.418	0.241		-1.725	-2.179	1.390	0.985
N4	0.994	0.991	0.018	0.013		-0.789	-1.684	0.407	0.298	0.772	0.734	0.392	0.248		0.107	-0.042	0.795	0.523
N5	0.572	0.358	0.156	0.115		0.759	0.639	0.149	0.116	0.988	0.986	0.090	0.051		0.732	0.687	0.435	0.376
N6	0.999	0.999	0.009	0.005		0.941	0.912	0.074	0.064	0.972	0.967	0.138	0.088		0.798	0.764	0.379	0.230
N7	0.999	0.999	0.009	0.006		0.977	0.966	0.046	0.041	0.806	0.774	0.362	0.160		-1074.913	-1254.232	27.609	10.132
N8	0.993	0.990	0.020	0.015		0.326	-0.011	0.250	0.174	0.970	0.965	0.142	0.077		0.919	0.906	0.239	0.165
N9	0.999	0.999	0.006	0.003		0.942	0.826	0.073	0.064	0.988	0.986	0.091	0.047		0.723	0.612	0.443	0.287
N10	0.999	0.999	0.008	0.005		0.884	0.652	0.104	0.070	1.000	1.000	0.011	0.005		-3.702	-5.583	1.825	0.981
N11	0.999	0.999	0.008	0.004		0.814	0.442	0.131	0.106	0.817	0.784	0.351	0.162		0.856	0.798	0.319	0.238
N12	0.999	0.999	0.007	0.004		0.908	0.724	0.092	0.078	1.000	1.000	0.011	0.007		0.890	0.846	0.279	0.184
N13	0.999	0.999	0.009	0.005		0.973	0.919	0.050	0.040	0.998	0.998	0.036	0.028		-3.337	-5.072	1.753	0.975
N14	0.999	0.999	0.007	0.004		0.918	0.754	0.087	0.066	0.699	0.644	0.451	0.228		-38.970	-54.958	5.322	2.121
N15	0.999	0.999	0.008	0.004		0.968	0.904	0.054	0.040	0.987	0.985	0.093	0.044		0.131	-0.217	0.784	0.540
N16	0.999	0.999	0.007	0.004		0.913	0.739	0.090	0.070	0.997	0.996	0.048	0.026		0.296	0.014	0.706	0.521
N17	0.999	0.999	0.007	0.004		0.855	0.565	0.116	0.090	0.997	0.996	0.047	0.033		0.861	0.805	0.314	0.198
N18	0.999	0.999	0.006	0.003		0.845	0.535	0.120	0.099	1.000	1.000	0.010	0.006		0.822	0.751	0.355	0.229
N19	0.999	0.999	0.009	0.005		0.951	0.853	0.067	0.058	0.991	0.989	0.076	0.038		0.656	0.518	0.493	0.283
N20	0.999	0.999	0.007	0.004		0.921	0.763	0.086	0.072	1.000	1.000	0.007	0.004		0.732	0.625	0.436	0.315
N21	1.000	1.000	0.005	0.003		0.949	0.847	0.069	0.058	1.000	1.000	0.002	0.001		0.677	0.548	0.478	0.330
N22	0.981	0.973	0.033	0.023		0.711	0.133	0.164	0.108	0.996	0.995	0.055	0.032		-2.072	-3.301	1.475	0.970
N23	0.999	0.999	0.008	0.004		0.924	0.772	0.084	0.072	0.999	0.999	0.028	0.016		0.844	0.782	0.333	0.228
N24	0.999	0.999	0.009	0.006		0.907	0.721	0.093	0.064	1.000	1.000	0.018	0.010		0.489	0.285	0.602	0.450

N25	0.999	0.999	0.009	0.006		0.879	0.637	0.106	0.075		0.997	0.996	0.046	0.026		-2.924	-4.494	1.667	1.021
N26	0.999	0.999	0.008	0.004		0.915	0.745	0.089	0.062		0.999	0.999	0.031	0.017		-0.435	-1.009	1.008	0.707
N27	0.999	0.999	0.007	0.004		0.515	-0.455	0.212	0.166		0.999	0.999	0.027	0.017		0.922	0.891	0.235	0.162
N28	0.999	0.999	0.008	0.004		0.967	0.901	0.055	0.046		1.000	1.000	0.013	0.008		0.937	0.912	0.212	0.156
N29	0.999	0.999	0.008	0.005		0.900	0.700	0.096	0.070		0.717	0.666	0.437	0.223		0.057	-0.320	0.817	0.493
N30	0.999	0.999	0.006	0.004		0.604	-0.188	0.192	0.153		0.997	0.996	0.042	0.025		0.682	0.555	0.475	0.352
N31	0.999	0.999	0.009	0.005		0.911	0.733	0.091	0.067		1.000	1.000	0.016	0.009		0.908	0.871	0.255	0.181
N32	0.999	0.999	0.006	0.004		0.925	0.775	0.083	0.057		1.000	1.000	0.002	0.001		0.492	0.289	0.600	0.355
N33	0.956	0.938	0.050	0.031		0.934	0.802	0.079	0.053		1.000	1.000	0.011	0.007		0.698	0.577	0.463	0.356
N34	0.999	0.999	0.009	0.005		0.910	0.730	0.091	0.071		0.998	0.998	0.039	0.028		-7.440	-10.816	2.445	1.059
N35	0.999	0.999	0.009	0.005		0.953	0.859	0.066	0.054		1.000	1.000	0.002	0.001		-0.105	-0.547	0.885	0.599
N36	0.999	0.999	0.007	0.004		0.941	0.823	0.074	0.054		1.000	1.000	0.001	0.001		0.638	0.493	0.507	0.295

Table S6.5. *Y-randomization for the selected SVM-based models developed from the internal and the combined dataset.*

Iteration	Internal dataset				Combined dataset			
	S12		S31		S12		S31	
	$R^2_{raining}$	R^2_{test}	$R^2_{raining}$	R^2_{test}	$R^2_{raining}$	R^2_{test}	$R^2_{raining}$	R^2_{test}
1	0.672	0.164	0.463	-0.117	0.672	-0.333	0.431	0.126
2	0.638	-0.291	0.738	-0.385	0.160	-0.633	0.060	-0.949
3	0.104	-0.017	0.096	-0.022	0.011	-0.159	0.070	-0.165
4	0.714	-1.399	0.815	-1.741	0.187	-0.083	0.295	-0.119
5	0.455	-0.874	0.577	-1.055	0.468	0.041	0.262	-0.823
6	0.088	-0.844	0.074	-0.885	0.419	-0.208	0.336	-0.596
7	0.322	-0.480	0.151	-0.512	0.363	-0.940	0.197	-0.872
8	0.306	0.697	0.238	0.683	0.336	-0.003	0.444	0.150
9	0.054	-0.199	0.050	-0.208	0.093	-0.232	0.131	-0.221
10	0.076	-0.166	0.096	-0.128	0.449	-2.598	0.369	-2.118
$^{c}R^2_p$	0.744	1.083	0.689	1.075	0.766	1.035	0.780	1.079

Table S6.6. *Y-randomization for the selected NN-based models developed from the internal and the combined dataset.*

Iteration	Internal dataset		Combined dataset	
	N12	N31	N12	N31
	R^2_{test}	R^2_{test}	R^2_{test}	R^2_{test}
1	0.646	0.553	-2.803	-1.770
2	-2.332	-2.158	-2.727	-4.690
3	-1.214	-8.204	-1.383	-1.091
4	-3.254	-2.693	-2.234	-4.516
5	-2.196	-2.042	-5.742	-0.433
6	-3.697	-863.167	-0.457	-0.786
7	-5.346	-2.146	-12.719	-7.102
8	0.256	0.306	-0.003	-0.382
9	-136.149	0.075	-9.853	-0.741
10	-18.164	0.167	-6.736	-6.876
$^cR^2_p$	4.049	8.966	2.183	1.844

Table S6.7. *Percental difference between the experimental and predicted values for the internal dataset* [a].

Mixture system of MO_X NPs	ML-based QSAR models				Mixture models	
	S12	S31	N12	N31	IA	CA
Int (*R*1)						
CuO + ZnO NPs	1.47	0.74	0.00	0.00	4.78	12.13
TiO_2 + ZrO_2 NPs	1.90	1.43	0.00	0.00	10.48	16.19
ZnO + TiO_2 NPs	1.38	0.46	0.46	0.46	36.41	38.25
ZnO + ZrO_2 NPs	3.04	6.96	3.04	3.04	3.91	10.43
CuO + TiO_2 NPs	1.44	1.08	3.97	1.08	2.53	1.08
CuO + ZrO_2 NPs	1.75	0.87	0.00	0.00	0.44	7.42
Int (*R*2)						
CuO + ZnO NPs	4.96	4.26	4.61	5.67	3.55	11.70
TiO_2 + ZrO_2 NPs	1.42	0.95	0.00	0.47	9.95	15.64
ZnO + TiO_2 NPs	0.45	0.91	0.45	0.91	25.91	38.64
ZnO + ZrO_2 NPs	5.91	9.70	0.00	0.00	0.84	7.17
CuO + TiO_2 NPs	1.09	0.73	0.36	0.36	1.46	2.19
CuO + ZrO_2 NPs	3.27	1.87	0.00	0.47	7.94	12.62
Average value	**2.34**	**2.50**	**1.08**	**1.04**	**9.02**	**14.46**

[a] *% difference = (experimental value - predicted value) / experimental value ×100.*

Table S6.8. *Percental difference between the experimental and predicted values for the combined dataset* [a].

Mixture system of MO_X NPs	ML-based QSAR models			
	S12	S31	N12	N31
Int (*R*1)				
CuO + ZnO NPs	2.94	6.25	0.00	0.00
TiO_2 + ZrO_2 NPs	3.81	2.38	0.00	0.48
ZnO + TiO_2 NPs	11.52	3.69	1.84	0.46
ZnO + ZrO_2 NPs	3.48	7.39	0.00	0.00
CuO + TiO_2 NPs	1.81	6.14	0.00	0.00
CuO + ZrO_2 NPs	0.87	7.86	0.87	1.31
Int (*R*2)				
CuO + ZnO NPs	2.13	3.55	2.84	2.48
TiO_2 + ZrO_2 NPs	3.32	2.84	0.00	0.00
ZnO + TiO_2 NPs	12.73	4.55	0.45	0.91
ZnO + ZrO_2 NPs	6.33	10.13	2.95	2.95
CuO + TiO_2 NPs	17.15	5.84	25.18	8.76
CuO + ZrO_2 NPs	3.74	7.94	1.40	2.34
Ext (*R*3)				
Al_2O_3 + ZnO NPs	7.75	8.92	0.00	0.00
Al_2O_3 + Fe_2O_3 NPs	3.88	2.43	0.00	0.49
Al_2O_3 + SiO_2 NPs	8.77	8.19	9.94	9.94
Al_2O_3 + TiO_2 NPs	14.71	10.00	0.59	0.00
ZnO + Fe_2O_3 NPs	2.06	4.37	0.00	0.00
ZnO + SiO_2 NPs	12.35	13.56	0.00	0.00
Fe_2O_3 + SiO_2 NPs	3.56	7.56	0.00	0.00
Fe_2O_3 + TiO_2 NPs	12.06	5.53	13.57	14.57
SiO_2 + TiO_2 NPs	4.44	11.67	0.56	0.00
ZnO + TiO_2 NPs	18.08	19.61	2.83	12.64
Average value	**7.16**	**7.29**	**2.87**	**2.61**

[a] *% difference = (experimental value - predicted value) / experimental value ×100*

Table S6.9. *Importance and statistical significance of studied descriptors to the mixture toxicity of MO_X NPs in the internal and the combined datasets.*

Descriptors	Internal dataset		Combined dataset	
	t value	Relative importance %	*t* value	Relative importance %
χ_{me}	0.132	1.45	-0.137	1.37
$\Sigma\chi_{me/nO}$	-1.110	12.17	-0.098	0.98
ζP	0.381	4.18	-1.432	14.37
D_H	-0.034	0.37	1.561	15.66
ΔH_{me+}	0.836	9.17	-4.706	47.22
ΔH_{sf}	5.672	62.19	0.613	6.15
E_C	-0.369	4.05	0.406	4.07
Z^2/r	0.586	6.43	1.013	10.16

Table S6.10. *The calculated AICc values for a set of models integrating the proposed descriptors in various combinations* [a].

Descriptors	Internal dataset		Combined dataset	
	K	*AICc*	*K*	*AICc*
χ_{me}	3	-2.46	3	60.42
ΔH_{me+}	3	0.98	3	45.19
ΔH_{sf}	3	-5.37	3	58.64
χ_{me}, ΔH_{me+}	4	0.89	4	48.19
χ_{me}, ΔH_{sf}	4	-0.69	4	61.30
ΔH_{me+}, ΔH_{sf}	4	-1.56	4	47.31
χ_{me}, ΔH_{me+}, ΔH_{sf}	5	3.12	5	48.08

[a] *K is the number of parameters in the model and its default value is 2.*